EPIGENETIC SIGNATURES OF PRENATAL ALCOHOL EXPOSURE

by

Alexandre André Lussier

B.Sc., McGill University, 2012

A THESIS SUBMITTED IN PARTIAL FULFILLMENT OF

THE REQUIREMENTS FOR THE DEGREE OF

DOCTOR OF PHILOSOPHY

in

THE FACULTY OF GRADUATE AND POSTDOCTORAL STUDIES

(Medical Genetics)

THE UNIVERSITY OF BRITISH COLUMBIA

(Vancouver)

September 2017

Abstract

Prenatal alcohol exposure (PAE) can alter the development, function, and regulation of neurobiological and physiological systems, causing lasting cognitive alterations, behavioral deficits, immune dysfunction, and increased vulnerability to mental health problems. In humans, the spectrum of these deficits is known as fetal alcohol spectrum disorder (FASD). Although the molecular underpinnings are not fully elucidated, epigenetic mechanisms are a prime candidate for the programming of physiological systems by PAE, as they may bridge environmental stimuli and neurodevelopmental outcomes. DNA methylation is also emerging as a potential biomarker of early-life events, which may aid in earlier FASD diagnoses. Thus, my overarching aim was to identify epigenetic mechanisms that may contribute to the deficits associated with FASD and act as biosignatures of PAE. Specifically, I used genome-wide approaches to assess underlying gene expression programs and epigenomic profiles in a rat model of PAE and clinical cohorts of individuals with FASD. In the rat model, I identified alterations to gene expression programs in the brain of adult PAE females under steady-state and immune challenge conditions. Building on these long-term alterations to transcriptomic programs, I identified altered DNA methylation patterns persisting from birth to weaning in the hypothalamus PAE animals, suggestive of early reprogramming of neurobiological systems. In parallel, I found concordant alterations to DNA methylation profiles in the hypothalamus and white blood cells of PAE animals, which may reflect systemic effects and potential biomarkers of PAE. To complement the animal model, I also investigated DNA methylation patterns in two clinical cohorts of FASD, where I identified an epigenetic signature of FASD in buccal epithelial cells. As these results raised the possibility of an epigenetic biomarker, I investigated the relevance of DNA methylation as a diagnostic method for PAE, and successfully generated a predictive algorithm that could classify

individuals with FASD versus controls. Overall, these findings provide evidence for the biological embedding of PAE's effects through changes in gene expression and DNA methylation, while setting the stage for the development of novel biomarkers. Ultimately, these may aid in the development of targeted interventions and early screening tools to mitigate the deficits associated with FASD.

Lay Summary

Prenatal alcohol exposure can result in abnormal brain development, causing Fetal Alcohol Spectrum Disorder (FASD), which is linked to a number of cognitive, behavioural, and immune deficits that last across the lifetime. Although the lasting effects of alcohol on development are well studied, the molecular changes causing these deficits remain relatively unknown. Recent evidence suggests that modifications to DNA structure and regulation, known as epigenetic mechanisms, may play a role in the long-term effects of alcohol on the developing brain and could act as a signature of prenatal alcohol exposure. This thesis presents new evidence for DNA methylation, a small chemical mark added to DNA, as a mechanism in the long-term programming of immune and brain functions. Furthermore, it provides a framework for the use of DNA methylation as a marker of alcohol exposure to diagnose children at-risk for FASD and help lessen some of their long-term problems.

Preface

Please note that all data chapters in this thesis (Chapters 2-5) are presented in manuscript format, as they are currently published (Chapters 2 & 4) or under submission (Chapters 3 & 5).

Portions of **Chapter 1** (introduction) have been adapted from previously published manuscripts:

- Lussier AA, Weinberg J, Kobor MS. 2017. Epigenetics studies of fetal alcohol spectrum disorder: where are we now? *Epigenomics*.
- Lussier AA*, Islam SA*, Kobor MS. Genetics and epigenetics of development. In Gibbs R. & Kolb B. (Eds.). *The neurobiology of brain and behavioural development.* Elsevier Inc. In press. *Authors contributed equally.

A version of **Chapter 2** has been published in the following manuscripts:

- Lussier AA*, Stepien KA*, Neumann SM, Pavlidis P, Kobor MS, Weinberg J. 2015. Prenatal alcohol exposure alters steady-state and activated gene expression in the adult rat brain. *Alcoholism: Clinical and Experimental Research*. *Authors contributed equally.
- Lussier AA, Stepien KA, Weinberg J, Kobor MS. 2015. Prenatal alcohol exposure alters gene expression in the rat brain: Experimental design and bioinformatic analysis of microarray data. *Data in Brief*.

The experimental design and animal work for this study was primarily performed by X. Zhang, with assistance from other members of the Weinberg lab. S. Neumann and K. Stepien ran the gene expression microarrays and performed the tissue extractions alongside T. Bodnar and L. Ellis. K. Stepien performed the differential expression analysis, with critical insight from P. Pavlidis. I verified the microarrays findings by RT-qPCR, and performed the bioinformatic

analyses related to verification experiments and pathway identification. I also wrote the vast majority of the manuscript. J. Weinberg and M. Kobor provided critical insight at all steps of the process. John Wiley & Sons license number: 4133251106844 (ACER).

Chapter 3 is original and unpublished. I developed the design for this study alongside T. Bodnar, J. Weinberg, and M. Kobor. I performed the animal experiments with the assistance of T. Bodnar, W. Comeau, and the members of the Weinberg lab. I performed the meDIP procedures with aid from M. Mingay from M. Hirst's lab at the UBC, and next-generation sequencing was performed by the Genome Sciences Centre in Vancouver, BC. I was responsible for all bioinformatic analyses of the meDIP-seq data, and was assisted by A. Morin from the Kobor lab for the pyrosequencing analysis. I was solely responsible for manuscript preparation, with critical feedback from J. Weinberg and M. Kobor.

A version of **Chapter 4** has been published as:

- Portales-Casamar E*, Lussier AA*, Jones MJ, MacIsaac JL, Edgar RD, Mah SM, Barhdadi A, Provost S, Lemieux-Perreault LP, Cynader MS, Chudley AE, Dubé MP, Reynolds JN, Pavlidis P, Kobor MS. 2016. DNA methylation signature of human fetal alcohol spectrum disorder. *Epigenetics & Chromatin*. *Authors contributed equally.

This study was designed by members of NeuroDevNet, a Canadian Network of Centres for Excellence, and collection of samples was performed at multiple FASD clinics across Canada. I was responsible for a portion of the bioinformatic analyses (gene ontology and differentially methylated regions) and wrote the majority of the manuscript. E. Portales-Casamar performed the differential methylation analysis. R. Edgar performed the brain gene expression analysis. J.

MacIsaac and S. Mah ran the DNA methylation arrays. A. Barhddi, S. Provost, LP Lemieux-Perreault and MP Dubé aided in the genetic analyses. M. Jones, P. Pavlidis, A. Chudley, J. Reynolds, and M. Kobor aided in the interpretation of results and manuscript feedback.

Chapter 5 is original and unpublished. This study was designed by members of NeuroDevNet and sample collection was performed in Winnipeg, MB by J. Salmon and A. Chudley. DNA methylation arrays were run by J. MacIsaac and A. Morin, whom also performed the pyrosequencing assay. I was responsible for all bioinformatic analyses and manuscript preparation, with critical feedback from J. Weinberg, M. Kobor, J. Reynolds, and P. Pavlidis.

Chapter 6 (discussion) contains excerpts from a published review:

- Lussier AA, Weinberg J, Kobor MS. 2017. Epigenetics studies of fetal alcohol spectrum disorder: where are we now? *Epigenomics*. The remainder is original and unpublished.

All animal protocols were approved by the University of British Columbia Animal Care Committee and are consistent with the NIH Guide for the Care and Use of Laboratory Animals (certificates: A06-0017, A07-0381, A10-0136, A10-0016, A12-0032).

Ethics for the clinical cohorts of FASD were reviewed and approved by the "Children's and Women's Research Ethics Board – Clinical" (H10-01149). Experimental procedures were reviewed and approved by the Health Research Ethics Boards at Queen's University, University of Alberta, Children's Hospital of Eastern Ontario, University of Manitoba, and the University of British Columbia.

Table of Contents

List of Tables

List of Figures

List of Abbreviations

450K array – Illumina HumanMethylation450 BeadChip array

AA – Adjuvant-induced arthritis

ADHD – Attention deficit hyperactive disorder

ANOVA – Analysis of variance

ARBD – Alcohol-related birth defect

ARND – Alcohol-related neurodevelopment disoder

ASD – Autism spectrum disorder

BEC – Buccal epithelial cell

BH – Benjamini-Hochberg

BWA – Burrows-Wheeler Alignment

C – Control

CBC/Diff – Complete blood count with differential

CFA – Complete Freund's adjuvant

CpG – Cytosine-guanine dinucleotide

CpH – Cytosine dinucleotide, where H = adenine, cytosine, or thymine

CGI – CpG island

CI – Confidence interval

CNS – Central nervous system

Ct – Cycle threshold

DM – Differentially methylated

DMR – Differentially methylated region

DNA – Deoxyribonucleic acid

DNAhm – DNA hydroxymethylation

E – Ethanol

FAS – Fetal alcohol syndrome

FASD – Fetal alcohol spectrum disorder

FC – Fold change

FDR – False discovery rate

GD – Gestational day

GEO – Gene expression omnibus

GO – Gene ontology

GSR – Gene score resampling

hmC – hydroxymethylated cytosine

HPA – Hypothalamic-pituitary-adrenal

HPC – Hippocampus

HSD – Honest significant different

HYP – Hypothalamus

KBHN – Kid's Brain Health Network

MACS – Model-based analysis of chromatin immunoprecipitation and sequencing

mCH – methylated CpH dinucleotide

MDS – Multidimensional scaling

meDIP-seq – Methylated DNA immunoprecipitation and next-generation sequencing

NDN – NeuroDevNet

NIH – National Institutes of Health

ORA – Over-representation analysis

P – Postnatal day

PAE – Prenatal alcohol exposure

PCR – Polymerase chain reaction

PF – Pair-fed

pFAS – Partial fetal alcohol syndrome

PFC – Prefrontal cortex

PND – Postnatal day

RNA – Ribonucleic acid

ROC – Receiver operator characteristic

RPKM – Reads per kilobase per million

RT-qPCR – Reverse-transcriptase quantitative polymerase chain reaction

SEP – Socio-economic position

SES – Socio-economic status

SNP – Single nucleotide polymorphism

SV – Surrogate variable

SVA – Surrogate variable analysis

TF – Transcription factor

TFBS – Transcription factor binding site

TSS – Transcriptional start site

UCSC – University of California, Santa Cruz Genome Browser

URA – Upstream regulator analysis

UTR – Untranslated region

WBC – White blood cell

Acknowledgements

Foremost, I would like to express my sincerest graduate to my two phenomenal supervisors, Dr. Michael S. Kobor and Dr. Joanne Weinberg. Thank you for your encouragement, critical insight and feedback, knowledge, "opportunities", and support throughout the past 5 years. I could not imagine having any better academic mentors and am honored to have had the privilege to learn from their experience and expertise. I cannot thank you enough. Many thanks to my committee members, Dr. Catharine Rankin, Dr. Daniel Goldowitz, and Dr. Wendy Robinson, whom have provided insightful feedback during my comprehensive exam, committee meetings, and many questions. Thank you for being available on short notice and putting up with sometimes tight deadlines.

Many thanks to past and present members of the Kobor and Weinberg labs – none of this would have been possible without your support. Special thanks to Dr. Tamara Bodnar, whom helped tremendously with the collection of my animal study and was always available to fill me in on the particularities of the immune system. Thank you, wonderful Weinbergers – Charlis, Kasia, Linda, Ni, Parker, Vivian, Wayne, and Wendy - for your friendship and feedback on my work. Thank you, Koborites – Alex, Alice, Alyssa, David, Eric, Evan, Grace, Josh, Julie, Kristy, Lisa, Maria, Meaghan, Olivia, Sachini, Sarah (x3), Sumaiya, Tanya, and Yasmin – for your friendship critical input on my many projects. Special thanks to Dr. David Lin for keeping me company during weekends/late nights and for always being there when I needed to vent. I would also like to thank the members Medical Genetic graduate program, including the many professors, fellow graduate students, and in particular, Cheryl Bishop, whom made navigating my various deadlines very easy.

This work would not have been possible without the aid of our many esteemed collaborators – Matthew Mingay (Hirst lab), Dr. Martin Hirst, Dr. Ab Chudley, Dr. James Reynolds, and Dr. Kristin Hamre. Particular thanks to Dr. Paul Pavlidis and Dr. Elodie Portales-Casamar, whom were always available to discuss my research and provided valuable insight into my methods and results. I have learned tremendously from their expertise and count myself lucky to have had the opportunity to collaborate with them. To Dr. Osman Ipsiroglu, thank you for your mentorship and advice, which has acted as a focal point for my future career path and lifelong goals.

I would like to acknowledge the funding support I have received over the years, including the Developmental Neurosciences Research Training Fellowship from NeuroDevNet and Brain Canada. I would also like to acknowledge the funding agencies that provided the grant support that made this work possible: US National Institutes of Health/National Institute on Alcohol Abuse and Alcoholism (R37 AA007789 and RO1 AA022460); NeuroDevNet (Canadian NCE); and the Canadian Foundation on Fetal Alcohol Research.

Finally, I would like to acknowledge all my family and friends that have been extremely supportive throughout my degree. I could never have made it this far without such a wonderful supporting cast and I cherish the relationships we have built over the years. Special thanks to my parents, who didn't mind me calling at odd hours of the night to share a success story or complain about not sleeping enough. Finally, I would like to thank Urshila Sriram for her love, acceptance of my many idiosyncrasies, and support of my work and career. I could not ask for a better partner and am extremely thankful for her companionship.

Chapter 1: Introduction

1.1 General overview and hypotheses

Adverse early-life conditions have the potential to permanently imprint or program physiological and behavioral systems during development and lead to long-term consequences in offspring (Godfrey & Robinson 1998; Hanson & Gluckman 2008). In particular, prenatal alcohol exposure (PAE) can alter the development, function, and regulation of numerous neurobiological and physiological systems, giving rise to lasting cognitive and behavioral deficits, immune dysfunction, motor impairments, and increased vulnerability to mental health problems in over the life course (Zhang, Sliwowska, & Weinberg 2005; Pei et al. 2011; Mattson, Crocker, & Nguyen 2011). In humans, the broad spectrum of these structural, neurocognitive, physiological, and behavioral abnormalities or deficits is known as fetal alcohol spectrum disorder (FASD) (Hoyme et al. 2016; Stratton, Howe, & Battaglia 1996). Although the exact molecular mechanisms underlying the effects of PAE on neurobiological systems are not yet fully elucidated, epigenetic mechanisms are prime candidates for the programming effects of environmental factors on physiological systems, as they may bridge environmental stimuli and neurodevelopmental outcomes to influence health and behavior well into adulthood (Yuen et al. 2011; Shulha et al. 2013; Kobor & Weinberg 2011). Furthermore, DNA methylation is emerging as a potential biomarker of early-life events and disease, which may prove useful in the early diagnosis of children at risk for FASD.

I hypothesized that PAE alters the transcriptional profiles and DNA methylation patterns of genes that are functionally related to the deficits associated with FASD. As such, my overarching aim was to identify genetic and epigenetic mechanisms that may contribute to the spectrum of physiological and neurobiological alterations associated with FASD and act as

potential biosignatures of PAE. To this end, I used genome-wide, discovery-driven approaches to assess underlying gene expression programs and epigenomic profiles in animal models of PAE and clinical cohorts of individuals with FASD.

I built on previous studies that showed physiological alterations following PAE. In particular, previous work demonstrated that female PAE rats display a more severe and prolonged course of adjuvant-induced arthritis (AA), suggestive of underlying alterations in immune regulation (Zhang et al. 2012). Following up on these results, I investigated gene expression profiles under basal and immune challenge conditions in the brain of adult PAE animals to determine whether I could identify long-term alterations to gene expression programs in the brain using an established rat model of PAE (Chapter 2). Based on previous research, I hypothesized that PAE animals would display altered baseline transcriptomic profiles in the hippocampus and prefrontal cortex, which have important regulatory inputs into the stress axis and immune system. I also hypothesized that PAE animals would show a differential gene expression response to AA compared to controls due to their increased vulnerability to this immune challenge. Building on the long-term programming effects of alcohol on the neural transcriptome identified through this investigation, I shifted my focus to the biological embedding of PAE through epigenetic mechanisms (Chapter 3). This particular study focused on the hypothalamus, rather than the hippocampus and prefrontal cortex, as it acts as the central common integrator of several physiological systems in the brain and plays key roles in the stress response, immune function, and homeostatic regulation. Given the persistent effects of PAE on these neurobiological systems, as well as the association between epigenetics and transcriptional regulation, I predicted that PAE would alter genome-wide DNA methylation programs in the hypothalamus across early development, particularly within genes associated with these vital

functions. I also predicted that some differential DNA methylation patterns would overlap between central nervous system (CNS) tissue and white blood cells (WBC), potentially reflecting systemic effects of alcohol and biomarkers of PAE.

Although the animal model provides important insight into the molecular underpinnings of PAE-induced deficits, it may not fully reflect the epigenetic changes found in individuals with FASD. As such, I assessed DNA methylation profiles in a clinical cohort of FASD, hypothesizing that I could identify genome-wide DNA methylation alterations in the buccal epithelial cells (BEC) of individuals with FASD versus controls (Chapter 4). Given the importance of replication in epigenome-wide association studies, I further assessed the findings from the first clinical cohort in a second, independent sample of individuals with FASD (Chapter 5). I predicted that some of the results from the initial study would validate here, representing a robust signature of PAE in humans. As DNA methylation patterns have previously been used to predict prenatal exposures, I further expected that the DNA methylation signature of FASD could be used to develop an early screening tool that could accurately classify individuals as FASD or controls.

Taken together, the identification of persistent gene expression changes and stable epigenetic alterations in the brain and peripheral tissues may provide insight into the etiology of PAE-induced deficits, while building a foundation for the development of accurate biomarkers of FASD.

1.2 Fetal alcohol spectrum disorder

PAE can result in a harmful *in utero* environment that can cause numerous adverse developmental consequences falling under the umbrella of FASD. At the most severe end of the

spectrum is fetal alcohol syndrome (FAS), which can occur with chronic exposure to high doses of alcohol (Jones & Smith 1973). The diagnostic criteria for FAS consist of pre- and post-natal growth retardation, a characteristic set of facial dysmorphologies, and central nervous system alterations, including neurological abnormalities, developmental delays, and intellectual impairment (Stratton, Howe, & Battaglia 1996). Exposure to alcohol at levels that do not produce full FAS can result in either partial FAS (pFAS), where only some of the diagnostic features occur, or in numerous alcohol-related effects that can be primarily physical (alcohol-related birth defects, ARBD) or primarily neurobehavioral (alcohol-related neurodevelopmental disorder, ARND), although ARBD and ARND are not mutually exclusive and both may occur in an individual exposed to alcohol *in utero* (Stratton, Howe, & Battaglia 1996). Importantly, neurobehavioral/-developmental deficits are consistently seen across the spectrum, and include neurocognitive impairment (cognitive function, learning and memory, executive function), impairment in self-regulation (attention, impulsivity, behavioral regulation, stress responsiveness, mood/affect, sleep abnormalities), and deficits in adaptive function (communication, social behavior, activities of daily living) (Carter et al. 2016; Lynch, Kable, & Coles 2015; Panczakiewicz et al. 2016; Doyle & Mattson 2015; Astley et al. 2009; Streissguth & O'Malley 2000).

Despite the recognition of FAS over four decades ago, PAE remains a leading cause of intellectual disability in North America and worldwide. Although current global estimates place the prevalence of FAS and FASD at 2.9 and 22.8%, respectively, regional incidences vary greatly, with some populations displaying up to an estimated 55% prevalence of FAS (Roozen et al. 2016). By contrast, recent active case ascertainment studies in the USA, Italy, Poland, and Croatia have found that FASD prevalence is approximately 2-5% in the general population (May

et al. 2009, 2014, 2015; Petković & Barišić 2013; Okulicz-Kozaryn, Borkowska, & Brzózka 2017; May et al. 2011). Importantly, approximately half of women under 30 years of age in the USA have unplanned pregnancies (May et al. 2004). As such, they may not realize they are pregnant until later in gestation and may continue to consume alcohol during the first trimester of their pregnancy. Indeed, it is estimated that 10-15% of women in Canada and the USA continue to drink throughout pregnancy, with approximately 3% continuing to binge drink, which is particularly deleterious to fetal development (Popova et al. 2017; Bonthius & West 1990).

The degree to which alcohol affects development depends on a variety of factors such as timing, pattern, and level of alcohol exposure, overall maternal health and nutrition, and genetic background, which may influence the disparity between maternal drinking rates and the prevalence of FASD (Pollard 2007). Importantly, the adverse neurodevelopmental outcomes of children with FASD often persist well into adulthood, including metabolic changes, immune dysfunction, altered stress responsitivity, and vulnerability to mental health disorders, such as substance use, depression, anxiety, psychosis, and bipolar disorder (Famy, Streissguth, & Unis 1998; Spohr & Steinhausen 2008; Lemoine et al. 2003; Weyrauch et al. 2017; Popova et al. 2016; Streissguth et al. 2004; Barr et al. 2006; Moore & Riley 2015).

1.3 Animal models of FASD

Animal models of PAE were first developed in response to the skepticism that greeted the first description of FAS by Jones and Smith in 1973 (Jones & Smith 1973; Jones et al. 1973). These were particularly important in that effects of alcohol could be investigated with a level of control not possible in the clinical setting, including timing, pattern (acute versus chronic), and dose of alcohol, genetic factors, environment, nutrition, and other drugs. An additional important

strength of animal models is the ability to make direct correlations between central and peripheral tissues, as clinical studies do not have ready access to critical tissues such as the brain and other organs, except through biopsy or postmortem specimens, and changes in peripheral tissues do not always reflect alterations in the brain. Furthermore, animal models can provide critical insight into the molecular mechanisms underlying effects of PAE, and can thus pave the way for identification of novel biomarkers. Important recent studies have made significant progress in characterizing the neurodevelopmental, physiological, and behavioral alterations associated with PAE, as well as elucidating molecular mechanisms through which these alterations occur at different doses and patterns of alcohol exposure. *In vitro* studies have provided further vital insights into the mechanisms by which alcohol affects cellular functions, allowing for the dissection of molecular pathways in highly specific and controlled environments (Liu et al. 2009; Zhou, Zhao, et al. 2011; Hicks, Middleton, & Miller 2010; Veazey et al. 2013, 2015; Balaraman, Winzer-Serhan, & Miranda 2012). These different strategies have provided key insights into the altered neurodevelopmental profiles resulting from PAE and highlight the complex and long-term programming effects of alcohol on numerous developmental processes. Overall, these studies have shown that alcohol is an early life insult that programs developing neurobiological systems and markedly increases risk for adverse outcomes, supporting the hypothesis that the effects of PAE on development may involve the reprogramming of physiological systems (Hellemans, Sliwowska, et al. 2010).

1.4 Reprogramming of physiological systems by PAE

1.4.1 PAE alters hypothalamic-pituitary-adrenal axis function

The HPA axis regulates the body's response to stress, reacting to stimuli threatening

homeostasis and/or survival. Briefly, stressors activate the parvocellular neurons of the paraventricular nucleus of the hypothalamus, resulting in secretion of corticotropin-releasing hormone (CRH) (reviewed in Jankord & Herman 2008). In turn, CRH stimulates release of adrenocorticotropic hormone (ACTH) from the anterior pituitary gland. ACTH then acts on the adrenal cortex, causing the secretion of glucocorticoids, cortisol in humans and mainly corticosterone in rodents. These feed back to multiple brain regions, such as the hypothalamus, to inhibit further HPA activation (Herman & Cullinan 1997). The hippocampus and prefrontal cortex are also important regulators of the HPA axis, partially controlling the extent of the stress response. While the prefrontal cortex provides both stimulatory and inhibitory inputs to the HPA axis, the hippocampus contains high levels of glucocorticoid receptors, dampening the stress response (Diorio, Viau, & Meaney 1993; Reul & De Kloet 1985; Jacobson & Sapolsky 1991). Under stressful conditions, glucocorticoids induce rapid physiological changes promoting survival, such as increased gluconeogenesis, reduced reproductive function, and suppressed immune response. However, prolonged exposure to high levels of glucocorticoids can produce deleterious effects, including metabolic, cognitive, and immune dysfunction (McEwen & Stellar 1993).

Furthermore, the HPA axis is highly susceptible to programming during early life (Matthews 2002; Eguchi 1969). Given that the pregnant mother and fetus constitute an interrelated functional unit, maternal exposures and hormone changes may shape developmental trajectories in the fetus (Weinberg 1993). In particular, the fetal HPA axis of an alcohol-consuming mother receives conflicting signals, as ethanol crosses the placenta to directly activate the fetal HPA axis, while activating the maternal HPA axis in parallel, which then exerts negative feedback on the fetal system (Eguchi 1969). However, the influence of the HPA axis on

the developing organism may be partially dampened by increased 11β-HSD levels in the placenta of PAE animals, which may reduce the degree to which glucocorticoids can cross the placenta (Lan et al. 2017). Nevertheless, these signals have been shown to reprogram the fetal HPA axis, increasing HPA axis activation and causing deficits in recovery following stress (Weinberg et al. 2008).

Importantly, data from both clinical cohorts and animal models of FASD suggest that PAE itself causes widespread reprogramming of HPA axis function. Infants exposed to alcohol *in utero* show elevated basal levels of cortisol at 2 and 13 months of age, as well as higher post-stress levels at 13 months (Ramsay, Bendersky, & Lewis 1996; Jacobson, Bihun, & Chiodo 1999). In addition, 5-7 month old children also display increased cortisol reactivity in response to the "still-face" procedure, which is used to assess emotion and stress regulation (Haley, Handmaker, & Lowe 2006). Animal models have identified a similar hyperresponsiveness to stressors following PAE, identifying alterations to central regulation of the HPA axis under basal and stress conditions (Ramsay, Bendersky, & Lewis 1996; Jacobson, Bihun, & Chiodo 1999; Haley, Handmaker, & Lowe 2006; Weinberg et al. 2008). Although basal serum levels of corticosterone and ACTH are not altered in PAE animals, CRH mRNA expression is increased in the hypothalamus of both weanling and adult PAE rats under basal conditions, as are POMC mRNA levels in the anterior pituitary (Lee et al. 1990, 2000; Lee & Rivier 1996; Gabriel et al. 2005, 2017; Redei, Clark, & McGivem 1989; Redei et al. 1993). PAE rats also display deficits in the intermediate range of HPA feedback regulation (2-10h), but not in the fast response (seconds to minutes), suggesting that deficits in feedback regulation may act through cellular programs, rather than direct hormonal signaling (Osborn et al. 1996; Hofmann et al. 1999). Taken together, these findings suggest that PAE reprograms the HPA axis, altering its basal tone and responsivity

to stressors, which may be influenced by underlying alterations to cellular programs within regions associated with the HPA axis.

1.4.2 PAE induces changes in homeostatic systems

In addition to its role in the stress response, the HPA axis is also intimately connected to the physiological systems regulating homeostasis. In particular, the hypothalamus acts not only as a key regulator of endocrine function but also for autonomic regulation and homeostatic control, regulating growth, sleeping patterns, metabolism, body temperature levels, and other vital functions through its many different nuclei (Squire et al. 2008). As glucocorticoids also play an important role in the regulation of these metabolic and physiological processes, their dysregulation following PAE may be due to both direct effects of ethanol on the function of hypothalamic centers and indirect effects caused by HPA axis dysfunction (Dickmeis 2009). Nevertheless, clinical and animal studies have shown that the hypothalamus is particularly vulnerable to the effects of alcohol during development, displaying broad alterations to homeostatic functions following PAE, including disrupted sleep patterns and circadian rhythms, deficiencies in thermoregulation, and disordered metabolism and feeding behavior (Jones & Smith 1973; Chen et al. 2012; Earnest, Chen, & West 2001; Sei et al. 2003; Zimmerberg, Ballard, & Riley 1987; Werts et al. 2014).

Indeed, children and adolescent with FASD show disrupted sleep patterns related to insomnia and parasomnia, with concomitant alterations to melatonin secretion profiles (Chen et al. 2012; Ipsiroglu et al. 2013; Goril et al. 2016). Rodent models have also identified sleep disturbances following PAE, including shorter circadian sleep-wake cycles and alterations to the structure and function of the suprachiasmatic nucleus (SCN) of the hypothalamus, which

synchronizes the circadian rhythm with light (Hilakivi 1986; Earnest, Chen, & West 2001; Spanagel et al. 2005; Chen et al. 2006). Additionally, PAE has lasting effects on the regulation of body temperature in response to circadian rhythms, while delaying the development of thermoregulation in rat pups, suggesting a disruption of the complex interplay between the different homeostatic systems of the hypothalamus (Zimmerberg, Ballard, & Riley 1987; Sei et al. 2003).

Disordered eating patterns are also common in alcohol-exposed children, particularly within feeding behaviors related to a lack of satiety, which suggest that regulatory pathways regulating feeding behavior may be dysregulated (Harper et al. 2014; Werts et al. 2014). Furthermore, children with FASD display higher rates of glucose intolerance and hyperinsulemia, suggesting that they may be more vulnerable to metabolic syndrome (Castells et al. 1981; Lee 2012; Fan et al. 2008). Animal models show similar findings of altered glucose homeostasis, as PAE rats display increased insulin resistance and glucose intolerance following a glucose challenge (Chen & Nyomba 2003). Furthermore, adult PAE animals show elevated serum triglyceride levels and alterations to adiposity, which may increase the risk of cardiovascular disease (Pennington, Shuvaeva, & Pennington 2002; Dobson et al. 2012). Although it is difficult to tease apart the molecular and biological pathways that may influence these phenotypes, they suggest a broad reprogramming of metabolic processes and regulatory mechanisms, which may be mediated through alterations in the hypothalamus.

As a whole, these findings suggest PAE may reprogram the developing homeostatic systems, potentially through indirect effects on HPA axis and direct effects on the hypothalamus, which may ultimately act as a final common integrator of the effects of PAE to mediate some of its widespread and lasting organizational effects on physiological systems.

1.4.3 PAE causes alterations to immune function and regulation

Beyond the lasting deficits in the stress response and homeostatic regulation, clinical studies and animal models of PAE have also identified broad alterations to immune function and response. Clinical data examining alcohol-induced alterations in immune competence in children and adults with FAS/FASD remain limited. Early investigation found that children with FAS show a higher incidence of a range of major and minor infections, including recurrent otitis media, upper respiratory tract infections, urinary tract infections, sepsis, pneumonia, and acute gastroenteritis (Johnson et al. 1981; Ammann et al. 1982; Church & Gerkin 1988). In addition, alcohol-exposed show decreased eosinophil and neutrophil cell counts in, as well as decreased leukocyte response to mitogens compared to non-exposed children (Johnson et al. 1981; Gottesfeld & Abel 1991). More recent studies have shown that very low birth weight newborns exposed to alcohol *in utero* have a 15-fold higher incidence of early-onset sepsis as compared to controls matched for race, sex, gestational age, and birth weight (Gauthier, Manar, & Brown 2004). High levels of maternal drinking (binge) during the second trimester have also been shown to increase the risk of infection by approximately 4-fold compared to that in unexposed newborns when controlling for smoking, low maternal income, and size for gestational age (Gauthier et al. 2005).

Animal models have corroborated clinical findings, as fetuses and newborn PAE animals display decreased thymus weight, size, and cell numbers, as well as suppressed B cell development (Ewald & Frost 1987; Ewald & Walden 1988; Clausing et al. 1996; Moscatello et al. 1999). These deficits persist into adulthood, with additional alterations to the immune response being revealed as the animal matures, such as deficits in the response of splenic T cells

and lymphoblasts to the mitogen Concanavalin A and/or interleukin-2, as well as increased vulnerability to infections (Weinberg & Jerrells 1991; Norman et al. 1991; Gottesfeld et al. 1990; McGill et al. 2009). PAE animals also display greater susceptibility to immune and inflammatory challenges, showing greater increases in plasma levels of pro-inflammatory cytokines and reduced proliferative responses of B-cells following lipopolysaccharide exposure (Zhang, Sliwowska, & Weinberg 2005). In addition, PAE females display increased severity of joint inflammation and a prolonged course of disease in an adjuvant-induced arthritis (AA) paradigm. This model is used to study the interactions between the neuroendocrine and immune systems, mimicking human rheumatoid arthritis, an auto-immune disorder influenced by early-life experiences and potentially mediated through altered neuroendocrine-immune interactions (Harbuz, Rees, & Lightman 1993; Harbuz, Chover-Gonzalez, & Jessop 2003; Chover-Gonzalez et al. 1999; Bomholt et al. 2004; Colebatch & Edwards 2011; Zhang et al. 2012).

Although the mechanisms underlying the immunoteratogenic effects of PAE on the immune system remain unclear, it has been shown that alcohol consumption increases cytokine levels with chronic alcohol consumption during pregnancy increasing levels of key cytokines in both the fetus and mother (Crews et al. 2006; He & Crews 2008; Ahluwalia et al. 2000). Evidence from other fields suggests that immune stimulation and alterations to the fine balance of pro- and anti-inflammatory cytokines during pregnancy is associated with increased risk for neurodevelopmental disorders, including schizophrenia and autism (Howard 2013; Goines et al. 2011). However, direct links between alcohol-related alterations in the prenatal maternal cytokine balance and immune, neurocognitive, or behavioral outcomes associated with FASD, have yet to be established. Recent work from a range of animal models has shown that alcohol exposure generally increases cytokine production within the brain, a marker of neuroimmune

activation. Using third trimester equivalent exposure models, cytokine levels were shown to increase in the cerebellum, cortex, and hippocampus in alcohol-exposed animals (Topper, Baculis, & Valenzuela 2015; Drew et al. 2015). In addition, cytokine levels are altered in the brain following PAE, with increased levels detected in the hippocampus and prefrontal cortex, but decreased levels in the hypothalamus (Bodnar, Hill, & Weinberg 2016). Despite inherent differences between these models, such as method and timing of alcohol administration, species, and cytokine detection method, the concordance of these findings highlights that neuroinflammation may be a cross-cutting feature in both FASD and animal models of PAE.

Importantly, exposure to stressors exacerbates immune deficits in PAE animals, suggesting a potential role for the stress response in these immune deficits (Giberson & Weinberg 1995; Giberson et al. 1997). Of note, the HPA axis and immune response display extensive bidirectional communication, sharing numerous ligands, receptors, and regulatory regions. In addition to its key role in the stress response, the hypothalamus is also an important feedback center for cytokines, while other brain regions regulating the HPA axis, such as hippocampus and prefrontal cortex display high levels of cytokine and immune receptors (Bernardini et al. 1990; Cunningham & De Souza 1993). Furthermore, pro-inflammatory cytokines can stimulate the HPA axis, which, in turn, has the ability to suppress immune function (Haddad, Saadé, & Safieh-Garabedian 2002). As such, PAE may affect the fine-tuned reciprocal interactions between these systems, leading to alterations in both HPA axis and immune function. Overall, the findings of persistent immune deficits and altered responses to immune stressors suggest a reprogramming of immune functions by PAE, potentially acting in concert with the rewiring of brain regions involved in both the stress and immune response.

1.5 Fetal programming as a framework for the interpretation of PAE-induced deficits

Overall, the persistence of FASD-associated deficits suggests that physiological and neurobiological systems may be reprogrammed by PAE during early life, resulting in a markedly increased risk for adverse outcomes later in life (Hellemans, Sliwowska, et al. 2010). These findings support a role for the interpretation of PAE-induced deficits through the fetal programming hypothesis. This concept suggests that early environmental or non-genetic factors, including maternal undernutrition, stress, and exposure to drugs or other toxic agents, can permanently organize or imprint physiological and neurobiological systems to increase adverse cognitive, adaptive, and behavioral outcomes, as well as vulnerability to diseases or disorders later in life (Godfrey & Robinson 1998; Hanson & Gluckman 2008; Swanson et al. 2009). This concept was first formulated based on epidemiological evidence that low birth weight and other indices of poor fetal growth are associated with increased biological risk for coronary heart disease, hypertension, and type II diabetes/impaired glucose tolerance (i.e., metabolic syndrome) in adult life (Barker et al. 1989, 1993, Barker 1997, 2003, 2004; Barker & Osmond 1986; Barker & Thornburg 2013). Subsequent research revealed that low birth weight *per se* is unlikely the cause of these risks for disease; rather, low birth weight is a proxy for prenatal environmental adversity, and common factors likely underlie both intrauterine growth retardation and altered physiological/metabolic function (Welberg & Seckl 2001).

Current thinking extends beyond these initial findings, suggesting that signals received during development, such as nutritional and hormonal status, may preemptively lead the organism towards a phenotype best adapted for the anticipated external environment (Hanson, Low, & Gluckman 2011). However, in the event of a mismatch between early and later life environments, this adaptive response may no longer confer a fitness advantage, but instead, lead

to deleterious phenotypes (Godfrey et al. 2007). This early-life programming is a manifestation of developmental plasticity, where a single genotype can lead to multiple phenotypic outcomes due to differing environmental conditions (Barker 2007). Importantly, epigenetic mechanisms are emerging as potential mediators for the biological embedding of these early-life environments, as they provide a link between *in utero* conditions and the genome in the modulation of subsequent developmental trajectories (Meaney 2010; Boyce & Kobor 2015).

1.6 Epigenetic mechanisms link environmental exposures and cellular programs

Although genetics may be considered the inscribed "blueprint" underlying the central dogma of molecular biology (i.e. DNA→RNA→protein), epigenetics can be thought of as the regulatory overlay of genetic sequence that fine-tunes gene activity during development and in response to external signals (Boyce & Kobor 2015). From a historical perspective, the term 'epigenetics' was first introduced by Conrad Waddington in the early 1940s to describe ''the branch of biology which studies the causal interactions between genes and their products which bring the phenotype into being" (Waddington 1968). Waddington argued that epigenetics play a critical role in the development of multicellular organisms by creating 'epigenetic landscapes' that drive cellular differentiation along a programmed trajectory towards a specific cell-type lineages (Waddington 1968). Since the first introduction of this concept, the field of epigenetics has flourished into a highly active area of study aimed at characterizing the molecular mechanisms underlying gene regulation and biological programming. Today, epigenetics is operationally defined as modifications of DNA and its regulatory components, including chromatin and non-coding RNA, to potentially modulate gene transcription without changing the DNA sequence itself (Bird 2007; Meaney 2010; Henikoff & Greally 2016). Notably,

Waddington's initial hypothesis still holds true: the ontogeny of the ~200 different cell types in the human body is largely shaped by the unique epigenomic profiles and transcriptional activity of each cellular subtype (Domcke et al. 2015; Schuebeler 2015). Accordingly, epigenetic regulation involves both dynamic tissue- and cell type-specific variation during development, as well as the preservation of the cellular memory required for developmental stability. In addition, epigenetic regulation is now becoming increasingly recognized as a potential biological mediator of environmental influences, which can contribute to sculpting the epigenome, although these effects tend to be subtler than those driven by cell type (Feil & Fraga 2012). Importantly, epigenetic mechanisms exist in a seeming paradox between the stability of cellular identity and plasticity of environmental responses, modulating cellular functions through both short- and long-term responses to stimuli (Boyce & Kobor 2015).

1.6.1 DNA modifications

Covalent modifications on DNA nucleotides, primarily cytosine, have long been an established form of epigenetic regulation. Specifically, DNA modifications are comprised of DNA methylation (which can occur in the context of cytosine-guanine (CpG) dinucleotides or at non-CpG positions) as well as oxidized derivatives of DNA methylation such as DNA hydroxymethylation.

1.6.1.1 DNA methylation

DNA methylation is arguably the most studied epigenetic mark and involves the covalent attachment of a methyl group to the 5' position of cytosine, typically at CpG dinucleotide sites (Jones & Takai 2001). These CpG dinucleotides occur relatively infrequently in the genome in

order to minimize the potential for DNA methylation-induced sequence mutability as methylated cytosines can undergo spontaneous deamination to thymine (Illingworth & Bird 2009; Weber et al. 2007; Gardiner-Garden & Frommer 1987). Areas with comparatively high CpG content in the genome have been termed "CpG islands" (CGIs) and these CGIs are thought to exist as regions that were either never methylated or only transiently methylated in the germline while the rest of the genome experienced a loss of CpGs at methylated sequences (Illingworth & Bird 2009; Weber et al. 2007; Gardiner-Garden & Frommer 1987). Importantly, the DNA methylation status of the ~ 28 million CpG sites in the human genome is often dependent on genomic context (Jones 2012; Ulahannan & Greally 2015). CGIs, which are associated with approximately 50-70% of known promoters, tend to contain low levels of methylation in somatic cells, while non-island CpGs exhibit generally higher methylation levels (Illingworth & Bird 2009; Weber et al. 2007; Saxonov, Berg, & Brutlag 2006). Moreover, DNA methylation is associated with the regulation of gene expression, although its effects on transcription are highly dependent on genomic context (Lam et al. 2012; Jones & Baylin 2007; Edgar et al. 2014). For example, DNA methylation at gene promoters is generally associated with gene expression silencing, although its role may be more variable within gene bodies (Schuebeler 2015; Jones & Baylin 2007). Conversely, in regions of lower CpG density which flank CGIs, known as "island shores", high DNA methylation levels are typically associated with highly expressed genes, especially if the associated CGI has low methylation (Edgar et al. 2014; Irizarry et al. 2008; Baubec & Schübeler 2014). While the exact mechanisms remain mostly unknown, transcriptional silencing by DNA methylation may potentially occur through the direct blocking transcription factor binding or the recruitment of transcriptional repressors to promoter, enhancers, or insulator regions (Tate & Bird 1993). Although DNA methylation in promoters and enhancer regions tend to negatively

correlate with gene expression within an individual, emerging evidence shows that when comparing a single gene across a population, the association between DNA methylation and gene expression can be negative, positive, or non-existent, highlighting the complex relationship between DNA methylation and transcription (Lam et al. 2012; Gutierrez-Arcelus et al. 2013; Jones, Fejes, & Kobor 2013). Moreover, DNA methylation can be both active, by being a likely cause of gene expression variation, or passive, by being a consequence or an independent mark of gene expression levels (Gutierrez-Arcelus et al. 2013; Jones, Fejes, & Kobor 2013). In addition to its role in transcriptional control, DNA methylation within introns has been associated with altered mRNA splicing, and its presence within certain exons potentially regulates alternative transcriptional start sites (Shukla et al. 2011; Maunakea et al. 2010, 2013) . Finally, DNA methylation in repetitive elements, which comprise more than half of the human genome including intergenic sequences, tends to occur at relatively high levels and is associated with maintenance of chromosome structure and genomic integrity (Cordaux & Batzer 2009; Donnelly, Hawkins, & Moss 1999). Perhaps most importantly, in addition to its role in the regulation of developmental programs, DNA methylation is also emerging as a potential biomarker for early-life exposures due to its stability over time and malleability in response to environmental cues (Bock 2009). For instance, DNA methylation signatures can predict an individual's risk for eczema or prenatal exposure to smoking with good accuracy, suggesting that DNA methylation profiles could potentially be used to screen for various environmental exposures or disorders (Quraishi et al. 2015; Reese et al. 2017).

1.6.2 Non-CpG DNA methylation

Although DNA methylation primarily occurs in the context of CpG dinucleotides, it can

also occur at CpH (where H = A/C/T) sites. Previous studies have shown that methylated CH dinucleotides (mCH) occur in cultured embryonic stem cells (ESCs) and induced pluripotent stem cells (Ramsahoye et al. 2000; Lister et al. 2009; Laurent et al. 2010; Ziller et al. 2011; Lister et al. 2012). Moreover, analysis of adult human and mouse CNS neurons found that mCH is specifically enriched in neurons compared to other cell types, as non-CpG methylation is nearly absent in non-neuronal adult somatic cells, but can reach up to ~ 25% of all cytosines in neurons of the adult mouse dentate gyrus (Guo et al. 2014; Ziller et al. 2011; Lister et al. 2013). Levels of mCH increase rapidly during early postnatal brain development (mouse, ~2-4 weeks; human 0-2 years), suggesting that it potentially plays an important role in the regulation of postnatal brain development. Genome-wide profiling also showed that in neurons, mCH is present throughout the 5' upstream, gene-body, and 3' downstream regions of genes, where it is negatively correlated with gene expression (Guo et al. 2014; Lister et al. 2013). Furthermore, *in vitro* plasmid reporter gene analyses have shown that CH methylation is associated with transcriptional repression in mouse neurons (Guo et al. 2014). However, mCH is not associated with gene silencing in all cell types, as non-CpG methylation in ESCs positively correlates with gene expression (Lister et al. 2009). It is thought that the distinct distribution and role in gene expression of mCH in different cell types relates to differences in the relative abundance and activity of specific "readers" and "writers" of non-CpG methylation (Kinde et al. 2015). Furthermore, in addition to CH methylation, very recent research has detected the presence of methylated adenosine nucleotides in vertebrates, suggesting that that DNA modification variants may be more diverse than previously thought (Meyer et al. 2012; Dominissini et al. 2013; Koziol et al. 2015; Meyer & Jaffrey 2016).

1.6.3 DNA hydroxymethylation

In contrast to the well-characterized mechanisms underlying the establishment and maintenance of DNA methylation, the process of DNA demethylation remains unclear. Thought to involve both active and passive pathways, this phenomenon is vital for typical development and genetic regulation, particularly in the brain (Ooi & Bestor 2008; Wu & Zhang 2014; Tognini, Napoli, & Pizzorusso 2015). Active DNA demethylation may potentially occur through the oxidation of 5-methylcytosine, catalyzed by the Ten-Eleven-Translocation (TET) family of enzymes (Tahiliani et al. 2009; Santiago et al. 2014). This process generates a series of oxidized cytosine base variants, including hydroxymethylcytosine (hmC), formylcytosine, and carboxycytosine (Tahiliani et al. 2009; Ito et al. 2010; Ulahannan & Greally 2015). Although the exact details of active DNA demethylation remain unclear, emerging evidence points to a process involving the coordinated activity of a number of key enzymatic players and intermediate modified cytosine species. These cytosine variants may also play a role in modulating chromatin structure or recruiting various factors to key regions of the genome (Sadakierska-Chudy, Kostrzewa, & Filip 2014). For instance, various members of the methyl-CpG-binding domain protein family display different affinities for hmC, and given their role in recruiting different chromatin modifying complexes, hmC could potentially alter chromatin landscapes throughout the genome (Pfeifer, Kadam, & Jin 2013).

DNA hydroxymethylation (DNAhm) is also present at high levels in pluripotent cells and the brain, where it has been implicated in neural stem cell functions, although its exact functional role remains to be uncovered (Ito et al. 2010; Kriaucionis & Heintz 2009; Santiago et al. 2014). Genome-wide mapping of DNAhm in various brain regions, including the frontal cortex, hippocampus, and cerebellum, identified an enrichment of hmC in gene bodies, which was

positively associated with gene transcription, particularly at developmentally activated genes (Lister et al. 2013; Wang et al. 2012). Active DNA demethylation and TET activity is also associated with memory formation and addiction in mice, further supporting its functional role in neural activity (Alaghband, Bredy, & Wood 2016).

1.7 Evidence for genetic and epigenetic changes following PAE

1.7.1 PAE causes both transient and persistent alterations to gene expression programs

Epigenetic factors provide an attractive mechanism to mediate the biological embedding of early life events, and their association with transcription makes gene expressions programs an easy target to first assess the molecular underpinning of PAE-induced deficits. Initial evidence of the genome-wide programming effects of alcohol on the genome was identified through changes in transcription. In particular, genome-wide investigations of gene expression programs have identified widespread alterations to gene expression levels in fetal, neonatal, and adult rodent models of PAE, providing important insight into potential mechanisms and pathways involved in PAE-induced deficits (Green et al. 2007; Hard et al. 2005; Zhou, Zhao, et al. 2011; Downing et al. 2012; Kleiber et al. 2012, 2013, 2014; Lussier et al. 2015).

Given the importance of spaciotemporal gene expression during developmental patterning, it is perhaps not surprising that many of the PAE-induced alterations to the transcriptome are closely related to the stage of development that was assessed. For example, differentially expressed genes during early gestation were generally associated with functions in cellular patterning, growth, and development, suggesting that PAE can interfere with typical developmental programs. As gene expression is highly dynamic, quickly responding to environmental and cellular inputs, transcriptional alterations measured soon after alcohol

exposure may reflect the intracellular response to the teratogen, rather than stable programming effects of PAE on the genome. By contrast, gene expression profiling in the adult brain, long after the removal of ethanol, may provide additional insight into the long-term effects of PAE on cellular programs. Although these effects are usually subtler, long-lasting changes to the transcriptome have been identified in the whole brain in male adult mice, suggesting that PAE can have lasting effects on the neural transcriptome.

Alterations identified in the entire embryo or brain likely reflect systemic effects of ethanol on the organism or CNS, respectively, and may reflect the broader alterations of PAE on biological functions. In particular, meta-analyses of gene expression patterns across multiple studies of PAE, ranging from whole embryos on embryonic day 9 in mice to the rat hippocampus on postnatal day 100, identified a general inhibition of transcription by PAE, regardless of the model (Rogic, Wong, & Pavlidis 2016). The differentially expressed genes identified in the combined analyses were mainly involved in protein synthesis, mRNA splicing, and chromatin function, suggesting that PAE may broadly influence the regulatory systems of the cell, irrespective of the timing and dosage of alcohol exposure. More recent studies are beginning to focus on specific brain regions, providing functional insight into some of the deficits observed following PAE. For instance, gene expression patterns in the postnatal day 70 mouse hippocampus are altered by a third trimester equivalent exposure to binge levels of alcohol, which may potentially be related to some of the deficits in spatial learning and memory impairment associated with PAE (Chater-Diehl et al. 2016). A recent study also profiled gene expression patterns in human fetal cortical tissue from late first trimester fetuses with PAE (n=2) (Kawasawa et al. 2017). These embryos displayed a shift in the typical balance of splicing

isoforms in addition to widespread alterations to transcriptomic programs, suggesting that PAE may influence the fine balance of splice variants in the brain.

Taken together, these findings support that PAE can have both transient and persistent effects on the genome, which may influence the cellular response to ethanol and mediate the vulnerability to adverse long-term health outcomes. Furthermore, PAE-induced deficits may potentially arise through the disruption of epigenetic programs, concurrent with alterations to gene expression patterns.

1.7.2 PAE alters DNA methylation programs

A large number of studies have identified changes in DNA modifications in response to prenatal alcohol exposure, and the current thesis will present a snapshot of the different approaches to assess these alterations, which range from "bulk" levels to candidate gene approaches and genome-wide investigations (here, bulk levels are defined as measures of epigenetic patterns that do not delineate specific regions, but rather represent the total levels within a given tissue or cell population). The first evidence of alcohol-induced changes to DNA methylation programs was generated in a mouse model, where embryos were exposed to alcohol during gestational days (GD) 9-11. This study demonstrated that alcohol reduced bulk levels of DNA methylation in the genome, potentially by inhibiting DNA methyltransferase 1 (DNMT1) activity, and opened the door for future studies of epigenetic mechanisms in FASD (Garro et al. 1991). Several studies have extended this line of evidence by studying the effects of alcohol exposure during various stages of development and identifying alterations to bulk levels of DNA methylation in different brain regions under basal and intervention conditions (Otero et al. 2012; Perkins et al. 2013; Chen, Ozturk, & Zhou 2013; Mukhopadhyay et al. 2013; Nagre et al. 2015;

Liyanage et al. 2015; Öztürk et al. 2017). For instance, PAE throughout gestation delays the accumulation of DNA methylation in neural stem cells, and increases DNA methylation levels in the mouse hippocampus, a brain region involved in learning and memory (Chen, Ozturk, & Zhou 2013). This same study assessed bulk DNA hydroxymethylation in parallel, identifying a decrease in the neural progenitor cells of the hippocampus, which suggests widespread alterations to DNA methylation programs (Chen, Ozturk, & Zhou 2013). In addition to assessing the impact of PAE on bulk DNA methylation levels, a number of studies have used bulk DNA methylation levels as a measurable outcome for dietary or therapeutic interventions in combination with different behavioral tasks. For example, choline supplementation has been proposed as a potential intervention due to its role as a methyl donor, and has been associated with the partial rescue of behavioral alterations and increased DNA methylation levels in the hippocampus and prefrontal cortex of PAE rats (Thomas et al. 2007; Otero et al. 2012). Similar outcomes are also observed in embryos and neural stem cells treated with alcohol or 5-azacytidine, a potent inhibitor of DNA methylation, suggesting that alcohol-induced deficits are likely related to altered epigenomic profiles and functions (Zhou, Zhao, et al. 2011). These findings demonstrate that developmental alcohol exposure tends to impair the establishment of typical DNA methylation levels, which may reprogram downstream cellular and biological functions.

Proof of principle of alcohol's programming effects was further exemplified using the agouti viable (A^{vy}) yellow mouse model, which contains a DNA methylation-sensitive element within the A^{vy} locus that regulates coat color (Wolff et al. 1998). In this model, PAE increased the incidence of pseudo-agouti animals, indicating that specific loci are responsive to the effects of alcohol during development and can influence phenotypic outcomes (Kaminen-Ahola et al.

2010). As such, more recent studies have sought to identify specific gene targets of PAE-induced epigenetic effects, either through hypothesis- or discovery-driven approaches. An initial study using cultured cells showed that, rather than a global demethylation of the genome, specific regions become more methylated and others less methylated in response to alcohol exposure, suggesting that some regions may be differentially sensitive to alcohol-induced reprogramming effects (Liu et al. 2009). Numerous groups have invested in targeted analyses of epigenetic patterns in genes associated with the deficits observed in individuals with FASD (e.g. immune, stress, cognitive, and otherwise-related) (Vallés et al. 1997; Maier et al. 1999; Downing et al. 2011; Bekdash, Zhang, & Sarkar 2013; Zhang et al. 2015; Ngai et al. 2015; Marjonen et al. 2015; Liyanage et al. 2015). In mice, the expression of *Igf2*, an imprinted gene involved in growth, is decreased in the embryo and placenta following PAE, concomitant with increased DNA methylation of the differentially methylated region 1 in its promoter and growth deficits in offspring. Choline supplementation during gestation partially rescues the effects of PAE on growth and DNA methylation within this locus, further highlighting a potential role for dietary supplements in the attenuation of alcohol-induced deficits (Downing et al. 2011). PAE also results in increased DNA methylation and decreased expression of proopiomelanocortin (*POMC*) in the hypothalamus, which is a key regulator of the stress response (Bekdash, Zhang, & Sarkar 2013). *Slc6a4*, an important serotonin transporter, also displays sex-dependent alterations to DNA methylation and gene expression patterns in the hypothalamus of adult PAE rats (Ngai et al. 2015). While the hypothesis-driven approach has proven fruitful in many regards, it relies heavily on previously identified biological pathways and has not been very successful in identifying novel targets of developmental alcohol exposure.

Researchers have also used genome-wide tools to study the effects of alcohol exposure beyond classical candidate pathways (Liu et al. 2009; Hicks, Middleton, & Miller 2010; F.C. Zhou, Chen, & Love 2011; Laufer et al. 2013; Krishnamoorthy et al. 2013; Khalid et al. 2014; Chater-Diehl et al. 2016; Laufer et al. 2015; Portales-Casamar et al. 2016). For example, widespread changes in DNA methylation patterns were identified in the brains of adult male mice, with some alterations overlapping with changes in gene expression profiles (Laufer et al. 2013; Chater-Diehl et al. 2016). These findings provide evidence for the lasting effects of developmental alcohol exposure on the DNA methylome, as well as identifying novel genes associated with alcohol exposure. Moreover, these PAE-related changes in the DNA methylome may alter transcriptional profiles and reprogram physiological systems. The analysis of DNA methylation profiles in buccal epithelial cells (BECs) of children with FASD has revealed widespread alterations to the epigenome, and provided preliminary evidence of a DNA methylation "signature" of FASD (Laufer et al. 2015; Portales-Casamar et al. 2016). While the use of a peripheral tissue, buccal epithelial cells, makes it difficult to readily interpret these findings in the context of FASD-associated deficits, these studies provide important insight into potential biomarkers of PAE in human populations.

These studies highlight the widespread effects of developmental alcohol exposure on DNA methylation patterns, although the direction of change varies depending on the model of alcohol exposure, the tissue analyzed, and the specific genes assessed. While most studies of bulk DNA methylation identify a decrease in methylation levels, potentially due to lower activity of DNA methyltransferases and the inhibition of 1-carbon metabolism by alcohol, results have varied across models due to a number of factors, including differences in levels and timing of alcohol exposure, developmental stage, analyzed tissue, and analysis methods. These findings

highlight the importance of using different models to assess the molecular mechanisms underlying the effects of ethanol at different stages, doses, etc. The analysis of DNA hydroxymethylation also remains an elusive topic of research in the context of FASD, only being investigated in a two studies of PAE (Chen, Ozturk, & Zhou 2013; Öztürk et al. 2017). Given its seemingly key role in neurons, it could potentially play an important role in the etiology of FASD. As a whole, multiple lines of evidence support a role for DNA methylation in the fetal programming of biological systems by PAE and represent an important avenue for the discovery of biomarkers of FASD.

1.8 Current diagnostic tools and biomarkers of FASD

Early identification and diagnosis of FASD is crucial to mitigate the long-term deficits caused by PAE. While FAS is readily distinguishable due to its well-characterized features (facial dysmorphisms, growth retardation, and CNS alterations), the identification and diagnosis of all individuals under the umbrella of FASD has proven more difficult, as the majority do not present with any physical manifestations of the disorder (Hoyme et al. 2016; Mattson et al. 2013). A diagnosis of ARND requires confirmation of prenatal alcohol, which is not always readily available from medical records or the biological mother (Riley, Infante, & Warren 2011). However, these individuals can still have considerable neurobiological/behavioral impairments, which are often not diagnosed until they reach school age, when their deficits become more apparent in the face of increased social and cognitive pressure (Senturias & Baldonado 2014). Furthermore, behavioral and cognitive interventions may be effective at mitigating some of the deficits caused by PAE and improving long-term health in individuals with FASD (Paley & O'Connor 2011). As earlier diagnosis of FASD is associated with increased positive outcomes,

and interventions may have the greatest impact during early development, early screening tools are being developed to aid in the identification and diagnosis of children at-risk of FASD (Streissguth et al. 2004; Fox, Levitt, & Nelson III 2010).

Self-report questionnaires and observations of alcohol-induced physical and neurobehavioral alterations are currently the gold standard for the initial screening of FASD. However, these can often lead to the underestimation of alcohol consumption behavior during pregnancy (Russell et al. 1996; Jones, Bailey, & Sokol 2013; Burns, Gray, & Smith 2010). Several groups have begun to investigate alternate molecular and physiological biomarkers of PAE to supplement these methods. Many of these have focused on the direct or indirect products of ethanol metabolism, which can be measured in a number of biological specimen, including maternal blood, urine, hair, saliva, and sweat; newborn blood, urine, hair, and meconium; and the placenta (Concheiro-Guisan & Concheiro 2014; McQuire et al. 2016). For instance, fatty acid ethyl esters (FAEE) are highly associated with PAE when measured in the meconium of newborns, but their specificity is inconsistent between different cohorts and markers, potentially due to the small number of cases in each study (Bakhireva et al. 2014; Bearer et al. 2003, 1999, 2005; Kwak, Han, Choi, Ahn, Kwak, et al. 2014; Ostrea et al. 2006). A composite measure of 4 FAEEs showed high levels of diagnostic accuracy in a very small cohort, though these results have yet to be fully assessed in large independent studies (Bakhireva et al. 2014). By contrast, FAEE measures in the placenta display high sensitivity and specificity, but 30-56% false positives, while maternal-based assays of ethanol metabolism blood, urine, and hair have not yet been shown to identify PAE at both high sensitivity and specificity (Gutierrez et al. 2015; Kwak, Han, Choi, Ahn, Ryu, et al. 2014; Sarkola et al. 2000). Importantly, these methods assess *in utero* exposure to alcohol and their use is restricted to a timeframe shortly after birth, limiting

their use in later-life diagnoses (Cabarcos et al. 2015). As such, other measures have been developed in order to identify a persistent biological signature of PAE.

Eye tracking measures have also been used in a small cohort of children to distinguish children with FASD, ADHD, or typically developing controls with relatively good accuracy using several features obtained from a short testing session (Tseng et al. 2013). Furthermore, the cardiac orienting response could also potentially be used to assess the effects of PAE on infants, as it performs slightly better than the Bayley Scales of Infant Development-II at classifying children as alcohol-exposure or controls (Mesa et al. 2017). A decision tree has also been developed using neurobehavioral and physical measures to distinguish individuals affected by PAE from typically developing controls (Goh et al. 2016).

Epigenetic marks are also emerging as potential biomarkers or signatures of early-life exposures, as they may provide a link between environmental factors and genetic regulation. For example, plasma microRNA (miRNA) in alcohol-exposed pregnant mothers, either alone or in conjunction with other clinical variables, could predict infant outcomes (Balaraman et al. 2016). A combination of high variance miRNAs, smoking history, and socioeconomic status could classify infants affected by PAE versus unexposed controls. These findings suggest that maternal plasma miRNAs may predict infant outcomes, and may be useful to classify difficult-to-diagnose FASD subpopulations.

These findings suggest that molecular screening tools may prove useful in early identification of children with FASD, although they require further optimization and validation. DNA methylation is now a unique position for the development of potentially accurate and stable biomarker of prenatal alcohol exposure given its stability over time and its malleability in response to environmental influences.

1.9 Thesis overview

The overarching goal of this thesis was to test the hypothesis that that PAE alters the transcriptional profiles and DNA methylation patterns of genes that are functionally related to the deficits associated with FASD. The experimental data will be presented through four separate chapters, which will address the specific aims outlined in section 1.1. **Chapter 2**, entitled "Prenatal alcohol exposure alters steady-state and activated gene expression in the adult rat brain" is based on the previous identification of PAE-induced alterations to an AA challenge by the Weinberg lab, and seeks to identify long-term changes to gene expression patterns in the rat brain. **Chapter 3**, entitled "Prenatal alcohol exposure alters DNA methylation patterns during early development", builds on the findings from the previous chapter, assessing the programming effects of PAE on DNA methylation patterns of the rat hypothalamus and white blood cells during early postnatal development. **Chapter 4**, entitled "DNA methylation signature of human fetal alcohol spectrum disorder", takes advantage of a clinical cohort of individuals with FASD, determining whether PAE in humans can influence DNA methylation in peripheral tissues. **Chapter 5**, entitled "DNA methylation as a predictive tool for fetal alcohol spectrum disorder", follows up on the findings from the previous chapter, attempting to validate the findings in an independent cohort, while simultaneously developing a predictive algorithm for the screening of individuals with FASD. Finally, the main findings from each data chapter will be integrated alongside a discussion of limitations and future directions for these studies.

Chapter 2: Prenatal alcohol exposure alters steady-state and activated gene expression in the adult rat brain

2.1 Background and rationale

The prevalence of fetal alcohol spectrum disorders (FASD) in North America is estimated at 2-5% of live births, making prenatal alcohol exposure (PAE) a leading cause of neurodevelopmental disorders (May et al. 2009; Sampson et al. 1997). In addition to lasting neurocognitive deficits, impairments in self-regulation, and deficits in adaptive functioning, children with FASD also display changes in a number of physiological systems, including the immune system, with adverse impacts on both innate and adaptive immunity (Johnson et al. 1981; Streissguth, Clarren, & Jones 1985; Gauthier et al. 2005).

Animal models have corroborated clinical findings, with PAE animals displaying behavioural and cognitive deficits, including delays in learning and memory, and altered responsivity to stressors (Hellemans, Sliwowska, et al. 2010). Moreover, PAE animals also exhibit altered development of the thymus, decreased lymphocyte proliferative responses to mitogens, increased susceptibility to infections, and greater vulnerability to immune and inflammatory challenges compared to controls (reviewed in Bodnar & Weinberg 2013). PAE animals also show larger increases in plasma levels of pro-inflammatory cytokines, as well as reduced proliferative responses of B cells to lipopolysaccharide (LPS), and splenic T cells and T lymphoblasts to Concanavalin A and/or interleukin-2 (Zhang, Sliwowska, & Weinberg 2005; Weinberg & Jerrells 1991). Likewise, in an adjuvant-induced arthritis (AA) paradigm, PAE animals show increased severity of joint inflammation and a prolonged course of disease (39 days post-injection, higher incidence of arthritis in PAE compared pair-fed [PF] and control [C]

animals) (Zhang et al. 2012). These findings suggest that although PAE causes deficits in adaptive immunity, PAE offspring show increased responses to some immune/inflammatory challenges.

The immune, neuroendocrine and central nervous systems have extensive bidirectional communication, sharing numerous ligands and receptors. Brain regions, such as the prefrontal cortex (PFC) and hippocampus (HPC) not only play a role in the regulation of neuroendocrine function, but also respond to immune/inflammatory molecules, including cytokines and neuropeptides (Crofford et al. 1992). For example, adjuvant injection induces c-Fos expression in the hippocampus for up to 4 months, suggesting a role for this region in AA (Carter et al. 2011). Thus, long-term changes in gene expression may modulate AA manifestation and progression. Indeed, mounting evidence suggests a role for altered gene expression in the etiology of FASD (Kobor & Weinberg 2011). Widespread changes to gene expression levels in fetal and neonatal brains following PAE, as well as long-lasting alterations to the neural transcriptome following alcohol exposure during the neonatal (third-trimester equivalent) period or across all three trimesters have been reported (Green et al. 2007; Hard et al. 2005; Zhou, Zhao, et al. 2011; Kleiber et al. 2012, 2013).

Using saline-injected animals (steady-state) as a baseline, the current study examined brains from adult PAE and control females from the lab's previous AA study to determine whether long-term alterations in gene expression mediate the altered severity and course of arthritis observed in PAE females (Zhang et al. 2012). Since the PFC and HPC play key roles in both neuroendocrine and neuroimmune processes and show altered function following PAE, PAE-induced alterations in the transcriptome of these regions could result in marked downstream effects, including dysregulation of the immune response and neuroendocrine-neuroimmune

interactions (Norman et al. 2009). Whole genome microarrays were utilized to assess gene expression in the PFC and HPC of adult PAE, PF and C females terminated at the peak or during resolution of inflammation (days 16 and 39 post-adjuvant injection, respectively); cohorts of saline-injected PAE, PF and C females were terminated in parallel. Under steady-state condition, we identified changes in gene expression and altered activation states of upstream regulators specific to PAE. Furthermore, at the peak of inflammation, we found not only changes in genes related to PAE, but also, a failure of PAE animals to mount appropriate responses to the immune challenge, showing no change in the activation or inhibition of inflammation-related genes and upstream regulators identified in controls.

2.2 Materials and Methods

2.2.1 Breeding and prenatal ethanol exposure

All animal protocols were approved by the University of British Columbia Animal Care Committee and are consistent with the NIH Guide for the Care and Use of Laboratory Animals (National Research Council 2011). Details of the breeding and feeding procedures have been published (Glavas et al. 2007). Briefly, male and female Sprague-Dawley rats (Animal Care Center, University of British Columbia) were paired; presence of a vaginal plug indicated gestation day (GD) 1. Pregnant dams were singly housed and assigned to experimental groups: Prenatal ethanol exposure (PAE; *ad libitum* access to liquid ethanol diet, 36% ethanol-derived calories); Pair-fed (PF; liquid-control diet, maltose-dextrin isocalorically substituted for ethanol, in the amount consumed by a PAE partner, g/kg body weight/GD); or *Ad libitum*-fed control (C; laboratory chow, *ad libitum*). All animals had *ad libitum* access to water. Experimental diets (Weinberg/Kiever Ethanol Diet #710324, Weinberg/Kiever Control Diet #710109, Dyets Inc.,

Bethlehem, PA) were fed from GD 1-21, then replaced with laboratory chow. Litters were weighed and culled at birth to 5 males and 5 females, when possible. Following weaning (postnatal day 22), offspring were group-housed by litter and sex. Female offspring were used in the present study due to their increased susceptibility to arthritis (Whitacre 2001).

2.2.2 Induction of arthritis and termination of animals

Details of the adjuvant-induced arthritis (AA) paradigm have been published (Zhang et al. 2012). Female offspring (50-65 days of age) from C, PF, and PAE groups received an intradermal injection of 0.1 ml of a 12 mg/ml suspension of complete Freund's adjuvant (CFA) or 0.1 ml physiological saline at the base of the tail. Animals were single-housed post-injection, and monitored for clinical signs of arthritis under light anesthesia with isofluorane. Paws were scored individually for redness and swelling on days 7, 10, and every other day thereafter until day 39 following injection (Zhang et al. 2012). Animals were terminated by decapitation, following brief exposure to CO_2, in two cohorts: day 16 post-injection or day 39 post-injection (peak or resolution phase of AA, respectively). Each cohort contained 9 adjuvant-injected animals and 5 saline-injected animals for each group (C, PF, and PAE). Brains were rapidly removed, immediately frozen on dry ice, and stored at -70 °C.

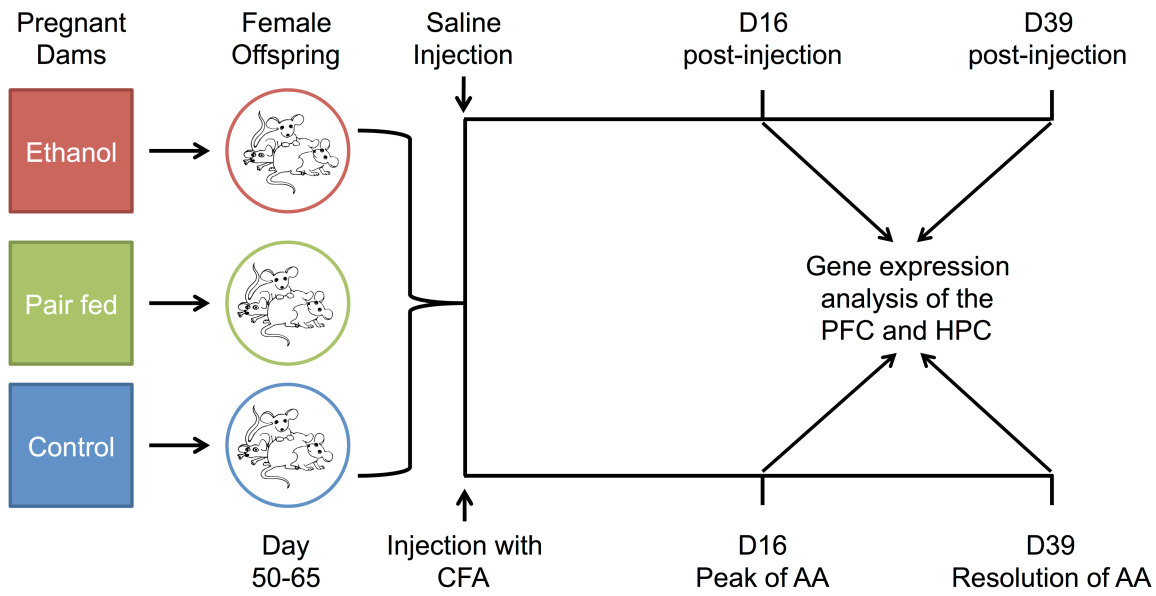

Figure 2.1 Overview of the experimental design prior to sample collection and microarray analysis

Adult female rats from one of three prenatal treatment groups, control (C), pair-fed (PF), and prenatal alcohol exposure (PAE), were injected with complete Freund's adjuvant (CFA) to cause adjuvant-induced arthritis (AA). Animals were terminated 16 or 39 days post-injection and microarray analysis of gene expression was performed on the prefrontal cortex (PFC) and hippocampus (HPC).

2.2.3 Tissue dissection and RNA extraction

Brains were thawed to 4 °C, and the PFC and HPC were dissected, placed in RNAlater, and stored at -20 °C. Total RNA and DNA were simultaneously extracted from the tissues (Qiagen AllPrep DNA/RNA Mini kit). RNA integrity was determined using the Agilent BioAnalyzer mRNA Nano assay.

2.2.4 Microarray assay of whole genome gene expression and quality control

The Ambion Illumina TotalPrep RNA Amplification kit was used to generate cRNA (750 ng) from total RNA (250 ng) for each sample. Expression data were obtained using the Illumina

RatRef-12 Expression BeadChip microarray with the Illumina iScan, which provides probe-level data for all expressed genes (~ 1 probe per gene). Datasets were filtered to remove control probes and probes with a detection p-value >0.05 in comparison to negative control probes. After filtering, 20215 and 20069 probes remained in the PFC and HPC, respectively (out of a total 23350 probes). The filtered, log2-transformed gene expression profiles were quantile-normalized within each tissue.

2.2.5 Differential gene expression analysis

Gene expression analysis utilized the *sva* and *limma* packages in the statistical program R (Smyth 2005). Using *sva*, surrogate variables representative of heterogeneity from sources other than experimental treatments (e.g. batch effects) were generated. These were included in linear modeling of gene expression with *limma*, which uses moderated F- and t-statistics to identify significant differences. Gene expression changes were modeled in two ways using separate sample means: effects of prenatal treatment alone on steady state levels of gene expression (saline-injected animals, n=5 per C, PF, PAE group), and interaction of prenatal treatment with an inflammatory challenge (adjuvant- versus saline-injected animals; n=5 for saline, n=9 for adjuvant per C, PF, PAE group). Each probe received a moderated F-statistic, and their p-values were corrected for multiple testing using Benjamini-Hochberg correction. The false-discovery rate (FDR) was controlled at <25% due to the moderate alcohol-exposure paradigm and its relatively subtle effects. Significant changes in PAE compared to controls had a moderated t-statistic p-value <0.05. Sequences for significant probes were queried against the RefSeq database for *Rattus norvegicus* to identify target transcripts.

2.2.6 Verification of microarray results

Differentially expressed genes were verified using reverse-transcription quantitative real time PCR (RT-qPCR) on the Corbett Rotorgene 6000 for both PFC and HPC, with the same RNA used for microarray analysis (n=4 in both tissues for each C, PF, and PAE). Primers were designed using well-established guidelines to obtain gene-level data and multiple reference genes were used to normalize expression data (Nolan, Hands, & Bustin 2006). Three reference genes across a spectrum of expression levels and no evidence for differences across groups (F-statistic p-value >0.05) were selected for each tissue (Supplementary table 2.4). The normalization factor for each sample was calculated using the geometric mean of cycle threshold (Ct) values (Vandesompele et al. 2002). Expression levels relative to the factor were determined, and analysis of variance (ANOVA) was conducted to test for significant differences between groups (Schmittgen & Livak 2008).

2.2.7 Gene Ontology and Pathway analysis

Gene ontology (GO) analysis was conducted to identify "Biological Processes" enriched for the effects of prenatal treatment and adjuvant exposure using the gene-score resampling (GSR) method in ermineJ (Lee et al. 2005). The set of candidate FASD genes from the curated Neurocarta database was included in the analysis as a custom GO term (Portales-Casamar et al. 2013) (Supplementary table 2.1). Benjamini-Hochberg correction was used with an FDR of 1% within single brain regions to identify more robust functional enrichment categories. By contrast, a 10% cutoff was used when comparing overlapping effects between brain regions to a broader picture of the effects of PAE on the brain's transcriptome. Where many GO categories were identified, these were mapped to their parent GO Slim terms using CateGOrizer to determine

common categories of altered function (Hu, Bao, & Reecy 2008). Following GO analysis, the Ingenuity© Upstream Regulator Analysis tool (URA, Ingenuity Systems Inc., Redwood City, CA) was used to predict master transcriptional regulators that explain the observed expression changes within the dataset. Genes with a fold-change ≥ 1.2 and $p < 0.05$ between treatments were analyzed for effects of PAE and adjuvant injection. For steady-state effects of PAE, prenatal groups were compared, while adjuvant effects were assessed by comparing adjuvant- to saline-injected animals in each prenatal group. Significantly activated and inhibited genes were identified through a Z-score > 2 or < -2 respectively, as well as an overlap p-value ≤ 0.1, calculated by Fisher's Exact test.

2.3 Results

2.3.1 Developmental Data

As expected, body weights of PAE dams were lower than those of controls ($p<0.001$) by the end of pregnancy (GD21) [Group x Day interaction, $F(6,99)=17.2$, $p<0.0001$], with PF dams intermediate to PAE and C; dams no longer differed in weight by lactation day 8. At birth, PAE (5.7± 0.17 g) females weighed less than their C (6.5± 0.18 g) counterparts (main effect of group, $F(2,66)=7.02$, $p<0.01$), which persisted until weaning (PAE, 51.2±1.4 g; PF, 55.3±1.6 g; C, 55.2±1.5 g) (group x day, $F(6,99)=1.96$, $p=0.079$). Blood ethanol levels for dams in this paradigm typically average ~100-150 mg/dl (Uban et al. 2010; Lan et al. 2006).

2.3.2 Prenatal ethanol exposure altered steady-state levels of gene expression in the PFC and HPC

PAE effects on steady-state levels of gene expression were examined in saline-injected females on Days 16 and 39 post-injection (~ PND 75 and 95, respectively). On Day 16, p-value distributions were skewed towards zero for contrasts of PAE vs C and PAE vs PF, suggesting gene expression differences in PAE compared to C and PF females (Supplementary figure 2.1). Following Benjamini-Hochberg correction, significant effects of prenatal treatment were found for 80 and 30 genes in the PFC and HPC, respectively, at 25% FDR (Figure 2.2). While many genes (43% in PFC, 37% in HPC) showed significant effects of ethanol exposure against both control groups, only a subset (15 in PFC, 4 in HPC; $p < 0.05$) showed changes specific to PAE, in that levels were similar between C and PF animals (Tables 1.1, 1.2; Figure 2.3). These had a number of annotated functions in common, including neurodevelopment, differentiation, neuronal signaling, and regulation of cell death and transcription.

By contrast, on day 39 post-injection, no relationship between gene expression and PAE was apparent in either brain region, according to p-value distributions (Supplementary figure 2.1). Moreover, only 2 probes met a 25% FDR, but were not specific to PAE effects (data not shown). Thus, subsequent analyses focused on brains from Day 16 post-injection.

Gene Symbol	Gene Name	Average Expression	F	p-value	q-value	Fold change		
						EvC	EvPF	PFvC
H2afv	Rattus norvegicus similar to H2A histone family, member V isoform 1 (LOC685909)	10.6	18.7	4.8E-05	0.11	**0.65**	**0.76**	0.86
Tcf4	transcription factor 4	11.2	11.4	7.0E-04	0.23	**0.67**	**0.66**	1.01
Rnasek	ribonuclease, RNase K	13.2	11.1	8.0E-04	0.23	**0.68**	**0.57**	1.19
Ppp1r14a	protein phosphatase 1, regulatory (inhibitor) subunit 14A	10.0	12.6	4.1E-04	0.23	**0.68**	**0.64**	1.05
Rps8	ribosomal protein S8	13.0	11.1	7.9E-04	0.23	**0.69**	**0.74**	0.93
ILMN_1372701	na	9.4	11.3	7.3E-04	0.23	**0.71**	**0.79**	0.90
ILMN_1374168	na	9.1	10.7	9.4E-04	0.25	**0.77**	**0.73**	1.05
Pex11g	peroxisomal biogenesis factor 11 gamma	7.0	11.5	6.7E-04	0.23	**0.82**	**0.71**	1.16
Ndfip1	Nedd4 family interacting protein 1	11.4	12.1	5.1E-04	0.23	**1.32**	**1.37**	0.97
Acsl3	acyl-CoA synthetase long-chain family member 3	10.2	12.2	4.9E-04	0.23	**1.36**	**1.36**	1.00
Dusp6	dual specificity phosphatase 6	9.9	12.5	4.4E-04	0.23	**1.41**	**1.21**	1.17
Rpl7	ribosomal protein L7	11.6	13.7	2.7E-04	0.22	**1.44**	**1.36**	1.05
Med28	mediator complex subunit 28	9.2	11.1	7.9E-04	0.23	**1.48**	**1.29**	1.15
Atp6ap1	ATPase, H+ transporting, lysosomal accessory protein 1	11.0	10.6	9.8E-04	0.25	**1.50**	**1.35**	1.11
Ap1s2	adaptor-related protein complex 1, sigma 2 subunit	9.7	12.4	4.6E-04	0.23	**1.60**	**1.35**	1.19

Table 2.1 Differentially expressed genes in the prefrontal cortex under steady-state conditions

Genes with a significantly expression under steady-state conditions in PAE compared to both C and PF animals (p <0.05) in the PFC (a) and HPC (b) at D16 post-saline injection. Bold = p <0.05. na = probe had no specific alignment to RefSeq RNA database.

Gene Symbol	Gene Name	Average Expression	F	p-value	q-value	Fold change		
						EvC	EvPF	PFvC
Cnih2	cornichon homolog 2 (Drosophila)	11.1	16.0	8.1E-05	0.14	**0.61**	**0.60**	1.01
Caap1	caspase activity and apoptosis inhibitor 1	9.2	15.2	1.1E-04	0.14	**0.68**	**0.71**	0.95
LOC688637	similar to WD repeat domain 36	8.8	15.4	1.0E-04	0.14	**1.46**	**1.36**	1.08
Rgs3	regulator of G-protein signaling 3	9.1	14.6	1.4E-04	0.15	**1.71**	**1.83**	0.93

Table 2.2 Differentially expressed genes in the hippocampus under steady-state conditions

Genes with a significantly expression under steady-state conditions in PAE compared to both C and PF animals (p <0.05) in the PFC (a) and HPC (b) at D16 post-saline injection. Bold = p <0.05. na = probe had no specific alignment to RefSeq RNA database.

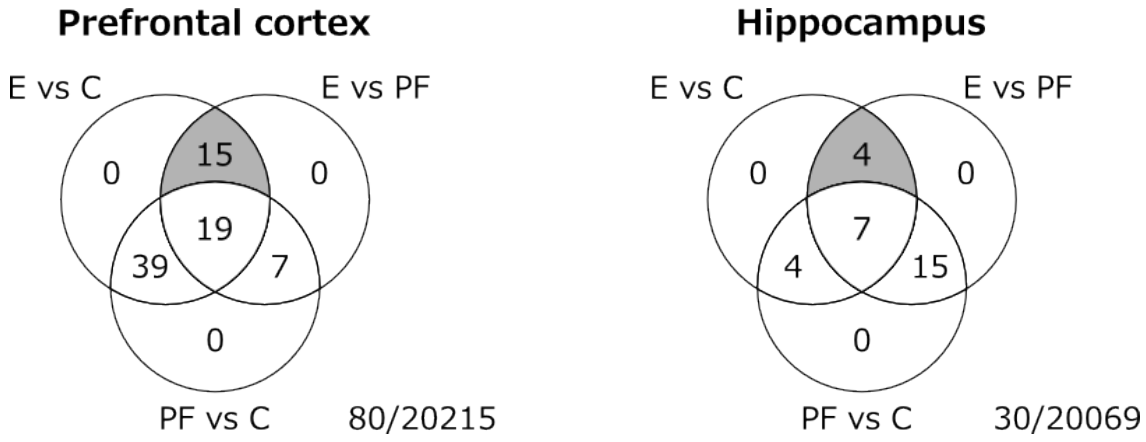

Figure 2.2 Prenatal treatment alters gene expression patterns under steady-state conditions.

Venn diagram of the number of the number of probes significantly altered in each contrast at Day 16 post-saline injection, with moderated F-statistic q <0.25 and moderated t-statistic p <0.05 (80 in the PFC, 30 in the HPC). The number of probes with unique effects in PAE versus both PF and C animals are highlighted in grey, and listed in Table 1. The center of each Venn diagram shows the number of probes differentially expressed among all three

prenatal treatment groups. The intersection on the left of each diagram shows the number of probes with a common effect of prenatal ethanol exposure and pair-feeding. The intersection on the right of each diagram shows the number of probes with a unique effect of pair-feeding.

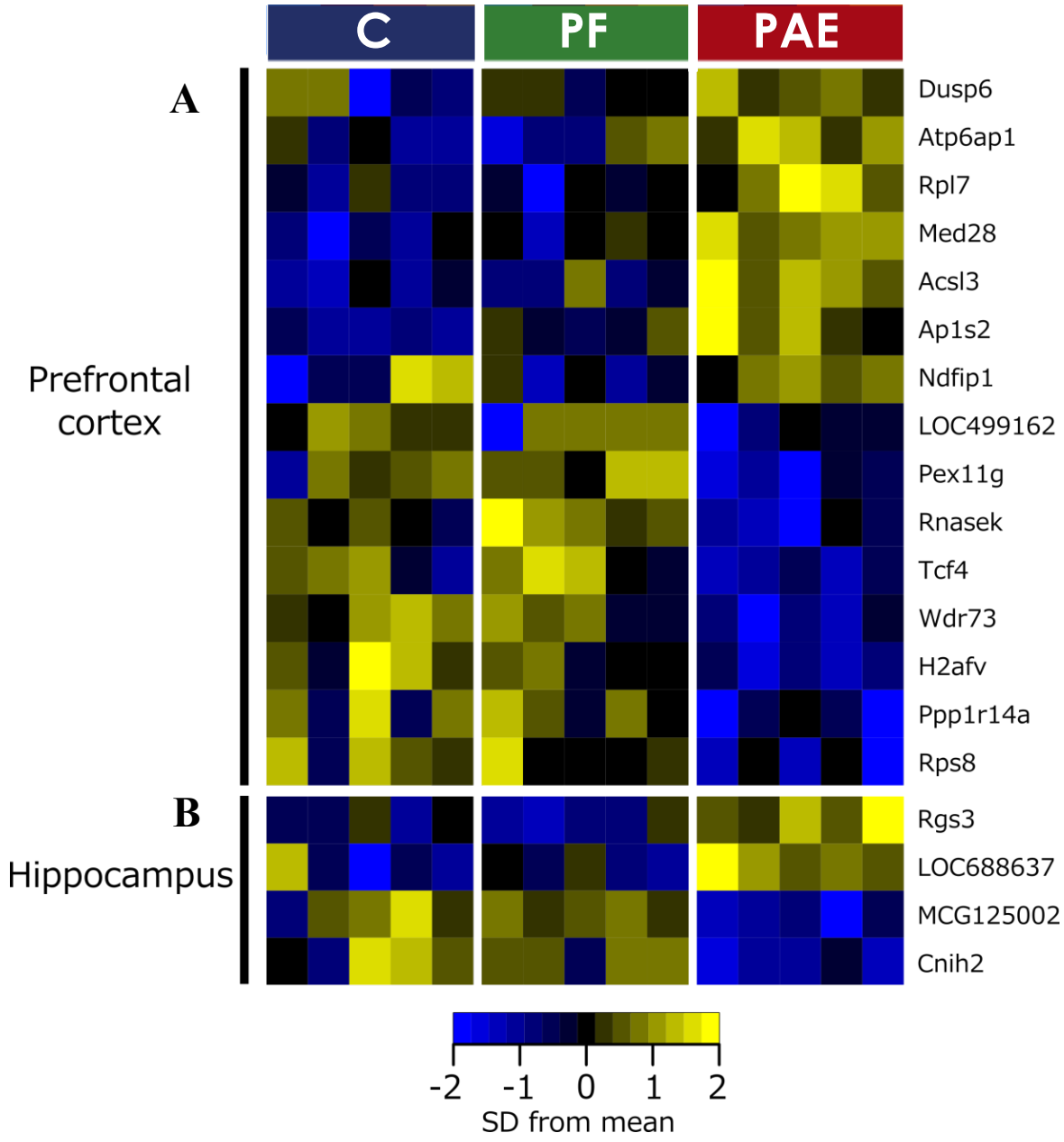

Figure 2.3 Prenatal alcohol exposure alters steady-state gene expression at Day 16 post-saline injection.

In the prefrontal cortex (a), 15 genes were differentially expressed in response to ethanol. In the hippocampus (b), 4 genes were differentially expressed in response to ethanol. F-statistic q-value <0.25 for all genes identified.

2.3.3 Verification of results related to prenatal ethanol exposure with RT-qPCR

Of 19 probes showing differential expression due to PAE (Tables 2.1, 2.2), 17 aligned to a sequence in the *Rattus norvegicus* RefSeq database (*ILMN_1372701* and *ILMN_1374168* were the exceptions). Specific RT-qPCR primers were successfully designed for 15 of the 17 genes (Supplementary table 2.3; *Rps8* and *Rpl7* were not analyzed).

Despite differences with microarray technology, RT-qPCR verified the differential expression of 2/11 genes in the PFC (*Ap1s2*, *Dusp6*) and 1/4 genes in the HPC (*Rgs3*), all of which showed increased expression ($p < 0.1$; Figure 2.4a). Moreover, for 7 significantly up-regulated genes in the microarray, changes trended in the same direction by RT-qPCR (Figure 2.4b). No down-regulated genes from microarray analysis showed significantly differences in PAE animals by RT-qPCR, but one gene (*Cnih2*) also trended downward. Importantly, positive correlation between microarray and RT-qPCR data was obtained for PAE effects ($r^2=0.35$, $p<0.02$ Figure 2.4b), and significant genes were corroborated by the small differences between methods shown in the Bland-Altman plot (Figure 2.4c). No correlation was found for PF animals (Supplementary figure 2.4). Collectively, the general agreement between qPCR and microarray data suggested that PAE caused persistent alterations to gene expression in the PFC and HPC.

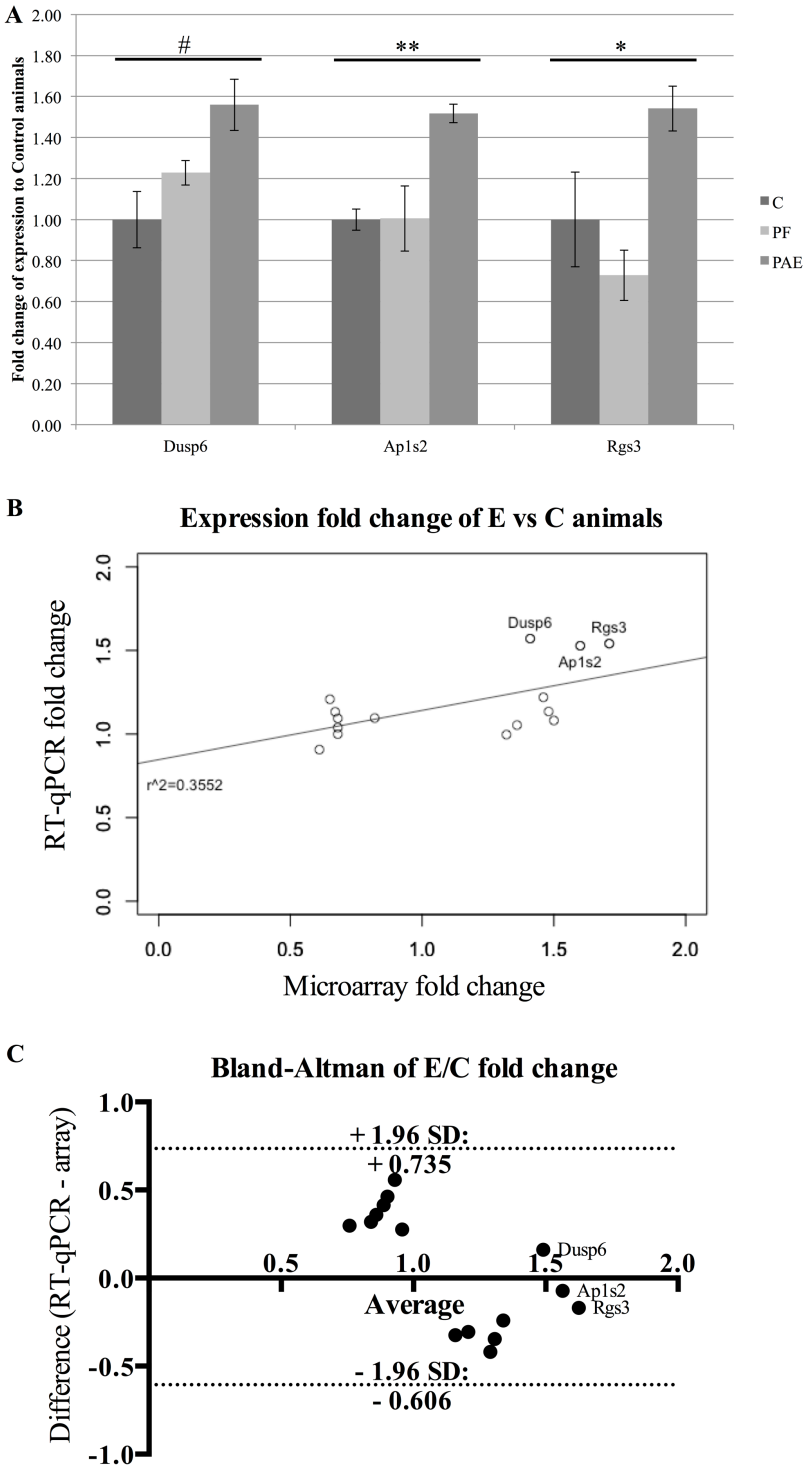

Figure 2.4 RT-qPCR verification of genes altered by prenatal alcohol exposure.

(a) Three genes were significantly upregulated in PAE animals (*Dusp6* and *Ap1s2* in PFC; *Rgs3* in HPC). Graphs were plotted as fold change to control animals (where C animals expression = 1) ± SEM. ** = $p<0.01$, * = $p<0.05$, #

= $p<0.1$. (b) Fold-changes in expression were positively correlated between microarray and RT-qPCR results for E vs C animals ($r^2=0.3552$, $p<0.02$). Annotated data points represent genes identified as significant in both methods. (c) Bland-Altman plot of genes identified by microarray analysis. Dotted lines represent the 95% limits of agreement (Bias = 0.06467) and annotated data points represent genes identified as significant in both methods.

2.3.4 Gene Ontology and Upstream Regulator Analysis of PAE effects under steady-state conditions

GO analysis was performed to ascertain the broad functional impact of PAE-induced changes in gene expression. Following multiple test correction, 6 processes were altered in the PFC of PAE compared to PF and C animals at a 1% FDR (Supplementary figure 2.2A): positive regulation of cell projection organization, chemical/ion homeostasis, response to virus, and regulation of intracellular transport. In the HPC, gene-score resampling (GSR) identified 79 processes specific to PAE, which were involved in metabolism (24%), cell communication (18%), development (18%), transport (15%), and signal transduction (10%) (Supplementary figure 2.2A). At a 10% FDR, several PAE-specific biological processes overlapped between brain regions: positive regulation of neuron differentiation, dorsal/ventral pattern formation, circadian rhythm, regulation of lymphocyte differentiation, and regulation of lipase activity (Supplementary figure 2.2B). Moreover, GSR also identified the NeuroCarta candidate gene list for FASD in the PFC of PAE females (Portales-Casamar et al. 2013).

As noted, gene sets were then analyzed using Ingenuity's Upstream Regulator Analysis (URA) to predict master regulators driving the observed expression changes within the dataset. In the PFC, a significant activation of *Gast* and an activation of *Lep* that approached statistical

significance were identified in PAE compared to PF and C animals (Table 2.3), whereas in the HPC, significant differential activation of *Laminin* and *Ifng* was observed (Table 2.4).

Gene Symbol	Gene Name	Predicted status	Z-score			Overlap p-value		
			EvC	EvPF	PFvC	EvC	EvPF	PFvC
Gast	Gastrin	Activated	**2.1**	**2.2**	NA	**0.05**	**0.009**	1.00
Lep	Leptin	Activated	**2.5**	**2.6**	NA	0.12	**0.04**	1.00

Table 2.3 Upstream Regulator Analysis in the PFC of animals under steady-state conditions

Genes identified using Ingenuity Pathway Analysis Upstream Regulator in the PFC of steady-state animals. Genes with a Z-score ≥2 or ≤-2 and an overlap p-value ≤0.1 are considered significant (bold). Those with no overlap had a p-value of 1 and no Z-score (NA).

Gene Symbol	Gene Name	Predicted status	Z-score			Overlap p-value		
			EvC	EvPF	PFvC	EvC	EvPF	PFvC
Ifng	Interferon-gamma	Activated	**3.8**	**2.5**	NA	**0.05**	**0.04**	1.00
Laminin	Laminin	Activated	**2.0**	**2.0**	NA	**0.01**	**0.04**	1.00

Table 2.4 Upstream Regulator Analysis in the HPC of animals under steady-state conditions

Genes identified using Ingenuity Pathway Analysis Upstream Regulator in the HPC of steady-state animals. Genes with a Z-score ≥2 or ≤-2 and an overlap p-value ≤0.1 are considered significant (bold). Those with no overlap had a p-value of 1 and no Z-score (NA).

2.3.5 Prenatal treatments resulted in common, graded, and differential effects under steady state conditions

A number of prenatal group effects not specific to PAE were observed in the microarray analysis (Figure 2.2). Of the probes affected by prenatal treatment, many showed the same levels of expression in PAE and PF compared to C animals (Supplementary table 2.5), while a handful

were altered in opposite directions by ethanol exposure and pair-feeding (Supplementary table 2.6). Conversely, several genes exhibited graded effects of prenatal treatment, with effects of ethanol greater than those of pair-feeding (PAE>PF>C), or vice versa (PF>PAE>C) (Supplementary table 2.6). Pair-feeding also had some unique effects, particularly in the HPC (Supplementary table 2.7), on genes involved in small molecule metabolism, transport, signal transduction, and stress responses. At a 10% FDR, GSR identified two PF-related processes overlapping between the PFC and HPC: negative regulation of neuron projection development and positive regulation of epithelial cell migration (Supplementary figure 2.2C). Moreover, the curated list of candidate FASD genes from NeuroCarta was also identified in the HPC of the PF group (Portales-Casamar et al. 2013).

2.3.6 PAE altered neural gene expression in response to an inflammatory challenge

Consistent with the findings on steady state gene expression, the greatest effects of immune challenge were observed on Day 16 post-injection (peak of inflammation). The dominant neural response to adjuvant across prenatal treatments was an up-regulation of mRNA levels. However, some genes (8 in PFC, and 4 in HPC) were differentially expressed in PAE compared to PF and C animals (Tables 2.5 and 2.6; Figure 1.5). For all hippocampal genes identified, C and PF animals showed a significant up-regulation of expression, while PAE animals showed no change in expression levels between the saline and adjuvant conditions (Figure 1.6). These genes (*Ctgf*, *Lcn2*, *Sgk*, *Vwf*) were multifunctional, with roles in growth, proliferation, adhesion, structural organization, and cellular response to immunological or stressful stimuli.

Gene Symbol	Gene Name	Average Expression	F	p-value	q-value	Fold change (Adjuvant/Saline)		
						C	PF	E
ILMN_1351665	na	7.0	7.9	3.4E-04	0.17	**0.80**	**0.80**	1.12
Ghrhr	growth hormone releasing hormone receptor	7.0	8.2	2.5E-04	0.14	0.87	**0.78**	**1.23**
ILMN_1354124	na	6.9	7.1	7.0E-04	0.24	0.94	0.99	**1.34**
ILMN_1364624	na	8.4	7.2	6.3E-04	0.24	1.22	1.06	**0.51**
ILMN_1372588	na	11.1	8.7	1.7E-04	0.13	**1.38**	1.10	**0.67**
ILMN_1351971	na	11.9	9.8	6.5E-05	0.08	**1.40**	**1.23**	**0.71**
Flna	filamin A, alpha	8.6	7.1	7.1E-04	0.24	**1.33**	**1.27**	0.99
Bhlhe40	basic helix-loop-helix family, member e40	9.5	8.1	2.8E-04	0.15	**1.42**	**1.45**	1.02

Table 2.5 Genes differentially expressed in PFC of Ethanol-exposed animals in response to adjuvant.

Genes with a significantly different response to Adjuvant in E compared to both C and PF animals ($p < 0.05$) in the PFC at the peak of inflammation (D16). Bold = $p < 0.05$. na = probe had no specific alignment to current RefSeq RNA database.

Gene Symbol	Gene Name	Average Expression	F	p-value	q-value	Fold change (Adjuvant/Saline)		
						C	PF	E
Sgk1	serum/glucocorticoid regulated kinase 1	11.4	9.1	1.1E-04	0.18	**1.63**	**1.67**	1.01
Vwf	von Willebrand factor	8.9	15.6	7.3E-07	0.00	**1.76**	**1.70**	1.06
Lcn2	lipocalin 2	7.4	18.6	1.1E-07	0.00	**1.55**	**1.92**	1.03
Ctgf	connective tissue growth factor	10.4	11.4	1.6E-05	0.05	**1.77**	**2.14**	0.85

Table 2.6 Genes differentially expressed in HPC of Ethanol-exposed animals in response to adjuvant.

Genes with a significantly different response to Adjuvant in E compared to both C and PF animals ($p < 0.05$) in the HPC at the peak of inflammation (D16). Bold = $p < 0.05$. na = probe had no specific alignment to current RefSeq RNA database.

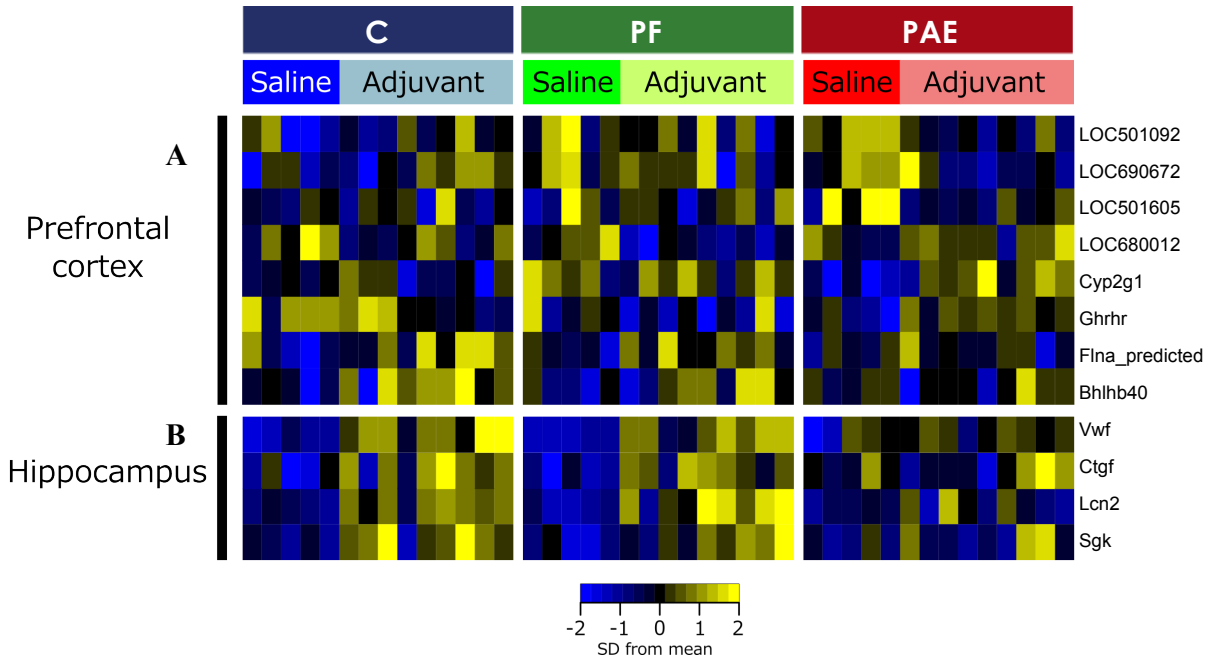

Figure 2.5 Adjuvant exposure alters gene expression at Day 16 post-injection.

8 genes showed significant changes in expression among treatment groups in prefrontal cortex (a). 4 genes demonstrated significant changes among treatment groups in the hippocampus (b). F-statistic q-value <0.25 for all genes identified.

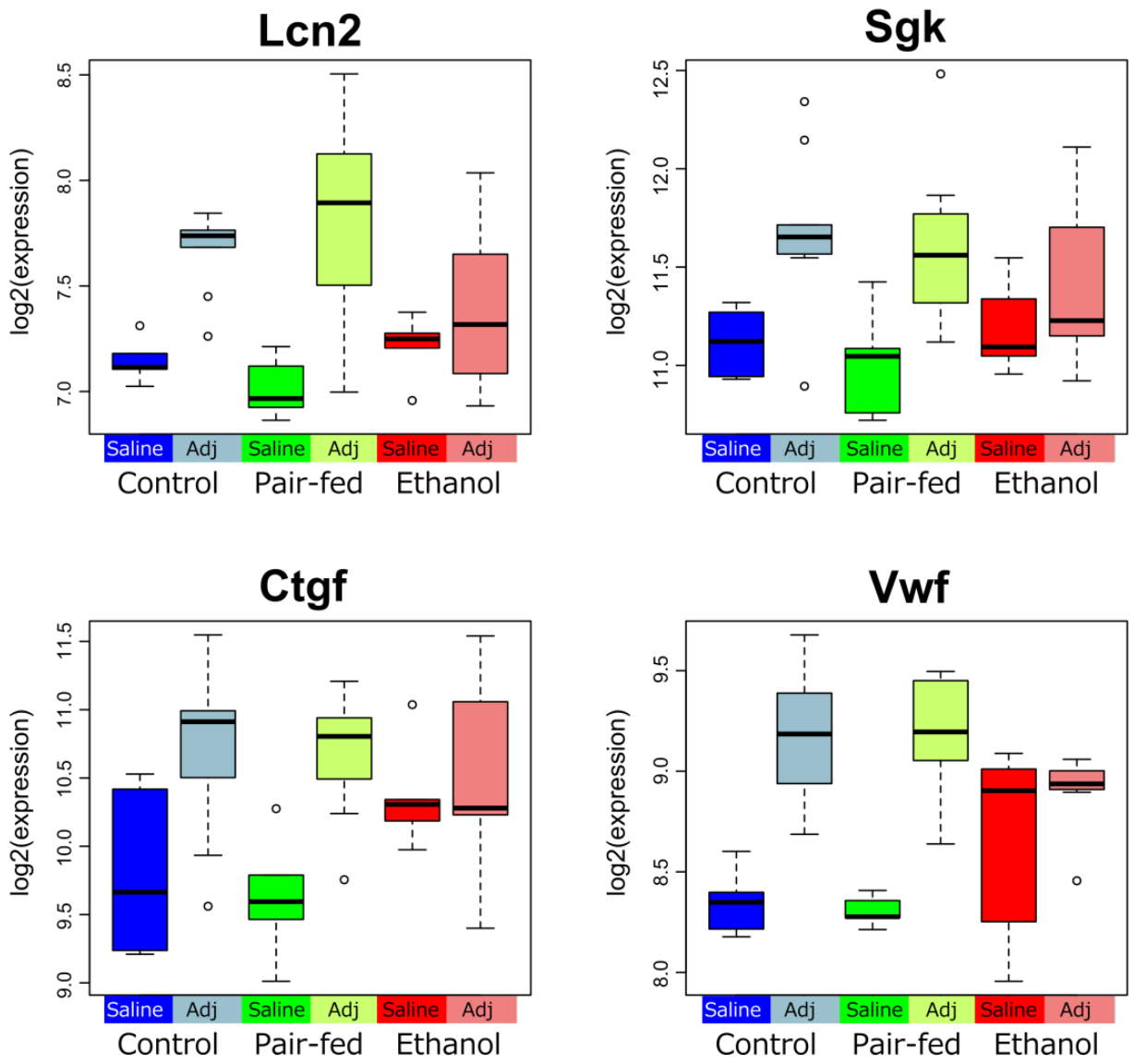

Figure 2.6 Ethanol-exposed animals show altered response to adjuvant.

In a subset of genes, Ethanol-exposed animals showed no response to Adjuvant, although pair-fed and control animals responded with an upregulation of the gene (*Lcn2*, *Sgk*). In others, gene expression levels in ethanol animals were already elevated compared to pair-feds and controls, but did not change in response to the extent of their control counterparts (*Ctgf*, *Vwf*).

2.3.7 Gene Ontology and Upstream Regulator Analysis of PAE effects in response to adjuvant

GSR identified numerous biological processes altered in response to adjuvant at a 1% FDR. In both the PFC and HPC, PAE animals had the fewest uniquely altered categories (8% in PFC, and 11% in HPC), while C animals had the most (25% in PFC and 30% in HPC) (Supplementary figure 2.3A). Four PAE-specific processes overlapped between brain regions (Supplementary figure 2.3B): regulation and positive regulation of epithelial cell proliferation, cellular protein complex assembly, and regulation of hormone level. In categories identified only in PF and C (normal response to adjuvant exposure), 6 overlapped between the PFC and HPC: response to organic nitrogen, actin filament-based process, actin cytoskeleton organization, regulation of cell morphogenesis, developmental growth, and mRNA metabolic process (Supplementary figure 2.3C).

Moreover, URA of gene sets for both the PFC and HPC predicted several master regulators of PAE-specific response to adjuvant, as well as some present only in PF and C animals. In the PFC, 2 PAE-specific genes (*Fn1*, *Dicer1*) and 4 PF/C-specific genes (*Agt*, *Foxo3*, *P38 Mapk*, *Osm*) were significantly activated, while a single PAE-specific gene, *Calmodulin*, was significantly inhibited (Table 2.7). In the HPC, 2 PAE-specific genes (*Adcyap1*, *Prl*) showed significant inhibition and one, *Nr1i3*, showed marginally significant activation (Table 2.8). As well, PF/C-specific effects were found for *Adamts12* (inhibited) and *Foxo4* (activated). Of note, *Foxo3* approached significance in the HPC of PF and C animals, representing the only overlap between brain regions.

Gene Symbol	Gene Name	Predicted status	Z-score			Overlap p-value		
			C	PF	E	C	PF	E
PAE-specific								
Calmodulin	Calmodulin	Inhibited	NA	0.4	**-2.0**	1.00	0.02	**0.02**
Dicer1	Dicer 1, ribonuclease type III	Activated	NA	NA	**2.0**	1.00	1.00	**0.09**
Fn1	Fibronectin 1	Activated	1.3	1.1	**2.1**	0.03	0.0002	**0.03**
NON-PAE								
Agt	Angiotensinogen	Activated	**2.5**	**2.2**	NA	**0.02**	**0.002**	1.00
Foxo3	Forkhead box O3	Activated	**2.3**	**3.1**	0.2	**0.02**	**0.002**	1.00
Osm	Oncostatin M	Activated	**2.9**	**2.7**	NA	**0.1**	**0.07**	1.00
P38 Mapk	p38 mitogen-activated protein kinase	Activated	**2.0**	**3.2**	NA	**0.04**	**0.005**	1.00

Table 2.7 Upstream Regulator Analysis of the PFC in adjuvant VS saline animals

Genes identified using Ingenuity Pathway Analysis Upstream Regulator in the PFC of adjuvant versus control animals. Genes with a Z-score ≥2 or ≤-2 and an overlap p-value ≤0.1 are considered significant (bold). Those with no overlap had a p-value of 1 and no Z-score (NA).

Gene Symbol	Gene Name	Predicted status	Z-score			Overlap p-value		
			C	PF	E	C	PF	E
PAE-specific								
Adcyap1	Adenylate cyclase activating polypeptide 1	Inhibited	NA	NA	**-2.2**	1.00	1.00	**0.09**
Nr1i3	Nuclear receptor subfamily 1, group I, member 3	Activated	NA	NA	**2.2**	1.00	1.00	0.12
Prl	Prolactin	Inhibited	2.3	NA	**-2.0**	0.24	1.00	**0.05**
NON-PAE								
Adamts12	ADAM metallopeptidase with thrombospondin type 1 motif, 12	Inhibited	**-2.4**	**-2.0**	NA	**0.0003**	**0.001**	1.00
Foxo4	Forkhead box O4	Activated	**2.0**	**2.0**	NA	**0.07**	**0.04**	1.00
Foxo3	Forkhead box O3	Activated	**2.6**	**2.6**	NA	0.13	0.13	1.00

Table 2.8 Upstream Regulator Analysis of the HPC in adjuvant VS saline animals

Genes identified using Ingenuity Pathway Analysis Upstream Regulator in the HPC of adjuvant versus control animals. Genes with a Z-score ≥2 or ≤-2 and an overlap p-value ≤0.1 are considered significant (bold). Those with no overlap had a p-value of 1 and no Z-score (NA).

2.4 Discussion

Prenatal ethanol exposure altered patterns of neural gene expression under both steady-state and immune challenge conditions. In saline-injected females, we identified PAE-induced changes in the expression of *Rgs3*, *Dusp6*, and *Ap1s2*, as well as activation of upstream regulators involved in metabolism and immune function. At the peak of inflammation, adjuvant injection caused PAE-specific changes in gene expression, and uncovered a failure to mount appropriate responses to inflammatory challenge in PAE animal, as evidenced by the absence of changes in inflammation-related genes and upstream regulators identified in controls.

2.4.1 Prenatal ethanol exposure altered neural gene expression under steady-state conditions

Microarray analysis identified unique effects of PAE on 15 and 4 genes in the PFC and HPC, respectively. These had roles in neurodevelopment, cell death, differentiation, transcriptional regulation, and neuronal signaling. Using RT-qPCR, we successfully verified the significant up-regulation of *Dusp6* and *Ap1s2* in the PFC, as well as *Rgs3* in the HPC. Furthermore, the majority of genes not verified by RT-qPCR trended in the same direction as the microarray. The discrepancy in technical verification may arise from the different methods of measurement between the technologies and the underpowered analysis resulting from a relatively low number of samples. Additional large-scale experiments will be required to fully validate these results at the biological level.

It is tempting to speculate that these genes play important roles in the cognitive and behavioural deficits observed in FASD. *Ap1s2* is involved in neurodevelopment and associated with intellectual disability and autism spectrum disorder, while *Dusp6* promotes apoptosis and is

linked to bipolar disorder (Borck et al. 2008; Kim et al. 2012). Activation of *Laminin* could also be involved in the altered neuronal migration patterns observed in PAE brains (Ozer, Sarioglu, & Gure 2000). Moreover, inappropriate feeding behaviour in children with FASD, as well as altered glucose metabolism and insulin tolerance in PAE animals have been reported (Werts et al. 2014; Harper et al. 2014). As *Rgs3* negatively regulates glucose output via cAMP production in hepatic cells, it may also play a role in altered energy metabolism within the brain when combined with the activation of gastrin and leptin in the PFC (Raab et al. 2005). Furthermore, the activation of interferon- γ in the HPC supports a role for this cytokine in the altered immune system activity and response to challenge in PAE offspring.

Previous studies on fetal and neonatal brains have uncovered ethanol-induced alterations in the expression of genes related to energy metabolism, adhesion, cytoskeletal remodeling, cell cycle, proliferation, differentiation, apoptosis, as well as neuronal growth and survival (Green et al. 2007; Hard et al. 2005; Zhou, Zhao, et al. 2011). Long-term PAE studies in brains of adult male mice identified networks related to cellular development, free radical scavenging, and small molecule metabolism, as well as genes involved in cognitive function, anxiety, ADHD, and mood disorders (Kleiber et al. 2012, 2013). Interestingly, none of the genes found here directly overlapped with those previously identified. These disparities are likely due to species- and sex-specific effects, differences between exposure paradigms, and different gene expression patterns in whole brains versus specific regions. As such, these discrepancies highlight the importance of examining both sexes and targeted brain regions to gain deeper insight into PAE effects. It is also possible that immediate changes in gene expression in response to PAE may not persist or that environmental influences cause alterations over the course of development. Moreover, the relatively moderate levels of ethanol exposure (BALs ~120-150 mg/dl) in this paradigm are

consistent with those reported for children with FASD who show functional and cognitive deficits (Mattson, Crocker, & Nguyen 2011). Perhaps most importantly, the genes identified here have not previously been examined in gene expression studies, suggesting that we have uncovered novel candidates for the effects of PAE in females. Whether our specific changes are mediated through epigenetic mechanisms remains to be investigated (Kobor & Weinberg 2011).

2.4.2 Prenatal ethanol exposure altered the gene expression response to adjuvant

PAE-specific responses to adjuvant were found for 8 and 4 genes in the PFC and HPC, respectively. These had roles in growth, proliferation, adhesion, structural organization, and cellular response to immunological or stressful stimuli. Across all prenatal treatments, adjuvant caused a global increase in gene expression compared to saline-injected animals. Importantly, PAE animals failed to exhibit the up-regulation in expression observed in controls for genes related to immune and cellular responses to stressful stimuli (*Ctgf*, *Lcn2*, *Sgk*, *Vwf*). Up-regulation of immune-related genes normally occurs in the CNS in response to peripheral inflammatory stimuli or neuroinflammation, which occurs in AA (Ousman & Kubes 2012; X. Liu et al. 2012). PAE animals may fail to detect these immune changes and/or launch the appropriate neuroendocrine/neuroimmune response, which could contribute to the prolonged inflammation observed in our previous AA study (Zhang et al. 2012). Consistent with this finding, most master regulators identified in the Upstream Regulator Analysis were involved in the immune response. For example, *P38 Mapk* plays a role in signal transduction within the normal inflammatory cascade and is only activated in PF and C animals (Cuadrado & Nebreda 2010). Moreover, *Adamts12* modulates neutrophil apoptosis during inflammation, while *Osm*

attenuates the inflammatory response (Dumas et al. 2012; Moncada-Pazos et al. 2012). Thus, inhibition of *Adamts12* and activation of *Osm* in control animals may blunt their responses to adjuvant. Furthermore, *Adcyap1* modulates anti-inflammatory responses and is neuroprotective in neurons following inflammation (Waschek 2013). Its inhibition in PAE animals suggests a lower level of protection against inflammation than the one that would occur in controls. In turn, as *Prl* promotes pro-inflammatory responses, its PAE-specific activation suggests an altered response to adjuvant (Brand et al. 2004). Failure of PAE animals to activate *Foxo*-related pathways may also play a role in their unique response to adjuvant, as knockdown of *Foxo3* or *Foxo4* increases inflammatory responses (Hwang et al. 2011; Zhou et al. 2009). The possibility that *Foxo3* is already up-regulated in PAE animals, and thus may not change further after adjuvant injection remains to be investigated (Kleiber et al. 2013). The activation of fibronectin in PAE animals is interesting, as it is involved in the development of inflammatory arthritis (Barilla & Carsons 2000). Greater production or sensitivity to this protein could underlie the altered course and severity of AA in PAE animals. Finally, activation of *Dicer1* in PAE animals suggests alterations to microRNA processing under stress conditions, previously demonstrated following PAE (Guo et al. 2011).

2.4.3 Limitations

Although these results suggest a long-term effect of PAE on the brain's transcriptome, the interpretability of this study is limited by the small number of animals and variability in transcriptomic profiles both at baseline and in response to AA. These factors could have influenced the identification of differential expressed genes and reproducibility of our results by RT-qPCR. In addition, as the FDR was set at a more relaxed threshold (25%) to capture a greater

number of differentially expressed genes, more false-positives may have been identified in the analysis, reflected in the low number of genes verified by RT-qPCR. The animals used in the present study were also obtained from an outbred population, and differences in genetic background could have influenced both the physiological response to AA and gene expression profiles.

An additional limitation of this study is that estrus stages were not determined at the time of termination. We have previously shown that PAE induces changes in basal levels of hippocampal glucocorticoid and serotonin Type 1A (5-HT1A) receptor mRNA as a function of estrous stage, which likely have widespread effects on global expression patterns in the brain (Sliwowska et al. 2008). While most females in the present study were likely in diestrus, estrus cycle variation might partially explain intra-group differences in gene expression (Lan et al. 2009). Taken together, these limitations temper our interpretation of the differential expression results, which require further validation in independent cohorts.

2.4.4 Effects of pair-feeding on neural gene expression: Pair-feeding is a treatment in itself

A number of genes were similarly altered, or showed graded and differential effects in PAE and PF compared to C animals (Figure 2.3). These may respond to common effects of ethanol exposure and pair-feeding, such as reduced caloric availability or altered stress system regulation. While both PAE and PF animals receive the same number of calories, PAE dams eat *ad libitum* whereas PF dams receive a reduced ration, likely resulting in hunger and stress (Harris & Seckl 2011). Moreover, PF dams tend to consume their daily ration within a few hours and are deprived until the next feeding, which may have unique metabolic effects associated with

"disordered" eating. Our results suggest that the HPC may be susceptible to fetal programming in response to energy-, and stress-related environmental factors. Interestingly, the curated list of candidate FASD genes from NeuroCarta was identified in the HPC of PF animals, suggesting that these genes are potentially related to common mechanisms underlying prenatal alcohol exposure, nutrition, and stress (Portales-Casamar et al. 2013). Studies such as ours are critical to separate the effects of prenatal stress and prenatal alcohol exposure at the level of gene expression.

2.4.5 Summary and conclusions

Our results support the hypothesis that PAE has long-term effects on gene expression patterns in the brain, as well as on the response to a systemic inflammatory insult. As both the PFC and HPC play important roles in cognitive, neuroendocrine, and immune function, the identified changes in steady-state and activated expression likely contribute to immune-related alterations, as well as cognitive and behavioural deficits arising from PAE. Moreover, an inability to mount appropriate response to immune/inflammatory challenges may contribute to the increased vulnerability of individuals with FASD to infections and immune problems. These findings extend our previous data demonstrating that PAE animals exhibit increased susceptibility to and impaired recovery from an inflammatory challenge, and suggest that the adverse impact of prenatal ethanol exposure on the neural transcriptome may underlie long-term health and developmental outcomes observed in individuals with FASD.

Chapter 3: Prenatal alcohol exposure alters DNA methylation patterns during early development

3.1 Background and rationale

Early-life environments have the potential to influence the development of biological systems, leading to long-term consequences in offspring (Godfrey & Robinson 1998; Hanson & Gluckman 2008). Of relevance, prenatal alcohol exposure (PAE) can lead to the development of Fetal Alcohol Spectrum Disorders (FASD) in humans, which is associated with a wide variety of adverse effects. Importantly, PAE can alter the development, function, and regulation of numerous neurobiological and physiological systems, giving rise to lasting deficits across the spectrum of FASD, including, but not limited to cognitive and behavioral deficits, impairment to self-regulation and adaptive functioning, immune dysregulation, and increased vulnerability to mental health problems across the lifespan (Zhang, Sliwowska, & Weinberg 2005; Pei et al. 2011; Mattson, Crocker, & Nguyen 2011).

Among the affected neurobiological systems, the hypothalamus is highly susceptible to the programming effects of PAE (Matthews 2002; Eguchi 1969). In addition to its vital role in neuroendocrine regulation, the hypothalamus also acts as the main center for autonomic regulation and homeostatic control, regulating growth, sleep/wake behavior, circadian rhythms, metabolism, body temperature, and other vital functions (Squire et al. 2008). Data from both clinical cohorts and animal models of FASD have identified alterations to physiological functions associated with the hypothalamus. For example, infants exposed to alcohol *in utero* show both elevated basal and post-stress levels of cortisol, and children with FASD and early life adversity exhibit dysregulation of the cortisol circadian rhythm (McLachlan et al. 2016).

Similarly, in animal models of PAE, exposed offspring exhibit hyperresponsiveness to stressors as well as altered central regulation of hypothalamic-pituitary-adrenal (HPA) activity (Ramsay, Bendersky, & Lewis 1996; Jacobson, Bihun, & Chiodo 1999; Haley, Handmaker, & Lowe 2006; Weinberg et al. 2008). Furthermore, PAE also alters sleep patterns and circadian rhythms, leads to deficits in thermoregulation, and is associated with inappropriate feeding behavior (Jones & Smith 1973; Chen et al. 2012; Earnest, Chen, & West 2001; Sei et al. 2003; Zimmerberg, Ballard, & Riley 1987; Werts et al. 2014).

These deficits often persist across the life course of individuals with FASD and PAE animals, suggesting that alcohol may alter developmental trajectories during prenatal life to increase the risk of adverse outcomes (Hellemans, Sliwowska, et al. 2010). Indeed, the fetal programming hypothesis suggests that early environmental or non-genetic factors, including maternal undernutrition, stress, and exposure to drugs or other toxic agents, can permanently organize or imprint physiological and neurobiological systems and increase adverse cognitive, adaptive, and behavioral outcomes, as well as vulnerability to diseases or disorders later in life (Godfrey & Robinson 1998; Hanson & Gluckman 2008; Swanson et al. 2009). As the underlying mechanisms of these effects begin to emerge, it has become apparent that epigenetic mechanisms are prime candidates for the programming effects of PAE on physiological systems, linking environmental factors and neurobiological outcomes while influencing health and behavior well into adulthood (Yuen et al. 2011; Shulha et al. 2013). The term epigenetics broadly refers to the modifications of DNA and its packaging that alter DNA accessibility, which modulate gene expression and cell functions without changes to underlying genomic sequences (Bird 2007). These include direct modifications to DNA, post-translational modification of histones, and non-coding RNAs.

DNA methylation is perhaps the most studied epigenetic modification and involves the covalent attachment of a methyl group to the 5' position of cytosine, typically occurring at cytosine-guanine dinucleotide (CpG) sites (Jones & Takai 2001). Although closely linked to the regulation of gene expression, the association between DNA methylation and transcription depends on genomic context. Whereas DNA methylation typically represses gene expression when located in promoter regions, its effects are more variable for CpGs residing in gene bodies and intergenic regions. DNA methylation can also directly control transcription factor binding to gene regulatory regions, such as enhancers, modulating gene expression patterns (Tate & Bird 1993). In addition to this role in transcriptional control, DNA methylation has been associated altered mRNA splicing when located within introns, and its presence within certain exons may potentially regulate alternative transcriptional start sites (Shukla et al. 2011; Maunakea et al. 2013, 2010). Furthermore, DNA methylation is closely linked to several crucial developmental processes, including genomic imprinting, as well as tissue specification and differentiation, suggesting a crucial role in the regulation of cellular functions and developmental trajectories (Ziller et al. 2013; Smith & Meissner 2013). Perhaps most importantly, DNA methylation is responsive to environmental influences and these changes may be inherited through cell divisions to potentially persist throughout the lifetime (Langevin et al. 2011; Hanson et al. 2011; Yuen et al. 2011). As such, an additional interesting aspect of DNA methylation is its emerging role as a potential biomarker of early-life exposures, as it is easily quantifiable, stable over time, and can be obtained from readily available peripheral tissues, such as buccal epithelial cells and white blood cells (Bock 2009).

Given their role in the regulation of gene expression and cell function, as well as their responsiveness to environmental factors, epigenetic alterations provide an attractive mechanism

for the biological embedding of the persistent deficits caused by PAE. Mounting evidence suggests a potential role for DNA methylation in the etiology of PAE-induced deficits, as numerous studies have identified alterations to epigenetic programs in the central nervous system of animals exposed to alcohol *in utero*. These range from differences in bulk levels of DNA methylation to genome-wide changes in DNA methylation patterns, suggesting that PAE can alter the epigenome (Bekdash, Zhang, & Sarkar 2013; Laufer et al. 2013). For example, PAE alters the DNA methylation status of the *POMC* gene in the hypothalamus (Ngai et al. 2015; Bekdash, Zhang, & Sarkar 2013). As a key regulator of the stress response, alterations to this gene may reflect broader alterations to the regulatory functions of the hypothalamus. Although genome-wide studies have been performed on whole brains in mice, few studies have focused on targeted brain regions. Studies from clinical cohorts of children with FASD have also identified widespread changes to DNA methylation patterns in peripheral tissues (Laufer et al. 2015; Portales-Casamar et al. 2016). However, alterations to central tissue are difficult to directly assess in clinical populations, and while peripheral tissues are more easily accessible, changes in these cells may not fully reflect alterations in the brain (Berko et al. 2014). Furthermore, biological embedding of PAE's effects earlier in development could potentially lead to more systemic effects on the epigenome, which would be reflected by alterations present across a variety of tissues.

Currently, the genome-wide impact of PAE on DNA methylation within the hypothalamus remains unknown (Ngai et al. 2015; Bekdash, Zhang, & Sarkar 2013). To address this gap, we assessed whether PAE alters DNA methylation profiles in the early postnatal period, and whether altered sites of methylation could serve as biomarkers of gestational alcohol

exposure if also identified in peripheral tissues. Using methylated DNA immunoprecipitation and next-generation sequencing (meDIP-seq), we identified statistically significant PAE-specific differentially methylated regions (DMR) that persisted across pre-weaning development of the hypothalamus, in regions that could potentially reflect the neurobiological alterations caused by PAE. In parallel, we identified concordant DNA methylation alterations between white blood cells and the hypothalamus of PAE animals compared to controls on postnatal day (P) 22. Our findings suggest that: 1) PAE causes widespread alterations to DNA methylation patterns in both central and peripheral tissues, potentially reprogramming physiological systems and influencing the deficits observed in FASD; and 2) DNA methylation patterns in peripheral tissue reflect some changes in brain, which could represent systemic effects on the organism and potential biomarkers of PAE.

3.2 Materials and methods

3.2.1 Prenatal treatment

Details of the procedures for breeding and handling have been published previously (Bodnar, Hill, & Weinberg 2016). Briefly, nulliparous females (n=39) were pair-housed with a male and vaginal lavage samples were collected daily for estrous cycle staging and to check for the presence of sperm, indicating gestation day 1 (GD1). Pregnant dams were singly housed and assigned to one of three prenatal treatment groups: Prenatal alcohol exposure (PAE) - *ad libitum* access to liquid ethanol diet, 36% ethanol-derived calories, 6.37% v/v, n =13; Pair-fed (PF) - liquid-control diet, maltose-dextrin isocalorically substituted for ethanol, in the amount consumed by an E partner, g/kg body weight/GD), n =14; or Control (Con) - pelleted version of the liquid control diet, *ad libitum*, n =12. All animals had *ad libitum* access to water.

Experimental diets (Weinberg/Kiever Liquid Ethanol Diet #710324, Weinberg/Kiever Liquid Control Diet #710109, and Pelleted Control Diet #102698, Dyets Inc., Bethlehem, PA) were fed from gestation days 1-21, and then replaced with laboratory chow. Litters were weighed and culled at birth to 6 males and 6 females, when possible.

3.2.2 Sample collection

On P1, 8, 15, and 22, female offspring (max 1/litter) were decapitated, trunk blood collected (at P22 only), and brains removed and weighed; the hypothalamus was then quickly dissected and frozen on dry ice in RNA*later* (n=7-11/age/group; Figure 3.1; Qiagen, Hilden, Germany). WBCs were isolated using *Ficoll-Paque* (GE Healthcare, Uppsala, Sweden), which isolates peripheral blood mononuclear cells (PBMC). All tissue collected was left at 4˚C for 1 day and then frozen at -80˚C until DNA extraction. WBCs were stored in RNA*later* at -80˚C until DNA extraction. Due to the large number of animals associated with the experimental design of this study, animals were collected across four different cohorts (breedings), spanning January 2012 – December 2013.

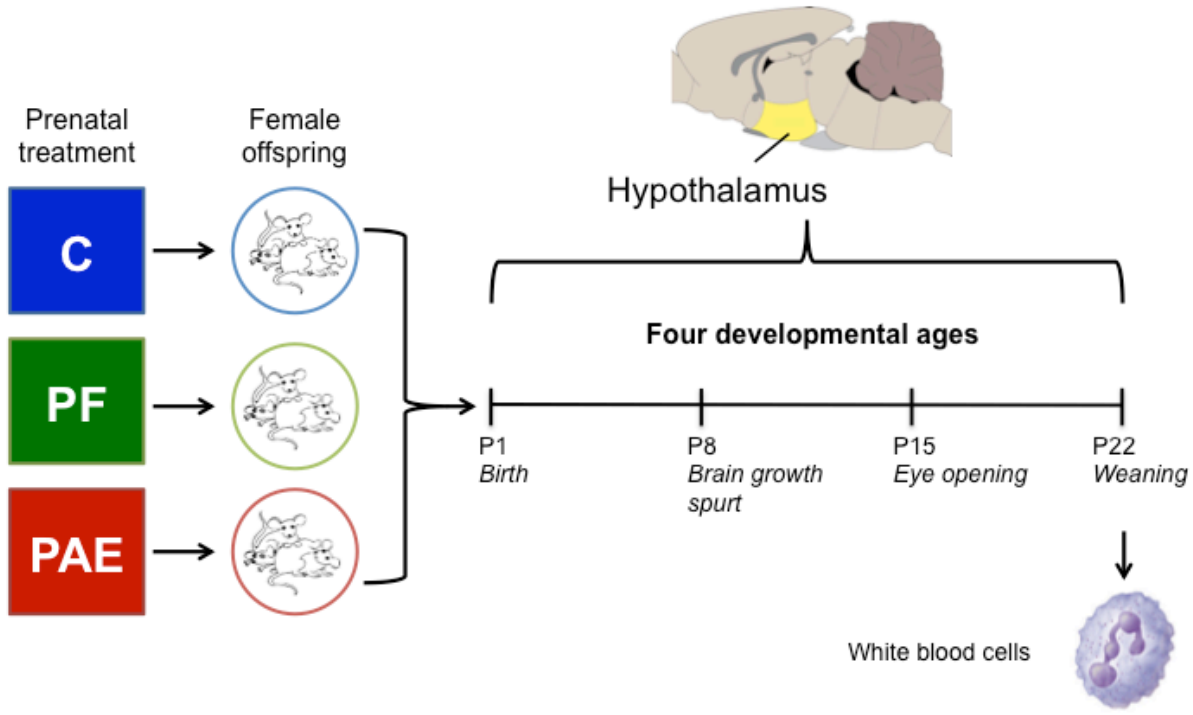

Figure 3.1 Overview of the experimental design

We collected the hypothalamus of female offspring from one of three prenatal treatment groups on postnatal days (P) 1, 8, 15, and 22. In parallel, white blood cells were collected on P22 from the same animals as the hypothalamus samples. Each group/age/tissue was composed of four samples for DNA methylation analysis by methylated DNA immunoprecipitated and next-generation sequencing (meDIP-seq).

3.2.3 Blood composition analysis

Analysis of blood composition was done on samples from a separate but parallel cohort of animals. Briefly, on P22, trunk blood was collected from female offspring (C: n = 6; PF: n = 5; PAE: n = 5), and analyzed using the Advia120 hematology system, which assesses complete blood counts and differential WBC counts (CBC/Diff function). The reported values include counts for neutrophils, lymphocytes, monocytes, eosinophils, basophils, and large unclassified cells (Supplementary table 3.1).

3.2.4 Statistical analyses of developmental data

Maternal data during gestation and lactation were analyzed using repeated measures analyses of variance (ANOVA), with prenatal treatment as the between-subjects factor, and postnatal day as the within-subjects factor. As separate cohorts of offspring from each prenatal group were terminated on P1, P8, P15, or P22 (n = 4/group/age/tissue), body weights were analyzed by ANOVAs for the factor of prenatal treatment at each age and in a group*age interaction model. Blood composition data were also analyzed using a two-way ANOVA to identify differences among groups for each WBC subtype.

Significant main effects and interactions were further analyzed by Tukey honest significant difference (HSD) *post hoc* tests ($p<0.05$).

3.2.5 DNA extraction

Total RNA and DNA were simultaneously extracted from the hypothalamus and white blood cells (n=4/group/age/tissue; Qiagen AllPrep DNA/RNA Mini kit, Hilden, Germany). Frozen tissue was thawed on ice, quickly weighed and placed in lysis buffer for 5 minutes. Homogenization was performed by 5 strokes of an 18G needle, 10 strokes of a 20G needle, and 10 strokes of a 23G needle. The resulting homogenate was centrifuged at 21,000g for 3 minutes and the supernatant was collected for DNA and RNA extraction. White blood cells were thawed on ice and then centrifuged at 10,000g for 10 minutes. RNA*later* was carefully removed without disturbing the cell pellet and cells were resuspended in lysis buffer. The cells were then frozen at -80˚C to disrupt cell membranes and then thawed on ice. The resulting homogenate was then used for DNA and RNA extraction. DNA concentration was assessed using Qubit Fluorometric Quantitation (Life Technologies, Carlsbad, USA). Full developmental data on the animals can be

found in Supplementary table 3.2.

3.2.6 Methylated DNA immunoprecipitation and next-generation sequencing

Our methylated DNA immunoprecipitation following by next-generation sequencing (MeDIP-seq) procedures were adapted from a previously published protocol, and are outlined in detail below (Taiwo et al. 2012).

3.2.6.1 Sequencing library preparation

For each sample, 500 nanograms of DNA were diluted in a total volume of 60µL of EB buffer (Qiagen, Hilden, Germany). DNA was then transferred to a 96-well plate and sheared for 1 hour using the Covaris Focused-ultrasonicator. DNA was purified using Ampure XP in 20% polyethylene glycol (PEG) beads to obtain fragments sized from 200-500 basepairs (Beckman-Coulter, Brea, USA). Library preparation was performed on the Bravo Automated Liquid Handling Platform (Agilent, Santa Clara, USA) using the TruSeq DNA PCR-Free Sample Preparation Kit (Illumina, San Diego, USA). Following end-repair and A-tailing, adapters were ligated overnight at room temperature. PCR-free library preparation allowed for the conservation of methylated cytosines for subsequent methylated DNA immunoprecipitation. Finally, DNA was resuspended in 35µL of EB buffer (Qiagen, Hilden, Germany). DNA was quality controlled using Qubit Fluorometric Quantitation and the DNA 1000 Bioanalyzer 2100 kit (Agilent, Santa Clara, USA) to verify concentration and fragment size (250-550bp).

3.2.6.2 Methylated DNA immunoprecipitation

For each sample, 400 nanograms of DNA were diluted in a total volume of 50µL of IP

Buffer (10mM sodium phosphate buffer, pH7.0, 140mM NaCl, 0.05% triton). DNA was denatured by incubation at 95˚C for 10 minutes, followed by the addition of 48µL ice-cold IP buffer and incubation on ice for 10 minutes. 2µL of anti-5-methylcytosine antibody (Eurogenetec, Liège, Belgium), diluted to 1/50 in IP buffer (1µL of antibody per 1µg of DNA ratio), was added to each sample. Immunoprecipitation reactions were incubated for 16 hours at 4˚C with overhead rotation. Following two 5 minute washes with 150uL of 0.1% BSA/PBS, 50µL of Dynabeads Protein G were incubated with 5µL of secondary antibody (rabbit anti-mouse IgG; Jackson Immunoresearch, West Grove, USA) in 45uL ice-cold IP buffer for 15 minutes at room temperature with overhead rotation. Beads were washed twice with IP buffer to remove unbound secondary antibody and resuspended in 50µL IP buffer. The antibody-bound beads were added to the immunoprecipitation reactions and incubated for 2 hours at 4˚C with overhead rotation. Beads were then washed 6 times with 150µL of ice-cold IP buffer and resuspended in 98.97µL of Proteinase K digestion buffer (TE with 0.5% SDS). Following the addition of 1.25µL Proteinase K (20mg/mL; Qiagen, Hilden, Germany), samples were incubated in a thermomixer for 2 hours at 55˚C with a rotation speed of 1250rpm. The reaction was then allowed to cool at room temperature for 15 minutes. Supernatant was collected and bead cleanup was performed using equal volume SeraMag beads with 30% PEG. DNA was resuspended in 35µL of EB buffer (Qiagen, Hilden, Germany).

3.2.6.3 Sample amplification and indexing

Two rounds of PCR amplification per sample were performed in order to reduce PCR amplification bias. The reaction mixes were as follows: 15µL DNA, 27µL H_2O, 12µL 5X HF buffer, 1.5µL DMSO, 1.0µL paired-end primer (Illumina), 0.5µL Phusion High-Fidelity DNA

polymerase (New England Biolabs), 2µL indexing primer (Illumina – specific to each sample). The amplification cycle was as follows: 98˚C for 1 minute, 12X (98˚C for 15 seconds, 65˚C for 30 seconds, 72˚C for 30 seconds), 72˚C for 5 minutes. Reactions from the same sample were pooled and bead cleanup was performed using SeraMag beads in 20% PEG (102µL of beads per 120µL of reaction). DNA was resuspended in a final volume of 35µL of EB buffer.

3.2.6.4 Next-generation sequencing

Indexed meDIP libraries were combined in 3 pools of 20 samples each, distributing samples evenly by tissue, age, and prenatal treatment across all three sets. Next-generation sequencing was performed on the three sample pools by the Genome Sciences Centre in Vancouver, BC, Canada. Each sample pool was run on two HiSeq lanes, which produced approximately 600,000,000 paired-end reads of 125 bases per lane.

3.2.6.5 Sequencing pre-processing and quality control

Fastq files were aligned to the most current rat genome (Rn6, July 2014) using the Burrows-Wheeler Transform (BWA) tool to obtain .bam files (Li & Durbin 2009). Bam files were filtered using *samtools* to remove duplicate reads, unpaired reads, and reads with a minimum quality score below 10. Following alignment and filtering, each the two runs for each sample were merged using *samtools* to obtain a single .bam file for each sample (Li et al. 2009). Supplementary table 3.3 shows sequencing related information: sample pool, sample index, number of raw reads, number of filtered reads, and total number of reads/sample.

3.2.7 Bioinformatic analyses

3.2.7.1 Peakset generation

Model-based analysis of ChIP-seq (MACS2; version 2.1.0.20140616) was used to identify enriched regions of DNA methylation across the genome (Zhang et al. 2008). This method models the distance between paired sequencing reads by using a sliding window (twice the bandwidth = 600 bp) to find enriched regions throughout the genome. Without a control, this method calculates a dynamic regional lambda for each peak (10000bp windows) to estimate the local bias to enrichment and compute background levels for fold enrichment. P-values for each peak are calculated through a dynamic Poisson distribution, which incorporates background levels estimated by the local lamba. These are corrected (q-values) using the Benjamini-Hochberg multiple-test correction method. The peak calling to identify peak regions (DNA methylation windows) was performed using the 'callpeaks' function on paired end bam files with no control input and the following options: –f BAMPE –m 5 50 –bw 300 –g 2.9e9 –q 0.05. Each sample was modeled individually, generating 60 total peaksets. These were imported into R using the *DiffBind* package (Stark & Brown 2011; Ross-Innes et al. 2012). As all samples had slightly different predicted peaks, peaksets were combined into common regions using the *dba.count* function in *DiffBind*, which removed peaks found in less than 3 samples across the entire dataset and provided the total number of reads within each peak/sample. This created a final dataset of 469,162 peaks and 48 samples from the developmental profile of the hypothalamus, and a final dataset of 350,960 peaks and 24 samples in the P22 hypothalamus and WBC (BvB) peakset.

3.2.7.2 Data preprocessing and normalization of the developmental dataset

First, the total reads within each peak were adjusted to reads/kilobase by dividing the number of reads within each region by their length. In turn, these were converted to reads per kilobase per million (RPKM) by dividing the reads/kilobase by the total number of reads found in the predicted peaks to account for differences in sequencing depth between samples. The samples in the developmental dataset were highly correlated ($r>0.95$ for all samples), with samples clustering most closely with animals of the same age (Supplementary figure 3.1). No outliers were detected in this first pass analysis.

Principal component analysis of the normalized RPKM data revealed significant levels of variation associated with batch effects. Notably, MeDIP and DNA extraction rounds were associated with a large proportion of variation within the dataset. However, both these factors were highly confounded with age, as all P22 samples were immunoprecipitated separately and separate ages were extracted together (Supplementary figure 3.2). Nevertheless, to account for these effects, ComBat correction was performed on the RPKM data from the hypothalamic samples to correct the effects of MeDIP round and DNA extraction round in the dataset. Age was also slightly confounded with the breeding from which animals were collected, as not all ages were samples from the different cohorts. Interestingly, some partial effects of breeding remained in the dataset following ComBat correction, suggesting that this covariate was not fully confounded with age. Furthermore, prenatal treatment accounted for a larger proportion of variance within the dataset following ComBat correction, suggesting that the removal of batch effects might allow for the identification of more subtle effects of PAE. The corrected and

normalized RPKM values obtained from ComBat were used for plotting purposes, but were converted back to reads/kilobase for downstream statistical analyses.

3.2.7.3 Data preprocessing and normalization of the BvB dataset

First, the total reads within each peak were adjusted to reads/kilobase by dividing the number of reads within each region by their length. In turn, these were converted to reads per kilobase per million (RPKM) by dividing the reads/kilobase by the total number of reads found in the predicted peaks to account for differences in sequencing depth between samples. Samples in the BvB peakset were highly correlated within tissue ($r>0.96$), the main driver of DNA methylation patterns, and well correlated within the same animals ($r>0.92$). However, one PF WBC sample clustered with the hypothalamus samples, suggesting that it may have been mislabeled during processing. As such, this sample was removed from the dataset, resulting in a dataset of 23 samples (Supplementary figure 3.3).

Principal component analysis of the normalized BvB RPKM data revealed significant levels of variation associated with DNA extraction round batch effects (Supplementary figure 3.4). Tissue type was the covariate most strongly associated with variance in the dataset, although it was slightly confounded with extraction round. While ComBat correction was used to account for the effects of DNA extraction round in the BvB dataset, this approach limited our ability to identify tissue-specific differences, as it removed the majority of tissue-associated variance from the dataset. Again, prenatal treatment was associated with a larger proportion of variance within the dataset following ComBat correction. Interestingly, breeding once again remained a major contributor to variability within the dataset, suggesting that differences between cohorts may have an important influence on epigenetic patterns. The corrected and

normalized RPKM values obtained from ComBat were used for plotting purposes, but were converted back to reads/kilobase for downstream statistical analyses.

3.2.7.4 Removing cell-type specific DMRs

Using previously characterized transcriptomic profiles from mouse neurons, oligodendrocytes, and astrocytes, we identified DNA methylation peaks within genes that are specifically expressed in each different subtype (1.5 fold expression difference compared to other cell types) (Cahoy et al. 2008). Given the relationship between gene expression and epigenetic patterns, it is possible that alterations to the DNA methylation levels of these genes could reflect changes in the cell-type proportions within this dataset. However, the majority of the peaks in the dataset were located within intergenic regions, with no annotated associations with these genes, reducing our ability to capture cell-type related differences. As such, only regions directed located within neuron-, oligodendrocytes-, or astrocyte-specific genes were removed from further analyses to reduce the potential confounding factor of cell type, resulting in a dataset of 451,112 peaks for downstream analyses of the hypothalamus.

3.2.7.5 DMR identification

Linear modeling was performed using *edgeR*, which is typically used to analyze RNA-seq count data and includes a factor to account for the number of reads in each sample (Nikolayeva & Robinson 2014; Robinson, McCarthy, & Smyth 2010). This method was used to identify differentially methylated regions (DMRs) that were consistently different between PAE animals and both control groups across difference ages and tissues. For both analyses, the model accounted for the effects of collection during different breedings, and p-values were corrected for

multiple-testing using the Benjamini-Hochberg method. Statistically significant DMRS at a false discovery rate (FDR) <0.05 were obtained for the following contrasts: PAE versus C, PAE versus PF, and Control versus PF. The final PAE-specific DMRs were statistically significant in both PAEvC and PAEvPF, and were not found in the CvPF contrasts.

3.2.7.6 Genomic enrichment

Custom annotations were built for each peakset using the UCSC genome browser gene annotations. Briefly, genomic coordinates of all CpG islands, exons, introns, promoters (TSS -200bp and TSS -1500bp), 3' untranslated regions (UTR), 5' UTRs for the rn6 genome were obtained as bed files from the table browser. In parallel, MeDIP-seq peaks were converted to the bed file format and the overlap of genomic features with MeDIP-seq peaks was computed iteratively using the *intersectBed* function from *bedtools*, retaining only the peaks that contained the assessed genomic feature (Quinlan & Hall 2010). The overlaps were concatenated into a single annotation set in R, where individual peaks contained information for each potential genomic feature. Of note, regions spanning both introns and exons were deemed intron/exons boundaries. P-values for genomic feature enrichment analyses were calculated by computing background levels of genomic features on 1,000 random subsets of DMRs, using the same number of PAE-specific DMRs.

3.2.7.7 Transcription factor binding site analysis

Enrichment of different transcription factors binding sites (TFBS) in PAE-specific DMRs was assessed using the *motifEnrichment* function of the *PWMEnrich* package (Stojnic & Diez 2013). DMR DNA sequences were obtained from the UCSC genome browser (Rn6 genome). As

no binding motifs were available for the *Rattus norvegicus* genome, motifs from the *Mus musculus* genome were obtained from the *PWMEnrich.Mmusculus.background*. Motifs were summarized using the *groupReport* function. P-values were calculated by performing enrichment analysis on 1,000 random subsets of DMRs, using the same number of PAE-specific DMRs for each analysis to assess background levels of each TFBS in the different peaksets.

3.2.7.8 Gene ontology analysis

The gene-score resampling (GSR) tool of ErmineJ (version 3.0.2) was used to identify gene function enrichment in the differentially methylated genes including the Gene Ontology (GO) annotations molecular function, biological process, and cellular component (Lee et al. 2005). The ermineJ GSR tool was set with the following parameters: max gene set size = 2,000; min gene set size = 2; iterations = 10,000. Once again, statistically significant associations ($p<0.05$ and multifunctionality score <0.05) were obtained for the following contrasts: PAE versus Control, PAE versus PF, and Control versus PF. The final PAE-specific GO terms were statistically significant in both PAEvC and PAEvPF, and were not found in the CvPF contrasts.

3.2.8 Bisulfite pyrosequencing

DNA from the same samples as above subjected to bisulfite conversion using the Zymo EZ DNA Methylation Kit (Zymo Research, Irvine, California), which converts DNA methylation information into sequence base differences by deaminating unmethylated cytosines to uracil while leaving methylated cytosines unchanged. Bisulfite pyrosequencing assays were designed with PyroMark Assay Design 2.0 (Qiagen, Hilden, Germany; Supplementary table 3.4). The regions of interest were amplified by PCR using the HotstarTaq DNA polymerase kit (Qiagen,

Hilden, Germany) as follows: 15 minutes at 95°C, 45 cycles of 95°C for 30s, 58°C for 30s, and 72°C for 30s, and a 5 minute 72°C final extension step. For pyrosequencing, single-stranded DNA was prepared from the PCR product with the Pyromark™ Vacuum Prep Workstation (Qiagen, Hilden, Germany) and the sequencing was performed using sequencing primers on a Pyromark™ Q96 MD pyrosequencer (Qiagen, Hilden, Germany). The quantitative levels of methylation for each CpG dinucleotide were calculated with Pyro Q-CpG software (Qiagen, Hilden, Germany). Of note, only PAE and Control animals were assessed by bisulfite pyrosequencing. We selected several DMRs for verification by bisulfite pyrosequencing based on their potential role in PAE-induced deficits, mainly focusing on their associated gene.

3.3 Results

3.3.1 Developmental data

To verify that our alcohol exposure paradigm performed as expected, we assessed whether our prenatal treatments influenced maternal weight gain over pregnancy and pup weights (Bodnar, Hill, & Weinberg 2016; Uban et al. 2010; Hellemans, Verma, et al. 2010). On average, alcohol intake of PAE dams was consistently high across pregnancy, ranging from 0.208 ± 0.014 to 0.268 ± 0.022 mL/kg body weight during *week 1*, 0.240 ± 0.016 to 0.305 ± 0.017 during *week 2*, and 0.236 ±0.014 to 0.285 ± 0.019 during *week 3* of gestation (Table 3.1). These levels of drinking typically result in blood alcohol levels ~100-150 mg/dL (Uban et al. 2010; Hellemans, Verma, et al. 2010). Separate analyses of maternal body weights during gestation (GD1, 7, 14, 21) and following parturition (P1, 8, 15, 22) showed significant main effects of group ($F_{(2,143)=}$13.609, p =0.0000039 and $F_{(2,91)}$=9.559, p =0.00017, respectively) and group X day interactions ($F_{(6,143)}$ = 2.869, p = 0.011 and $F_{(2,91)}$ = 2.566, p = 0.082, respectively)

during both gestation and lactation. Both PAE and PF dams weighed significantly less than controls on GD14 and 21, and following parturition (P1). However, catch-up weight gain occurred after birth, when the diets were normalized, and maternal weight differences among groups were no longer significant by P8. We did not observe any significant group differences in the number of live-born pups, or in the average weight of female pups/litter at any of the collection days. These results suggested that our paradigm was performing as expected, with PAE dam showing gaining less weight over the course of pregnancy, though these effects were not reflected in the weight of pups.

	C	PF	PAE	N
Number of pups	14.7 ± 0.5	14.0 ± 0.8	14.4 ± 0.5	39 (12C; 14PF; 13PAE)
Dam weight				
GD 1	295.9 ± 5.1	297.3 ± 5.1	299.4 ± 6.9	39 (12C; 14PF; 13PAE)
GD 7	327.8 ± 3.9	314.4 ± 5.6	313.2 ± 6.6	39 (12C; 14PF; 13PAE)
GD 14	380.4 ± 5.2	356.6 ± 6.1†	353.1 ± 5.4††	39 (12C; 14PF; 13PAE)
GD 21	478.9 ± 9.5	446.0 ± 6.6††	434.0 ± 5.8†††	39 (12C; 14PF; 13PAE)
P1	393.9 ± 9.1	365.1 ± 7.8†	348.0 ± 6.3†††	39 (12C; 14PF; 13PAE)
P8	373.3 ± 8.4	356.5 ± 8.4	361.6 ± 5.2	28 (9C; 10PF; 9PAE)
P15	367.9 ± 8.7	356.7 ± 8.6	356.9 ± 1.5	19 (6C; 7PF; 6PAE)
P22	346.8 ± 7.1	333.0 ± 11.4	334.0 ± 1.3	12 (4C; 4PF; 4PAE)
Pup weight				
P1	6.6 ± 0.2	6.5 ± 0.2	6.4 ± 0.1	39 (12C; 14PF; 13PAE)
P8	17.4 ± 0.4	16.8 ± 0.8	16.3 ± 0.7	28 (9C; 10PF; 9PAE)
P15	36.6 ± 2.4	33.1 ± 0.9	35.3 ± 1.3	19 (6C; 7PF; 6PAE)
P22	59.9 ± 0.9	57.2 ± 2.7	59.1 ± 4.2	12 (4C; 4PF; 4PAE)

†PAE = PF < C; $^{\dagger}p < 0.05$; $^{\dagger\dagger}p < 0.01$; $^{\dagger\dagger\dagger}p < 0.001$

Table 3.1 Pregnancy outcomes and body weights during gestation and postnatal development

3.3.2 The developmental profile of the rat hypothalamus

Our initial analysis of this dataset aimed to identify persistent alterations to DNA methylation patterns in the rat hypothalamus across early development (P1 to P22). More specifically, we analyzed the hypothalamus of female offspring on P1, 8, 15, and 22 using methylated DNA immunoprecipitation (meDIP-seq). These ages were selected as they represent

key developmental periods, including birth (P1), the brain growth spurt (P8), eye opening (P15), and weaning (P22) and females were utilized due to their underrepresentation in molecular and genome-wide studies of PAE. (Dobbing & Sands 1979; McCormick & Mathews 2010).

3.3.2.1 PAE caused persistent alterations to DNA methylation patterns in the hypothalamus

As cell type proportions are a major driver of DNA methylation patterns, we first removed peaks that were located within genes specifically expressed in neurons, astrocytes, or oligodendrocytes, resulting in a dataset of 48 samples and 451,112 peaks. We assessed the cell-type associated peaks independently by linear modeling (18,050 peaks), identifying few differences between prenatal groups, which suggested that few cell-type associated differences were present in the dataset (Supplementary figure 3.5). To assess persistent alterations to DNA methylation patterns caused by PAE, we performed linear modeling on the hypothalamic samples across all ages with a model that also accounted for differences across breeding cohorts. Using contrast analyses to assess PAE-specific alterations, we successfully identified 118 PAE-specific DMRs at an FDR <0.05 that persisted across all four developmental ages and showed consistently different DNA methylation levels between PAE animals and controls (Figure 3.2; Supplementary table 3.2). Of these, 47 were up-methylated and 75 were down-methylated in PAE animals versus control groups, and their sizes ranged from 316 to 1027bp (median = 494.5bp). Importantly, meDIP-seq provides relative levels of DNA methylation based on enrichment scores, and thus, the magnitude of change (i.e. % methylation) was not assessed using this method.

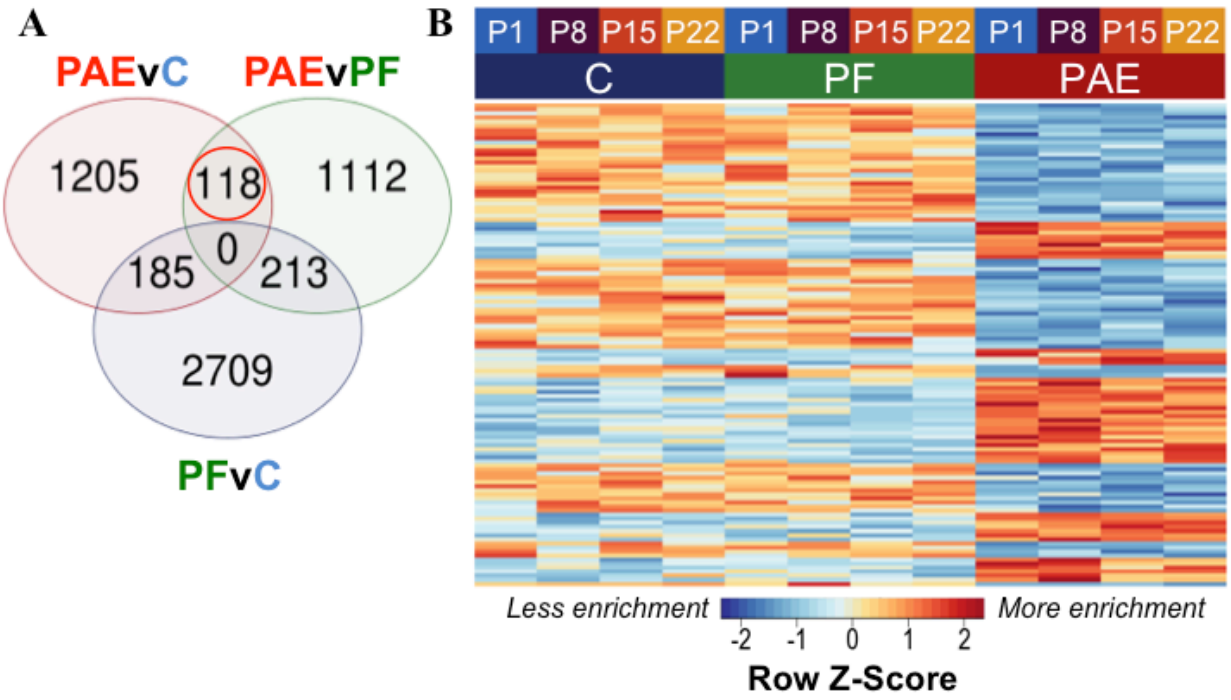

Figure 3.2 PAE-specific DMRs across pre-weaning development of the hypothalamus

A) Contrast analysis revealed 118 PAE-specific differentially methylated regions (DMR), which were significantly different in PAE versus C animals and PAE versus PF animals, but not significantly different between PF versus C. B) The DMRs showed consistent difference between PAE animals and controls across ages. Each row represents a different DMR, while each column shows the mean for all animals within that group/age. Reads per kilobase per million (RPKM) data were scaled and centered to produce a Z-score for each DMR, where those in blue showed less DNA methylation enrichment and those in red showed more enrichment.

Overall, 34 DMRs were located in genes, particularly within those involved in dopamine signaling (*Drd4*), the immune response (*Ifih1*, *Ccrl2*, *Il20ra*), and blood-brain barrier function (*Plvap*). Of note, two overlapping genes, *Golga4* and *Ctdspl,* contained two separate DMRs, and were the only genes with multiple DMRs. Although the entire DMRs set did not show any significant differences in genomic location enrichment compared to the background of the dataset, the up-methylated DMRs displayed significantly less enrichment in CGI and exons

(p<0.05), as no up-methylated DMRs were located in these regions (Figure 3.3). Furthermore, the majority of DMRs were located in intergenic regions, and while these were not significantly enriched compared to the entire dataset, these results suggested that intergenic regions may be more responsive to the influence of PAE on the epigenome, and may contain important regulatory regions that are not yet annotated in the rat genome.

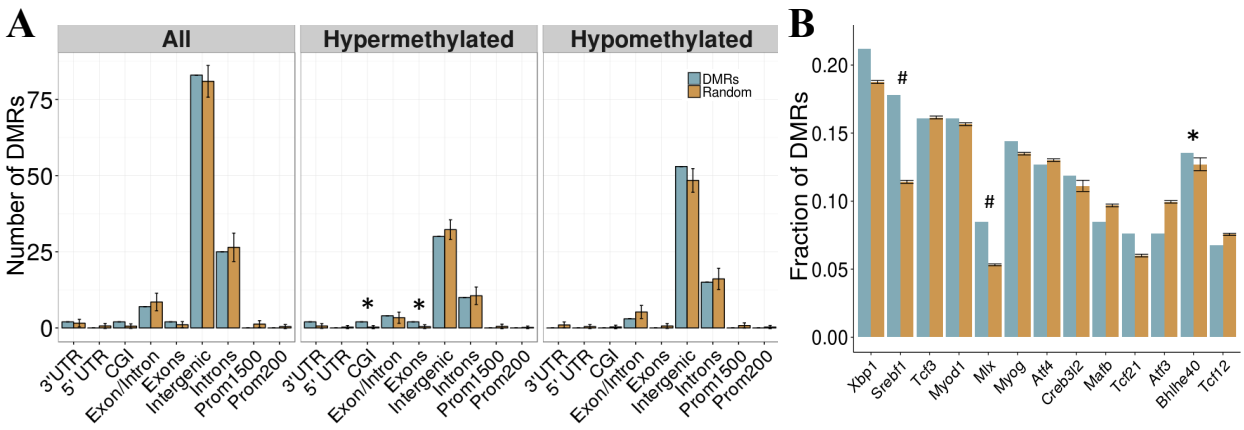

Figure 3.3 Enrichment patterns of the developmental DMRs

A) Genomic feature enrichment profile of all, up-methylated, and down-methylated DMRs. The probe counts for each feature (blue) were compared to the results from permutation analyses of 118 random regions (orange), which were used to compute the p-value. The majority of DMRs were located in intergenic regions or introns. Up-methylated regions in PAE animals did not contain any CpG islands (CGI) or exons, which is lower than expected by chance (p<0.05). B) Overrepresentation analysis of transcription factor binding sites in the DMRs. Only Bhlhe40 showed higher enrichment in the PAE-specific DMRs (blue) than by random chance (orange) (p<0.05), although Srebf1 and Mlx trended towards significance (p<0.1). *p<0.05, #p<0.1.

3.3.2.2 PAE-specific DMRs contained a greater proportion of bioinformatically predicted Bhlhe40 and Srebf1 TFBS

To follow up on the large proportion of intergenic regions in the PAE-specific DMRs, we assessed the enrichment of transcription factor binding sites (TFBS) within these regions using

binding motifs from the mouse genomes. Although the overlap between the rat and mouse genomes is not perfect, the rodent family shares many genomic characteristics and this analysis provides an important first pass analysis of potential regulatory factors within these regions. Following multiple-test correction (FDR<0.05), few TFBS were enriched within these regions compared to background levels. However, the Bhlhe40 binding motif was significantly enriched within the PAE-specific DMRs ($p<0.05$), while the Srebf1 and Mlx motifs trended towards significance ($p<0.10$) (Figure 3.3B). These results suggested that certain transcription factors may play a role in the long-term reprogramming of hypothalamic functions by PAE and may act in concert with other factors to sculpt the epigenome and downstream phenotypes.

3.3.2.3 Genes in PAE-specific DMRs were enriched for biological processes associated with hypothalamic functions

We performed GO analysis to ascertain the broad functional impact of PAE-induced changes in DNA methylation patterns of the hypothalamus across early development. We identified 20 PAE-specific biological processes (PAEvC and PAEvPF, $p<0.05$; PFvC, $p>0.05$; Table 3.2). Of note, the top GO terms were associated with steroid receptor signaling (GO:0042921, GO:0030518, GO:0031958, GO:0030520), a key function of the hypothalamus. Several processes associated with epigenetic regulation (GO:0016577, GO:0006482, GO:0070932) were also enriched in the PAE-specific DMRs, as were processes involved in immune function (GO:0030885, GO:0030886, GO:0002314), and cellular metabolism (GO:0050812).

Name	ID	Number of genes	Multi-functionality	P-value			Multifunctionality p-value		
				PAEvC	PAEvPF	PFvC	PAEvC	PAEvPF	PFvC
Glucocorticoid receptor signaling pathway	0042921	4	0.475	0.00117	0.00432	0.06853	0.0011	0.00456	0.07096
Intracellular steroid hormone receptor signaling pathway	0030518	27	0.681	0.00146	0.00865	0.09115	0.00148	0.00765	0.09009
Corticosteroid receptor signaling pathway	0031958	5	0.442	0.0025	0.01919	0.10193	0.00269	0.01955	0.1019
Regulation of myeloid dendritic cell activation	0030885	2	0.129	0.00816	0.0198	0.14194	0.00843	0.01869	0.14077
Negative regulation of myeloid dendritic cell activation	0030886	2	0.129	0.00816	0.02063	0.1637	0.00843	0.01978	0.163
Histone demethylation	0016577	13	0.397	0.01224	0.02727	0.18051	0.01204	0.02756	0.17928
Protein demethylation	0006482	15	0.365	0.01636	0.0284	0.18496	0.01597	0.02785	0.18571
Protein dealkylation	0008214	15	0.365	0.01636	0.02926	0.2578	0.01597	0.02805	0.26243
Calcium ion export	1901660	3	0.345	0.0166	0.02927	0.32371	0.01739	0.02926	0.32667
Protein sumoylation	0016925	11	0.328	0.01845	0.03449	0.33119	0.01688	0.03389	0.33539
Regulation of protein targeting to membrane	0090313	11	0.631	0.01845	0.03449	0.42205	0.01688	0.03389	0.42409
Intracellular estrogen receptor signaling pathway	0030520	6	0.523	0.01891	0.0354	0.42205	0.01913	0.0354	0.42409
Histone H3 deacetylation	0070932	8	0.419	0.02819	0.04091	0.56227	0.03028	0.04161	0.56796
Relaxation of smooth muscle	0044557	6	0.679	0.03185	0.04117	0.56279	0.03219	0.04121	0.56348
Midbrain-hindbrain boundary development	0030917	3	0.267	0.03285	0.04178	0.72697	0.03382	0.04319	0.72413
GDP-mannose metabolic process	0019673	5	0.252	0.03451	0.04275	0.7401	0.03368	0.04445	0.73884
Protein deacetylation	0006476	20	0.664	0.04114	0.04456	0.76723	0.04009	0.04284	0.76878
Regulation of acyl-CoA biosynthetic process	0050812	4	0.358	0.04459	0.04469	0.89405	0.04633	0.04556	0.89682
Germinal center B cell differentiation	0002314	2	0.073	0.0467	0.04469	0.89405	0.04618	0.04556	0.89682
Negative regulation of nuclear division	0051784	24	0.774	0.04736	0.04683	0.97779	0.04927	0.04737	0.97771

Table 3.2 Biological processes enriched in the developmental profile DMRs

3.3.2.4 The *Ddr4* DMR was verified by bisulfite pyrosequencing

Given that meDIP-seq provides a relative signal of DNA methylation levels, we verified the PAE-specific DMRs using bisulfite pyrosequencing, a quantitative measure of DNA methylation, to ensure that MeDIP-seq could accurately detect alterations in DNA methylation patterns. Importantly, this technique also detects DNA hydroxymethylation, but cannot differentiate between the different cytosine modifications, while MeDIP-seq is specific to DNA methylation. We assessed four different DMRs, based on their potential role in the etiology of PAE-induced deficits.

We first assayed 16 CpGs within the 3' UTR of the *Drd4* DMR (chr1:214,281,174-214,281,640) in the same samples as the meDIP-seq analysis (Figure 3.4). This analysis detected a >5% change in DNA methylation across the DMR on P1 in PAE compared to Control animals. At older ages, several of the CpGs remained significantly different between PAE and controls, with several remaining present on P22. Overall, bisulfite pyrosequencing showed the same direction of change as the meDIP-seq analysis in this DMR.

We also used this method to verify three additional DMRs, located within *Ifih1* (chr3:48,561,559-48,561,925), *Mycbp* (chr5:141,565,784-141,566,172), and *Plvap* (chr16:19,912,813-19,913,185) (Supplementary figure 3.6). These showed less consistent changes in DNA methylation between the two methods, as some ages appeared to drive DNA methylation patterns more than others and some CpGs showed opposite direction of change between meDIP-seq and pyrosequencing. Nevertheless, small differences were identified between groups, suggesting that meDIP may be sensitive enough to detect small changes in DNA methylation levels. Of note, only a portion of CpGs within each DMR were assessed by bisulfite pyrosequencing due to limitations in read length, suggesting that additional CpGs within

the DMR may partially drive some of the differential DNA methylation enrichment identified by meDIP-seq.

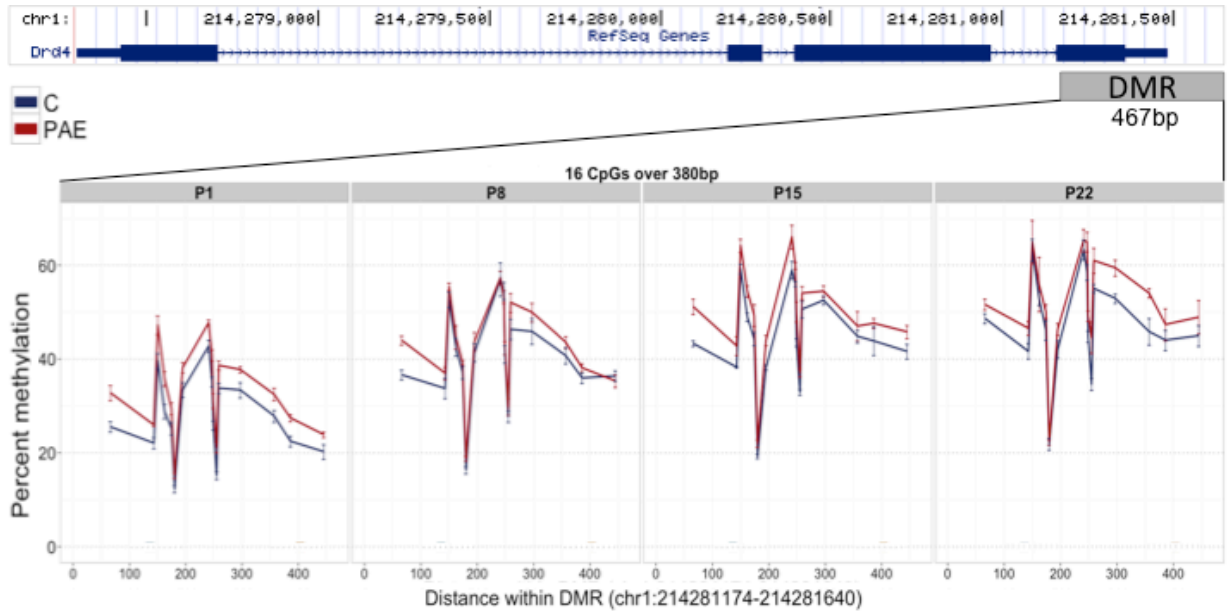

Figure 3.4 Bisulfite pyrosequencing verification of the *Drd4* DMR

16 CpGs spanning 380 base pairs (bp) of the DMR located in the 3' UTR of *Drd4* were verified by pyrosequencing in the same animals as the meDIP-seq analysis. All CpGs on P1 displayed >5% change in DNA methylation levels between PAE (red) and controls (blue). Of these, several were consistently different across all ages and a number persisted until P22. The total levels of DNA methylation in the DMR also increased with age across all groups.

3.3.3 Tissue-concordant alterations to DNA methylation patterns

In parallel to the analysis of developmental DNA methylation in the hypothalamus, we used meDIP-seq to assay DNA methylation in the hypothalamus and WBC of the same P22 females. This analysis aimed to identify tissue-concordant alterations present in both the CNS and peripheral tissue in response to PAE.

3.3.3.1 White blood cell proportions were not different across groups

As noted, cell type proportions are a major driver of epigenetic variability. However, the volume of blood collected from P22 animals was too small to perform both epigenetic and blood composition analyses on the same animals. As such, we collected samples from P22 animals from an independent but parallel cohort to determine whether PAE alters the proportion of the different WBCs that would be collected using the *Ficoll-Paque* method. Composition analysis of whole blood indicated the proportions of lymphocytes, neutrophils, monocytes, basophils, eosinophils, and large unclassified cells. Linear modeling revealed no significant differences among prenatal treatment groups, suggesting that PAE does not alter the proportion of the major WBC subtypes (Supplementary figure 3.7). These findings suggested that WBC proportions might not influence differences in DNA methylation patterns between groups in the present dataset.

3.3.3.2 Tissue-concordant alterations to DNA methylation patterns

To identify tissue-concordant alterations to DNA methylation patterns associated with PAE, we performed linear modeling on the BvB dataset with a model that also accounted for differences across breeding cohorts: ~Group+tissue+breeding. This method results in the identification of 300 PAE-specific DMRs at an FDR <0.05 that were present in both tissues and showed the same direction of change in PAE animal compared to controls (Figure 3.5; Supplementary table 3.6). Of these, 105 were up-methylated and 195 were down-methylated in PAE animals, and their size ranged from 355 to 2038bp (median = 574). The majority of DMRs also displayed tissue-specific effects in the relative enrichment of DNA methylation, although the magnitude of change was similar between PAE and controls across both tissues (Figure 3.6).

Moreover, unsupervised hierarchical clustering of samples using only the PAE-specific DMRs caused the control groups to cluster by tissue, rather than group. By contrast, the PAE were more closely related than those of the PF and C animals, regardless of tissue-type, highlighting that these DMRs likely reflect a mark of alcohol exposure (Figure 3.5).

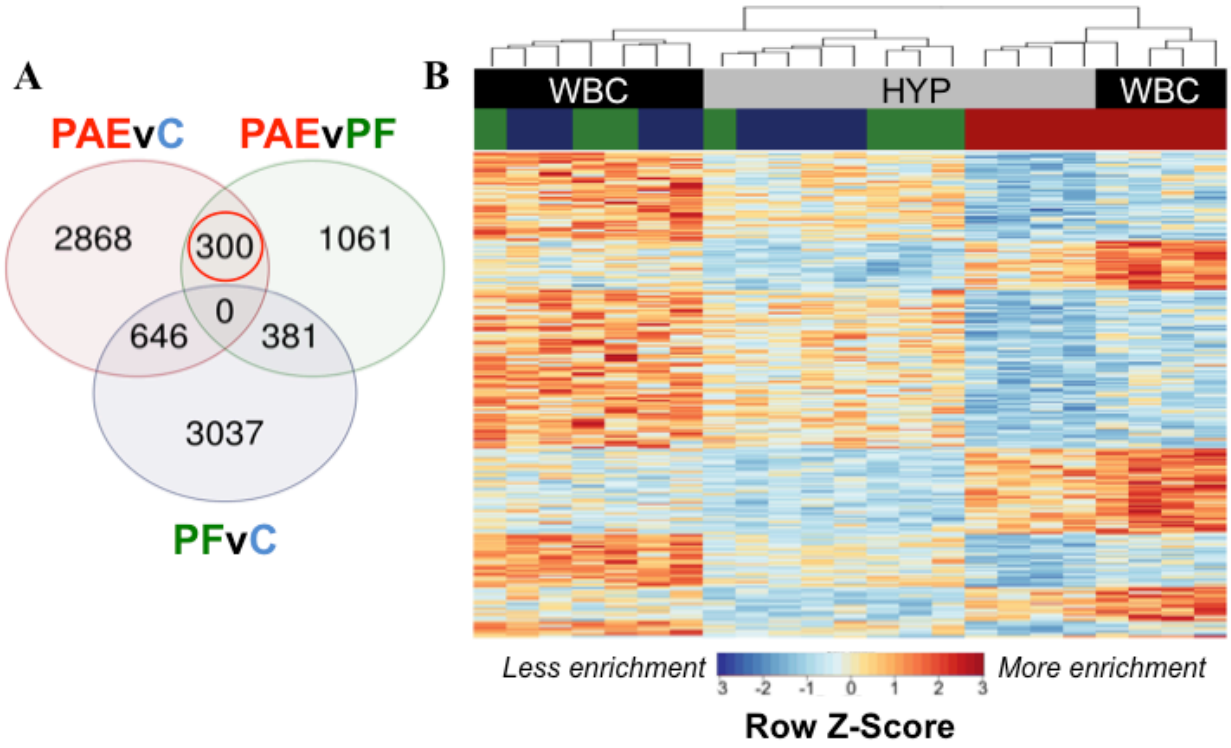

Figure 3.5 PAE-specific DMRs concordant across the hypothalamus and white blood cells

A) Contrast analysis revealed 300 PAE-specific differentially methylated regions (DMR) between both tissues, which were significantly different in PAE versus C animals and PAE versus PF animals, but not significantly different between PF versus C. B) Heatmap of the DMRs. Each row represents a different DMR, while each column shows the meDIP-seq data for each animal (n=4, except PF WBC: n =3). Reads per kilobase per million (RPKM) data were scaled and centered to produce a Z-score for each DMR, where those in blue showed less DNA methylation enrichment and those in red showed more enrichment. Samples were grouped using unsupervised hierarchical clustering, causing PAE samples to first cluster together and samples in general to separate by tissue. PAE-specific DMRs showed the same direction of change in both tissues, with some graded effects of tissue type.

Again, the majority of DMRs were located in intergenic regions, and were not associated with any gene (Figure 3.6A). However, the DMRs showed decreased enrichment in intergenic regions compared to background levels and more enrichment in intron/exons boundaries, which was driven mainly by the down-methylated regions. These results may reflect the role of DNA methylation in the regulation of splice variants, which could potentially be affected by PAE. Overall, 75 DMRs were located in genes, although the majority of these were once again located in intronic regions. Several DMRs were located in genes involved in immune function (*Fgf9*, *Il18r1*) and alcohol metabolism (*Adh4*). Of note, one DMR spanned 9 different isoforms of the Utg1a family of genes, while *Caln1* and *Cntnap5c* each contained three separate DMRs.

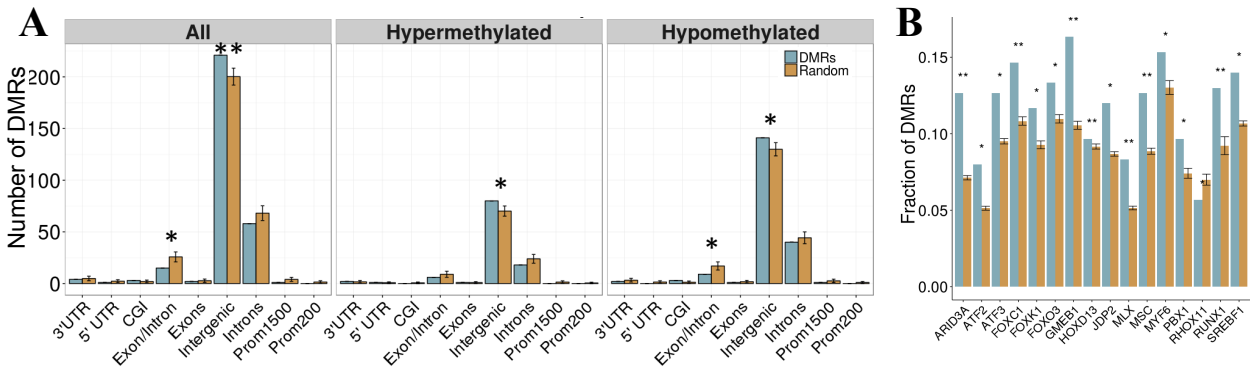

Figure 3.6 Enrichment patterns of the tissue-concordant DMRs

A) Genomic feature enrichment profile of all, up-methylated, and down-methylated DMRs. The probe counts for each feature (blue) were compared to the results from permutation analyses of 300 random regions (orange), which were used to compute the p-value. While the majority of DMRs were located in intergenic regions, they showed a lower proportion than expected by random change ($p<0.01$). By contrast, exon/intron boundaries were overrepresented in the DMRs, particularly within the regions that were down-methylated in PAE animals. B) Overrepresentation analysis of transcription factor binding sites in the DMRs. Several TFBS showed higher enrichment in the tissue-concordant DMRs (blue) than expected by random chance (orange), with GMEB1 showing the highest enrichment at 17% of all DMRs. *$p<0.05$, **$p<0.01$.

3.3.3.3 Several bioinformatically-predicted TFBS were enriched in cross-tissue PAE-specific DMRs

We assessed the enrichment of TFBS within these cross-tissue PAE-specific DMRs to follow up on potential regulatory regions. Following multiple-test correction (FDR<0.05), we identified 16 TFBS enriched within these regions compared to background levels (Figure 3.6B). The most frequent motif belonged to GMEB1, which was found in 16% of all DMRs. Several binding sites for the forkhead box (FOX) family of transcription factors were also enriched in these regions. Of note, the enrichment of Mlx and Srebf1 motifs in the cross-tissue DMRs overlapped with the results from the developmental profile.

3.3.3.4 Genes in cross-tissue PAE-specific DMRs were enriched for various biological processes

We performed GO analysis to ascertain the broad functional impact of PAE-induced changes in DNA methylation patterns across the hypothalamus and WBC. We identified 35 PAE-specific biological processes ($p<0.05$ in PAEvC and PAEvPF, $p>0.05$ in PFvC; Table 3.3). Of note, the top GO terms were associated with metabolic processes, including aldehyde metabolism (GO:0006081). Several processes were also associated with immune function (GO:0045063, GO:0071351, GO:0032733, GO:0070673, GO:2674), chromatin remodelling (GO:6338, GO:90239), and the stress response (GO:42320).

Name	ID	Number of genes	Multi-functionality	P-value			Multifunctionality p-value		
				PAEvC	PAEvPF	PFvC	PAEvC	PAEvPF	PFvC
Cellular aldehyde metabolic process	6081	29	0.785	0.00089	0.00081	0.0531	0.00094	0.00093	0.05423
T-helper 1 cell differentiation	45063	5	0.483	0.0026	0.00284	0.0531	0.00261	0.00319	0.05423
Amino-acid betaine metabolic process	6577	10	0.484	0.00275	0.00383	0.05739	0.0028	0.0034	0.058
Carnitine metabolic process	9437	7	0.36	0.00284	0.00414	0.06279	0.00321	0.00391	0.06181
Osteoblast fate commitment	2051	2	0.224	0.0044	0.00465	0.09845	0.00413	0.00434	0.09938
Plasma membrane repair	1778	7	0.109	0.00599	0.0051	0.1162	0.00631	0.00474	0.11789
Negative regulation of circadian sleep/wake cycle, REM sleep	42322	2	0.324	0.00788	0.0051	0.14968	0.00829	0.00474	0.15006
Chromatin remodeling	6338	43	0.753	0.01171	0.00597	0.17051	0.01135	0.00569	0.17029
Negative regulation of axon regeneration	48681	3	0.41	0.01139	0.0092	0.17521	0.01204	0.00896	0.17422
Regulation of natural killer cell cytokine production	2727	2	0.293	0.01217	0.01155	0.17521	0.01348	0.01048	0.17422
Positive regulation of natural killer cell cytokine production	2729	2	0.293	0.01217	0.01082	0.22896	0.01348	0.01057	0.2317
Amino-acid betaine biosynthetic process	6578	5	0.219	0.01428	0.01082	0.25627	0.01367	0.01057	0.25577
Glucose 1-phosphate metabolic process	19255	2	0.0827	0.01405	0.0106	0.29844	0.01546	0.01064	0.30042
Cellular response to interleukin-18	71351	2	0.23	0.01587	0.0114	0.31438	0.01748	0.01094	0.317
Protein K63-linked deubiquitination	70536	12	0.126	0.02072	0.01396	0.33657	0.02115	0.01351	0.33588
Carnitine biosynthetic process	45329	3	0.085	0.02242	0.01864	0.34572	0.02301	0.02005	0.34264
Positive regulation of interleukin-10 production	32733	15	0.81	0.02457	0.02429	0.34572	0.02509	0.02327	0.34264
Response to jasmonic acid	9753	3	0.405	0.02597	0.02429	0.37241	0.02675	0.02327	0.36841
Cellular response to jasmonic acid stimulus	71395	3	0.405	0.02597	0.02776	0.38417	0.02675	0.02755	0.38807
Response to interleukin-18	70673	3	0.404	0.02741	0.03021	0.44431	0.02814	0.02905	0.44259
Cofactor catabolic process	51187	13	0.638	0.0291	0.03294	0.44477	0.02836	0.03162	0.44499
Extracellular polysaccharide biosynthetic process	45226	2	0.12	0.02809	0.03374	0.50515	0.02987	0.03253	0.50571

Name	ID	Number of genes	Multi-functionality	P-value			Multifunctionality p-value		
				PAEvC	PAEvPF	PFvC	PAEvC	PAEvPF	PFvC
Extracellular polysaccharide metabolic process	46379	2	0.12	0.02809	0.03382	0.53397	0.02987	0.03259	0.53274
Acetaldehyde metabolic process	6117	2	0.216	0.03048	0.03547	0.53397	0.03224	0.03553	0.53274
Protein K48-linked deubiquitination	71108	12	0.0357	0.0314	0.03784	0.58202	0.03277	0.03703	0.57955
Cellular response to light stimulus	71482	38	0.821	0.03665	0.03755	0.58809	0.03621	0.03751	0.58519
Podosome assembly	71800	3	0.0518	0.03607	0.03755	0.61294	0.03643	0.03751	0.61412
Micturition	60073	5	0.536	0.04093	0.03865	0.65836	0.03964	0.0376	0.65844
Regulation of histone H4 acetylation	90239	5	0.465	0.04093	0.03969	0.66132	0.03964	0.03965	0.66174
Adenylate cyclase-activating G-protein coupled receptor signaling pathway	7189	26	0.73	0.038	0.04176	0.7519	0.03969	0.04102	0.75163
ER to Golgi ceramide transport	35621	2	0.11	0.03821	0.04171	0.76157	0.03982	0.04149	0.75818
Ceramide transport	35627	2	0.109	0.03821	0.04174	0.81677	0.03982	0.04231	0.81613
Glycolipid transport	46836	2	0.0288	0.03821	0.04318	0.84505	0.03982	0.0426	0.84661
Regulation of circadian sleep/wake cycle, REM sleep	42320	4	0.439	0.04575	0.04318	0.86337	0.04542	0.0426	0.86292
Negative regulation of acute inflammatory response	2674	6	0.674	0.04567	0.04881	0.94037	0.04575	0.04964	0.93962

Table 3.3 Biological processes enriched in the tissue-concordant DMRs

3.3.3.5 Verification of DMRs by bisulfite pyrosequencing

We used bisulfite pyrosequencing to compare quantitative levels of DNA methylation between PAE and Control animals in three cross-tissue DMRs. More specifically, we analyzed DNA methylation in the final exon and 3' UTR of *Adh4* (chr2: 243,719,416-243,720,233), the first exon and 5' UTR of *Ctnnbip1* (chr5: 166,485,057-166,485,637), and the first intron of *Ffg9* (chr15: 38,377,629-38,378,027) (Supplementary figure 3.8). The main differences in DNA methylation levels were identified between tissues, which sometimes showed different directions of change between PAE and Controls. In particular, a CpG within the *Adh4* DMR showed a close to 5% methylation difference in the hypothalamus of PAE animals, but this effect was not present in WBC. Another CpG within the *Adh4* locus showed small changes that were consistent between tissues. This pattern was also observed in the *Fgf9* locus, which suggested that these may be small, but systemic effects of PAE. By contrast, the *Ctnnbip1* locus showed opposite effects between tissues (decreased in the hypothalamus; increased in WBC), suggesting that other factors may come into play. Moreover, as we did not assess quantitative DNA methylation level across the entire DMR due to pyrosequencing limitations, other CpGs may drive the enrichment patterns previously identified by meDIP-seq.

3.4 Discussion

Alcohol exposure *in utero* appears to reprogram physiological and neurobiological systems, increasing the risk of adverse developmental outcomes across the lifespan (Zhang, Sliwowska, & Weinberg 2005; Pei et al. 2011; Mattson, Crocker, & Nguyen 2011). Given the potential role of epigenetic mechanisms in mediating the long-term effects of PAE, the present study aimed to extend previous work on the influence of *in utero* alcohol exposure on the

epigenome, using an animal model of PAE to assess genome-wide DNA methylation patterns during early postnatal development. We identified 118 differentially methylated regions (DMRs) that were altered in the hypothalamus of PAE versus control animals across the pre-weaning period. In parallel, we found 300 DMRs displaying concordant DNA methylation alterations between the hypothalamus and WBC of PAE animals at weaning. Several differentially methylated genes were functionally related to the PAE-induced deficits, including roles in the immune response, neurobiological function, and mental health, while functional enrichment revealed several PAE-specific biological processes, including those related to immune function, the stress response, and epigenetic regulation. In addition, we identified several transcription factor bindings sites that were enriched in the DMRs, which may potentially reflect broader programming effects of PAE on the epigenome. Overall, these findings suggested that PAE causes broad alterations to epigenomic programs in both the CNS and peripheral tissues, suggesting that alterations to DNA methylation patterns could influence broader neurobiological and physiological systems and potential act as biomarkers of PAE.

Our initial analysis of the DMRs revealed several differentially methylated genes that could potentially be relevant to PAE-induced deficits. In particular, the dopamine receptor D4 (*Drd4*) gene contained a DMR that persisted across the early developmental period. Given its crucial role in dopaminergic function, as well as interactions among dopaminergic, neuroendocrine, and immune systems, alterations to this gene could reflect broader alterations to signaling in the brain. Interestingly, differential DNA methylation patterns of *Drd4* are also present in the buccal epithelial cells of individuals with FASD, suggesting that this may be a robust effect of PAE on the epigenome (Portales-Casamar et al. 2016; Fransquet et al. 2016). In

addition to this association with FASD, genetic and epigenetic variation in *Drd4* has been linked to attention deficit hyperactivity disorder (ADHD), schizophrenia, bipolar disorder, substance-use disorders, and several other neurobiological disorders (Dadds et al. 2016; Ji et al. 2016; Cheng et al. 2014; Kordi-Tamandani, Sahranavard, & Torkamanzehi 2013; Docherty et al. 2012; Ptáček, Kuželová, & Stefano 2011; Bau et al. 2001; Zhang H. et al. 2013; Faraone, Bonvicini, & Scassellati 2014; Chen et al. 2011). Moreover, *Golga4* contained 2 PAE-specific DMRs across hypothalamic development, and is known to be overexpressed in the prefrontal cortex of individuals with bipolar disorder (Iwamoto et al. 2004). As a member of the Golgi secretory pathway, it could also potentially influence the secretion of neuropeptides by cells of the hypothalamus, possibly playing a role in altered function or responsivity following PAE (Wong & Munro 2014). Similarly, *Plvap* expression increases the breakdown and permeability of the blood-brain barrier (BBB) (Shue et al. 2008). As such, slight alterations to its DNA methylation profile could reflect broader effects on the BBB, which, in turn, could affect downstream neurobiological functions.

The tissue-concordant DMRs also contained several genes previously associated with mental health disorders. In particular, *Adh4* was differentially methylated across the hypothalamus and WBC of PAE animals, and has been previously associated with alcohol dependence and substance abuse (Luo et al. 2005). Importantly, it is a key component of alcohol metabolism pathways, and could reflect increased susceptibility to the effects of alcohol during development. Furthermore, *Caln1* contained 3 separate DMRs, and as it contains a risk allele for schizophrenia in some human populations, it could also play a role in the etiology of FASD (Li et al. 2015).

Of note, two genes displayed differential DNA methylation patterns in both the developmental profile and tissue-concordance analysis, *Cntnap5c* and *Ush2a*, which may reflect robust alterations to DNA methylation patterns across both age and tissue types. In humans, genetic variation in *Cntnap5* is associated with risk for Alzheimer's disease and bipolar disorder, while its deletion is associated with autism and dyslexia, suggesting that common pathways may come into play between these disorders and FASD (Schott et al. 2016; Xu et al. 2014; Pagnamenta et al. 2010). By contrast, mutations in *Ush2a* cause Usher syndrome II, which is associated with hearing deficiencies, deficits also commonly found in individuals with FASD (Church & Gerkin 1988). Finally, several DMRs in both datasets were located in genes associated with immune function and response. In particular, *Ifih1* was identified across all ages in the hypothalamus; as a receptor for double stranded RNA that responds to viral infections, it could be associated with vulnerability to neuroimmunological deficits (Rice et al. 2014). *Fgf9*, a key factor in embryonic and glial cell development, was also differentially methylated in both the hypothalamus and WBC (Thisse & Thisse 2005). Furthermore, this growth factor promotes pro-inflammatory environments through Ccl2 and Ccl7 chemokine secretion, consistent with several DMRs that were located in genes associated with pro-inflammatory cytokine and chemokine signaling (Lindner et al. 2015). These included *Il20ra* and *Ccrl2* in the developmental profile, and *Il18r1* in the tissue-concordance analysis, suggesting that PAE can influence inflammatory pathways through epigenetic pathways, and ultimately, alter the cellular response to immune challenges.

We also assessed the functional enrichment of genes located within PAE-specific DMRs, identifying a number of biological processes associated with differential DNA methylation

patterns in PAE animals compared to controls. In the DMRs identified across hypothalamic development, a large number of GO processes were associated with functions in steroid receptor signaling. The hypothalamus is central to numerous physiological systems that function through steroid hormones, many of which are dysregulated by PAE. As such, this enrichment pattern suggests that DNA methylation may play a role in the reprogramming of hormonal systems during early development, potentially priming physiological systems to new set-points. In addition, several processes in both the developmental and tissue-concordant DMRs were associated with epigenetic regulation, which may reflect the complex interplay between different layers of the epigenetic machinery. Several studies have identified alterations to histone modifications in the brain following developmental alcohol exposure, further highlighting their potential role in FASD (Goldowitz et al. 2014; Chater-Diehl et al. 2016; Veazey et al. 2015; Subbanna et al. 2014, 2013; Zhang et al. 2015; Lussier, Weinberg, & Kobor 2017; Guo et al. 2011; Govorko et al. 2012; Bekdash, Zhang, & Sarkar 2013). A large number of immune-related biological processes were also identified through this analysis, which further highlights the bidirectional communication between the stress response and immune system. Given the close relationship between these systems, altered responsivity of the hypothalamus to immune challenge could potentially alter the organism's ability to defend against disease or infection. In addition, the top GO term associated with PAE in the tissue-concordant DMRs was "cellular aldehyde metabolic process", which may reflect lasting effects of PAE on the organism's ability to metabolize alcohol's metabolic byproducts and possibly modulate susceptibility to substance abuse later in life. While no overlaps were identified between the specific biological processes identified in the developmental profile and tissue-concordance analyses, both contained a high proportion of processes with immune, endocrine, or epigenetic functions. These findings suggest

that PAE may cause systemic effects on the epigenome across multiple tissue types, which may, in turn, influence downstream neurobiological and physiological processes.

Previous studies have identified subtle effects of PAE on gene expression programs and epigenomic patterns, which is consistent with the effects of other prenatal exposures (Laufer et al. 2013; Chater-Diehl et al. 2016; Zhou, Balaraman, et al. 2011; Ladd-Acosta et al. 2014; Berko et al. 2014; Rakyan et al. 2011; Lussier et al. 2015). Regions containing lower CpG density appear to be more responsive to environmental exposures, highlighting the importance of selecting a method that covers a large portion of the epigenome when analyzing an exposure with rather subtle effects (Irizarry et al. 2009a). Thus, we analyzed genome-wide DNA methylation using MeDIP-seq, which is unbiased towards less variable CpG-rich regions and simultaneously reduces the complexity of the dataset by omitting unmethylated regions. As expected, few DMRs across both analyses were identified in CpG-dense regions, such as promoters and CpG islands, while the majority of DMRs were located in intergenic regions and introns, and several were located in intron/exon boundaries, particularly within the down-methylated tissue-concordant DMRs. Given that DNA methylation plays a role in regulating alternative splice variants, these findings may reflect alterations to the balance of different isoforms within the cell, which could influence downstream cellular profiles and phenotypes (Shukla et al. 2011; Maunakea et al. 2013, 2010). Although isoform balance has not been investigated in the context of PAE, studies have shown that alcohol consumption in general can influence the proportions of different splice variants in the brain, supporting a potential role in early-life exposures as well (MacKay et al. 2011; Farris et al. 2015; Lee, Mayfield, & Harris 2014; Mathew et al. 2016). Interestingly, a larger proportion of down-methylated DMRs were

identified in both analyses, which is consistent with several studies showing that PAE decreases bulk DNA methylation levels (Otero et al. 2012; Perkins et al. 2013; Chen, Ozturk, & Zhou 2013; Mukhopadhyay et al. 2013; Nagre et al. 2015; Liyanage et al. 2015). These findings provide important insight into different outcomes in different paradigms of alcohol exposure and suggest that similar upstream mechanisms may impact DNA methylation across models, potentially involving changes in one-carbon metabolism or in the activity of DNA methyltransferases.

The large proportion of DMRs located in intergenic regions suggested that these could contain regulatory regions susceptible to the influence of PAE. Given that the rat genome is poorly annotated for regulatory features, we assessed the enrichment profiles of different transcription factor binding sites in the DMRs, which could be influenced by DNA methylation levels within specific loci. While only the binding site for the BHLHE40 transcription factor was significantly enriched in PAE-specific DMRs across early development, we previously identified this gene as differentially expressed in the adult brain of PAE (Lussier et al. 2015). This gene negatively regulates the circadian rhythm, a key function of the hypothalamus that is dysregulated in individuals with FASD (Nakashima et al. 2008). The BHLHE40 transcription factor could potentially play a role in early programming effects of PAE on neurobiological systems, with persistent expression and downstream effect into later life. By contrast, the tissue-concordant DMRs contained a high proportion of significantly enriched TFBS, including SREBF1, which trended towards significance in the developmental profile DMRs. SREBF1 is associated with key metabolic processes for hormonal signaling, as it plays a role in the regulation of cholesterol production (Osborne 2001). It is also associated with Smith–Magenis

syndrome, which is characterized by intellectual disability, disordered sleeping, and behavioral problems (Smith et al. 2002). Furthermore, additional TFBS enriched in the BvB dataset included several members of the forkhead box (FOX) family of genes, FOXC1, FOXK1, and FOXO3. In particular, FOXO3 was identified as a hub gene in the brain PAE animals following an immune challenge, suggesting that it may prime biological systems from early in life (Lussier et al. 2015). Finally, the highest represented TFBS in the BvB dataset belonged to GMEB1, which is involved in signal transduction of the glucocorticoid response (Zeng, Kaul, & Simons 2000). Taken together, these findings suggest that the DMRs identified in both the developmental and tissue-concordance analyses may contain key regulatory regions, and that various transcription factors likely act in concert with DNA methylation to mediate the effects of PAE.

Although meDIP-seq allows for the investigation of more variable regions of the epigenome, it presents a particular caveat when assessing DNA methylation levels, as it provides relative levels of DNA methylation across broad regions of the genome, rather than quantitative and granular data. As such, we undertook to verify our findings from the meDIP-seq analysis through bisulfite pyrosequencing, the gold standard for targeted DNA methylation analyses. A limitation of this approach is that bisulfite pyrosequencing detects both methylated and hydroxymethylated cytosines, and there is no way to distinguish the two when analyzing the results from pyrosequencing, resulting in a mixed signal. By contrast, meDIP-seq specifically enriches DNA methylation, as the antibody is highly specific to 5-methylcytosine (Taiwo et al. 2012). In this context, we found that some of the bisulfite pyrosequencing results did not fully confirm the effects observed by meDIP-seq. However, given that neuronal cells contain a high

proportion of DNA hydroxymethylation compared to other cell types, it is possible that the observed differences in methodologies are due to the confound of additional epigenetic patterns not assessed in the meDIP-seq analysis. Indeed, a number of studies have shown that developmental alcohol exposure can alter DNA hydroxymethylation programs in neuronal cells in addition to DNA methylation, suggesting that it may also play a role in the etiology of FASD (Chen, Ozturk, & Zhou 2013; Öztürk et al. 2017). In addition, the lack of confirmation could potentially be due to the small number of animals used in the present study, as well as increased variability in the enrichment profiles obtained from meDIP-seq, given the broader regions assessed. Nevertheless, the *Drd4* locus identified in the developmental profile of the hypothalamus displayed consistent DNA methylation alterations in both methods, suggesting that meDIP-seq can capture differences in DNA methylation patterns, regardless of the influence of DNA hydroxymethylation. Additional studies are required to fully validate these findings and assess their relationship to the deficits observed following PAE.

One of the main strengths of animal models derives from their ability to directly compare central and peripheral tissue to ascertain potential correlations between the two, which may identify potential biomarkers reflective of brain function in a tissue that is available for study in human populations. In that regard, however, cell type heterogeneity is a major driver of DNA methylation patterns (Farré et al. 2015). Thus, we attempted to partially correct for cellular heterogeneity between groups by removing regions that were associated with the major cell types in the brain, neurons, astrocytes, and oligodendrocytes (Cahoy et al. 2008). However, additional cellular subtypes, such as glia, are also present in the hypothalamus, and could have influenced the results here without our knowledge. We were also limited by the use of regions located

within genes, and thus could not correct for intergenic regions that may be associated with cell type.

By contrast, we measured the proportion of different WBC subtypes in an independent cohort of animals. The fact that we did not identify any significant differences in WBC composition of whole blood among groups suggests that this may not have been a factor in driving the DMRs identified in the tissue-concordant analysis. However, as *Ficoll-Paque* is a highly technical procedure, differences between WBC extractions could have influenced the proportions of cells analyzed in the present study, and we could not correct for such effects. Additionally, as these subtypes can be further subdivided through more sophisticated methods such as fluorescence-activated cell sorting, there is still a possibility that group differences may exist. In contrast to clinical studies of DNA methylation, no bioinformatic tools exist to predict the proportion of different cell types using epigenomic profiles in rats, and future studies should take this into consideration. Nevertheless, we successfully identified several PAE-specific DMRs that showed the same direction of change between the two tissues, suggesting that these regions may be responsive to ethanol across multiple tissues and may represent more stable biomarkers of PAE.

3.5 Summary and conclusions

Our results support a role for DNA methylation in the early-life reprogramming of hypothalamic functions by PAE, and suggest that DNA methylation patterns in WBC could potentially be used as a surrogate for alterations in the central nervous system. We identified persistent PAE-induced alterations to the DNA methylome of the hypothalamus, including several DMRs that could, at least in part, underlie some of the deficits observed in FASD.

Although PAE-induced alterations to DNA methylation profiles at any of these development ages may not persist into adulthood, changes early in development could alter the developmental trajectory and induce lasting alterations in brain structure and connectivity, or prime physiological systems to different set-points. Of note, we demonstrate for the first time that PAE-specific DMRs can occur across central and peripheral tissues, which potentially represent systemic effects of PAE on the epigenome, and could serve as an epigenetic biomarker or signature of FASD. Taken together, these findings provide insight into the important role of epigenetic alterations in the short and long-term deficits observed in FASD, and provide a foundation for the development of robust biomarkers of PAE.

Chapter 4: DNA methylation signature of human fetal alcohol spectrum disorder

4.1 Background and rationale

The prenatal environment has the potential to permanently imprint physiological and behavioural systems during development, leading to both short and long-term health consequences. In particular, prenatal alcohol exposure (PAE) can alter the development, function, and regulation of numerous neural and physiological systems, resulting in a variety of deficits falling under the umbrella of Fetal Alcohol Spectrum Disorder (FASD) (Mattson, Crocker, & Nguyen 2011). Over the lifetime, the effects of prenatal alcohol exposure are manifested through cognitive and behavioural deficits, persistent alterations to stress responsivity and immune function, and increased vulnerability to mental health disorders and other comorbidities in individuals with FASD (Zhang, Sliwowska, & Weinberg 2005; Pei et al. 2011; Mattson, Crocker, & Nguyen 2011; Popova et al. 2016). However, the degree to which alcohol exposure causes alterations during development varies, depending on factors such as timing and level of exposure, overall maternal health and nutrition, and genetic background (Pollard 2007). As such, only a small proportion of affected children present with the phenotype of Fetal Alcohol Syndrome (FAS), which is distinguished by growth deficits and facial dysmorphisms in addition to central nervous system dysfunction (Jones & Smith 1973; Astley & Clarren 2000). Nevertheless, the vast majority of children with FASD display physiological and neurobehavioral impairments lasting into adulthood, suggesting persistent programming effects of PAE across the spectrum of FASD (Jacobson et al. 2011).

While the etiology of the FASD currently remains unclear, epigenetics is emerging as an attractive candidate for the biological embedding of prenatal and early life experiences in general, and thus is a promising avenue for the study of FASD (Feil & Fraga 2012). Epigenetics refers to modifications of DNA and its packaging that alter the accessibility of DNA, to potentially regulate gene expression and cellular function without changes to the underlying genomic sequences (Bird 2007). The most studied epigenetic modification in human populations is DNA methylation, which refers to the covalent attachment of a methyl group to the 5' position of cytosine, typically occurring in the context of cytosine-guanine dinucleotide (CpG) sites (Jones & Takai 2001). CpG sites are relatively rare in the human genome, yet do not occur at random; regions containing higher than expected levels of these dinucleotides have been termed 'CpG islands' (CGIs) (Illingworth & Bird 2009). The 2kb regions flanking CGIs are known as CGI 'shores', while the areas located beyond shores are known as 'shelves' (Doi et al. 2009; Irizarry et al. 2009a; Bibikova et al. 2011). Of note, these regions typically are more variable than CGIs themselves, as they have a greater range of DNA methylation across individuals (Irizarry et al. 2009a). DNA methylation is associated with the regulation of gene expression, although its effects on transcription are highly dependent on genomic context. For example, when located within gene promoters, DNA methylation generally represses gene expression, but this relationship is less well defined for CpGs located within gene bodies and intergenic regions (Jones 2012). Furthermore, DNA methylation is closely associated with several key developmental processes, including genomic imprinting, as well as tissue specification and differentiation (Ziller et al. 2013; Smith & Meissner 2013). DNA methylation patterns are also population-specific, as a number of CpG sites are associated with ethnicity (Fraser et al. 2012; Moen et al. 2013; Heyn et al. 2013). There are a number of possible reasons for this association,

including shared environments or associations of epigenetic marks with specific genetic variants (Gutierrez-Arcelus et al. 2013; Wagner et al. 2014; Banovich et al. 2014).

Importantly, DNA methylation is malleable in response to environmental factors and these changes may be inherited through cell divisions, potentially persisting throughout the lifetime (Langevin et al. 2011; Hanson et al. 2011; Yuen et al. 2011). For example, prenatal exposure to cigarette smoke is associated with long-term changes in DNA methylation of the *AHRR* gene, and maternal under-nutrition during pregnancy leads to altered DNA methylation of *IGF2* (Joubert et al. 2012; Heijmans et al. 2008). Several studies have also characterized epigenetic changes following prenatal and postnatal ethanol exposure (Haycock 2009; Haycock & Ramsay 2009; Kobor & Weinberg 2011; Ungerer, Knezovich, & Ramsay 2013; Laufer, Diehl, & Singh 2013; Resendiz et al. 2013; Ramsay 2010). Early work in pregnant mice demonstrated that acute ethanol exposure during mid-gestation (gestational days 9 to 11) causes global genomic loss of DNA methylation in the fetus (Garro et al. 1991). However, recent studies of embryonic cultures exposed to ethanol show that rather than a global demethylation of the genome by ethanol, some regions become more methylated and others less methylated (Liu et al. 2009). Moreover, genome-wide studies in adult mice that were exposed to ethanol prenatally have also identified widespread changes in DNA methylation patterns in the entire brain, further suggesting an important role for epigenetics in the etiology of FASD (Laufer et al. 2013). Finally, a recent study characterized the DNA methylation profile in buccal epithelial cells (BECs) from a small cohort of human FASD samples, identifying alterations in the epigenome of children with FASD, particularly within the protocadherin gene clusters (Laufer et al. 2015).

Collectively, these findings support epigenetic mechanisms as potential contributors to the deficits observed following PAE. However, no large-scale investigations of DNA

methylation in individuals with FASD have been performed to date. In order to ascertain the effect of PAE on the human epigenome, the present study investigated the DNA methylation patterns of BECs from 110 children with FASD and 96 age- and sex-matched controls, to our knowledge representing the largest investigation on PAE effects on the human epigenome. Statistically significant alterations between FASD cases and controls were successfully identified following ethnic background correction, with a number of differentially methylated sites and regions located in genes previously associated with alcohol exposure (Liu et al. 2009; Laufer et al. 2015). Taken together, these results support a potential role for DNA methylation in the etiology of the neurobiological deficits observed in children with FASD and represent a potential epigenetic signature of FASD.

4.2 Materials and methods

4.2.1 Participants and samples

Children with FASD were recruited from multiple FASD diagnostic clinics across Canada and age- and sex-matched typically developing children were recruited in parallel. Saliva samples and buccal epithelial cells (BECs) were collected for genotyping and DNA methylation analysis respectively (Reynolds et al. 2011). Written informed consent was obtained from a parent or legal guardian and assent was obtained from each child before study participation. The majority of clinics used previously described guidelines for the diagnosis of FASD (Chudley et al. 2005). Briefly, samples were collected from 112 FASD and 102 age- and sex-matched control children aged between 5 and 18. Saliva samples were collected using the Oragene DNA kit (DNA Genotek Inc., Ontario, Canada) according to the manufacturer's instructions. BECs were collected using the Isohelix buccal swabs and Dri-Capsule (Cell Projects Ltd., Kent, UK). To

collect buccal cells, the swab was inserted into the participants' mouth and rubbed firmly against the inside of the left cheek for 1 minute. The swab was then placed into a sterile tube with a Dri-Capsule and the tube sealed. An identical procedure was followed for the right cheek. Participants did not have any dental work performed 48 hours prior to collection, and no food was consumed less than 60 minutes prior to collection to avoid contamination.

4.2.2 DNA methylation 450K assay

DNA was extracted from buccal swabs using the Isohelix DNA isolation kit (Cell Projects, Kent, UK). 750ng of genomic DNA was subjected to bisulfite conversion using the Zymo EZ DNA Methylation Kit (Zymo Research, Irvine, California), which converts DNA methylation information into sequence base differences by deaminating unmethylated cytosines to uracil while leaving methylated cytosines unchanged. 160ng of converted DNA was applied to the HumanMethylation450 BeadChip array from Illumina (450K array), which enables the simultaneous quantitative measurements of 485,512 CpG sites across the human genome, following the manufacturer's instructions. Chips were scanned on an Illumina HiScan, with the 214 samples run in two batches and each containing an equal number of FASD and control samples, randomly distributed across the chips. Two pairs of technical replicates were included and showed a Pearson correlation coefficient $r>0.996$ in both cases, highlighting the technology's reproducibility.

4.2.3 DNA methylation data quality control and normalization

The raw DNA methylation data were subjected to a set of rigorous quality controls, first of the samples, and then of the probes. Of the 214 initial samples, 8 were removed from the final

dataset due to various quality and concordance issues. Of these, five were removed based on poor quality data, which were identified through skewed internal controls and/or >=5 % of probes with a detection p-value > 0.05. One sample was removed due to a chromosomal abnormality identified in the genotyping and DNA methylation data (XXY; Klinefelter syndrome). The genotypes of the samples, based on the 65 SNP probes contained on the 450K array, were compared to the genotypes from the SNP arrays. The genotypes were highly correlated for all samples (Pearson correlation coefficient r > 0.9), except one, which was excluded from further analyses. Finally, as a pair of monozygotic twins was present in the control group, only one of their samples was chosen at random and retained in the analysis to remove any genetic bias. Next, probes were removed from the dataset according to the following criteria: (1) probes on X and Y chromosomes (N = 11648); (2) SNP probes (N = 65); (3) probes with beadcount <3 in 5 % of samples (N = 3029); (4) probes with 1% of samples with a detection p-value > 0.05 (N = 10163); or (5) probes with a polymorphic CpG and non-specific probes as defined by the Price annotation (N = 20869 SNP-CpG and 41937 non-specific probes; (Price et al. 2013)). A final filtering step was performed to set the methylation values to NA for any remaining probe-sample pair where beadcount <3 or detection p-value > 0.05. Data normalization was performed using the Beta-Mixture Quantile Normalization method on the final dataset, composed of 206 samples (110 FASD and 96 control) and 404,030 probes (Teschendorff et al. 2012). All analyses were performed using M-values, which represent the log2 ratio of methylated/unmethylated, where negative values indicate less than 50% methylation and positive values indicate more than 50% methylation (Du et al. 2010). Percent methylation changes (beta-values) were used in graphical representations of the data and indicate the

percentage of methylation calculated by methylated/(methylated + unmethylated), ranging from 0 (fully unmethylated) to 1 (fully methylated).

4.2.4 Differential methylation analysis

Given that DNA methylation changes are typically small and that unknown sources of variation, including cellular heterogeneity, may influence the data, surrogate variable analysis (SVA) was performed to identify surrogate variables (SVs) representative of unwanted heterogeneity using the SVA package in R (Leek et al. 2012). Using DNA methylation data from all 206 samples, SVA identified 15 SVs not associated with clinical status (FASD vs control), which, as expected, were only partially correlated with known covariates (Supplemental methods & Supplementary figure 4.2). Linear regression analysis was performed on the dataset with the *limma* package in R, utilizing a model that included clinical status and all identified SVs as covariates (Smyth 2004). Statistically significant differences between groups were required to show a false-discovery rate (FDR) <0.05 following multiple test correction by the Benjamini-Hochberg method (Benjamini & Hochberg 1995). Further evaluation of potential biological significance was assessed by mean percent DNA methylation differences between FASD and controls.

4.2.5 Analysis of effects due to familial and diagnosis status

As the cohort included several sets of siblings and cousins, a sensitivity analysis was performed to identify potential family effects in the dataset. However, little effect of familial origin was observed, indicating that the presence of families in the cohort did not significantly impact the study's results or require statistical correction (Supplemental methods). Furthermore,

this cohort also included children with prenatal alcohol exposure (PAE) that were not formally diagnosed with FASD (27 children). As such, additional differential DNA methylation analyses were performed on the two individual subgroups of FASD cases compared to controls (Supplemental methods & Supplementary figure 4.9). However, as these did not reveal any significant differences between diagnosed FASD cases and PAE children, the PAE cases were included in the FASD group for all analyses.

4.2.6 Genotyping

Genomic DNA was extracted from saliva samples following standard procedures. Briefly, 161 DNA samples were genotyped for 2,443,177 markers using the Infinium HumanOmni2.5-Quad v1.0 BeadChip (Illumina Inc., San Diego, CA, USA) and 54 samples were genotyped for 2,379,855 markers using the Infinium HumanOmni2.5-8 v1.0 BeadChip (Illumina Inc., San Diego, CA, USA) according to the manufacturer's protocol. For both microarrays, 200ng of DNA (4uL at 50ng/uL) was independently amplified, labeled, and hybridized to BeadChips, then scanned with default settings using the Illumina iScan. Analysis and intra-chip normalization of resulting image files was performed using Illumina's GenomeStudio Genotyping Module software v.2011 with default parameters. Genotype calls were generated using the Illumina-provided genotype cluster definitions files (HumanOmni2.5-4v1_H.egt and HumanOmni2.5-8v1_C.egt generated using HapMap project DNA samples) with a Gencall cutoff of 0.15. Only the 2 368 900 common SNPs were used for analysis. pyGenClean v1.2.2 and PLINK v1.07 were used for quality control and genetic data cleanup process. SNPs with completion rate <98%, uninformative (MAF=0) and failed for Hardy-Weinberg equilibrium

exact test (P value <2.9x10-8) were removed. Samples with completion rate <95% were excluded.

4.2.7 Sub-sample definition

Multi-dimensional scaling (MDS) was performed on the participants' genotype data including 83 founder individuals from the Caucasian population (CEU), 186 from the Japanese and Han Chinese population (JPT-CHB), and 88 from the Yoruba population (YRI) (HapMap; (International HapMap 3 Consortium et al. 2010)). All 195 samples that had both genotyping and DNA methylation data were hierarchically clustered based on the first 4 principal components from the MDS analysis. One individual of African descent was excluded because of their unique ethnicity compared to the rest. All other samples clustered in two major groups: Cluster 1 = 136 samples (49 FASD: 87 Control; mainly Caucasian) and Cluster 2 = 58 samples (53 FASD: 5 Control; mainly First Nations) (Supplementary figure 4.3).

A large imbalance in ethnicities was present between groups, with the majority of controls being Caucasian and most FASD cases being of First Nation descent. Thus, cluster 1, the largest major cluster, was selected as a more balanced sub-sample, both in terms of ethnicity and cases vs. controls, for further analysis (See Figure 4.1 for a summary of the bioinformatic analyses).

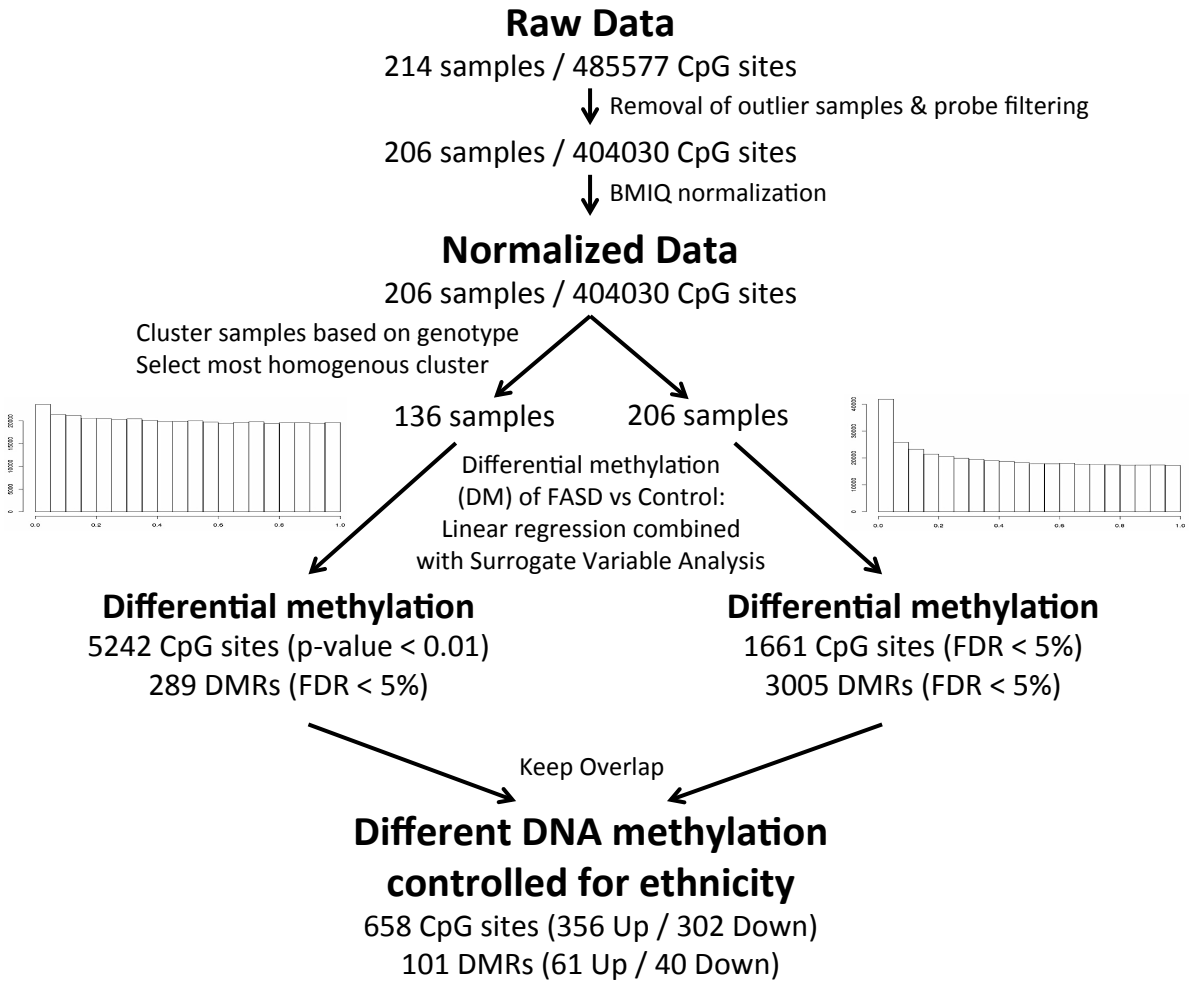

Figure 4.1 Flowchart of bioinformatic analyses

Two analyses were performed in parallel to assess differential DNA methylation between FASD cases and controls. The first analysis, using 206 samples (110 FASD and 96 controls), identified 1661 differentially methylated (DM) sites and 3005 differentially methylated regions (DMR). The second, using a more genetically homogenous subgroup composed of 49 FASD cases and 87 controls, identified 5242 DM sites and 289 DMRs. This second analysis used a p-value threshold of 0.01 to obtain a more conservative list of probes not associated with ethnicity. These were used to filter out the sites identified in the first analysis that might have been confounded by differences in ethnic proportions between the two groups, resulting in a final list of 658 DM CpGs and 101 DMRs free of the confounding effects of ethnicity.

4.2.8 Ethnic group adjustment

Differential DNA methylation analysis was performed as previously described on the more genetically-homogenous sub-sample defined as "Cluster 1" in the MDS analysis above to identify difference between FASD cases and controls. SVA using this sub-sample identified 11 SVs that were added as covariates in linear modeling as described for the full sample. In addition, the inclusion of principal components from the MDS analysis into the regression model to correct for ethnicity was also explored. However, as ethnicity was confounded with the phenotype of interest, direct correction in the model also removed the signal of interest.

4.2.9 DNA methylation pyrosequencing assay

Bisulfite pyrosequencing assays were designed with PyroMark Assay Design 2.0 (Qiagen; Supplementary table 4.3). The regions of interest were amplified by PCR using the HotstarTaq DNA polymerase kit (Qiagen) as follows: 15 minutes at 95°C, 45 cycles of 95°C for 30s, 58°C for 30s, and 72°C for 30s, and a 5 minute 72°C final extension step. For pyrosequencing, single-stranded DNA was prepared from the PCR product with the Pyromark™ Vacuum Prep Workstation (Qiagen) and the sequencing was performed using sequencing primers on a Pyromark™ Q96 MD pyrosequencer (Qiagen). The quantitative levels of methylation for each CpG dinucleotide were calculated with Pyro Q-CpG software (Qiagen).

4.2.10 Brain concordance analysis

Human brain and blood DNA methylation data from a previously published cohort was used to assess concordance, which was calculated as the Spearman correlation coefficient of DNA methylation at all CpGs between healthy human blood and brain (Farré et al. 2015).

Human brain microarray data were obtained from the Allen Brain Atlas (http://human.brain-map.org/static/download; August 1st 2015), which contains normalized expression values for 58,692 probes and 896 brain regions from 6 individuals. Probes were ranked based on their average expression level for each brain region separately and the mean was calculated across all brain regions. All 29,191 genes assayed (which included 389 out of our 404 differentially methylated genes) were sorted based on their highest ranked probe.

4.2.11 CpG island distribution

The probes categorization into "North Shelf", "North Shore", "Core Island", "South Shore", "South Shelf" or "Non-island" was based on the Illumina "RELATION_TO_UCSC_CPG_ISLAND" annotation. The expected counts were calculated with the 404,030 probes remaining after filtering. Statistics were calculated using multinomial goodness of fit chi-square test. As a post-hoc test to evaluate which category is driving the effect, additional chi-square tests were run on each category vs. the sum of all of the other categories.

4.2.12 Functional enrichment analysis

The list of imprinted genes was extracted from http://www.geneimprint.com/site/genes-by-species.Homo+sapiens.imprinted-All (June 1st 2014; Supplementary table 4.4), which includes 80 genes with at least one probe among the 404,030 probes remaining after filtering (3035 probes total). The Illumina "UCSC_REFGENE_NAME" annotation was used to map the probes to genes (479 out of 658 DM probes had such annotation and could be mapped). In the event of probes mapping to several genes, the gene with the closest transcription start site (TSS) was selected using the Price annotation (Price et al. 2013). The over-representation analysis

(ORA) tool of ErmineJ (version 3.0.2) was used to identify gene function enrichment in the list of up- and down-methylated genes including the Gene Ontology (GO) annotations molecular function, biological process, and cellular component (Lee et al. 2005). The ermineJ ORA tool was set with the following parameters: max gene set size = 1,000; min gene set size = 2; background genes = all genes mapping to the 404,030 probes remaining after filtering.

4.2.13 Co-expression analysis

The Gemma tools and database for meta-analysis of functional genomics data were used to perform a co-expression analysis based on existing studies (Zoubarev et al. 2012). The methods used by Gemma have been previously described (Lee et al. 2004). Data sets were obtained from public sources, primarily the Gene Expression Omnibus (Wheeler et al. 2004). For each data set included in the meta-analysis, the Pearson correlation matrix of gene co-expression profiles was computed. Thresholds were applied for statistical significance of correlation, and the resulting sparse co-expression networks were aggregated across data sets. The degree to which a link is replicated across studies is a measure of its reliability; a threshold was set based on a benchmark permutation-based analysis, scaled to the number of data sets aggregated. Using the Gemma on-line tools, a co-expression network was extracted for the 199 up-methylated genes in the master set of microarray experiments for human (282 usable experiments across multiple tissues and experimental conditions) at the stringency recommended by the software, and visualized the results in Cytoscape (Smoot et al. 2011). The resulting network shows the co-expression relationship of the genes in the input list only.

4.2.14 Differentially methylated region analysis

The identification of differentially methylated regions (DMRs) was performed using previously established guidelines and the *DMRcate* package in R (Peters et al. 2015; Peters & Buckley, n.d.). Briefly, results from linear modeling with surrogate variables were analyzed using a Gaussian kernel smoother with a bandwith of 1000 base pairs (bp) and scaling factor of 2 to model all CpG sites in the genome in parallel and identify broad regions of differential DNA methylation. P-values were corrected for multiple testing using the BH method, and an FDR cutoff of 0.05 was used to select significant probes between the FASD and control groups. DMRs were then assigned by clustering significant CpGs located within 1000 bp windows that contained two or more CpGs. This analysis was performed on both the full dataset and the more ethnically homogeneous subset of individuals, and the final list of DMRs was obtained through the same process as previously described in the differential methylation analysis. Genomic locations for all DMRs were assigned using the Illumina hg19 annotation.

4.3 Results

4.3.1 The NeuroDevNet FASD epigenetics cohort

Participants in the NeuroDevNet Canadian FASD study cohort were recruited from six clinical sites across Canada (Vancouver, BC; Edmonton, AB; Cold Lake, AB; Winnipeg, MB; Ottawa, ON; and Kingston, ON) (Reynolds et al. 2011). More specifically, 110 children with FASD or confirmed PAE and 96 typically developing controls were matched for sex and age, ranging from 5 to 18 years of age, for the analysis of genome-wide DNA methylation patterns (Table 4.1). We note that self-declared ethnicity differed considerably between the FASD and control participants, necessitating stringent statistical corrections, as described below.

	FASD cases	Controls
N	110	96
Age	11.55 ± 3.37	11.28 ± 3.38
Sex		
- Male	41%	47%
- Female	59%	53%
Self-declared ethnicity		
- Caucasian	27% (48%)*	91% (96%)
- Other	73% (52%)	9% (4%)

*Percentages in brackets include participants with mixed ethnicities including Caucasian

Table 4.1 Characteristics of the NeuroDevNet FASD cohort

4.3.2 Children with FASD displayed altered DNA methylation patterns

The DNA methylation profiles of BECs from the complete NeuroDevNet cohort were assessed using the Illumina HumanMethylation450 array, which assays DNA methylation at 485,512 sites across the human genome. Following quality control and normalization to remove probes with bad detection p-values and low bead counts, or those associated with sex chromosomes, SNPs, and polymorphic CpGs, 404,430 sites remained in the final dataset of 206 samples (Price et al. 2013). Although BECs typically represent a relatively homogenous population of cells, they can occasionally be contaminated by white blood cells during collection, thus possibly affecting the results of differential DNA methylation analyses (Jones et al. 2013). To assess whether BEC from the present study had high levels of contamination, principal component analysis of BECs and blood samples obtained from GEO was performed. This analysis did not reveal any considerable blood contamination in our dataset, as evidenced by the distant clustering of samples from both tissue types, though some cell type differences may be present (Supplementary figure 4.1). Having thus established that cellular heterogeneity was unlikely to confound our results, we next set out to identify alterations in DNA methylation patterns specific to the FASD group. For this, differential DNA methylation analysis using a

two-group design was coupled with surrogate variable analysis (SVA), which corrects for batch effects and any other undesirable variation in the data. This analysis identified 1661 differentially methylated (DM) CpG sites between the FASD group and controls at a false discovery rate (FDR) <0.05, indicating substantial differences in DNA methylation patterns between the two groups. However, self-declared ethnicity in the cohort was strongly confounded with FASD status (Table 4.1). Given that ethnicity has been associated with altered DNA methylation levels, these differences could potentially drive alterations in DNA methylation at these 1661 DM CpG sites (Fraser et al. 2012; Moen et al. 2013; Heyn et al. 2013).

4.3.3 Ethnic background correction identified FASD-specific DNA methylation patterns

To account for ethnicity on a genetic basis, the Illumina HumanOmni2.5 array was used to obtain genotypes at nearly 2.4 million single nucleotide polymorphisms (SNPs) for each child. Participants were clustered by multi-dimensional scaling (MDS) of genotypic data along with publicly accessible data from the HapMap project (Thorisson et al. 2005). Linear regression of the first four genetic clusters from this analysis with the SVs revealed little correlation with the majority of DNA methylation variation, suggesting that further correction for differences in ethnicity was required to isolate the effect of PAE beyond ethnicity (Supplementary figure 4.2). As such, individuals clustering within the larger and more genetically homogeneous subgroup were selected for further analysis, consisting of 49 FASD cases and 87 controls (Table 4.2; Supplementary figure 4.3 & Supplementary table 4.2). Differential DNA methylation analysis was performed on the more genetically-homogeneous sub-sample to isolate the effects of PAE in the absence of an ethnic confound. In support of less ethnicity-related effects in this subsample, SVA identified fewer SVs compared to the full dataset. Furthermore, the results from DNA

methylation analysis in this subgroup displayed only a moderate correlation with those obtained from the full sample (Spearman rank correlation: 0.43), suggesting that ethnicity indeed may have influenced differential DNA methylation patterns in the full cohort, despite our efforts to use SVA to remove the effects of ethnicity. Therefore, the subsample was used to filter out ethnically confounded CpG loci to obtain a subset of DM sites unbiased for ethnicity (Figure 4.1). More specifically, the top 5242 probes (unadjusted p-value <0.01) in the genetically-homogeneous sub-sample were selected as a conservative set of differentially methylated CpG sites between FASD cases and controls that were unaffected by ethnic background. This set was compared to the 1661 DM sites identified in the full sample, and only the probes present in both lists were considered specific effects of FASD, unlikely to be related to effects of ethnicity. Following this strategy, a final list of 658 DM CpG sites significantly altered in FASD cases was obtained at an FDR<0.05 (Supplementary table 4.1), composed of 356 down-methylated and 302 up-methylated sites compared to controls (Figure 4.2AB).

To determine whether this corrective analysis removed some or all effects of ethnicity, differential DNA methylation analysis was performed on FASD cases from the two main ethnic clusters from MDS to tease apart ethnicity and FASD-specific effects between the groups (Supplemental methods). As expected, the ethnicity-corrected CpGs were less, but still partially associated with ethnicity differences in DNA methylation patterns than the uncorrected set of CpGs, as evidenced by the decreased area under the ROC curve (Supplementary figure 4.4). (Supplemental methods). Furthermore, reflecting the economic realities of our study populations, socio-economic status (SES) scores were slightly confounded between groups (p=0.00017; Supplementary figure 4.5), with the FASD group displaying lower overall scores than controls. However, the more ethnically homogeneous subgroup showed less skewing towards low SES in

the FASD group (p=0.16; Supplementary figure 4.5), suggesting that the effects of SES might also have been partially accounted for during the correction for ethnic biases between groups.

As such, the ethnicity-corrected set of 658 CpG loci associated with FASD was used in all subsequent analyses. The changes observed in the absolute methylation levels of these DM CpGs were relatively small, consistent with previous human studies of neurological and neurodevelopmental disorders, with percent methylation changes ranging from 0.16% to 13.1% after correction for surrogate variables (Ladd-Acosta et al. 2014). However, 41 DM sites passed an arbitrary threshold for possible biological relevance of greater than 5% difference in DNA methylation levels between groups. Taken together, these results support the hypothesis that FASD is associated with altered DNA methylation patterns, largely free of identified confounding effects due to ethnicity and SES.

	FASD cases	**Controls**
N	49	87
Age	11.29 ± 3.16	11.29 ± 3.37
Sex		
- Male	43%	41%
- Female	57%	59%
Self-declared ethnicity		
- Caucasian	51% (76%)*	93% (97%)
- Other	49% (24%)	7% (3%)

*Percentages in brackets include participants with mixed ethnicities including Caucasian

Table 4.2 Characteristics of the more genetically-homogenous sub-sample

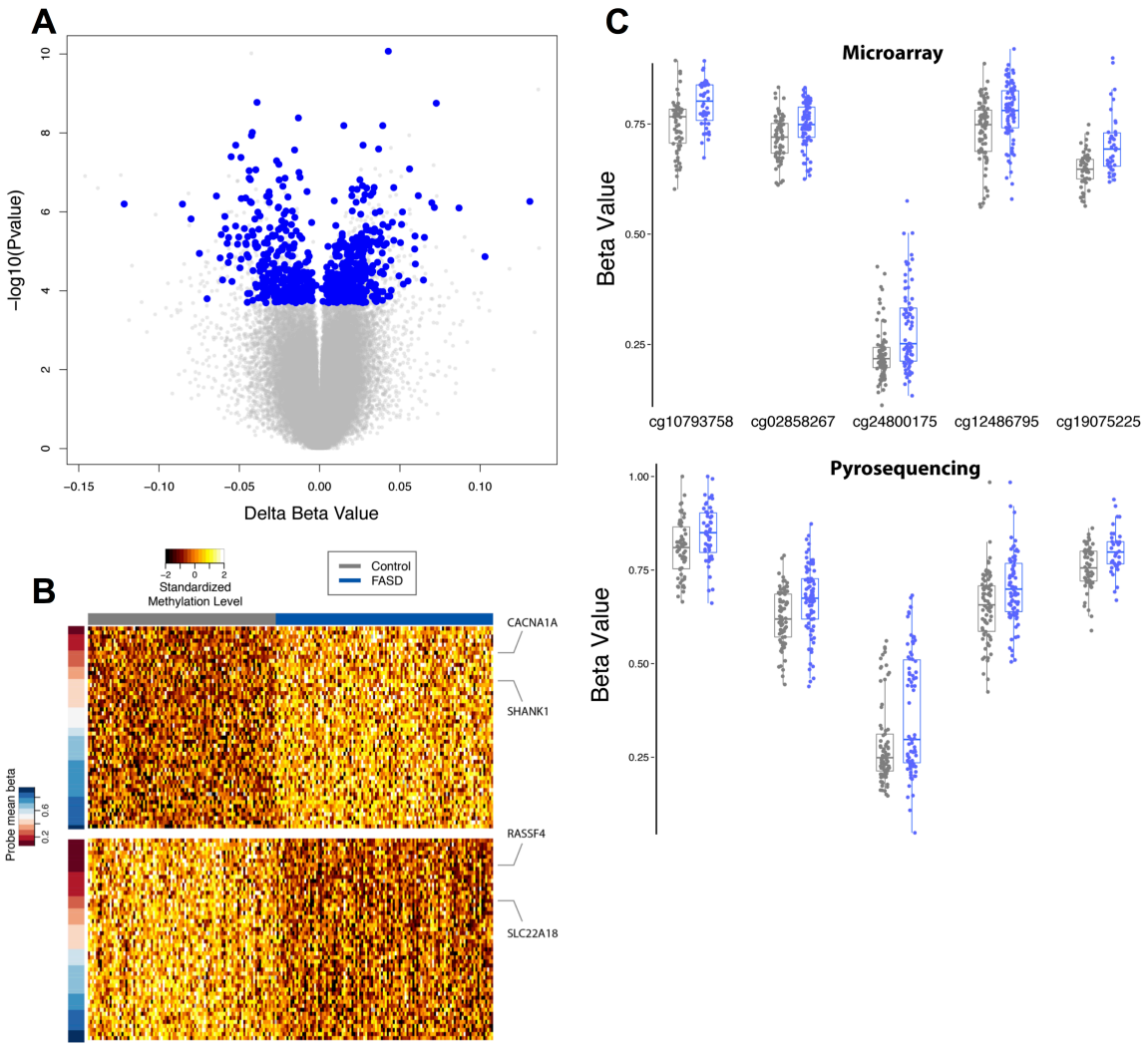

Figure 4.2 Visualization and verification of differentially methylated probes

A. Volcano Plot showing mean methylation differences between FASD and control (x axis) versus log transformed p-values (y axis). 1661 CpG sites with an FDR<0.05 were considered significantly differently methylated between FASD and control, but 1003 of these were ethnically confounded, resulting in the final 658 probes shown in blue. B. Heatmap of top 50 most significant up- (top) and down-methylated (bottom) probes in control (left, grey) versus FASD cases (right, blue). The percent methylation values (ranging from 0 to 1) are adjusted for the covariates from the regression model, then centered, scaled, and trimmed, resulting in a standardized DNA methylation level ranging from -2 to +2 (black to white scale). The mean percent methylation value for each probe (red to blue scale) is the mean methylation value, after adjustment for covariates, for all samples. C. Verification with pyrosequencing in

both FASD (blue) and control (grey) samples. The top panel displays DNA methylation levels measured by the 450k array, the bottom panel, the levels for the same CpG sites measured with pyrosequencing. These CpGs were located in the gene body of *SHANK3* (cg10793758), *NOS1AP* (cg02858267), *CACNA1A* (cg24800175), and *SNED1* (cg19075225), or in the 3'UTR of *NOS1AP* (cg12486795). Those found in *NOS1AP* were located in a CpG island, while those in *SHANK3* and *CACNA1A* were located in a north shelf or shore, respectively. The CpG associated with *SNED1* was not located near any CpG island. All pyrosequencing data showed significant differences between FASD and controls ($p<0.01$).

4.3.4 Technical verification of FASD DM loci by bisulfite pyrosequencing

To ensure that the results from the differential DNA methylation analysis were not dependent on the method used to measure them, five CpG sites with a difference in percent methylation change greater than 5% in the vicinity of genes with potential biological relevance were selected for verification using bisulfite pyrosequencing on the same samples. Pyrosequencing results confirmed the DNA methylation levels observed on the 450K array, showing similar DNA methylation levels and significant differences between groups ($p<0.01$) for CpGs located in *SHANK3*, *NOS1AP*, *CACNA1A*, and *SNED1* (Figure 4.2C). Pearson correlations ranged from 0.421 to 0.801 and Bland-Altman plots showed little difference when comparing both methods, suggesting a strong concordance between DNA methylation data from microarray and the different pyrosequencing method (Supplementary figure 4.6). Perhaps more importantly, linear regression analysis of pyrosequencing data confirmed differential DNA methylation between FASD cases and controls in this subset of biologically relevant sites, even in the absence of covariates, as the p-value ranges from 3.7e-04 to 5.5e-03. Collectively, pyrosequencing data verified the findings from the 450K array, suggesting that individuals with FASD had altered DNA methylation patterns compared to typically developing children.

4.3.5 Overlap of BEC FASD signatures with brain tissue gene expression and DNA methylation

As alterations to DNA methylation patterns in children with FASD were identified in BECs, it is important to note that changes in peripheral tissues do not necessarily reflect alterations in a relevant tissue, such as the brain, even though these two tissues originate from the same germ layer and thus might share some epigenetic concordance (Berko et al. 2014). Therefore, two complimentary approaches were used to obtain an approximation for the relationship of these FASD-associated DM loci to brain biology and possible the etiology of FASD. First, DM genes were compared to publically available gene expression data from 896 post-mortem brain regions (Allen Institute for Brain Science) to determine whether they were expressed at biologically relevant levels in neural tissue (Hawrylycz et al. 2012). This analysis revealed that 56% of DM genes identified in BECs displayed mRNA expression levels in the brain above the median expression for all genes, with 68% ranked in the top 2/3 of the genes based on mean ranking across ~900 brain regions (Farré et al. 2015). These findings held true whether all DM genes or only the down-/up-methylated genes were considered for analysis. Next, the FASD BEC DNA methylation patterns were compared to DNA methylation patterns from unrelated post-mortem cortical brain specimens previously published by our group (Farré et al. 2015). The overall correlation of mean DNA methylation between BEC and brain samples for all 658 DM CpGs was 0.76 (Supplementary figure 4.7). Taken together, these results indicated that BEC may be a suitable surrogate tissue for brain cells, and that the DM loci presented here could potentially report on biological alterations in neural tissues.

4.3.6 FASD DM loci were enriched in regions of high DNA methylation variability

Given that genomic location plays an important role in sculpting DNA methylation landscapes and mediating its effects, we ascertained the relative enrichment of FASD DM loci in distinct genomic features. Overall, DM probes had a significantly different distribution than the proportions present on the entire 450K array (Figure 4.3A; down-methylated probes: $\chi 2 = 33.63$, $p = 2.8e\text{-}06$; up-methylated probes: $\chi 2 = 13.30$, $p = 2.1e\text{-}02$). Compared to all 450K probes, both down- and up-methylated CpGs in FASD cases were significantly under-represented in CpG island cores, which generally show the least amount of variability in DNA methylation levels (down-methylated p= 1.62e-6; up-methylated p= 7.53e-4). By contrast, down-methylated sites were enriched in CpG island shores and shelves (p= 0.04; p= 0.0003), which tend to be more variable than CpG island cores (Irizarry et al. 2009b). Up-methylated sites were over-represented in non-CpG island regions (p=0.009), further supporting a greater effect of PAE on malleable regions of the epigenome. Moreover, the distribution of average methylation levels for DM sites was significantly different than that of all 404,030 sites (Student's t test; p = 2.5e-09; Supplementary figure 4.8). Further analysis of this phenomenon revealed a significant enrichment for DM CpG sites in the intermediate 20-80% range of methylation levels, while showing a concordant under-representation in the hypo- (<20%) and hyper- (>80%) methylated categories (Figure 4.3B) (Eckhardt et al. 2006). These findings suggested that DM loci in the FASD cases versus controls were mostly located in more variable regions of the epigenome.

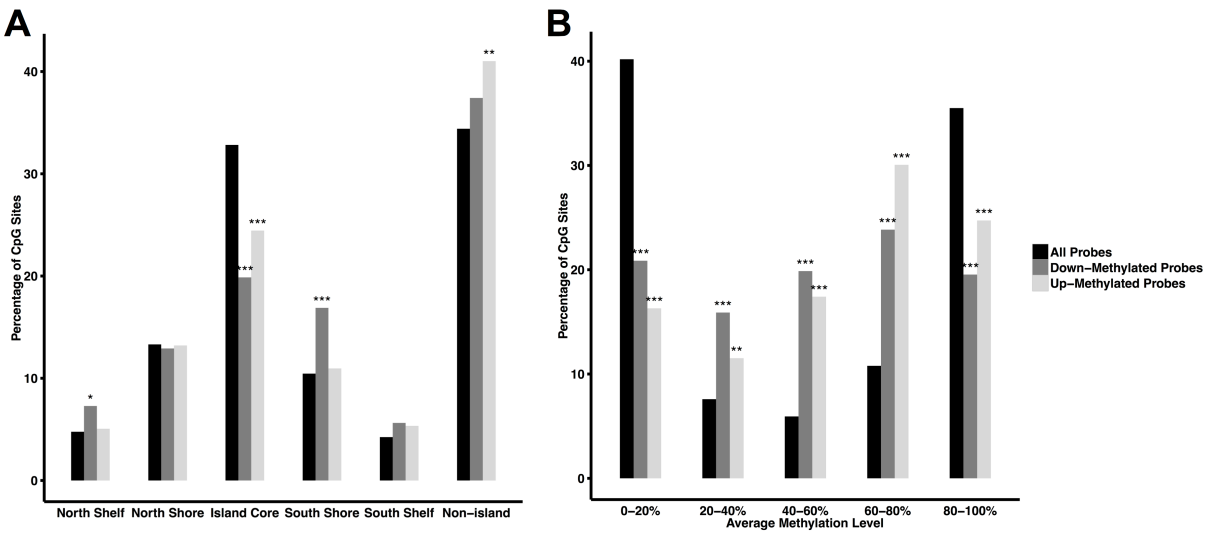

Figure 4.3 Differentially methylated probes are located in regions of variable and intermediate DNA methylation

A. The 658 probes differentially methylated between FASD and control were under-represented in CGI cores (down-methylated p= 1.62e-6; up-methylated p= 7.53e-4), while down-methylated probes were overrepresented in CGI shores/shelves (p= 0.04; p= 0.0003) and up-methylated probes were over-represented in non-CpG island regions (p=0.009). B. The same probes' average methylation levels are over-represented in the mid-range categories (**p<0.01, ***p<0.0001).

4.3.7 Multiple DM sites were associated with imprinted genes and the protocadherin gene cluster

Next, the association of DM loci with different genes was assessed, particularly with regards to whether some of these harbored more than one CpG differentially methylated between FASD and controls. Using genome location annotations from UCSC, the DM sites were mapped to 403 different genes. Of these, 190 were down-methylated, 208 were up-methylated, and 5 displayed inconsistent differences between FASD cases and controls, containing both up- and down-methylated sites, which were likely due to different genomic locations within the genes

(Supplementary table 4.2). The Phenocarta resource for gene-disease associations has previously curated a list of susceptibility genes for FASD, identifying 123 potential candidates from both human and animal studies of PAE (Portales-Casamar et al. 2013). However, DNA methylation analysis of the 115 FASD candidate genes assayed on the 450K array did not reveal significant alterations in FASD cases. Nonetheless, twelve genes contained three or more DM loci, including several genes previously involved in studies of alcohol exposure and dependence, but not present in the Phenocarta list, such as *SLC6A3* and *DRD4* (Table 4.3) (Hillemacher et al. 2009; Zhang H. et al. 2013; Bau et al. 2001; Sánchez-Mora et al. 2011). This short list of DM genes also showed a slight but statistically significant enrichment for imprinted genes (Fisher's exact test; p=0.02317). The geneimprint website (www.geneimprint.com; June 1st 2014) currently lists 96 human genes as imprinted, 80 of which were assayed by the 404,030 filtered probes on the 450K array. Of these, 5 were differentially methylated in FASD cases versus controls (*ATP10A*, *CPA4*, *H19*, *KCNQ1OT1*, *SLC22A18*), with twelve out of fifteen DM CpGs showing lower methylation levels in the FASD group, which resulted in a strong enrichment for imprinted probes in the list of differentially methylated probes (Fisher's exact test; p = 1.8e-04). In particular, the 6 CpGs located within the *SLC22A18* promoter were clustered together, showing a similar pattern between FASD cases and controls, suggesting a robust regional effect of PAE on this gene's DNA methylation profile (Figure 4.4). Furthermore, fifteen of the 658 DM sites were located within protocadherin genes, including 6 in the *PCDHB* cluster, 6 in the *PCDHGA* cluster, 2 in the *PCDHA* cluster, and 1 in *PCDH9*. Given the presence of multiple DM CpGs within these genes, these results provide support for imprinted genes and protocadherin clusters as strong candidates for the effects of PAE on the epigenome.

Gene	# of probes	Direction of change	Previous reports (PMID)
PCDHB gene cluster	6	Up	-
PCDHGA gene cluster	6	Up	-
SLC22A18	6	Down	20009564
H19	5	Down	21382472 19519716 19279321 20009564 23580197
HLA-DPB1	5	Up	-
DES	4	Down	-
FAM59B (*GAREML*)	4	Down	-
SLC38A2	4	Down	-
CAPN10	3	Up	-
DRD4	3	Down	20009564*
RASSF4	3	Inconsistent	-
SLC6A3	3	Up	18504048

Table 4.3 Genes containing 3 or more differentially methylated probes

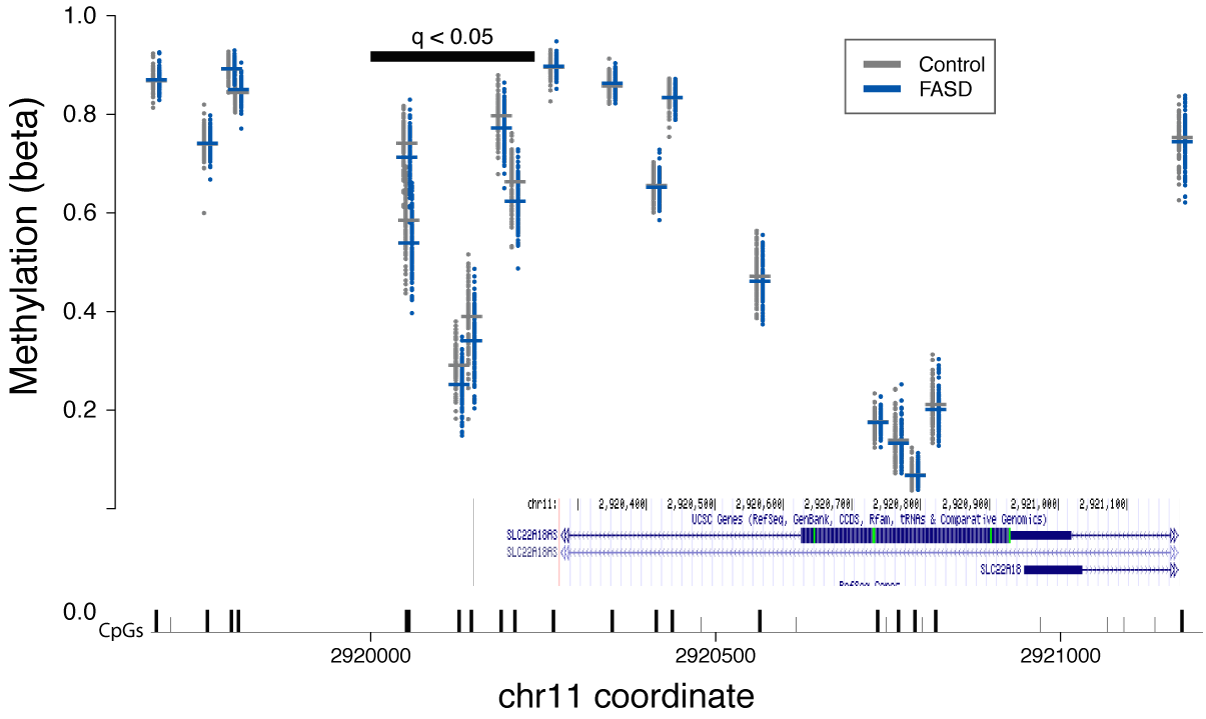

Figure 4.4 Several CpGs associated with SLC22A18 displays down-methylation in FASD cases

The covariate-adjusted DNA methylation levels for control (grey) and FASD (blue) samples are shown for SLC22A18AS (top), with the gene structure aligned (bottom). Exons are represented by blocks, and transcriptional

direction is indicated by arrows. All CpG sites are noted, those present on the 450K array are black while CpGs not present are grey. The six significantly differentially methylated probes located in the SLC22A18 promoter region are indicated with the horizontal black bar (FDR-adjusted p-value (q) <0.05).

4.3.8 Association of FASD differentially methylated loci with neurodevelopmental processes and disorders

In order to identify broad biological processes associated with altered DNA methylation patterns in FASD children, gene function enrichment analysis was performed on the dataset. As no significant results were obtained from the entire list of DM genes following multiple-test correction, the analysis was performed separately on both the up- and down-methylated gene lists. Given that the up-methylated gene list included several members of the protocadherin beta (*PCDHB*) and gamma A (*PCDHGA*) clusters, which are not differentiated by gene function annotations, a single gene from each cluster was conserved for the analysis to avoid any redundancy that may skew the results. As such, only 199 up-methylated genes and 190 down-methylated genes were analyzed for functional annotations using the over-representation analysis (ORA) tool in ermineJ (Lee et al. 2005). While no significant results were obtained using the Gene Ontology (GO) annotation with the list of down-methylated genes, the up-methylated gene list showed enrichment for genes associated with neurodevelopmental processes (Table 4.4), such as neuron parts (20 genes; FDR = 0.051) and projections (19 genes; FDR = 0.082) (Ashburner et al. 2000; Portales-Casamar et al. 2013). Furthermore, using the Phenocarta annotation for associations with diseases, the list of up-methylated genes was enriched for several neurodevelopmental disorders (Table 4.5), including ‘epilepsy syndrome’ (15 genes; FDR = 0.081), ‘autistic disorder’ (12 genes; FDR = 0.092), and ‘anxiety disorder’ (8 genes; FDR

= 0.071) (Ashburner et al. 2000; Portales-Casamar et al. 2013). Of note, the up-methylated genes were also marginally enriched for genes associated with substance-related disorder (15 genes; FDR = 0.192). To further examine the regulatory circuitry associated with FASD DM genes, a co-expression analysis of the up-methylated genes across 282 human expression microarray experiments, spanning multiple tissues and experimental conditions, was performed using the Gemma web tools (Zoubarev et al. 2012). Of the up-methylated genes, 86 could be included in the co-expression network (Figure 4.5). The most strongly co-expressed pair was caldesmon 1 (*CALD1*)-Palladin (*PALLD*), which are both cytoskeleton-associated proteins (Jin et al. 2009). In addition, a small cluster of the network showed co-expression of several genes (*NRXN1*, *CACNA1A*, *CDH10*, and others) associated with autism and/or epilepsy. Taken together, these findings suggest that altered DNA methylation patterns may potentially relate to the neurobiological deficits of children with FASD.

GO Name	GO ID	P-value	FDR	Genes
neuron part	GO:0097458	1.38E-05	0.051	*ATP2B2, CDH13, GABRB1, HEPACAM, KCNAB2, KCND3, KCTD16, NFASC, NMU, NRSN1, NRXN1, P2RX7, PAM, ROBO3, SHANK1, SHANK3, SLC6A1, SLC6A3, SLC8A1, TIAM2, UCN3*
vocalization behavior	GO:0071625	1.18E-05	0.066	*NRXN1, SHANK1, SHANK3*
neuron projection	GO:0043005	7.31E-06	0.082	*CDH13, GABRB1, HEPACAM, KCNAB2, KCND3, NFASC, NMU, NRSN1, NRXN1, P2RX7, PAM, ROBO3, SHANK1, SHANK3, SLC6A1, SLC6A3, SLC8A1, TIAM2, UCN3*

Table 4.4 Gene ontology function enrichment in genes up-methylated in FASD

Disease Name	Disease ID	P-value	FDR	Genes
anxiety disorder	DOID_2030	1.44E-04	0.071	*CRHR2, CYP3A4, GRM8, NOS1AP, P2RX7, PAM, SHANK1, SLC6A3*
pervasive developmental disorder	DOID_0060040	1.15E-04	0.076	*AGAP1, ARID1B, ATP2B2, ATP10A, CDH10, DCUN1D1, DPP6, ESRRB, GABRB1, GRM8, HEPACAM, NOS1AP, NRXN1, PCDHAC2, ROBO3, SDK1, SHANK1, SHANK3, SLC6A3, ST8SIA2*
epilepsy syndrome	DOID_1826	2.07E-04	0.081	*BRD2, CACNA1A, CCR3, CIT, GJD2, GRM1, GRM8, KCNAB2, NRXN1, NTNG2, P2RX7, PAM, SLC6A1, SLC6A3, SLC8A1*
autistic disorder	DOID_12849	4.70E-05	0.092	*AGAP1, ATP10A, CDH10, GABRB1, GRM8, HEPACAM, NOS1AP, NRXN1, ROBO3, SHANK1, SHANK3, ST8SIA2*
autism spectrum disorder	DOID_0060041	1.01E-04	0.099	*AGAP1, ARID1B, ATP2B2, ATP10A, CDH10, DCUN1D1, DPP6, ESRRB, GABRB1, GRM8, HEPACAM, NOS1AP, NRXN1, PCDHAC2, ROBO3, SDK1, SHANK1, SHANK3, SLC6A3, ST8SIA2*
substance-related disorder	DOID_303	6.85E-04	0.192	*ADARB2, ANPEP, CACNA1A, CDH13, CRHR2, FRMD4A, GRM8, KCND3, KISS1R, NMU, NRXN1, SLC6A1, SLC6A3, TIAM2, TRPM4*

Table 4.5 Disease-association enrichment in genes up-methylated in FASD

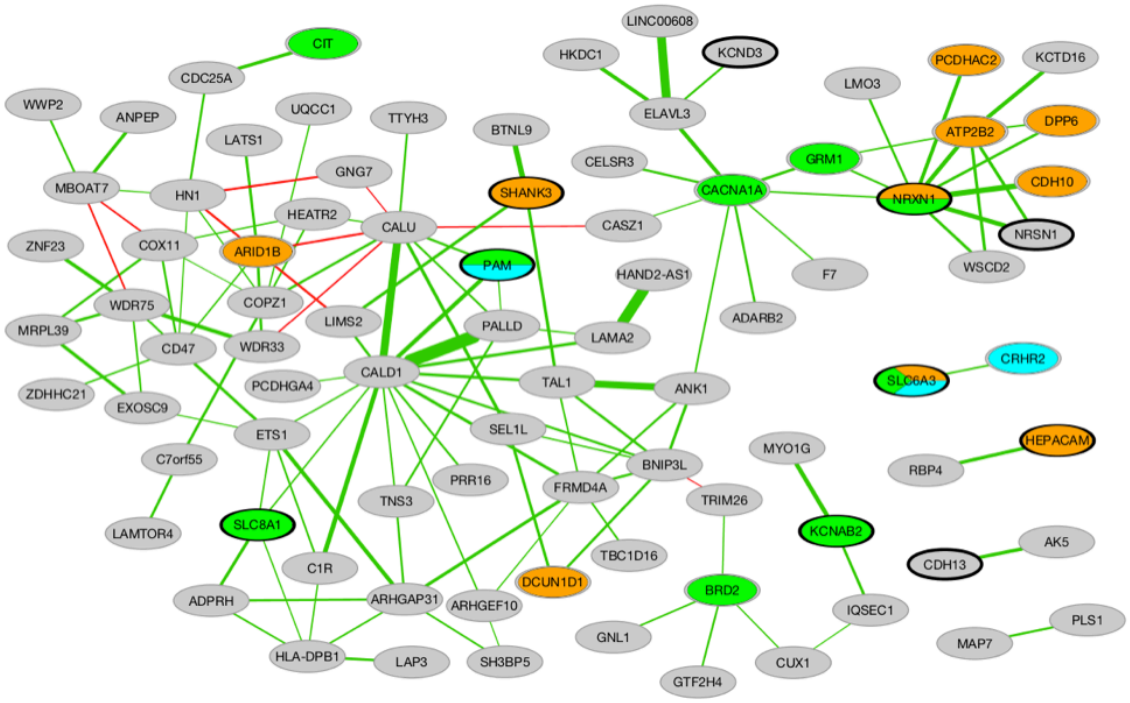

Figure 4.5 FASD up-methylated genes coexpression network

Nodes represent the up-methylated genes while edges represent their coexpression link. Nodes colored in orange, green, cyan are genes associated with autism spectrum disorder, epilepsy, and anxiety, respectively. The edge width represents the number of experiments in which the coexpression link was identified. The green edges show positive correlations, while the red edges are negative correlations.

4.3.9 Differentially methylated regions were identified between FASD cases and controls

To complement the site-specific analysis of differential DNA methylation, which identified several genes with multiple DM CpGs, we next attempted to identify broader patterns of differential DNA methylation using an unbiased approach. Specifically, the identification of region-specific clusters of DM CpGs between children with FASD and controls was performed using *DMRcate*, an established method that uses a Gaussian kernel smoother to identify broad regions of differential DNA methylation (Peters et al. 2015). In the full dataset, 3005 differentially methylated regions (DMRs) containing two or more CpGs were identified at an

FDR<0.05, while in the more homogeneous subset of samples, 289 statistically significant DMRs were identified between groups. Using the same approach to correct for the confounding effects of ethnicity as described in the site-specific analysis, 101 DMRs unbiased by ethnicity were uncovered between individuals with FASD and controls (Supplementary table 4.5).

On average, DMRs spanned 471 nucleotides, with lower and upper limits of 31 and 2,450 base pairs, respectively. DMRs each contained between 2 and 20 CpGs assayed on the 450K array, for a total of 504 unique sites, 75 of which were also identified in the first differential methylation analysis. Of these, 74 overlapped with 95 different genes, and 27 were located in intergenic regions. Of those associated with genes, 25 overlapped with promoter regions (within 1500 bp of the transcriptional start site), 23 with the 5'UTR, 16 with the first exon, 49 with the gene body, and 6 with the 3'UTR, as annotated from the hg19 genome assembly. Moreover, 15 of the top DMRs associated with one or more genes overlapped with those containing multiple DM CpG in the previous analysis, including *SLC22A18*, *SLC38A2*, *HLA-DBP1,* and *NOS1AP* (Table 4.6; Figure 4.6AB). These showed the same direction of change across the entire DMR, consistent with the individual CpG differential methylation analysis and verification by pyrosequencing, in the case of *NOS1AP*. Moreover, two DMRs were identified within the protocadherin genes, with 8 CpGs spanning the *PCDHGA* and *PCDHGB* clusters and 4 CpGs spanning the promoter of *PCDH12*, further supporting a potential role for the protocadherin genes in FASD. Importantly, in addition to the genes overlapping with the previous DM analysis, several additional DM genes were identified through this analysis, including *UCN3* and *ITGAL*, key components of the stress and immune response, respectively (Figure 4.6CD). Taken together, these results suggested that the effects of PAE on the DNA methylation went beyond single CpG loci to affect broader chromosomal neighborhoods.

Gene symbol(s)	DMR location	Chr	Start position	End position	# of probes	Min FDR	Mean FDR	Max beta FC
HLA-DPB1	Body	6	33047056	33049505	17	2.59E-50	1.61E-06	0.087
SLC22A18, SLC22A18AS	Body, TSS1500, TSS200, 5'UTR	11	2919689	2921176	20	1.21E-29	1.46E-05	-0.049
PPP1R2P1	Body	6	32846924	32847845	18	1.81E-20	9.39E-10	0.026
SLC38A2	TSS1500	12	46767132	46768016	8	1.98E-16	9.78E-09	-0.039
HKR1	TSS1500, TSS200, 1st Exon, 5'UTR	19	37825307	37825679	7	7.51E-16	9.51E-16	0.022
WDR52	5'UTR, 1st Exon, TSS200, TSS1500	3	113160071	113160821	10	1.34E-14	6.02E-13	-0.037
C3orf24	5'UTR, 1st Exon, TSS200, TSS1500	3	10149466	10150487	11	4.41E-13	1.88E-11	0.034
NOS1AP	Body, 3'UTR	1	162336877	162337375	5	4.69E-13	8.79E-13	0.039
KCNAB2	5'UTR	1	6093770	6094993	6	9.78E-13	2.86E-07	0.026
F7	TSS1500, TSS200, Body	13	113759771	113760286	6	1.55E-10	1.96E-10	0.029
IFT140, TMEM204	Body	16	1598866	1599150	4	1.81E-10	4.34E-10	-0.036
RGL3	Body	19	11517079	11517436	4	3.06E-10	5.34E-10	0.036
STRA6	5'UTR, 1st Exon, TSS200, TSS1500	15	74494781	74496040	12	4.80E-10	1.06E-04	0.035
TXNRD1, EID3	5'UTR, Body, TSS1500, TSS200, 1st Exon	12	104697193	104697983	11	5.49E-10	3.98E-08	0.024
RNMTL1	Body, 3'UTR	17	695156	695661	3	5.77E-10	3.23E-09	-0.026
C22orf42	Body, TSS200	22	32554848	32555310	5	7.95E-10	7.91E-09	0.022
RADIL	Body	7	4869981	4870162	3	2.40E-09	2.48E-09	0.026
ITGAL	Body	16	30485383	30485966	6	7.18E-09	5.13E-08	0.022

Gene symbol(s)	DMR location	Chr	Start position	End position	# of probes	Min FDR	Mean FDR	Max beta FC
ZNF710	5'UTR	15	90547692	90548043	3	4.18E-08	5.44E-07	-0.023
PCDHA7, PCDHAC2, PCDHA12, PCDHA6, PCDHA10, PCDHA4, PCDHA11, PCDHA8, PCDHA1, PCDHA2, PCDHA9, PCDHA13, PCDHA5, PCDHAC1, PCDHA3	Body, TSS1500	5	140344290	140344745	4	4.73E-08	1.20E-07	0.019
MAL2	TSS200, 1st Exon, Body	8	120220410	120221797	8	1.26E-07	2.35E-03	-0.022
UCN3	TSS1500, TSS200, 1st Exon, 5'UTR	10	5406543	5407020	8	1.32E-07	3.03E-07	0.016
HKDC1	TSS1500, 5'UTR, 1st Exon	10	70979777	70980067	4	1.37E-07	1.40E-07	0.023
ARHGEF19	Body	1	16533422	16534579	8	1.88E-07	1.11E-04	-0.035
LOC154822	Body	7	158815555	158816392	3	2.36E-07	1.90E-05	-0.043
NDST4	1st Exon, 5'UTR, TSS200, TSS1500	4	116034871	116035232	4	5.96E-07	6.45E-07	0.031
SNED1	Body	2	242009513	242009588	2	6.41E-07	6.48E-07	0.040
PRKDC	Body	8	48739161	48739256	2	7.94E-07	8.04E-07	-0.045
CASZ1	5'UTR	1	10847541	10847594	2	2.92E-06	2.92E-06	0.025
HEATR2	Body	7	807596	809109	9	3.11E-06	3.69E-04	0.036

Table 4.6 Top 30 gene-annotated differentially methylated regions associated with FASD

Max fold changes (FC) represented in percent methylation change (beta) in DNA methylation levels of FASD compared to control

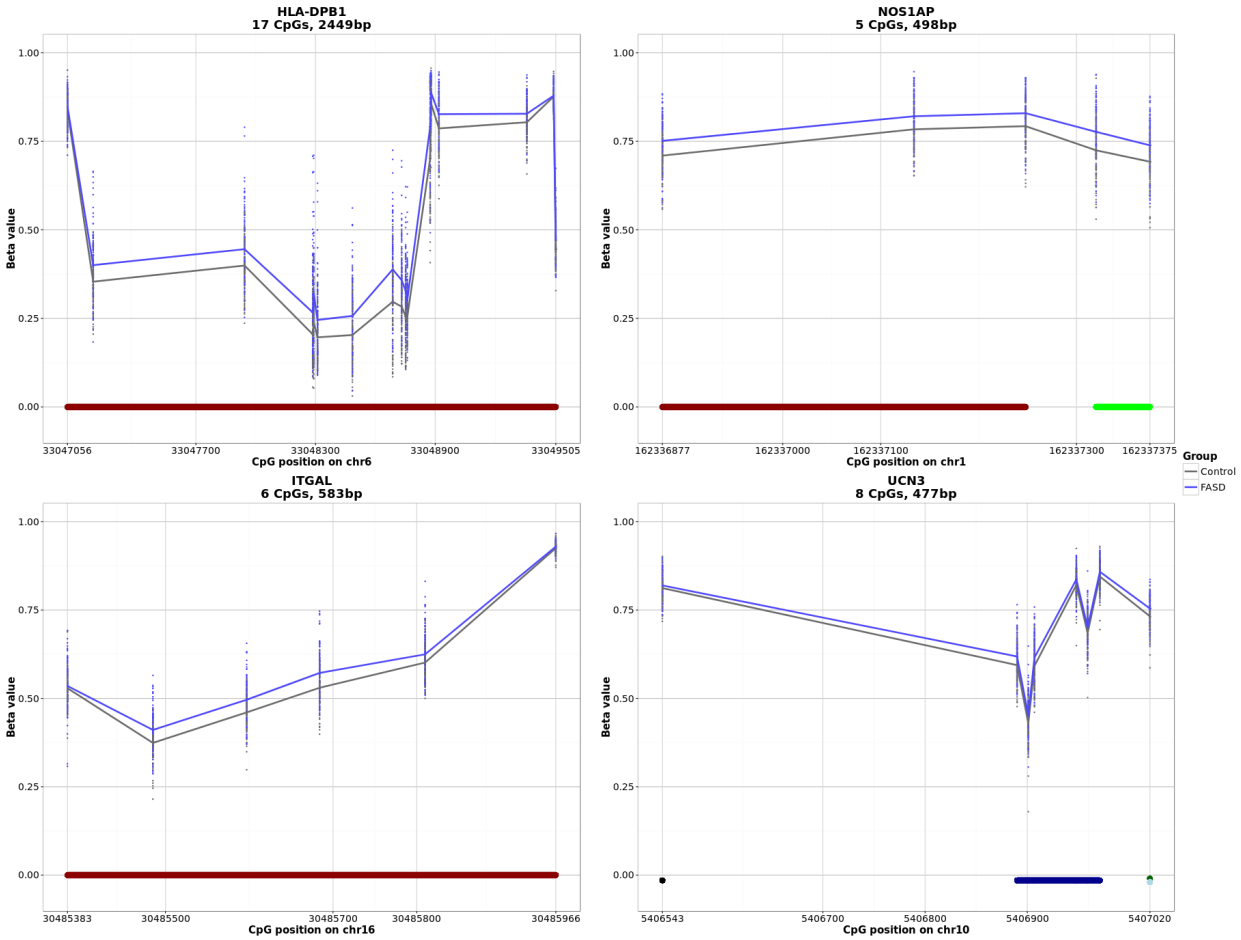

Figure 4.6 Differentially methylated regions associated with FASD.

Percent methylation values adjusted for covariates were plotted across four statistically significant differentially methylated regions (DMRs) between FASD (blue) and controls (grey) identified by DMRcate. A. The HLA-DPB1 DMR spanned 2449 base pairs (bp) of the gene body (red bar) and contained 17 CpGs from the 450K array. B. The NOS1AP DMR contained 5 CpGs over 498 bp, and was located within the body and 3' UTR (green bar) of the gene. C. The 477 bp UCN3 DMR contained 8 CpGs. One was located within the 5'UTR (dark green dot) and 1st exon (light blue dot), while the remainder were located upstream of the gene's transcriptional start site (TSS), 1 CpG falling within 1500 bp (black dot) of TSS and 6 located within 200 bp of the TSS (blue bar). D. The ITGAL gene contained 6 unique DMRs over 583 bp of the gene body (red bar).

4.4 Discussion

This study aimed to assess the effects of PAE on genome-wide DNA methylation patterns and identify an epigenetic signature of FASD, using a large cohort of human subjects. Significant changes to the DNA methylation profiles in BECs of children with FASD compared to age- and sex-matched typically developing controls were identified, with 658 CpGs displaying significantly altered DNA methylation levels, of which 41 had a greater than 5% methylation change. Moreover, 101 DMRs containing two or more sequential DM CpGs were identified throughout the genome, spanning 95 different genes, overlapping with several from the initial differential methylation analysis at single CpG level. The majority of DM genes were highly expressed in postmortem brain samples from the Allen Brain Institute. Moreover, BEC and independent cortical samples showed relatively high concordance of DNA methylation levels. As discussed in more detail below, several lines of evidence converge to support the validity of our data. First, a number of DM sites and regions were identified within genes and pathways previously associated with PAE. Second, novel DM sites and regions tended to be involved in pathways implicated in functional deficits of FASD. Third, broader patterns related to altered neurodevelopmental disorders were identified in sets and networks of genes associated with FASD in our study.

Differential DNA methylation analysis in our case control study comparing children with FASD to children with normal development replicated several associations from previous studies of PAE. One of the most striking similarities is the altered DNA methylation patterns observed in imprinted genes. Several studies have demonstrated the effect of PAE on the *H19* imprinted gene in both mice and humans (Stouder, Somm, & Paoloni-Giacobino 2011; Ouko et al. 2009; Haycock & Ramsay 2009). A genome-wide DNA methylation study in mouse embryos exposed

to ethanol also identified significant changes within several imprinted genes including both *H19* and *SLC22A18* (Liu et al. 2009). Results from our study further confirmed these findings, as 5 down-methylated probes in *H19*, and 6 in *SLC22A18* were altered in the FASD cohort, with the latter being identified as a broader DMR as well. Given that imprinting plays a key role in the regulation of normal growth and development, its alteration by alcohol exposure could be a factor in the neurodevelopmental defects observed in children with FASD (Falls et al. 1999). Furthermore, the only other study of genome-wide DNA methylation patterns in individuals with FASD also identified several DM protocadherin genes within the alpha, beta, and gamma clusters, though only one CpG overlapped with the results presented here (Laufer et al. 2015). The differences in specific CpGs within these gene clusters between the two studies might be due to the much larger sample size of our study, as well as our use of multiple test correction to mitigate spurious patterns of differential DNA methylation associated with the FASD group. In addition, the protocadherin clusters are coordinately regulated and are highly susceptible to environmental influences, which may be reflected by their overrepresentation in these studies (Hirayama & Yagi 2017). However, we note that the single CpG site from our study that overlapped with the previous findings (cg21117330) was located in *PCDHGA8* and displayed the same direction of change between FASD cases and controls, and thus might represent a reproducible effect of PAE.

In addition to genes previously identified in studies of PAE, DNA methylation changes were also uncovered in a number of additional genes with functional relevance to the deficits observed in FASD. More specifically, analysis of DM probes and regions identified altered DNA methylation patterns within genes related to the immune response, such as *HLA-DPB1*, a HLA class II histocompatibility antigen, and *ITGAL* (or *CD11A*), the integrin alpha L chain. Given

that children with FASD often present with numerous deficits in immune function, epigenetic alterations of these genes might reflect functionally relevant underlying biology (Bodnar & Weinberg 2013). A DMR between FASD cases and controls was also identified in *UCN3*, an antagonist of the CRF type 2 receptor that plays a key role in the stress response. As this gene acts downstream of stress signaling pathways, this alteration might be linked to altered basal levels of corticosterone found in individuals with FASD (Mattson, Crocker, & Nguyen 2011; Ergang et al. 2015). Finally, two members of the dopaminergic system, *SLC6A3* and *DRD4*, each contained three differentially methylated CpGs in FASD cases compared to controls. Both of these genes have also been proposed as modifiers and/or risk factors in alcohol abuse disorders and attention deficit disorder, and thus might potentially play a role in the deficits of attention and executive function in children with FASD (Bau et al. 2001; Sánchez-Mora et al. 2011).

Moving beyond alterations in specific genes related to PAE, broader associations to neurodevelopmental processes and disorders were identified in genes containing differentially methylated CpGs. In particular, the gene co-expression network contained a small sub-network of genes associated with autism and/or epilepsy, and up-methylated genes in FASD cases were enriched for functions related to neurodevelopmental disorders. These results could reflect the pleiotropy of these genes, or perhaps their involvement in developmental functions dysregulated in neurodevelopmental disorders with partially overlapping phenotypes. As many of these genes were also functionally enriched for neuron parts and projections, they could influence processes necessary for typical brain development and partially underlie some deficits observed in children with FASD and other neurodevelopmental disorders.

Comparing epigenetic patterns associated with FASD and autism presented an interesting conundrum. While we identified a small sub-network of genes associated with autism and/or

epilepsy in our analysis of the FASD related gene co-expression network, this relationship did not extent to the level of individual CpGs. Comparing the 14 DM genes from BECs recently reported to be associated with autism spectrum disorder, we did not find any overlap with the DM loci identified in our study of FASD children (Berko et al. 2014). The differences between the gene lists may reflect the different origins and phenotypes between the conditions, or that the effects of PAE are more easily identifiable in peripheral tissue than those of autism, or simply false positives and/or false negatives. Regardless, these results imply that at the single CpG level, genes showing differences in DNA methylation between FASD cases and controls are reflective of FASD-specific alterations, rather than broad neurodevelopmental functions.

Although it is tempting to speculate that our collective results may be partially related to the functional deficits observed in FASD, it is important to consider that the DNA methylation patterns were derived from BECs. We feel that this concern is partially mitigated by our finding of the majority of DM genes in BECs being consistently expressed across multiple brain regions, and by the DNA methylation patterns in neural tissue displaying high correlation with those in BEC. Moreover, it has been noted by others that BECs might be a good surrogate tissue for human DNA methylation studies, as both buccal and brain cells are derived from the ectoderm (Lowe et al. 2013). Lastly, while our study did not measure DNA methylation in additional tissues, evidence from animal models is emerging to support lasting alterations to both epigenetic and gene expression patterns in neural tissue following PAE (Lussier et al. 2015; Kleiber et al. 2012, 2013; Laufer et al. 2013). Nevertheless, our results must be interpreted with caution in the context of neurodevelopment, as additional studies in postmortem samples from humans are required to rigorously assess the concordance of epigenetic changes associated with FASD between peripheral and central tissues.

A further challenge in the interpretation of alterations to DNA methylation patterns in FASD cases versus controls lies in the small effect sizes of environmental exposures on the epigenome. Although the small magnitude of DNA methylation changes observed here are consistent with genome-wide DNA methylation studies in other neurodevelopmental and psychiatric disorders, it is unclear whether such small changes can have a strong effect on cellular functions (Ladd-Acosta et al. 2014; Berko et al. 2014; Rakyan et al. 2011). As a 5% change in DNA methylation levels is typically interpreted as biologically significant, the 41 CpGs displaying >5% differences between FASD cases and controls may reflect more robust PAE-induced alterations to the epigenome. However, slight alterations accumulating in several genes involved in similar processes could combine to have strong effects on biological processes. For instance, as many of the up-methylated genes were co-expressed, small alterations to multiple members of this network could potentially affect the biological functions they regulate.

While our data are very consistent with published work in human epigenome-wide association studies, it is of course possible that the relatively small changes to DNA methylation levels reflect biological biases or even technical noise (Rakyan et al. 2011). These could originate from a variety of sources, which we attempted to address to the best of our abilities. For example, while differences in cell type composition can play an important role in driving DNA methylation variation, little to no contamination of the BEC from the present study with white blood cells was identified. These findings suggest that differences in cell type composition may not have affected the observed alterations to DNA methylation patterns in the FASD group, although few blood cell types were covered in our analysis and additional subtypes that were not assessed could potentially have been present in some samples. In addition to differences in cell types, differing postnatal environments between groups might also influence the observed DNA

methylation patterns, skewing the results to represent possibly confounding variables other than PAE, such as diet, socio-economic status (SES), and postnatal alcohol exposure. However, the majority of children in the FASD group were living in foster or adoptive homes, rather than the biological family, which hopefully would reduce differences in the rates of alcohol use or food security between groups. By contrast, SES scores were slightly confounded between groups, although this effect was partially mitigated by the focus on the more ethnically homogeneous subgroup, which showed less skewing towards low SES in the FASD cases. Finally, we feel that potential technical issues were reduced through the use of strict quality control and statistical procedures to eliminate unwanted variation in the data. As such, the technical validity of our approach was supported by the verification of 5 DM loci by bisulfite pyrosequencing, the gold standard for targeted DNA methylation analysis.

We note that although most biological and technical issues were addressed by our study design and methods, a particular caveat in the identification of DM loci was manifested by the imbalance in ethnicity across FASD cases and control groups. Given the close relationship between genetic variation and DNA methylation patterns, differences in genetic background between groups may have contributed to the DNA methylation alterations we identified between FASD cases and controls. Other studies have included ethnicity as a covariate during linear modeling to correct for its effects, but no significant DM probes were identified using this approach in our study, as FASD status was confounded with ethnic background (Supplemental methods). Given that self-reports do not always accurately assess ethnicity, SNP genotyping data were used to objectively assign participants to different ethnic groups, based on HapMap samples of known ethnicity. This analysis resulted in the identification of a more homogeneous subgroup of samples, which was used as a comparative control to filter out the influences of

ethnicity and related effects, such as SES and cultural confounders, on differential DNA methylation within FASD cases. In turn, this strategy facilitated the removal of ethnically biased probes from the original DM loci, resulting in the successful identification DM CpG sites specific to children with FASD and not confounded for ethnicity. Given the prevalence of ethnically diverse populations in large-scale studies of DNA methylation, this unique approach driven by genetic stratification of subgroups might prove a useful way of dealing with the effects of ethnicity in case control studies beyond the one presented here.

4.4.1 Summary and conclusions

Despite the recognition of FAS over 40 years ago, PAE remains the leading cause of developmental disability in the developed world. While several animal studies have investigated the role of epigenetic mechanisms in context of PAE, most human studies have been limited to alcohol consumption and dependence in adults, or a small cohort of children with FASD (Zhang H. et al. 2013; Zhang R. et al. 2013; Philibert et al. 2012; Laufer et al. 2015). As such, this study is the single largest investigation of genome-wide DNA methylation patterns in children with FASD. While one of the greatest challenges with this large cohort was the ethnicity imbalance between the FASD and Control groups, ethnic background correction reduced this confound and allowed the reliable identification of 658 DM CpG sites specific to children with FASD. Although the effect size of changes was small in most cases, 41 sites displayed a greater than 5% change in DNA methylation, which is consistent with previous studies and may reflect the subtle effects of PAE on the epigenome. We also identified 101 DMRs containing two or more DM CpGs, located within 95 different genes and spanning promoter regions, gene bodies, and both 3' and 5' UTRs. While these data were collected from BEC, rather than neural tissue, the vast

majority of DM genes were highly expressed in the brain, suggesting a potential concordance between peripheral and central tissues. These alterations occurred in several genes previously implicated with PAE and altered neurodevelopment, and displayed functional enrichments for neural process and neurodevelopmental disorders. Although it will be essential to validate these changes in separate cohorts from a different population, these findings provide initial insight into the molecular mechanisms underlying the effects of PAE on children and present a potential role for role for DNA methylation in the etiology of FASD.

Chapter 5: DNA methylation as a predictive tool for fetal alcohol spectrum disorder

5.1 Introduction

Prenatal alcohol exposure (PAE) can alter the development, function, and regulation of numerous neural and physiological systems, giving rise to lasting cognitive and behavioural deficits, immune dysfunction, motor impairments, and increased vulnerability to mental health problems in adulthood (Zhang, Sliwowska, & Weinberg 2005; Pei et al. 2011; Mattson, Crocker, & Nguyen 2011). In humans, PAE can result in fetal alcohol spectrum disorder (FASD), a leading preventable cause of developmental disability with a North American prevalence currently estimated between 2-5% (May et al. 2009, 2014, 2015). FASD presents through a wide spectrum of phenotypes, ranging from growth deficits and physical abnormalities to cognitive and behavioral deficits. On the most severe end of the spectrum lies Fetal Alcohol Syndrome (FAS), which is characterized by growth retardation, microcephaly, a distinct set of facial dismorphisms, and central nervous system abnormalities (Jones & Smith 1973; Astley & Clarren 2000). By contrast, Alcohol-Related Birth Defects (ARBD) and Alcohol-Related Neurodevelopmental Disorders (ARND) describe the less severe end of the spectrum, where individuals with confirmed maternal drinking during pregnancy show primarily physical abnormalities or behavioural and/or cognitive abnormalities, respectively (Jacobson et al. 2011).

Although the degree of alcohol's effects during development varies among individuals, depending on factors such as timing and level of alcohol exposure, overall maternal health and nutrition, and genetic background, individuals across the spectrum show cognitive and behavioral deficits, which can be as serious in those with full FAS as those without any physical

features (Pollard 2007). Importantly, FASD has proven difficult to identify at an early age in the absence of overt physical manifestations of the disorder, as ARND requires confirmation of maternal alcohol consumption for diagnosis. As such, many children with FASD are not identified until they reach school age, where they begin to struggle with increased social pressure and cognitive challenges (Senturias & Baldonado 2014). However, early cognitive and behavioral interventions may potentially alleviate some of the deficits caused by PAE and improve the long-term outcomes of individuals with FASD (Paley & O'Connor 2011). As earlier diagnosis is a strong predictor of positive outcomes in individuals with FASD and habilitative care may be have a greater impact during infancy, early screening tools are necessary to help identify at-risk children at a young age and potentially buffer some of the deficits caused by prenatal alcohol exposure (Streissguth et al. 2004; Fox, Levitt, & Nelson III 2010).

Self-report methods are most commonly used to assess PAE and the child's risk of FASD, these are not always accurate and can lead to underestimation of alcohol consumption behavior during pregnancy (Russell et al. 1996; Jones, Bailey, & Sokol 2013; Burns, Gray, & Smith 2010). Over the past decades, various biomarkers of PAE have been developed to complement self-report questionnaires in the absence of direct alcohol-induced pathologies. More specifically, the latter have focused on the direct or indirect products of ethanol metabolism, which can be measured in biological specimens from both the mother and infant (Concheiro-Guisan & Concheiro 2014). Although these biomarkers are very sensitive to fetal alcohol exposure, they may not be directly related to the biological underpinnings of PAE-induced deficits or the developmental profiles associated with FASD. Furthermore, their use is limited to a short window after birth, which may not be useful in cases where alcohol exposure is

not suspected (Cabarcos et al. 2015). As such, objective measures of PAE are needed to aid in the screening and diagnosis of children at risk for FASD.

Importantly, epigenetic marks are now emerging as potential biomarkers or signatures of early-life exposures. Broadly defined, epigenetics refers to modifications of DNA and its regulatory components, including chromatin and non-coding RNA, that potentially modulate gene transcription without changing underlying DNA sequences (Bird 2007; Meaney 2010; Henikoff & Greally 2016). In addition to their role in the regulation of cellular processes, these may also bridge environmental factors and genetic regulation to capture a lasting signature of early environments. In particular, DNA methylation is emerging as a candidate biomarker for environmental exposures and disease. Typically found on the cytosine residues of cytosine-guanine dinucleotides (CpG), this epigenetic mark is both stable over time and dynamic in response to environmental factors (Boyce & Kobor 2015). Several pre- and postnatal environmental influences have been associated with altered DNA methylation patterns, such as maternal nutrition and smoking, supporting their responsiveness to early-life environments and potential use as biomarkers (Joubert et al. 2012; Heijmans et al. 2008). For example, prenatal exposure to cigarette smoke is associated with lasting alterations to DNA methylation patterns, which are now being used as biomarkers of cigarette smoke exposure in infants (Reese et al. 2017).

While in its infancy in relation to PAE, this field shows promise for FASD, as the DNA methylome retains a lasting signature of prenatal alcohol exposure in both the central nervous system and peripheral tissues (reviewed in Lussier, Weinberg, & Kobor 2017). Numerous studies have been performed using animal models, and have shown both short term and persistent

alterations to DNA methylation patterns in the brain, suggesting that this epigenetic mark may play a role in PAE-induced deficits (Chater-Diehl et al. 2016; Laufer et al. 2013; Liu et al. 2009; Hicks, Middleton, & Miller 2010; Zhou, Chen, & Love 2011; Lussier, Weinberg, & Kobor 2017). By contrast, fewer studies have investigated DNA methylation patterns in children with FASD. More targeted methods identified changes in DNA methylation levels in the promoter region of *DRD4* among a large cohort of children exposure to alcohol during breastfeeding in Australia (Fransquet et al. 2016). Others have employed discovery-driven approaches, assessing genome-wide DNA methylation patterns in case-control studies of FASD. The first of these came from a small cohort of children, where the main findings were alterations to DNA methylation patterns in the protocadherin (PCDH) gene clusters (Laufer et al. 2015). Recently, we analyzed DNA methylation profiles in a large cohort of children with FASD, identifying a signature of 658 differentially methylated CpGs (Portales-Casamar et al. 2016). Although few results have been validated across different cohorts, these findings have set the stage for broader applications of DNA methylation in the context of FASD, creating a framework upon which to build future epigenomic studies of PAE.

To validate the findings from our previous DNA methylation signature of FASD, we assessed the genome-wide DNA methylation profiles of buccal epithelial cells (BEC) from an independent cohort of 24 individuals with FASD and 24 sex- and age-matched typically developing controls. Given that our initial study provided a robust framework for genome-wide assessment of DNA methylation patterns in FASD, we used the findings from our initial study as a foundation for the identification of replicable epigenetic alterations following PAE. Notably, nearly 25% of statistically significant associations from the NDN study were validated in this new cohort at a false-discovery rate (FDR) <0.05. In addition to the validation analyses, we also

assessed whether DNA methylation profiles could be used to identify individuals with FASD, generating classification algorithms that use DNA methylation levels to predict FASD status with high accuracy. Taken together, these results support a role for DNA methylation in FASD and suggest that it could potentially be used as an early screening tool for at-risk children.

5.2 Materials and methods

5.2.1 The Kids Brain Health Network cohort of children with FASD

The present cohort was collected as a replication study by Kids Brain Health Network (KBHN), formerly NeuroDevNet, and is hereby referred to as the KBHN cohort (Reynolds et al. 2011). Written informed consent was obtained from a parent or legal guardian and assent was obtained from each child before study participation. The clinics used previously described guidelines for the diagnosis of FASD (Chudley et al. 2005). Children with FASD and age- and sex-matched typically developing children were recruited from FASD diagnostic clinics in Winnipeg, Manitoba, Canada. Briefly, buccal epithelial cell (BEC) samples were collected for DNA methylation analysis from 25 FASD and 26 age- and sex-matched control children aged between 5 and 18 (Table 1). BECs were collected using the Isohelix buccal swabs and Dri-Capsule (Cell Projects Ltd., Kent, UK). To collect buccal cells, the swab was inserted into the participants' mouth and rubbed firmly against the inside of the left cheek for 1 minute. The swab was then placed into a sterile tube with a Dri-Capsule and the tube sealed. An identical procedure was followed for the right cheek. Participants did not have any dental work performed 48 hours prior to collection, and no food was consumed less than 60 minutes prior to collection to avoid contamination.

5.2.2 DNA methylation 450K assay

DNA was extracted from BECs using the Isohelix DNA isolation kit (Cell Projects, Kent, UK). 750ng of genomic DNA was subjected to bisulfite conversion using the Zymo EZ DNA Methylation Kit (Zymo Research, Irvine, California), which converts DNA methylation information into sequence base differences by deaminating unmethylated cytosines to uracil while leaving methylated cytosines unchanged. 160ng of converted DNA was applied to the HumanMethylation450 BeadChip array from Illumina (450K array), which enables the simultaneous quantitative measurements of 485,512 CpG sites across the human genome, following the manufacturer's instructions. Chips were scanned on an Illumina HiScan, with the 53 samples run in two batches and each containing a similar number of FASD and control samples, randomly distributed across the chips. Two pairs of technical replicates were included and showed a Pearson correlation coefficient $r>0.994$ in both cases, highlighting the technology's reproducibility on our in house-platform. Inter-sample correlations ranged from 0.926-0.99.

5.2.3 DNA methylation data quality control and normalization

The raw DNA methylation data was subjected to a rigorous set of quality controls, first of the samples, and then of the probes. Of the 51 initial samples, 3 were removed from the final dataset based on poor quality data, which was identified through skewed internal controls and/or >=5 % of probes with a detection p-value > 0.05 (2 controls and 1 FASD). Next, probes were removed from the dataset according to the following criteria: (1) probes on X and Y chromosomes (n = 11,648); (2) SNP probes (n = 65); (3) probes with beadcount <3 in 10 % of samples (n = 726); (4) probes with 10% of samples with a detection p-value > 0.01 (n = 11,864);

or (5) probes with a polymorphic CpG and non-specific probes (N = 19,337 SNP-CpG and 10,484 non-specific probes) (Price et al. 2013). A final filtering step was performed to set the methylation values to NA for any remaining probe-sample pair where beadcount <3 or detection p-value > 0.01. Data normalization was performed using the SWAN method on the final dataset, composed of 48 samples (24 FASD and 24 control) and 431,544 probes (Teschendorff et al. 2012). Finally, batch effects (chip number and chip position) were removed using the ComBat function from the *SVA* package in R. All analyses were performed using on ComBat-corrected M-values, which represent the log2 ratio of methylated/unmethylated, where negative values indicate less than 50% methylation and positive values indicate more than 50% methylation (Du et al. 2010). Percent methylation changes (beta-values) were used in graphical representations of the data and indicate the percentage of methylation calculated by methylated/(methylated + unmethylated), ranging from 0 (fully unmethylated) to 1 (fully methylated).

5.2.4 Differential methylation analysis and validation of NeuroDevNet (NDN) findings

Cell type deconvolution was performed to assess the proportions of CD14, CD34, and buccal epithelial cells in each sample using DNA methylation levels at CpGs highly correlated with these cell types (Smith et al. 2015). Surrogate variable analysis (SVA) was also performed on ComBat-corrected, normalized data using the *SVA* package in R to identify surrogate variables (SVs) representative of unwanted heterogeneity (Leek et al. 2012). Using DNA methylation data from all 48 samples, SVA identified 6 SVs not associated with clinical status (FASD vs control). As these were partially associated with known covariates, such as cell type proportions and age, the SVs were included in the linear regression analysis to account for their effects. More specifically, linear modeling was performed on the 648 differentially methylated

probes identified in the initial NDN study and found in the present dataset using the *limma* package in R and a model that included clinical status and all identified SVs as covariates(Smyth 2004; Portales-Casamar et al. 2016). Significant differentially methylated probes between groups were identified at a false-discovery rate (FDR) <0.05 following multiple test correction by the Benjamini-Hochberg method and were required to show the same direction of change as the NDN cohort's findings (Benjamini & Hochberg 1995). Further evaluation of potential biological significance was performed using an arbitrary threshold of >5% mean percent DNA methylation differences between FASD and controls.

5.2.5 DNA methylation pyrosequencing assay

Bisulfite pyrosequencing assays were designed with PyroMark Assay Design 2.0 (Qiagen; Supplementary table 5.1). The regions of interest were amplified by PCR using the HotstarTaq DNA polymerase kit (Qiagen) as follows: 15 minutes at 95°C, 45 cycles of 95°C for 30s, 58°C for 30s, and 72°C for 30s, and a 5 minute 72°C final extension step. For pyrosequencing, single-stranded DNA was prepared from the PCR product with the Pyromark™ Vacuum Prep Workstation (Qiagen) and the sequencing was performed using sequencing primers on a Pyromark™ Q96 MD pyrosequencer (Qiagen). The quantitative levels of methylation for each CpG dinucleotide were calculated with Pyro Q-CpG software (Qiagen).

5.2.6 The NDN cohort of children with FASD

DNA methylation data from the our previous cohort of children with FASD were obtained from GEO (GSE80261), and normalized as in described in our original publication (Portales-Casamar et al. 2016). This cohort was collected by NeuroDevNet, a Canadian Network

of Centers for Excellence, and is hereby referred to as the NDN cohort (Portales-Casamar et al. 2016). Briefly, this dataset was composed of 110 children with FASD or confirmed PAE and 96 age- and sex-matched typically developing controls. The mean age (in years) for individuals with FASD was 11.55 and 11.28 for controls, both ranging from 5-18 years old. A skew in self-declared ethnicity was present between the groups, as the majority of controls identified as Caucasian, while the majority of children in the FASD group identified as First Nations. This skew was addressed in the initial epigenome-wide association study through the use of a more ethnically homogeneous subset of the cohort. DNA methylation data were obtained from buccal epithelial cells using the Illumina 450K array and were normalized using the beta-mixture quantile normalization method.

5.2.7 Cohort of individuals with autism spectrum disorder

Normalized DNA methylation data from a publically available dataset of individuals with autism spectrum disorder (ASD) were obtained from GEO (GSE50759). Briefly, this dataset was composed of 48 individuals with ASD and 48 typically developing controls. The samples consisted of 57 males and 39 females, consistent with the skew towards males in ASD. The mean age (8.84) and range (1-28 years old) differed from the NDN and KBHN studies and the genetic ancestry of most individuals was Caucasian (European), though a proportion of the cohort was of Nigerian ancestry. DNA methylation data of these samples were obtained from buccal epithelial cells using the Illumina 450K array.

5.2.8 DNA methylation as a predictor of FASD status

A predictive model of FASD status was created using DNA methylation data and the *caret* package in R. First, a predictive model was created using stochastic gradient boosting on the NDN cohort (110 FASD: 96 control) using both the differentially methylated probes identified in the NDN study (648 probes) and those validated in the KBHN validation cohort (161 probes) (Portales-Casamar et al. 2016). The parameters of the modeling were optimized for area under the receiver operating characteristic (ROC) curve by grid tuning for repeated cross-validation (number of trees 50-1500; 1,5, or 9 interaction depth; 0.1 shrinkage). The optimal model for predicting clinical FASD status using 648 probes was 1500 trees, 5 of interaction depth, and 20 minimum observations per node. The optimal model for predicting clinical FASD status using 161 probes was 1400 trees, 1 of interaction depth, and 20 minimum observations per node. Next, the KBHN cohort (24 FASD: 24 control) was used as a positive control to verify the predicted sensitivity and specificity of the predictive model. In parallel, 450K data from a cohort of children with autism spectrum disorder (ASD) were tested as a negative control of the model to verify the predicted specificity of the models. Verification of the predictor with these datasets was performed on normalized, uncorrected data to better mimic the potential use of the predictive model by independent groups.

5.3 Results

5.3.1 The KBHN cohort of children with FASD

As noted, we analyzed genome-wide DNA methylation patterns from 24 children with FASD or confirmed PAE and 24 typically developing controls, matched for sex and age, ranging from 2 to 18 years of age (Table 5.1). We found that self-declared ethnicity, primary caregiver,

and mean age were significantly different between the FASD and control participants ($p<0.05$). We corrected for the potential effects of age on DNA methylation through the statistical methods outlined below. However, given the heavy confound in self-declared ethnicity and caregiver status, we could not correct for these effects, and relied on the previous correction of ethnic bias in the initial NDN study (see below) (Portales-Casamar et al. 2016).

	FASD cases	Controls
N	24	24
Age		
Range	2-18	5-17
Mean	9.1	11.6
Sex		
Female	9	13
Male	15	11
Self-declared ethnicity		
Caucasian	4 (2)*	22
First Nations	17 (20)*	1
Asian	1 (0)*	1
Not reported	2	0
Caregiver status		
Biological parents	7	24
Biological grandparents	3	0
Adopted/legal guardian	8	0
Foster care	6	0

*including individuals with mixed First Nations lineage

Table 5.1 Characteristics of the NeuroDevNet II FASD cohort

5.3.2 Children with FASD and typically developing controls showed differential DNA methylation patterns

Following quality control and normalization, 431,544 sites of the 485,512 sites remained in the final dataset of 48 samples, which were corrected for batch effects using ComBat. While BECs are mostly homogeneous population of cells, they contain small proportions of CD34- and CD14-positive white blood cells, which can potentially skew DNA methylation analyses. As

such, cell type deconvolution was performed to identify any blood contamination in the samples, identifying a trend toward significance in the proportions of different cells types between groups (CD34: $p = 0.115$; CD14: $p = 0.224$; BEC: $p = 0.068$). To account for this factor in addition to other additional potential confounding variables within the dataset, we performed surrogate variable analysis to identify patterns of variation, identifying 6 surrogate variables when protecting the effects of group (FASD vs Control). These were correlated with known sources of variation within the data, including cell type proportions and age (Supplementary figure 5.1).

To identify alterations in DNA methylation patterns specific to the FASD group, we coupled differential DNA methylation analysis using a two-group design with the surrogate variables to correct for undesirable variation in the data. Given that ethnicity-related probes were already accounted for in the NDN study as much as possible, it was concluded that the effects of ethnic background would be lessened by using the final 658 differentially methylated CpGs (Portales-Casamar et al. 2016). As such, we performed linear modeling on the probes that were differentially methylated in the first study and remained in the dataset after pre-processing (648 CpGs of 658 from NDN). Of these, 161 CpGs displayed differential methylation in the same direction as the initial cohort in the KBHN FASD group compared to the controls at a FDR<0.05 (Figure 5.1A; Supplementary table 5.2). To assess the probability of validating this many probes, random group subsampling and probe subsampling were performed 10,000 times. As none showed more differentially methylated probes than the original replication cohort (maximum = 31 differentially methylated probes), the probability of validating 161/648 probes was < 1e-4 (Supplementary figure 5.2). Of the 161 validated probes, 82 were up-methylated while 79 were down-methylated in FASD compared to control samples. Several genes contained multiple differentially methylated CpGs across both cohorts, including *HLA-DPB1* (5), *FAM59B* (4),

CAPN10 (3), *DES* (3), *SLC6A3* (3), *SLC38A2* (3), *FAM24A* (2), *H19* (2), and *TGFB1I1* (2) (Table 5.2). Moreover, 53 CpGs showed >5% change in methylation, an arbitrary cutoff often used to gauge potential biological significance. Of note, three genes contained 2 or more DM probes that showed both an FDR<0.05 and change in percent methylation >5%, *FAM59B* (4 probes), *HLA-DPB1* (2 probes), and *SLC6A3* (2 probes). In particular, the *FAM59B* CpGs were located within a CpG island and showed very strong differences in DNA methylation levels between FASD and control groups, with an average 13% methylation change across the array probes in the CpG island (Figure 5.2).

Overall, the percent methylation changes between groups of the 648 analyzed probes were highly correlated between the NDN and KBHN cohorts (r=0.638; figure 5.1B). Across the entire 648 probes analyzed, 462 had the same direction of change, even though the majority did not achieve statistical significance. We also compared the ranking of probes by p-value from linear modeling between the NDN and KBHN cohorts; no significant similarities were identified (p=0.91). Of note, 21 of the significant probes with >5% methylation change in the NDN study were validated in the present analysis (39 of 41 were present in KBHN). This proportion (54%) was much higher than all validated probes (25%), suggesting that these represented potentially more robust effects of alcohol exposure on the epigenome. When using a 5% methylation change as a cutoff, rather than an FDR < 0.05, 62 probes were validated in the KBHN cohort (p<0.1, max FDR = 0.177), of which 25 displayed > 5% change in both cohorts (64% of the NDN probes).

Gene	# of CpGs	Direction of change
HLA-DPB1	5	UP
FAM59B	4	DOWN
DES	3	DOWN
SLC6A3	3	UP
SLC38A2	3	DOWN
CAPN10	3	UP
FAM24A	2	UP
H19	2	DOWN
TGFB1I1	2	DOWN

Table 5.2 Genes containing multiple differentially methylated CpGs in FASD

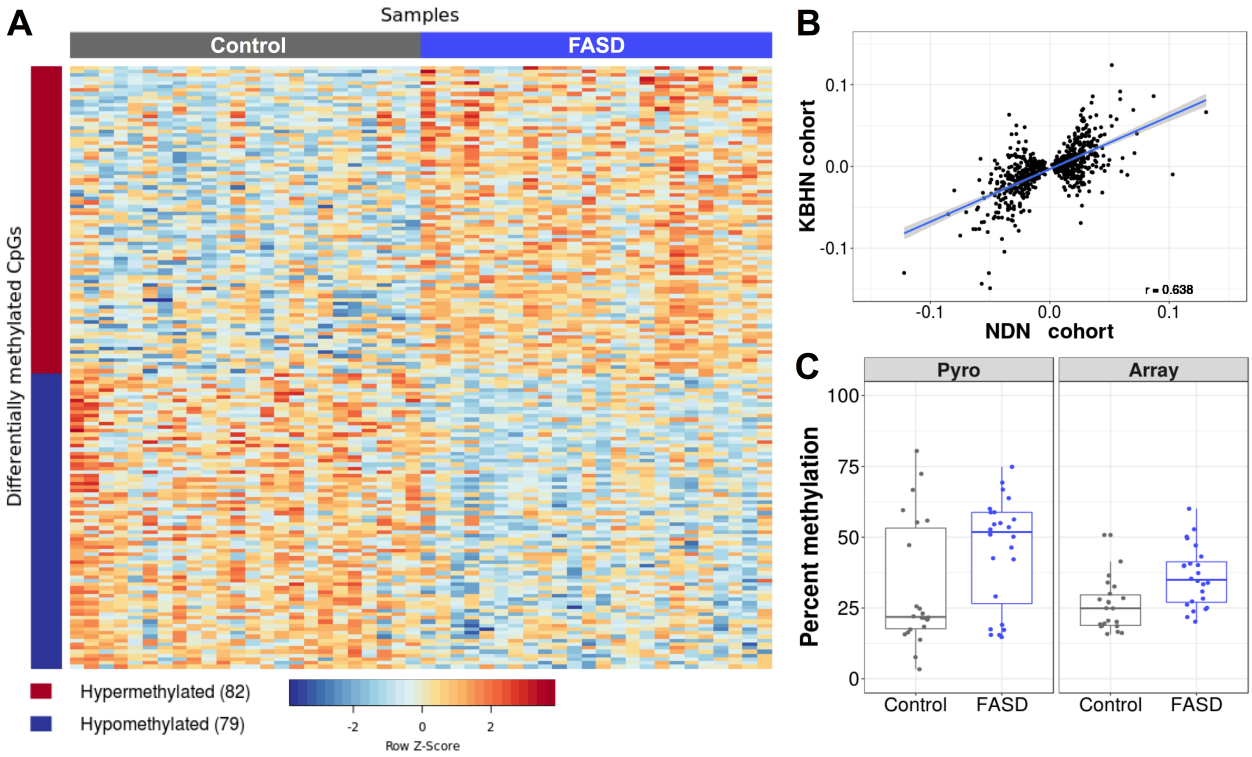

Figure 5.1 Visualization and verification of the differentially methylated probes

A) Heatmap of the 161 validated probes validated in the KBHN cohort at an FDR <0.05 (79 hypermethylated in FASD; 82 hypomethylated in FASD). The percent methylation values (ranging from 0 to 100) were centered, scaled, and trimmed, resulting in a standardized DNA methylation level ranging from −2 to +2 (blue-red scale). B) Scatter plot of the differences in percent methylation between FASD and controls for the 648 differentially probes identified in the NDN cohort. The mean changes between groups were highly correlated between both the NDN and KBHN

cohorts (r = 0.638). C) Verification by bisulfite pyrosequencing in FASD (*blue*) and control (*gray*) samples verified the difference observed on the 450K array (p=0.0501). The left panel shows the DNA methylation levels from the pyrosequencing assay, while the right panel shows the results from the 450K array. The CpG assayed was located in the *CACNA1A* gene body (*cg24800175*).

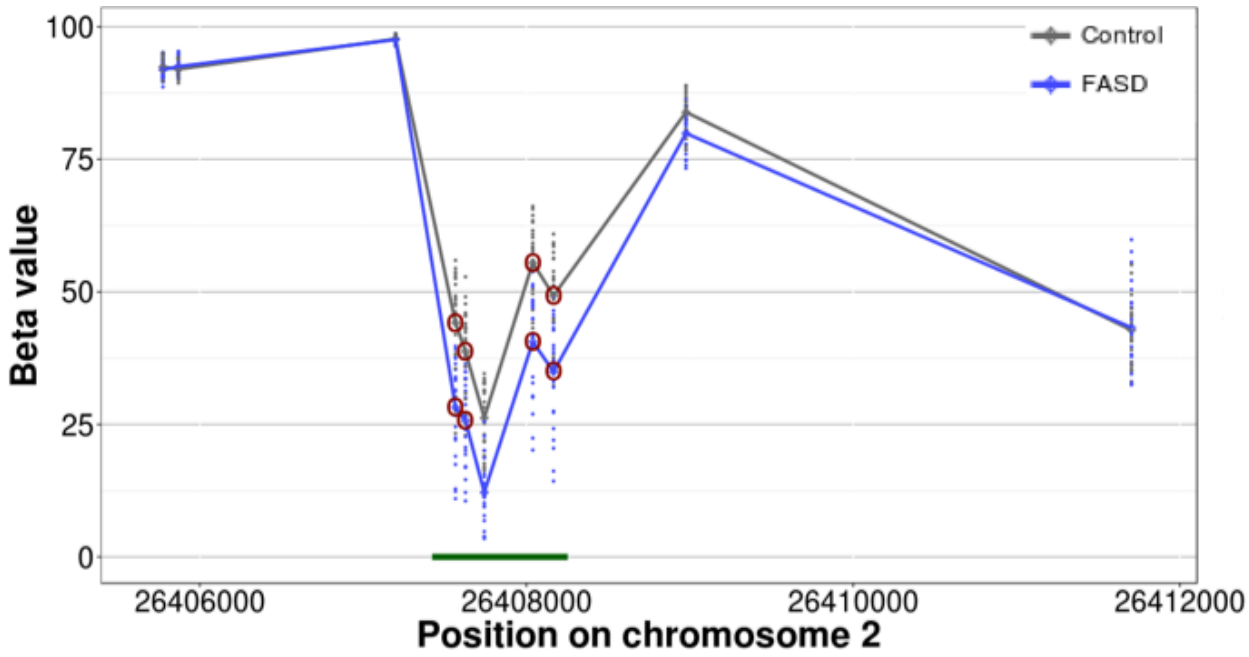

Figure 5.2 Several differentially methylated CpGs were located in the *FAM59B* gene body

DNA methylation levels for FASD (*blue*) and controls (*grey*) are shown for 10 CpGs within the gene, with the red circles representing the validated hits in KBHN (FDR <0.05). These were located in a CpG island, illustrated by the green bar at the bottom, which showed an average 13% change in DNA methylation levels in individuals with FASD versus controls across all 5 CpGs covered by the 450K array.

5.3.3 Bisulfite pyrosequencing verified the differential DNA methylation of *CACNA1A*

To verify that the differential DNA methylation results did not depend on the method used to measure them, we assessed DNA methylation levels of the cg24800175 probe in *CACNA1A*. We selected this probes as it was also verified in the initial NDN study, where it similarly showed a >5% change in DNA methylation between individuals with FASD and

controls (p=0.0501). Pyrosequencing results confirmed the DNA methylation levels observed on the 450K array, showing similar DNA methylation levels and differences between groups for CpGs located in *CACNA1A* (Figure 5.1C). The Pearson correlation between these two methods was 0.826 and the Bland–Altman plot showed little difference when comparing the 450K array to pyrosequencing, suggesting good concordance between DNA methylation data from the two methods (Supplementary figure 5.3). Linear regression analysis of pyrosequencing data between FASD cases and controls confirmed differential DNA methylation in this site, even without correcting for covariates (p = 0.04).

5.3.4 DNA methylation patterns classified individuals with FASD versus controls

To assess whether DNA methylation data could be used to predict FASD status, we created a predictive algorithm of FASD using machine learning approaches. First, we selected normalized DNA methylation data from the 206 samples in the NDN cohort (110 FASD: 96 control) in both the 648 initial probes that were also found in the KBHN data. In addition, we also assessed the 161 probes that were validated across both cohorts, though this model may have resulted in over-fitting of the data. Our strategy was to build both predictors (648 probes vs 161 probes) using an initial training cohort (NDN), followed by subsequent testing in the test cohort (KBHN). See Figure 5.3 for an overview of steps used to build the FASD predictor.

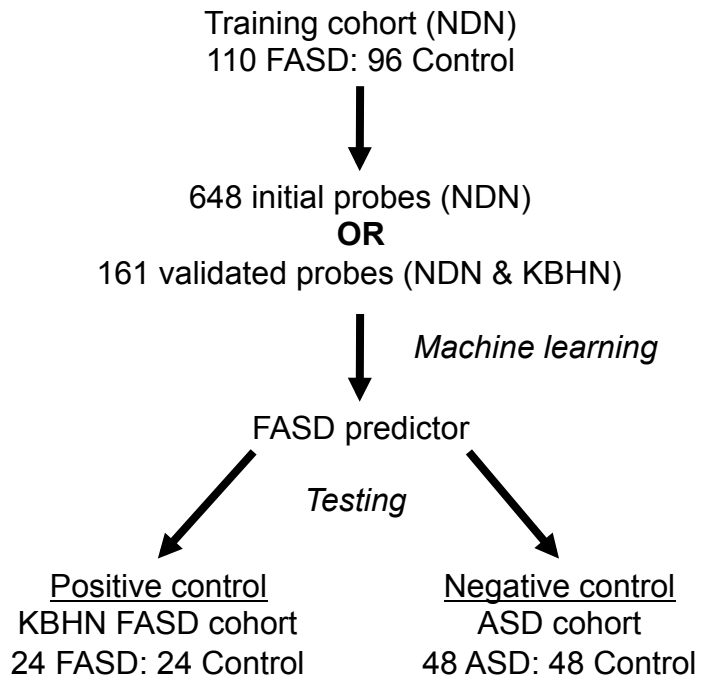

Figure 5.3 Flowchart of bioinformatic analyses for the DNA methylation predictor of FASD

Briefly, samples from the NDN cohort were used as the training set, and machine learning was performed on either the 648 probes from the initial NDN study, or the 161 probes validated in the present study. The resulting FASD predictor was tested on the KBHN test set, as well as a negative control set composed of individuals with autism spectrum disorder and typically developing controls.

Using a gradient boosting model in the *caret* package to optimize both sensitivity and specificity (area under the ROC curve), we created two predictive models to assess the probability of FASD based on DNA methylation patterns (Supplementary table 5.3). For the 648 initial probes model, the predicted sensitivity and specificity for the training cohort were 0.922 and 0.978, respectively, for an area under the curve of 0.993 (95% confidence intervals: 0.990-0.995; Figure 5.4A). By contrast, for the 161 probes model, the predicted sensitivity and specificity were 0.887 and 0.892, respectively, forming an area under the curve of 0.955 (95%

confidence intervals: 0.947-0.963; Figure 5.4B). As expected, the 648 model performed much better in the training set, given that the NDN cohort was used to generate these findings.

We next assessed the predictive models using the normalized, batch-corrected DNA methylation data of the KBHN cohort as a test set. Of note, these data were not corrected for any covariates or surrogate variables other than batch correction. In this cohort, the 648 initial probes model performed more poorly, displaying 0.875 sensitivity, 0.542 specificity, and 0.819 area under the ROC curve (Table 5.3; Figure 5.4A). The balanced accuracy of the model in this cohort was 0.708% (95% CI: 0.559-0.830), and the ROC curve was significantly different from the one obtained in the training cohort (p=0.0051). Overall, 11 controls were misclassified as FASD and 3 children with FASD were misclassified as controls, giving a negative predictive value (NPV) of 81.3% and a positive predictive value (PPV) of 65.6%. In contrast to the 648 probes model, the test set confirmed the predictive accuracy of the 161 probes model, though it was potential over-fitting the data. This model displayed 0.917 sensitivity, 0.875 specificity, and 0.944 area under the ROC curve, while the balanced accuracy in this cohort was 0.896% (95% CI: 0.773-0.965), similar to the training dataset (Table 5.3; Figure 5.4B). Overall, 3 controls were misclassified as FASD and 2 children with FASD were misclassified as controls, giving a negative predictive value (NPV) of 88% and a positive predictive value of 91.3%. Moreover, the ROC from the training set and test set were not significantly different (p=0.78), suggesting that the predictor functioned correctly in a similar dataset. Given the discrepancies in ethnic backgrounds between FASD and control groups, the misclassified samples were assessed for differences in self-reported ethnicity, caregiver status, age, or cell-type proportions in the classification. However, no patterns emerged between the correctly and incorrectly classified

individuals, suggesting that differences in demographic variables between the groups do not drive their classification.

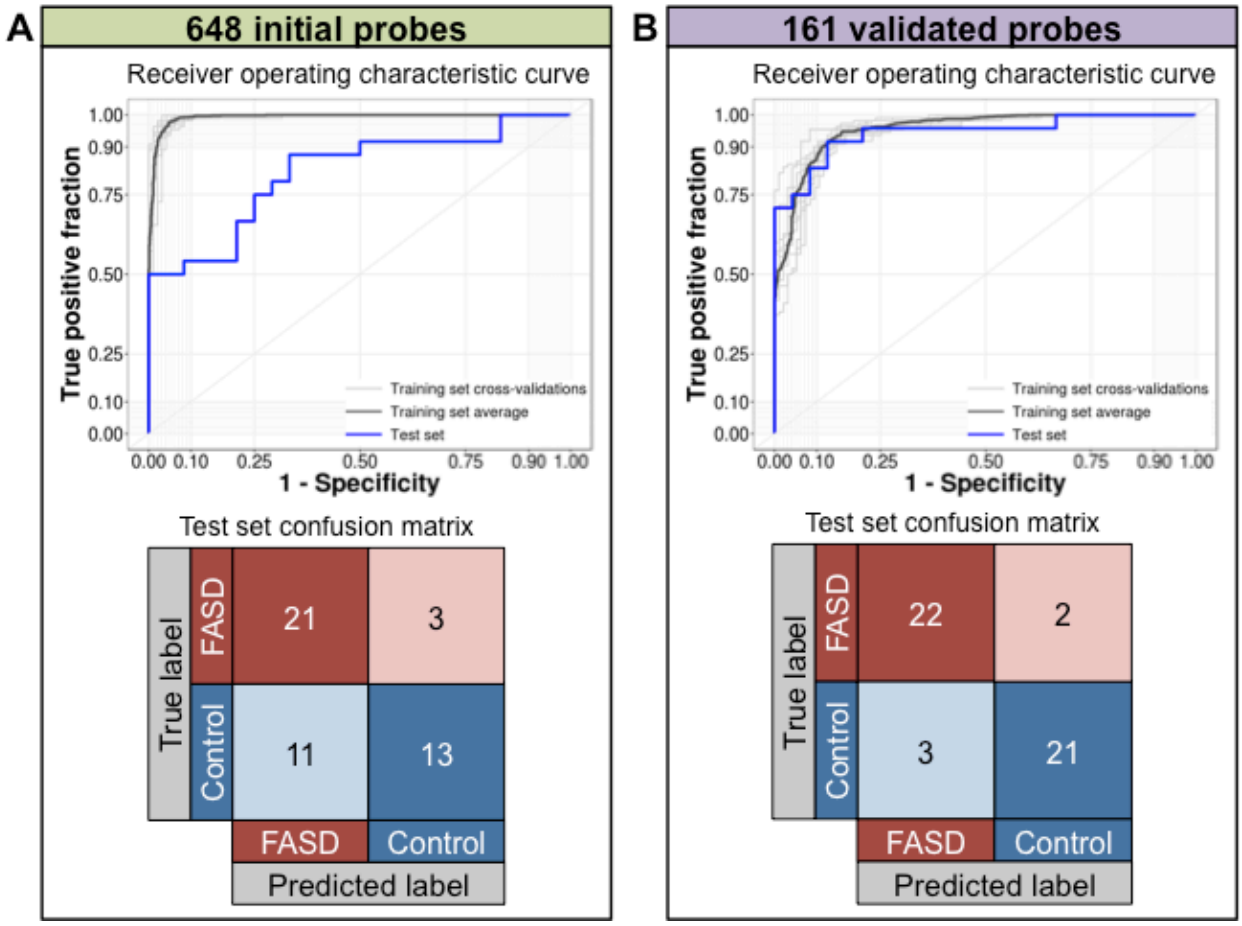

Figure 5.4 Visualization of the training and test set performance for both DNA methylation predictors

A) The DNA methylation predictor created using the 648 probes identified in NDN showed high accuracy in the training cohort (*dark grey*; area under the curve = 0.99), but poorer accuracy in the KBHN test set (*blue*; area under the curve = 0.82; $p<0.01$). In particular, 11 control samples in the test set were misclassified as FASD, while only 3 individuals with FASD were classified as controls. B) The DNA methylation predictor created using the 161 validated probes also showed high accuracy in the training cohort (*dark grey*; area under the curve = 0.96), and similar accuracy in the test set (*blue*; area under the curve = 0.94, $p=0.77$). Only 3 controls were misclassified as FASD and 2 individuals with FASD were classified as controls.

	648 probes	161 probes
Training set (NDN)		
AUC	0.993	0.955
Accuracy	0.943	0.890
Sensitivity	0.922	0.887
Specificity	0.978	0.892
Test set (KBHN)		
AUC	0.819	0.944
Accuracy	0.708	0.896
Sensitivity	0.875	0.917
Specificity	0.542	0.875
False positives	11	3
False negatives	3	2
PPV	0.656	0.880
NPV	0.813	0.913
Negative control (ASD)		
Accuracy	0.823	0.875
Sensitivity	NA	NA
Specificity	0.823	0.875
False positives	17	12

Table 5.3 Summarized results from the classification algorithms

5.3.5 The DNA methylation predictors were not biased by ASD in an independent cohort

BEC samples from an independent ASD cohort served as a negative control to assess the validity of the model in the FASD cohorts. To this end, we used a publically available dataset of 450K array data from the BECs of 48 individuals with autism spectrum disorder (ASD) and 48 typically developing controls from the gene expression omnibus (GSE50759). Using uncorrected, normalized data from this cohort, the two predictors correctly identified the vast majority of individuals in the cohort as non-FASD. The 648 initial probes model misclassified 17 individuals (9 ASD and 8 controls) as FASD, for a specificity of 0.823 (95% CI: 0.732-0.893), slightly lower than the predicted specificity in the training set. By contrast, 12 individuals (7 ASD and 5 controls) were misclassified as individuals with FASD using the 161 probes model, for a specificity of 0.875 (95% CI: 0.792-0.934), which was consistent with predicted values from the model (Table 5.3). The samples did not have any distinguishing features from the

correctly classified sample, suggesting that the predictive model is not biased for ASD, sex, age, or Nigerian ancestry in independent cohorts.

5.4 Discussion

Epigenetic mechanisms are emerging as potential biomarkers and mediators of environmental exposures, and a growing body of literature suggests that epigenetic factors may be involved in the etiology of FASD. In particular, our recent study using the largest cohort of children with FASD to date identified a signature of 658 differentially methylated CpGs in the BEC of individuals with FASD compared to typically developing controls (Portales-Casamar et al. 2016). Here, we present the first validation of genome-wide DNA methylation data in a small cohort of individuals with FASD, where we successfully validated 161 of the 658 differentially methylated CpGs identified in the initial NDN cohort. Furthermore, we demonstrated that DNA methylation data could be utilized to successfully generate predictive algorithms to classify individuals as FASD or controls with high accuracy. These results indicated that DNA methylation in BEC could potentially be used as a biomarker of PAE to screen children at risk for FASD.

Our present findings represent the first validation of genome-wide DNA methylation alterations in individuals with FASD. Of the 161 validated CpGs at an FDR<0.05, 53 had >5% change in DNA methylation levels, the arbitrary threshold for potential biological relevance. When using a DNA methylation change >5% as a cutoff, rather than a stringent FDR, 62 CpGs were validated, with 25 of those showing this magnitude of change in the NDN cohort as well, suggesting that these regions are more responsive to alcohol's effects. Importantly, the majority

of the CpGs showed the same direction of change between FASD and controls in both cohorts (462/648), and while they did not achieve statistical significance, potentially due to the small size of this cohort, they may reflect consistent alterations of PAE on the epigenome. In addition, we verified the results from the 450K array by bisulfite pyrosequencing, confirming the differential DNA methylation results for a CpG located in *CACNA1A* and supporting that our findings were not an artifact of array technology.

Although the effects of alcohol on the epigenome were relatively subtle, we note that several genes previously associated with PAE or FASD contained multiple differentially CpGs, including *FAM59B*, *H19*, *HLA-DPB1*, and *SLC6A3*. In particular, DNA methylation alterations in the imprinted gene *H19* have been previously associated with PAE in both animal models and clinical cohorts of FASD, and may reflect broader alterations to imprinted genes caused by PAE (Stouder, Somm, & Paoloni-Giacobino 2011; Ouko et al. 2009; Haycock & Ramsay 2009; Portales-Casamar et al. 2016). Moreover, the *HLA-DPB1* locus, a member of the major histocompatibility complex proteins, contained several differentially methylated CpGs, which overlapped with a differentially methylated region identified in the NDN study. Given its key function in immune regulation and potential role in rheumatoid arthritis, these alterations could potentially reflect some of the immune changes associated with FASD (Liu et al. 2013). Furthermore, the *FAM59B* gene contained several CpGs with large changes in DNA methylation levels between individuals with FASD and controls, potentially representing a particularly sensitive locus with regards to PAE. Of note, only one validated CpG was located in a protocadherin gene (*PCDHB18*), which were considerably enriched in previous genome-wide studies of DNA methylation in individuals with FASD (Laufer et al. 2015; Portales-Casamar et al. 2016). Given that these only showed one overlapping probe, this could indicate higher

variability within these gene clusters that may be associated with other variables not present in the current dataset, such as differences in age, BMI, ethnicity, and SES.

Of particular interest, we replicated the differential DNA methylation patterns of the two genes involved in dopamine signaling from the NDN cohort, the dopamine transporter *SLC6A3* and the dopamine receptor D4 (*DRD4*). Given the key role of the dopaminergic system in brain development and its interactions with neuroendocrine and immune systems, these alterations could potentially reflect broader changes to signaling pathways in the organism. Of note, the buccal epithelial cells of children exposed to alcohol during prenatal life and breastfeeding also display altered DNA methylation patterns in the promoter region of *DRD4* (Fransquet et al. 2016). Furthermore, several disorders previously associated with allelic variation and DNA methylation in this gene show either overlaps or co-morbidities with FASD, including ADHD, bipolar disorder, anxiety disorder, schizophrenia, and substance abuse (Sánchez-Mora et al. 2011; Dadds et al. 2016; Ji et al. 2016; Cheng et al. 2014; Kordi-Tamandani, Sahranavard, & Torkamanzehi 2013; Docherty et al. 2012; Ptáček, Kuželová, & Stefano 2011; Bau et al. 2001; Zhang et al. 2013; Faraone, Bonvicini, & Scassellati 2014; Chen et al. 2011). Given that dopamine signaling plays a key role in brain development and function, it is tempting to interpret these findings in the context of PAE-induced deficits. However, DNA methylation alterations in buccal epithelial cells may not fully reflect alterations in the central nervous system. Nevertheless, it has been suggested that BEC may act as a suitable surrogate tissue in human studies of DNA methylation, as they are also derived from the ectoderm (Lowe et al. 2013). While we did not measure these genes in additional tissues, evidence from animal models suggest that PAE can cause lasting alterations to the epigenome of central nervous system

tissues, and as such, these results may represent potentially broader alterations to epigenomic patterns in the brain (Lussier, Weinberg, & Kobor 2017).

Although these findings represent the first validation of genome-wide DNA methylation data in children with FASD, a few particularities of the KBHN cohort limit the interpretability and generalizability of these results. Similar to the initial cohort, the KBHN replication cohort was heavily confounded by ethnicity, as the vast majority of FASD cases were from First Nations communities, while controls were mainly Caucasian. Given that ethnicity influences DNA methylation patterns, differences between groups may have been due to genetic background. Unfortunately, the KBHN cohort was too small to separate the groups into more ethnically homogeneous subsets, a method we had previously used to account for ethnicity-related differences in DNA methylation. As such, we performed linear modeling on the sites that had been previously identified in the NDN study, which were partially filtered for ethnicity-related differences during the analysis of the first cohort. However, some of the top differentially methylated genes could potentially be influenced by ethnicity differences between groups in spite of our best efforts. For instance, three known polymorphisms are located within the *FAM59B* locus (dbSNP minor allele frequencies: rs774397935: 1.04%; rs4665833: 5.1%; rs181971256: 21.4%). Although none of these are known methylation quantitative trait loci (mQTL), the *FAM59B* gene body contains several mQTLs in the developing human brain, and genetic variation outside the region could potentially influence DNA methylation levels (Hannon et al. 2015). In addition, nearby genetic variation can also influence DNA methylation patterns in the promoter of *DRD4*, which may be reflected in this cohort through the skew in ethnicity between groups (Docherty et al. 2012). Although the frequencies of these alleles in First Nation populations have not been assessed, genetic differences between groups could potentially

influence DNA methylation levels within this differentially methylated region. Nonetheless, our results suggest that the regulation of these genes might be altered in individuals with FASD, which may potentially occur through direct effects of alcohol on the epigenome or through increased susceptibility to the effects of alcohol due to genetic variation.

In addition to self-declared ethnicity, significant differences in the primary caregiver were present between groups, as all controls lived with their biological families, while the majority of children with FASD were typically in foster care. While the effects of this disparity on the epigenome are unclear, they could influence DNA methylation patterns through a number of factors, including nutrition, early-life adversity, and socio-economic status (SES) (Esposito et al. 2016). However, we also used SVA to account for differences between groups that may have influenced DNA methylation, including cell type proportions, age, and sex. As such, we feel that the potential confounds associated with the cohort design were reduced through our statistical procedures, though future studies with groups balanced for ethnicity and additional variables will be necessary to tease out these differences and further validate our findings.

Finally, we show for the first time that DNA methylation patterns could be used as biomarkers of PAE in clinical populations and can be utilized as predictive variables for FASD. These findings complement and extend previous studies that investigated different molecular and physiological markers to help screen children for potential prenatal alcohol exposure, including alcohol metabolites in mothers and children, circulating miRNA in mothers, and cardiac orienting response in children (Balaraman et al. 2016; Mesa et al. 2017; Goh et al. 2016; McQuire et al. 2016) . In particular, eye tracking measures have been used in a small cohort of children to distinguish children with FASD, ADHD, or typically developing controls with

relatively good accuracy (Tseng et al. 2013). In contrast to these studies, the present cohorts were composed of both children diagnosed with FASD and some with confirmed PAE/high-risk of developing FASD. As no follow-up was performed to determine if all children with PAE were ultimately diagnosed with FASD at a later date, the classification models were essentially tuned to screen children at a higher risk for developing FASD with both high sensitivity and specificity. Importantly, our results suggest that DNA methylation predictors can achieve high accuracy in the classification of individuals with FASD versus controls across multiple cohorts. Although the prediction algorithm that used the 161 validated probes showed more consistent results across different cohorts (NDN: 88.9%; KBHN: 89.6%; ASD: 87.5 %) than the 648 probes algorithm (NDN: 94.3%; KBHN: 70.8%; ASD: 82.3%), the use of the validated probes may have caused some over-fitting in the KBHN test set. Nevertheless, it provides an important second validation of the strongest associations with FASD, which likely represent the more robust DNA methylation alterations caused by PAE. Moreover, both predictive algorithms appear to be largely independent of typical confounding factors, such as age, sex, ethnicity, and cell type composition of the samples, as well as ASD. Collectively, these results support the use of DNA methylation as a potential biomarker of PAE and screening tool for FASD.

5.4.1 Summary and conclusions

Given the broad spectrum of cognitive, behavioral, and biological deficits caused by PAE, FASD places an important strain on both societal resources and the affected individuals and families. As such, accurate biomarkers are necessary to identify children at risk for FASD at an early age, when interventions are most effective. Our findings provide an important stepping-stone towards epigenetic biomarkers of FASD and set the stage for broader screening tools for

neurodevelopmental disorders. Nevertheless, validation of these tools across different cohorts, with varying ages, ethnicities, and environmental exposures will be essential to parse out the strongest associations and create a successful molecular diagnostic tool for FASD.

Chapter 6: Conclusion

6.1 Summary and cross-cutting features

The work presented in this dissertation highlights the programming effects of PAE on the developing organism, and provides a framework for the use of DNA methylation as a biomarker for FASD. More specifically, I took advantage of an animal model of PAE and two clinical cohorts of children with FASD to identify genome-wide alterations to gene expression programs and DNA methylation patterns.

I profiled genome-wide transcriptomic alterations using gene expression microarrays in the hippocampus and prefrontal cortex of adult female PAE rats under steady-state (basal, saline-injected) and immune challenge (adjuvant-injected) conditions. I identified significant changes in gene expression in PAE compared to controls in response to ethanol exposure alone (saline-injected females), including genes involved in neurodevelopment, apoptosis, and energy metabolism. Moreover, in response to an adjuvant-induced arthritis challenge, PAE animals showed unique gene expression patterns, while failing to exhibit the activation of genes and regulators involved in the immune response observed in control and pair-fed animals. These results support the hypothesis that PAE affects neuroimmune function at the level of gene expression, demonstrating long-term effects of PAE on the CNS response under steady-state conditions and following an inflammatory insult.

Building on these findings of persistent alterations to the brain's transcriptome, I investigated the early programming effects of PAE on the brain's epigenome. Specifically, I probed for alterations to DNA methylation programs across early postnatal development in the hypothalamus. As a key regulatory region of the stress response, immune system, and both autonomic and homeostatic regulation, the hypothalamus is a central target for the biological

embedding of PAE and I hypothesized that this region would be more responsive to the effects of PAE on the epigenome. I identified numerous differentially methylated regions (DMRs) that showed persistent differences in PAE compared to control animals across pre-weaning development. Importantly, these contained genes enriched for functions in immune regulation, hormonal response, and epigenetic mechanisms, suggesting that epigenetic mechanisms may play a role in PAE-induced alterations to hypothalamic functions. Furthermore, these DMRs also contained a higher proportion of BHLHE40 binding sites, a transcription factor that was also differentially expressed in the prefrontal cortex of PAE animals exposed to adjuvant compared to controls. As BHLHE40 is an important regulator of the circadian rhythm, it could potentially play a role in mediating some of the long-term deficits associated with FASD (Nakashima et al. 2008). Given that central nervous system tissue is not accessible in clinical settings, other than in postmortem specimens, I also assessed the concordance of PAE-induced differential DNA methylation patterns between the hypothalamus and WBC. I identified 300 DMRs that showed the same direction of change in response to PAE in both tissues, which contained genes enriched for functions in immune regulation, the stress response, and chromatin remodeling. These may represent systemic effects of PAE on the developing organism and suggest that WBC could potentially act as a surrogate for CNS alterations in a subset of the epigenome.

Overall, the epigenomic analyses revealed more differential DNA methylation in intergenic regions, suggestive of underlying regulatory regions that could have subtle but broader effects on gene expression profiles and cellular regulation. Furthermore, a number of DMRs were located around intron/exon boundaries, which have been associated with alternative splicing of genes (Shukla et al. 2011; Maunakea et al. 2013, 2010). Although I could not measure the proportions of different isoforms through the gene expression microarray analyses, these

findings suggests that PAE could potentially alter the balance of gene isoforms in the developing organism, which could have important ramifications on the developmental trajectories of neurobiological systems.

Finally, across the three different analyses in our rat model of PAE, I identified several alterations to genes involved in immune regulation, suggesting that, even at baseline levels, PAE animals display differential overall cellular responses to immune factors. In addition, the differentially expressed genes in the brain of adult PAE rats were enriched for functions related to lymphocyte differentiation, further highlighting the prevalence of immune-related changes across different studies. Furthermore, all three analyses identified alterations to genes involved in epigenetic regulation, highlighting the complex interplay between the various layers of genetic regulation and stressing the importance of investigating multiple levels of regulatory mechanisms following PAE.

To complement the findings from animal models of PAE, I investigated DNA methylation patterns in a cohort of children and adolescents with FASD. After correcting for the effects of ethnicity, I found 658 significantly differentially methylated CpGs between FASD cases and controls in buccal epithelial cells. Furthermore, over-representation analysis of genes with up-methylated CpGs revealed a significant enrichment for neurodevelopmental processes and diseases, such as anxiety, epilepsy, and autism spectrum disorders. These findings suggest that prenatal alcohol exposure is associated with distinct DNA methylation patterns in children and adolescents. Importantly, I validated these findings in an independent cohort of individuals with FASD, replicating the differential DNA methylation levels at 161 CpGs throughout the

genome. These were located in several genes involved in immune function, highlighting the parallels between animal models and clinical cohorts of FASD.

Of particular note, children and adolescents with FASD had altered DNA methylation levels in several genes from the complement system (*C1RL*), and cytokine/chemokine signaling (*CXXC11*, *IL1R1*), as well as alterations to *HLA-DPB1*, a component of the major histocompatibility complex previously associated with rheumatoid arthritis (Liu et al. 2013; Raychaudhuri et al. 2012). While these findings were identified in a peripheral tissue not directly involved in immune modulation, they may provide insight into changes in global epigenetic patterns associated with altered immune profiles in individuals with FASD. Furthermore, *DRD4*, a crucial regulator of the dopaminergic system, had altered DNA methylation levels associated with PAE in both the hypothalamus of PAE animals and BEC of individuals with FASD. Given that genetic variation and DNA methylation in this gene has previously been associated with several disorders comorbid with FASD, such as ADHD, depression, schizophrenia, and substance use, this finding suggests that it could potentially play a role in the etiology of several PAE-induced deficits (Ptáček, Kuželová, & Stefano 2011; Bau et al. 2001; Sánchez-Mora et al. 2011; Abdolmaleky et al. 2008; Cheng et al. 2014; Faraone, Bonvicini, & Scassellati 2014; D. Chen et al. 2011; Dadds et al. 2016; Ji et al. 2016; Kordi-Tamandani, Sahranavard, & Torkamanzehi 2013). Taken together, these results highlight the value of animal models in assessing the molecular underpinnings of FASD in the central nervous system, and suggest a potential role for DNA methylation in the etiology of some PAE-induced deficits, including those in self-regulation and immune function.

Finally, as these findings raised the possibility of an epigenetic biomarker of FASD, I investigated the potential relevance of DNA methylation in developing a predictive algorithm for

PAE. Using these the two clinical cohorts at our disposal, I successfully generated a bioinformatic tool that could classify individuals with FASD versus controls. Importantly, this algorithm could also successfully differentiate between autism spectrum disorder and FASD, suggesting that these epigenetic patterns were likely specific to individuals with PAE.

As a whole, I propose that PAE can leave a lasting impression on the epigenome of central and peripheral tissues, which may potentially influence the deficits observed in individuals with FASD. In turn, these could also be used a biomarkers of PAE to identify individuals with FASD earlier in life, or aid in diagnoses at later ages.

6.2 Limitations

These results represent an important step towards understanding the molecular underpinnings of fetal programming by PAE and the deficits associated with FASD. However, their interpretation may be limited by our use of female offspring in the animal model, tissue and cell-type differences in epigenetic patterns, genetic background, and their correlative nature. In addition, while these findings also suggest a potential role for DNA methylation as a biomarker of FASD, our clinical cohorts also contained several individuals with confirmed PAE, but were not yet diagnosed with an FASD.

6.2.1 Sexual dimorphisms

In the animal model, I focused our investigation of PAE-induced gene expression and epigenetic alterations on female animals, partially due to their increased vulnerability to autoimmune disorders such as rheumatoid arthritis and the underrepresentation of females in molecular and genome-wide studies of FASD. However, this approach presents an important

caveat in the interpretation of our results, as males and females often display sexually dimorphic responses to the effects on alcohol on various neurobiological systems. In particular, males generally show different cognitive and behavioral phenotypes, as well as differential susceptibilities to stressors and mental health disorders compared to their female counterparts (Hellemans et al. 2008; Bale & Epperson 2015; Oldehinkel & Bouma 2011). Given that genetic and epigenetic patterns are highly associated with sex, our findings must also be validated in male animals to fully assess the effects of PAE on the transcriptome and DNA methylome and to understand the sexually dimorphic effects that may exist (Zhang et al. 2011).

6.2.2 Tissue specificity and cellular heterogeneity

Given the key role of epigenetic mechanisms in driving cellular identity, cellular heterogeneity is a major drivers of epigenetic variation in large datasets, which may influence the differences identified between groups (Smith & Meissner 2013). As PAE causes neuronal apoptosis, it is possible that slight differences in cell composition are present between prenatal treatment groups (Ikonomidou et al. 2000). As such, DMRs identified in the animal model could potentially be due to underlying differences in cell composition of the hypothalamus or total WBC. Furthermore, as the entire hypothalamus was analyzed, the impact of PAE on its different nuclei, which have widely varying functions, cannot be conclusively assessed (Squire et al. 2008). Nevertheless, differences in genes related to the functions of a particular hypothalamic center could be tentatively assigned and validated in independent studies. Additionally, while cellular composition could also have affected the results obtained from the tissue concordance analysis, I did not identify any difference in the proportions of different WBC subtypes. While these result may suggest few differences between groups, more sensitive methods could

potentially subdivide these cell types further to provide a more granular signal of cellular heterogeneity (De Souza et al. 2016).

Furthermore, alterations to the epigenetic patterns of central tissues are not easily measurable in humans, other than in postmortem brain samples. Thus, the vast majority of epigenome-wide association studies are performed in peripheral tissues such as blood and buccal epithelial cells in the hope that they reflect epigenomic variation in the brain. As epigenetic patterns are highly dependent on cell types that may respond differently in the face of the same exposures, these surrogate tissues may not fully portray the true changes driving disease. However, the establishment of common epigenetic profiles between central and peripheral tissues is an ongoing and essential topic of research, and several studies suggest that peripheral tissue could potentially be used as a surrogate for CNS alterations in humans (Walton et al. 2016; Farré et al. 2015; Kaminsky et al. 2012; Davies et al. 2012; Smith et al. 2015; Horvath et al. 2012). These further highlight the power of our animal model study, as it allowed us to make direct correlations between central and peripheral tissue in the same animals and identify concordant alterations to DNA methylation patterns in the hypothalamus and WBC.

6.2.3 Genetic background

Genetic background can also influence DNA methylation patterns throughout the genome, as a large number of CpG sites are associated with genetic variation (Fraser et al. 2012; Moen et al. 2013; Heyn et al. 2013). Of note, our animal model is based on an outbred population of Sprague-Dawley rats, which display a range of genetic diversity. As such, differing genetic backgrounds among prenatal treatment groups could potentially have influenced the DMRs identified in the developmental and tissue-concordant analyses. This issue was further

highlighted in the clinical cohorts, where the majority of individuals with FASD were of First Nation descent, while the controls were primarily of Caucasian descent. Although this limitation was at least partially mitigated through the use of statistical methods, they could potentially have influenced the PAE-induced epigenetic alterations identified in these studies. By contrast, I could not account for this potential genetic influence in the animal model, and further studies are required to fully investigate the interaction between genetic variants and epigenomic patterns in the context of PAE.

6.2.4 Correlation versus causation

Although the data presented in this thesis lend support to hypothesis that PAE can influence neurobiological systems through epigenetic alterations, they were not designed to examine the exact mechanisms of alcohol's effects. More specifically, even though gene expression profiles and epigenetic mechanisms are correlated with PAE in cross-sectional clinical cohorts and animal models, it is not yet clear whether their reversal would dampen PAE phenotypes, which would indicate a more causal role. Emerging technologies, such as CRISPR fused to chromatin modifiers, could potentially be used to selectively alter the epigenetic profiles of key genes and provide a more causal link between epigenetic alterations and PAE-induced deficits (Enríquez 2016). Moreover, while epigenetic patterns are associated with gene expression, these relationships are inconsistent across individuals and the functional implications of epigenetic alterations have yet to be fully established (Lam et al. 2012; Gutierrez-Arcelus et al. 2013). In particular, it is not yet clear whether DNA methylation regulates transcription or if it is a result of thereof, making its functional interpretation difficult. As such, prior to making inferences concerning cognitive, behavioral, or physiological outcomes from alcohol-induced

epigenetic alterations, a direct line of evidence must first be established between epigenetic patterns, gene expression profiles, and the phenotype in question, either through genetic manipulation or therapeutic interventions in model organisms.

6.2.5 PAE versus FASD biomarkers

The present clinical cohorts were composed of both children diagnosed with FASD and some with confirmed PAE/high-risk of developing FASD. Due to constraints of the clinical situation, it was not possible to do follow-up assessments to determine if all children with PAE were ultimately diagnosed with FASD at a later date. As such, the classification models were tuned to screen children at a higher risk for developing FASD, rather than act as a diagnostic tool. Conversely, this method may cast a wider net and help identify children who might benefit from early interventions. Furthermore, it remains unclear whether higher specificity (low false-negative rate) or specificity (low false-positive rate) is preferable when screening for FASD. On the one hand, higher sensitivity would promote early interventions in a greater number of at-risk children, which could mitigate some of their deficits. On the other hand, high specificity would potentially prevent unnecessary interventions with some individuals and reduce the strain on health care resources. As both issues are important for child health and wellbeing, it appears that a balance between the two may be the best compromise, although much higher values and overall accuracy will be necessary before these methods are implemented in the clinic.

6.3 Broader considerations for future epigenome-wide studies of FASD

Much headway has been made in characterizing the epigenetic patterns associated with developmental alcohol exposure and their role in fetal programing by PAE. However, a number

of key considerations will be crucial for the next wave of genetic and epigenetic studies in FASD. First, most studies of alcohol exposure in animal models focus exclusively on male animals or do not highlight sex-specific differences, an issue found throughout many research fields and recently highlighted by the new funding guidelines from the National Institutes of Health (Clayton & Collins 2014). Since epigenetic patterns are highly associated with sex, this further reduces the generalizability and applicability of findings from animal models of PAE to clinical settings (Zhang et al. 2011). This is particularly relevant to the domain of FASD, as males in general typically display different cognitive and behavioral phenotypes, as well as differential susceptibilities to stressors and mental health disorders compared to their female counterparts (Hellemans et al. 2008; Bale & Epperson 2015; Oldehinkel & Bouma 2011). As such, the paucity of data on females in the FASD research field must be addressed in order to fully assess the role of epigenetics in the etiology of alcohol-induced deficits. Given the wide variety of PAE models, we must also begin to integrate findings from different models of exposure, which vary in terms of dosage (low to high), pattern of exposure (acute or chronic), trimester of exposure, and type of ethanol administration, to identify the most robust epigenetic signatures of PAE.

Additionally, a large portion of whole-genome analyses of genomic and epigenomic patterns have been performed either in cell culture or whole brains, which does not necessarily reflect the downstream functional implications of alcohol-induced alterations. Future studies should begin to assess changes within specific brain regions and primary tissues to further dissect the role of the transcriptome and epigenetics in the various deficits associated with developmental alcohol exposure. Cell type differences must also be taken into account when analyzing these data, as tissue type and cellular heterogeneity are major drivers of epigenetic

patterns and may be altered by alcohol exposure. Various strategies can be used to address this issue, including the isolation of single cell types prior to genome-wide analyses, the inclusion of cell type proportions in statistical models, or bioinformatic methods such as cell type deconvolution and surrogate variable analysis. Large-scale network analyses may also provide an alternative method to analyze these types of data, allowing researchers to identify broader patterns of PAE-induced alterations and draw links between the different changes observed (Zoubarev et al. 2012; Zhang & Horvath 2005).

In addition, robust statistical methods must be used in the analysis of genome-wide alterations to prevent spurious associations with alcohol exposure. These considerations include the use of multiple-test correction and other methods to correct for discrepancies between groups (age, ethnicity, smoking, etc.), which tend to occur frequently in population studies. Of note, the phenotypes associated with FASD have been rather heterogeneous in human studies. This is perhaps not surprising, given that numerous environmental and genetic influences can modulate the effects of alcohol on the developing organism, including maternal nutrition, dose and timing of alcohol exposure, as well as overall maternal health and genetics (Pollard 2007). Furthermore, these phenotypes are also possibly confounded with genetic ancestry, highlighting our need for large and diverse cohorts to tease apart the subtle influences of PAE on the genome and identify critical periods of vulnerability.

Finally, to fully assess the role of epigenetic mechanisms in PAE-induced associated physiological functions, we must begin to integrate the multiple layers of genetic and epigenetic machinery, from chromatin alterations and DNA methylation to miRNA and lncRNA expression (Lister et al. 2013). Future studies should also assess the concordance of these changes with mRNA expression, as the relationship between epigenetic patterns and transcription is highly

complex and has yet to be fully elucidated. Some studies of PAE have already begun to fill this niche, identifying concomitant changes in gene expression, histone modification levels, and DNA methylation patterns of *POMC* and *VGLUT2* (Bekdash, Zhang, & Sarkar 2013; Zhang et al. 2015). However, much work is needed before we can successfully integrate the multiple layers of genome-wide epigenomic regulation in the etiology of FASD.

6.4 Future directions

Although the study of genetic and epigenetic patterns following PAE is progressing at a relatively rapid rate, a number of key issues remain elusive in regards to both mechanisms of fetal programming and biomarkers of FASD. For one, early evidence from some groups suggests that developmental alcohol exposure could potentially have lasting impacts on the epigenome of future generations, suggesting a possible role for inter- or transgenerational epigenetic inheritance (Govorko et al. 2012). While these data are certainly intriguing and raise important ethical considerations in the study and prevention of FASD, they must be interpreted with relative caution due to severe limitations in studying such effects. First, the interpretation of these results must take into consideration the number of generations to determine whether they are considered inter or transgenerational, which are commonly confounded due to the presence of cells for the F2 generation in the pregnant F0 female (van Otterdijk & Michels 2016). Second, these studies were performed in rodent models, which have not yet been shown to display the same inheritance patterns as humans. Third, no cohorts are currently available for the study of transgenerational inheritance in humans, and the current evidence remains tenuous at best. Nevertheless, although much work must be done to fully assess the implications of inter- or

transgenerational epigenetic inheritance in FASD, this remains an intriguing and important area of research that certainly warrants further investigation.

Another issue facing the field is that as of yet, and perhaps not surprisingly at this time, the vast majority of epigenetic studies rely on correlation, rather than causation. Given that different environmental factors have been shown to modulate PAE-induced deficits, including stress, immune challenges, nutrition, and early-life adversity, futures studies must also begin to address the differences and similarities between basal and inducible alterations to gene expression and epigenetic patterns. Model organisms, such as mice, rats, zebrafish, *M. drosophila*, *C. elegans,* etc. will play a crucial role in addressing this issue, as they allow for finer manipulations of biological systems and tighter control of environmental conditions. Perhaps most importantly, we must begin to position epigenetic mechanisms at the nexus of exposure paradigms and phenotypic outcomes to provide better insight into the etiology of FASD. Furthermore, analysis of both central and peripheral tissues in animal models will be vital before we can begin to make functional inferences in clinical settings, as human epigenetic studies mainly rely on peripheral tissues such as BEC and blood.

Although the degree to which peripheral alterations are linked to the mechanisms underlying FASD remains unknown, they may present a unique opportunity to develop accurate epigenetic biomarkers of PAE. In many cases, the deficits associated with FASD only become evident long after exposure, highlighting the importance of early biomarkers as tools to identify at risk children and mitigate the long-term effects of alcohol. More recent studies in animal models and clinical populations of individuals with FASD are beginning to provide a solid foundation for biomarker discovery with hopes for definitive markers in the relatively near future. Of the utmost importance in this line of research are additional studies to validate current

findings and to begin to assess the accuracy and specificity of these types of markers. While a characteristic epigenomic signature appears to occur in the buccal cells of children with FASD, these finding requires additional validation and testing in a clinical setting. Furthermore, strong correlations have been identified between genetic background and epigenetic patterns, particularly in the case of gene by environment (GxE) interactions (Fraser et al. 2012; Heyn et al. 2013; Moen et al. 2013). This work also points to the functional effects of methylation quantitative trait loci (mQTL), defined as an allelic variant that correlates with CpG methylation levels in its vicinity (Jones, Fejes, & Kobor 2013). A number of studies have explored the occurrence of mQTLs in the human brain, showing that mQTLs tend to occur as *cis* associations in different brain regions and may underlie risk loci of various neuropsychiatric diseases, such as schizophrenia and bipolar disorder (Zhang et al. 2010; Gibbs et al. 2010; Gamazon et al. 2013; Hannon et al. 2015; Jaffe et al. 2015). Given the challenges in obtaining cohorts of children with homogenous ethnicities, it will be vital to assess the relevance and implications of methylation quantitative trait loci or allelic variants correlating with nearby CpG methylation levels in the context of FASD.

Longitudinal studies will also be integral to the identification of PAE-associated alterations to epigenetic profiles, as cross-sectional studies may not fully reflect the diversity of individuals with FASD across development and aging. Importantly, the field must also begin to move beyond early life outcomes and extend its focus into adolescence and adulthood, as data on adolescents and adults with FASD remain sparse. These studies will further develop a role for altered epigenetic programming in FASD and long-term health outcomes, be they immune, neurological, or stress-related (Moore & Riley 2015). In addition, these may prove crucial to our understanding of the etiology of FASD, particularly given the relationship between aging,

disease, and DNA methylation (Jones, Goodman, & Kobor 2015). These longitudinal cohorts will also be necessary to assess the persistence of epigenetic reprogramming by PAE and the potential validity of biomarkers over time. Epigenetic profiles may also serve as better markers of FASD if they are developed in conjunction with different stratification tools, such as magnetic resonance imaging (MRI), eye tracking, physical and mental health diagnostics, and immune markers, to parse out the wide range of deficits associated with FASD and create more accurate diagnostic tools. Finally, we must also begin to assess the overlaps, or lack thereof, in epigenetic patterns among different neurodevelopmental disorders, as they may display similar deficits and share common or overlapping molecular etiologies (Kelleher & Corvin 2015). The integration of these findings will provide important insight into the root causes of these disorders and may provide additional strategies for both diagnostic tools and therapeutic interventions.

6.5 Conclusions

Despite the recognition of FAS over 40 years ago, PAE remains the leading cause of developmental disability in the developed world, as recent North American estimates place the incidence between 2-5% (Jones & Smith 1973; Lemoine et al. 1968; May & Gossage 2001; May et al. 2014, 2015). However, early identification of individuals with FASD remains difficult, limiting the effectiveness of current interventions, which still lack specific molecular or neurobiological targets (Murawski et al. 2015). Although the study of genetic and epigenetic patterns in FASD remains an emerging field, it has provided important contributions to our understanding of the molecular underpinnings of FASD. To date, epigenetic research has identified numerous alterations to gene expression, DNA methylation patterns, chromatin states, and ncRNA expression levels, which provide important neurobiological insight into the deficits

associated with FASD, while also potentially uncovering targets for therapeutic intervention. This work has also begun to lay the groundwork for the development of epigenetic biomarkers of PAE, which may be the key to identifying children at risk for FASD. In turn, the identification of valid biomarkers will eventually support the creation of strategies for earlier diagnoses and targeted interventions to improve the lives of children and families affected by FASD.

References

Abdolmaleky H.M., Smith C.L., Zhou J.-R., & Thiagalingam S. 2008. "Epigenetic Alterations of the Dopaminergic System in Major Psychiatric Disorders." *Methods in Molecular Biology* 448: 187–212.

Ahluwalia B., Wesley B., Adeyiga O., Smith D.M., Da-Silva A., & Rajguru S. 2000. "Alcohol Modulates Cytokine Secretion and Synthesis in Human Fetus: An in Vivo and in Vitro Study." *Alcohol* 21 (3): 207–13.

Alaghband Y., Bredy T.W., & Wood M.A. 2016. "The Role of Active DNA Demethylation and Tet Enzyme Function in Memory Formation and Cocaine Action." *Neuroscience Letters* 625 (June): 40–46.

Ammann A., Wara D., Cowan M., Barrett D., & Stiehm E. 1982. "The Digeorge Syndrome and the Fetal Alcohol Syndrome." *American Journal of Diseases of Children* 136 (10): 906–8.

Ashburner M., Ball C.A., Blake J.A., Botstein D., Butler H., Cherry J.M., Davis A.P., et al. 2000. "Gene Ontology: Tool for the Unification of Biology. The Gene Ontology Consortium." *Nature Genetics* 25 (1): 25–29.

Astley S.J., & Clarren S.K. 2000. "Diagnosing the Full Spectrum of Fetal Alcohol-Exposed Individuals: Introducing the 4-Digit Diagnostic Code." *Alcohol and Alcoholism* 35 (4): 400–410.

Astley S.J., Olson H.C., Kerns K., Brooks A., Aylward E.H., Coggins T.E., Davies J., et al. 2009. "Neuropyschological and Behavioral Outcomes from a Comprehensive Magnetic Resonance Study of Children with Fetal Alcohol Spectrum Disorders." *Canadian Journal of Clinical Pharmacology* 16 (1): e178-201.

Bakhireva L.N., Leeman L., Savich R.D., Cano S., Gutierrez H., Savage D.D., & Rayburn W.F. 2014. "The Validity of Phosphatidylethanol in Dried Blood Spots of Newborns for the Identification of Prenatal Alcohol Exposure." *Alcoholism: Clinical and Experimental Research* 38 (4): 1078–85.

Balaraman S., Schafer J.J., Tseng A.M., Wertelecki W., Yevtushok L., Zymak-Zakutnya N., Chambers C.D., & Miranda R.C. 2016. "Plasma miRNA Profiles in Pregnant Women Predict Infant Outcomes Following Prenatal Alcohol Exposure." *PLoS One* 11 (11): e0165081.

Balaraman S., Winzer-Serhan U.H., & Miranda R.C. 2012. "Opposing Actions of Ethanol and Nicotine on MicroRNAs Are Mediated by Nicotinic Acetylcholine Receptors in Fetal Cerebral Cortical-Derived Neural Progenitor Cells." *Alcoholism: Clinical and Experimental Research* 36 (10): 1669–77.

Bale T.L., & Epperson C.N. 2015. "Sex Differences and Stress across the Lifespan." *Nature Neuroscience* 18 (10): 1413–20.

Banovich N.E., Lan X., McVicker G., Geijn B. van de, Degner J.F., Blischak J.D., Roux J., Pritchard J.K., & Gilad Y. 2014. "Methylation QTLs Are Associated with Coordinated Changes in Transcription Factor Binding, Histone Modifications, and Gene Expression Levels." *PLoS Genetics* 10 (9): e1004663.

Barilla M.L., & Carsons S.E. 2000. "Fibronectin Fragments and Their Role in Inflammatory Arthritis." *Seminars in Arthritis and Rheumatism* 29 (4): 252–65.

Barker D.J.P. 1997. "Fetal Nutrition and Cardiovascular Disease in Later Life." *British Medical Bulletin* 53 (1): 96–108.

Barker D.J.P. 2003. “Editorial: The Developmental Origins of Adult Disease.” *European Journal of Epidemiology* 18 (8): 733–36.
———. 2004. “The Developmental Origins of Adult Disease.” *Journal of the American College of Nutrition* 23 (sup6). Taylor & Francis: 588S–595S.
———. 2007. “The Origins of the Developmental Origins Theory.” *Journal of Internal Medicine* 261 (5): 412–17.
Barker D.J.P., Godfrey K.M., Gluckman P.D., Harding J.E., Owens J.A., & Robinson J.S. 1993. “Fetal Nutrition and Cardiovascular Disease in Adult Life.” *The Lancet* 341 (8850): 938–41.
Barker D.J.P., & Osmond C. 1986. “Infant Mortality, Childhood Nutrition, and Ischaemic Heart Disease in England and Wales.” *The Lancet* 327 (8489): 1077–81.
Barker D.J.P., Osmond C., Winter P.D., Margetts B., & Simmonds S.J. 1989. “Weight in Infancy and Death from Ischaemic Heart Disease.” *The Lancet* 334 (8663): 577–80.
Barker D.J.P., & Thornburg K.L. 2013. “The Obstetric Origins of Health for a Lifetime.” *Clinical Obstetrics and Gynecology* 56 (3).
Barr H.M., Bookstein F.L., O’Malley K.D., Connor P.D., Huggins J.E., & Streissguth A.P. 2006. “Binge Drinking during Pregnancy as a Predictor of Psychiatric Disorders on the Structured Clinical Interview for DSM-IV in Young Adult Offspring.” *American Journal of Psychiatry* 163 (6): 1061–65.
Bau C.H., Almeida S., Costa F.T., Garcia C.E., Elias E.P., Ponso A.C., Spode A., & Hutz M.H. 2001. “DRD4 and DAT1 as Modifying Genes in Alcoholism: Interaction with Novelty Seeking on Level of Alcohol Consumption.” *Molecular Psychiatry* 6 (1): 7–9.
Baubec T., & Schübeler D. 2014. “Genomic Patterns and Context Specific Interpretation of DNA Methylation.” *Current Opinion in Genetics and Development* 25 (1): 85–92.
Bearer C.F., Jacobson J.L., Jacobson S.W., Barr D., Croxford J., Molteno C.D., Viljoen D.L., Marais A.-S., Chiodo L.M., & Cwik A.S. 2003. “Validation of a New Biomarker of Fetal Exposure to Alcohol.” *The Journal of Pediatrics* 143 (4): 463–69.
Bearer C.F., Lee S., Salvator A.E., Minnes S., Swick A., Yamashita T., & Singer L.T. 1999. “Ethyl Linoleate in Meconium: A Biomarker for Prenatal Ethanol Exposure.” *Alcoholism: Clinical and Experimental Research* 23 (3): 487–93.
Bearer C.F., Santiago L.M., O’Riordan M.A., Buck K., Lee S.C., & Singer L.T. 2005. “Fatty Acid Ethyl Esters: Quantitative Biomarkers for Maternal Alcohol Consumption.” *The Journal of Pediatrics* 146 (6): 824–30.
Bekdash R.A., Zhang C., & Sarkar D.K. 2013. “Gestational Choline Supplementation Normalized Fetal Alcohol-Induced Alterations in Histone Modifications, DNA Methylation, and Proopiomelanocortin (POMC) Gene Expression in Beta-Endorphin-Producing POMC Neurons of the Hypothalamus.” *Alcoholism: Clinical and Experimental Research* 37 (7): 1133–42.
Benjamini Y., & Hochberg Y. 1995. “Controlling the False Discovery Rate: A Practical and Powerful Approach to Multiple Testing.” *Journal of the Royal Statistical Society. Series B (Methodological)* 57 (1): 289–300.
Berko E.R., Suzuki M., Beren F., Lemetre C., Alaimo C.M., Calder R.B., Ballaban-Gil K., et al. 2014. “Mosaic Epigenetic Dysregulation of Ectodermal Cells in Autism Spectrum Disorder.” *PLoS Genetics* 10 (5): e1004402.
Bernardini R., Kamilaris T.C., Calogero A.E., Johnson E.O., Gomez M.T., Gold P.W., &

Chrousos G.P. 1990. “Interactions between Tumor Necrosis Factor-Alpha, Hypothalamic Corticotropin-Releasing Hormone, and Adrenocorticotropin Secretion in the Rat.” *Endocrinology* 126 (6): 2876–81.
Bibikova M., Barnes B., Tsan C., Ho V., Klotzle B., Le J.M., Delano D., et al. 2011. “High Density DNA Methylation Array with Single CpG Site Resolution.” *Genomics* 98 (4): 288–95.
Bird A. 2007. “Perceptions of Epigenetics.” *Nature* 447 (7143): 396–98.
Bock C. 2009. “Epigenetic Biomarker Development.” *Epigenomics* 1 (1): 99–110.
Bodnar T.S., Hill L.A., & Weinberg J. 2016. “Evidence for an Immune Signature of Prenatal Alcohol Exposure in Female Rats.” *Brain, Behavior, and Immunity* 58: 130–41.
Bodnar T.S., & Weinberg J. 2013. *Neural-Immune Interactions in Brain Function and Alcohol Related Disorders*. Edited by Changhai Cui, Lindsey Grandison, and Antonio Noronha. Boston, MA: Springer US.
Bomholt S.F., Harbuz M.S., Blackburn-Munro G., & Blackburn-Munro R.E. 2004. “Involvement and Role of the Hypothalamo-Pituitary-Adrenal (HPA) Stress Axis in Animal Models of Chronic Pain and Inflammation.” *Stress* 7 (1): 1–14.
Bonthius D.J., & West J.R. 1990. “Alcohol-Induced Neuronal Loss in Developing Rats: Increased Brain Damage with Binge Exposure.” *Alcoholism: Clinical and Experimental Research* 14 (1): 107–18.
Borck G., Mollà-Herman A., Boddaert N., Encha-Razavi F., Philippe A., Robel L., Desguerre I., et al. 2008. “Clinical, Cellular, and Neuropathological Consequences of AP1S2 Mutations: Further Delineation of a Recognizable X-Linked Mental Retardation Syndrome.” *Human Mutation* 29 (7): 966–74.
Boyce W.T., & Kobor M.S. 2015. “Development and the Epigenome: The ‘synapse’ of Gene-Environment Interplay.” *Developmental Science* 18 (1): 1–23.
Brand J.M., Frohn C., Cziupka K., Brockmann C., Kirchner H., & Luhm J. 2004. “Prolactin Triggers pro-Inflammatory Immune Responses in Peripheral Immune Cells.” *European Cytokine Network* 15 (2): 99–104.
Burns E., Gray R., & Smith L.A. 2010. “Brief Screening Questionnaires to Identify Problem Drinking during Pregnancy: A Systematic Review.” *Addiction* 105 (4): 601–14.
Cabarcos P., Álvarez I., Tabernero M.J., & Bermejo A.M. 2015. “Determination of Direct Alcohol Markers: A Review.” *Analytical and Bioanalytical Chemistry* 407 (17): 4907–25.
Cahoy J.D., Emery B., Kaushal A., Foo L.C., Zamanian J.L., Christopherson K.S., Xing Y., et al. 2008. “A Transcriptome Database for Astrocytes, Neurons, and Oligodendrocytes: A New Resource for Understanding Brain Development and Function.” *The Journal of Neuroscience* 28 (1): 264–78.
Carter J.L., Lubahn C., Lorton D., Osredkar T., Der T.C., Schaller J., Evelsizer S., et al. 2011. “Adjuvant-Induced Arthritis Induces c-Fos Chronically in Neurons in the Hippocampus.” *Journal of Neuroimmunology* 230 (1–2): 85–94.
Carter R.C., Jacobson J.L., Molteno C.D., Dodge N.C., Meintjes E.M., Jacobson S.W., May P., et al. 2016. “Fetal Alcohol Growth Restriction and Cognitive Impairment.” *Pediatrics* 138 (2): 176192.
Castells S., Mark E., Abaci F., & Schwartz E. 1981. “Growth Retardation in Fetal Alcohol Syndrome. Unresponsiveness to Growth-Promoting Hormones.” *Developmental Pharmacology and Therapeutics* 3 (4): 232–41.

Chater-Diehl E.J., Laufer B.I., Castellani C.A., Alberry B.L., & Singh S.M. 2016. "Alteration of Gene Expression, DNA Methylation, and Histone Methylation in Free Radical Scavenging Networks in Adult Mouse Hippocampus Following Fetal Alcohol Exposure." *PLoS ONE* 11 (5): e0154836.

Chen C.P., Kuhn P., Advis J.P., & Sarkar D.K. 2006. "Prenatal Ethanol Exposure Alters the Expression of Period Genes Governing the Circadian Function of β-Endorphin Neurons in the Hypothalamus." *Journal of Neurochemistry* 97 (4): 1026–33.

Chen D., Liu F., Shang Q., Song X., Miao X., & Wang Z. 2011. "Association between Polymorphisms of DRD2 and DRD4 and Opioid Dependence: Evidence from the Current Studies." *American Journal of Medical Genetics Part B: Neuropsychiatric Genetics* 156 (6): 661–70.

Chen L., & Nyomba B.L.G. 2003. "Effects of Prenatal Alcohol Exposure on Glucose Tolerance in the Rat Offspring." *Metabolism* 52 (4): 454–62.

Chen M., Olson H., Picciano J., Starr J., & Owens J. 2012. "Sleep Problems in Children with Fetal Alcohol Spectrum Disorders." *Journal of Clinical Sleep Medicine* 8: 421–29.

Chen Y., Ozturk N.C., & Zhou F.C. 2013. "DNA Methylation Program in Developing Hippocampus and Its Alteration by Alcohol." *PLoS ONE* 8 (3): 1–11.

Cheng J., Wang Y., Zhou K., Wang L., Li J., Zhuang Q., Xu X., et al. 2014. "Male-Specific Association between Dopamine Receptor D4 Gene Methylation and Schizophrenia." *PLoS ONE* 9 (2): e89128.

Chover-Gonzalez A.J., Harbuz M.S., Tejedor-Real P., Gibert-Rahola J., Larsen P.J., & Jessop D.S. 1999. "Effects of Stress on Susceptibility and Severity of Inflammation in Adjuvant-Induced Arthritis." In *Annals of the New York Academy of Sciences*, 876:276–86.

Chudley A.E., Conry J., Cook J.L., Loock C., Rosales T., & LeBlanc N. 2005. "Fetal Alcohol Spectrum Disorder: Canadian Guidelines for Diagnosis." *Canadian Medical Association Journal* 172 (5 Suppl): S1–21.

Church M.W., & Gerkin K.P. 1988. "Hearing Disorders in Children with Fetal Alcohol Syndrome: Findings from Case Reports." *Pediatrics* 82 (2): 147–54.

Clausing P., Ali S.F., Taylor L.D., Newport G.D., Rybak S., & Paule M.G. 1996. "Central and Peripheral Neurochemical Alterations and Immune Effects of Prenatal Ethanol Exposure in Rats." *International Journal of Developmental Neuroscience* 14 (4): 461–69.

Clayton J. a., & Collins F.S. 2014. "NIH to Balance Sex in Cell and Animal Studies." *Nature* 509 (7500): 282–83.

Colebatch A.N., & Edwards C.J. 2011. "The Influence of Early Life Factors on the Risk of Developing Rheumatoid Arthritis." *Clinical and Experimental Immunology* 163 (1): 11–16.

Concheiro-Guisan A., & Concheiro M. 2014. "Bioanalysis during Pregnancy: Recent Advances and Novel Sampling Strategies." *Bioanalysis* 6 (23): 3133–53.

Cordaux R., & Batzer M.A. 2009. "The Impact of Retrotransposons on Human Genome Evolution." *Nature Reviews Genetics* 10 (10): 691–703.

Crews F.T., Bechara R., Brown L.A., Guidot D.M., Mandrekar P., Oak S., Qin L., Szabo G., Wheeler M., & Zou J. 2006. "Cytokines and Alcohol." *Alcoholism: Clinical and Experimental Research* 30 (4): 720–30.

Crofford L.J., Sano H., Karalis K., Webster E.L., Goldmuntz E.A., Chrousos G.P., & Wilder R.L. 1992. "Local Secretion of Corticotropin-Releasing Hormone in the Joints of Lewis Rats with Inflammatory Arthritis." *Journal of Clinical Investigation* 90 (6): 2555–64.

Cuadrado A., & Nebreda A.R. 2010. “Mechanisms and Functions of p38 MAPK Signalling.” *The Biochemical Journal* 429 (3): 403–17.
Cunningham E.T., & Souza E.B. De. 1993. “Interleukin 1 Receptors in the Brain and Endocrine Tissues.” *Immunology Today* 14 (4): 171–76.
Dadds M.R., Schollar-Root O., Lenroot R., Moul C., & Hawes D.J. 2016. “Epigenetic Regulation of the DRD4 Gene and Dimensions of Attention-Deficit/hyperactivity Disorder in Children.” *European Child & Adolescent Psychiatry* 25 (10): 1081–89.
Davies M.N., Volta M., Pidsley R., Lunnon K., Dixit A., Lovestone S., Coarfa C., et al. 2012. “Functional Annotation of the Human Brain Methylome Identifies Tissue-Specific Epigenetic Variation across Brain and Blood.” *Genome Biology* 13 (6): R43.
De Souza R.A.G., Islam S.A., McEwen L.M., Mathelier A., Hill A., Mah S.M., Wasserman W.W., Kobor M.S., & Leavitt B.R. 2016. “DNA Methylation Profiling in Human Huntington’s Disease Brain.” *Human Molecular Genetics* 25 (10): 2013–30.
Dickmeis T. 2009. “Glucocorticoids and the Circadian Clock.” *Journal of Endocrinology* 200 (1): 3–22.
Diorio D., Viau V., & Meaney M.J. 1993. “The Role of the Medial Prefrontal Cortex (Cingulate Gyrus) in the Regulation of Hypothalamic-Pituitary-Adrenal Responses to Stress.” *The Journal of Neuroscience* 13 (9): 3839–47.
Dobbing J., & Sands J. 1979. “Comparative Aspects of the Brain Growth Spurt.” *Early Human Development* 3 (1): 79–83.
Dobson C.C., Mongillo D.L., Brien D.C., Stepita R., Poklewska-Koziell M., Winterborn A., Holloway A.C., Brien J.F., & Reynolds J.N. 2012. “Chronic Prenatal Ethanol Exposure Increases Adiposity and Disrupts Pancreatic Morphology in Adult Guinea Pig Offspring.” *Nutrition and Diabetes* 2 (December): e57.
Docherty S.J., Davis O.S.P., Haworth C.M. a, Plomin R., D’Souza U., & Mill J. 2012. “A Genetic Association Study of DNA Methylation Levels in the DRD4 Gene Region Finds Associations with Nearby SNPs.” *Behavioral and Brain Functions* 8 (1): 31.
Doi A., Park I.H., Wen B., Murakami P., Aryee M.J., Irizarry R., Herb B., et al. 2009. “Differential Methylation of Tissue- and Cancer-Specific CpG Island Shores Distinguishes Human Induced Pluripotent Stem Cells, Embryonic Stem Cells and Fibroblasts.” *Nature Genetics* 41 (12): 1350–53.
Domcke S., Bardet A.F., Ginno P.A., Hartl D., Burger L., & Schuebeler D. 2015. “Competition between DNA Methylation and Transcription Factors Determines Binding of NRF1.” *Nature* 528 (7583): 575–79.
Dominissini D., Moshitch-Moshkovitz S., Schwartz S., Salmon-Divon M., Ungar L., Osenberg S., Cesarkas K., et al. 2013. “Topology of the Human and Mouse m6A RNA Methylomes Revealed by m6A-Seq.” *Nature* 485 (7397): 201–6.
Donnelly S.R., Hawkins T.E., & Moss S.E. 1999. “A Conserved Nuclear Element with a Role in Mammalian Gene Regulation.” *Human Molecular Genetics* 8 (9): 1723–28.
Downing C., Flink S., Florez-McClure M.L., Johnson T.E., Tabakoff B., & Kechris K.J. 2012. “Gene Expression Changes in C57BL/6J and DBA/2J Mice Following Prenatal Alcohol Exposure.” *Alcoholism: Clinical and Experimental Research* 36 (9): 1519–29.
Downing C., Johnson T.E., Larson C., Leakey T.I., Siegfried R.N., Rafferty T.M., & Cooney C.A. 2011. “Subtle Decreases in DNA Methylation and Gene Expression at the Mouse Igf2 Locus Following Prenatal Alcohol Exposure: Effects of a Methyl-Supplemented Diet.”

Alcohol 45 (1): 65–71.
Doyle L.R., & Mattson S.N. 2015. "Neurobehavioral Disorder Associated with Prenatal Alcohol Exposure (ND-PAE): Review of Evidence and Guidelines for Assessment." *Current Developmental Disorders Reports* 2 (3): 175–86.
Drew P.D., Johnson J.W., Douglas J.C., Phelan K.D., & Kane C.J. 2015. "Pioglitazone Blocks Ethanol Induction of Microglial Activation and Immune Responses in the Hippocampus, Cerebellum, and Cerebral Cortex in a Mouse Model of Fetal Alcohol Spectrum Disorders." *Alcoholism: Clinical & Experimental Research* 39.
Du P., Zhang X., Huang C.-C., Jafari N., Kibbe W.A., Hou L., & Lin S.M. 2010. "Comparison of Beta-Value and M-Value Methods for Quantifying Methylation Levels by Microarray Analysis." *BMC Bioinformatics* 11 (1): 587.
Dumas A., Lagarde S., Laflamme C., & Pouliot M. 2012. "Oncostatin M Decreases Interleukin-1 β Secretion by Human Synovial Fibroblasts and Attenuates an Acute Inflammatory Reaction in Vivo." *Journal of Cellular and Molecular Medicine* 16 (6): 1274–85.
Earnest D.J., Chen W.J., & West J.R. 2001. "Developmental Alcohol and Circadian Clock Function." *Alcohol Research & Health : The Journal of the National Institute on Alcohol Abuse and Alcoholism* 25 (2): 136–40.
Eckhardt F., Lewin J., Cortese R., Rakyan V.K., Attwood J., Burger M., Burton J., et al. 2006. "DNA Methylation Profiling of Human Chromosomes 6, 20 and 22." *Nature Genetics* 38 (12): 1378–85.
Edgar R., Tan P.P., Portales-Casamar E., & Pavlidis P. 2014. "Meta-Analysis of Human Methylomes Reveals Stably Methylated Sequences Surrounding CpG Islands Associated with High Gene Expression." *Epigenetics & Chromatin* 7 (1): 28.
Eguchi Y. 1969. *Physiology and Pathology of Adaptation Mechanisms*. Edited by E. Bajusz. Pergamon Press.
Enríquez P. 2016. "CRISPR-Mediated Epigenome Editing." *The Yale Journal of Biology and Medicine* 89 (4). YJBM: 471–86.
Ergang P., Vodička M., Soták M., Klusoňová P., Behuliak M., Řeháková L., Zach P., & Pácha J. 2015. "Differential Impact of Stress on Hypothalamic-Pituitary-Adrenal Axis: Gene Expression Changes in Lewis and Fisher Rats." *Psychoneuroendocrinology* 53: 49–59.
Esposito E.A., Jones M.J., Doom J.R., MacIsaac J.L., Gunnar M.R., & Kobor M.S. 2016. "Differential DNA Methylation in Peripheral Blood Mononuclear Cells in Adolescents Exposed to Significant Early but Not Later Childhood Adversity." *Development and Psychopathology* 28 (4pt2): 1385–99.
Ewald S.J., & Frost W.W. 1987. "Effect of Prenatal Exposure to Ethanol on Development of the Thymus." *Thymus* 9 (4): 211–15.
Ewald S.J., & Walden S.M. 1988. "Flow Cytometric and Histological Analysis of Mouse Thymus in Fetal Alcohol Syndrome." *Journal of Leukocyte Biology* 44 (5): 434–40.
Falls J.G., Pulford D.J., Wylie A.A., & Jirtle R.L. 1999. "Genomic Imprinting: Implications for Human Disease." *The American Journal of Pathology* 154 (3): 635–47.
Famy C., Streissguth A.P., & Unis A.S. 1998. "Mental Illness in Adults with Fetal Alcohol Syndrome or Fetal Alcohol Effects." *The American Journal of Psychiatry* 155 (4): 552–54.
Fan A.Z., Russell M., Naimi T., Li Y., Liao Y., Jiles R., & Mokdad A.H. 2008. "Patterns of Alcohol Consumption and the Metabolic Syndrome." *The Journal of Clinical Endocrinology & Metabolism* 93 (10): 3833–38.

Faraone S. V, Bonvicini C., & Scassellati C. 2014. “Biomarkers in the Diagnosis of ADHD – Promising Directions.” *Current Psychiatry Reports* 16 (11): 497.
Farré P., Jones M.J., Meaney M.J., Emberly E., Turecki G., & Kobor M.S. 2015. “Concordant and Discordant DNA Methylation Signatures of Aging in Human Blood and Brain.” *Epigenetics & Chromatin* 8 (1): 19.
Farris S.P., Arasappan D., Hunicke-Smith S., Harris R.A., & Mayfield R.D. 2015. “Transcriptome Organization for Chronic Alcohol Abuse in Human Brain.” *Molecular Psychiatry* 20 (11): 1438–47.
Feil R., & Fraga M.F. 2012. “Epigenetics and the Environment: Emerging Patterns and Implications.” *Nature Reviews Genetics* 13 (2): 97–109.
Fox S.E., Levitt P., & Nelson III C.A. 2010. “How the Timing and Quality of Early Experiences Influence the Development of Brain Architecture.” *Child Development* 81 (1): 28–40.
Fransquet P.D., Hutchinson D., Olsson C.A., Wilson J., Allsop S., Najman J., Elliott E., Mattick R.P., Saffery R., & Ryan J. 2016. “Perinatal Maternal Alcohol Consumption and Methylation of the Dopamine Receptor DRD4 in the Offspring: The Triple B Study.” *Environmental Epigenetics* 2 (4): dvw023-dvw023.
Fraser H.B., Lam L.L., Neumann S.M., & Kobor M.S. 2012. “Population-Specificity of Human DNA Methylation.” *Genome Biology* 13 (2): R8.
Gabriel K.I., Glavas M.M., Ellis L., & Weinberg J. 2005. “Postnatal Handling Does Not Normalize Hypothalamic Corticotropin-Releasing Factor mRNA Levels in Animals Prenatally Exposed to Ethanol.” *Developmental Brain Research* 157 (1): 74–82.
Gabriel K.I., Yu C.L., Osborn J.A., & Weinberg J. 2017. “Prenatal Ethanol Exposure Alters Sensitivity to the Effects of Corticotropin-Releasing Factor (CRF) on Behavior in the Elevated plus-Maze.” *Psychoneuroendocrinology* 31 (9): 1046–56.
Gamazon E.R., Badner J.A., Cheng L., Zhang C., Zhang D., Cox N.J., Gershon E.S., et al. 2013. “Enrichment of Cis-Regulatory Gene Expression SNPs and Methylation Quantitative Trait Loci among Bipolar Disorder Susceptibility Variants.” *Molecular Psychiatry* 18 (3): 340–46.
Gardiner-Garden M., & Frommer M. 1987. “CpG Islands in Vertebrate Genomes.” *Journal of Molecular Biology* 196 (2): 261–82.
Garro A.J., McBeth D.L., Lima V., & Lieber C.S. 1991. “Ethanol Consumption Inhibits Fetal DNA Methylation in Mice: Implications for the Fetal Alcohol Syndrome.” *Alcoholism: Clinical and Experimental Research* 15 (3): 395–98.
Gauthier T.W., Drews-Botsch C., Falek A., Coles C., & Brown L.A.S. 2005. “Maternal Alcohol Abuse and Neonatal Infection.” *Alcoholism: Clinical and Experimental Research* 29 (6): 1035–43.
Gauthier T.W., Manar M.H., & Brown L.A.S. 2004. “Is Maternal Alcohol Use a Risk Factor for Early-Onset Sepsis in Premature Newborns?” *Alcohol* 33 (2): 139–45.
Gibbs J.R., Brug M.P. van der, Hernandez D.G., Traynor B.J., Nalls M.A., Lai S.-L.L., Arepalli S., et al. 2010. “Abundant Quantitative Trait Loci Exist for DNA Methylation and Gene Expression in Human Brain.” *PLoS Genetics* 6 (5): 29.
Giberson P.K., Kim C.K., Hutchison S., Yu W., Junker A., & Weinberg J. 1997. “The Effect of Cold Stress on Lymphocyte Proliferation in Fetal Ethanol-Exposed Rats.” *Alcoholism: Clinical and Experimental Research* 21 (8): 1440–47.
Giberson P.K., & Weinberg J. 1995. “Effects of Prenatal Ethanol Exposure and Stress in

Adulthood on Lymphocyte Populations in Rats." *Alcoholism: Clinical and Experimental Research* 19 (5): 1286–94.
Glavas M.M., Ellis L., Yu W.K., & Weinberg J. 2007. "Effects of Prenatal Ethanol Exposure on Basal Limbic-Hypothalamic-Pituitary-Adrenal Regulation: Role of Corticosterone." *Alcoholism: Clinical and Experimental Research* 31 (9): 1598–1610.
Godfrey K.M., Lillycrop K.A., Burdge G.C., Gluckman P.D., & Hanson M.A. 2007. "Epigenetic Mechanisms and the Mismatch Concept of the Developmental Origins of Health and Disease." *Pediatric Research* 61 (5R–10R).
Godfrey K.M., & Robinson S. 1998. "Maternal Nutrition, Placental Growth and Fetal Programming." *Proceedings of the Nutrition Society* 57 (1): 105–11.
Goh P.K., Doyle L.R., Glass L., Jones K.L., Riley E.P., Coles C.D., Hoyme H.E., et al. 2016. "A Decision Tree to Identify Children Affected by Prenatal Alcohol Exposure." *The Journal of Pediatrics* 177 (October): 121–127.e1.
Goines P.E., Croen L.A., Braunschweig D., Yoshida C.K., Grether J., Hansen R., Kharrazi M., Ashwood P., & Water J. Van de. 2011. "Increased Midgestational IFN-Γ, IL-4 and IL-5 in Women Bearing a Child with Autism: A Case-Control Study." *Molecular Autism* 2 (August): 13.
Goldowitz D., Lussier A.A., Boyle J.K., Wong K., Lattimer S.L., Dubose C., Lu L., Kobor M.S., & Hamre K.M. 2014. "Molecular Pathways Underpinning Ethanol-Induced Neurodegeneration." *Frontiers in Genetics* 5 (July): 203.
Goril S., Zalai D., Scott L., & Shapiro C.M. 2016. "Sleep and Melatonin Secretion Abnormalities in Children and Adolescents with Fetal Alcohol Spectrum Disorders." *Sleep Medicine* 23 (July): 59–64.
Gottesfeld Z., & Abel E.L. 1991. "Maternal and Paternal Alcohol Use: Effects on the Immune System of the Offspring." *Life Sciences* 48 (1): 1–8.
Gottesfeld Z., Christie R., Felten D.L., & LeGrue S.J. 1990. "Prenatal Ethanol Exposure Alters Immune Capacity and Noradrenergic Synaptic Transmission in Lymphoid Organs of the Adult Mouse." *Neuroscience* 35 (1): 185–94.
Govorko D., Bekdash R.A., Zhang C., & Sarkar D.K. 2012. "Male Germline Transmits Fetal Alcohol Adverse Effect on Hypothalamic Proopiomelanocortin Gene across Generations." *Biological Psychiatry* 72 (5): 378–88.
Green M.L., Singh A. V., Zhang Y., Nemeth K.A., Sulik K.K., & Knudsen T.B. 2007. "Reprogramming of Genetic Networks during Initiation of the Fetal Alcohol Syndrome." *Developmental Dynamics* 236 (2): 613–31.
Guo J.U., Su Y., Shin J.H., Shin J., Li H., Xie B., Zhong C., et al. 2014. "Distribution, Recognition and Regulation of Non-CpG Methylation in the Adult Mammalian Brain." *Nature Neuroscience* 17 (2): 215–22.
Guo W., Crossey E.L., Zhang L., Zucca S., George O.L., Valenzuela C.F., & Zhao X. 2011. "Alcohol Exposure Decreases CREB Binding Protein Expression and Histone Acetylation in the Developing Cerebellum." *PLoS ONE* 6 (5): e19351.
Gutierrez-Arcelus M., Lappalainen T., Montgomery S.B., Buil A., Ongen H., Yurovsky A., Bryois J., et al. 2013. "Passive and Active DNA Methylation and the Interplay with Genetic Variation in Gene Regulation." *eLife* 2 (2): e00523.
Gutierrez H.L., Hund L., Shrestha S., Rayburn W.F., Leeman L., Savage D.D., & Bakhireva L.N. 2015. "Ethylglucuronide in Maternal Hair as a Biomarker of Prenatal Alcohol

Exposure." *Alcohol* 49 (6): 617–23.
Haddad J.J., Saadé N.E., & Safieh-Garabedian B. 2002. "Cytokines and Neuro-Immune-Endocrine Interactions: A Role for the Hypothalamic-Pituitary-Adrenal Revolving Axis." *Journal of Neuroimmunology* 133 (1–2): 1–19.
Haley D.W., Handmaker N.S., & Lowe J. 2006. "Infant Stress Reactivity and Prenatal Alcohol Exposure." *Alcoholism: Clinical and Experimental Research* 30 (12): 2055–64.
Hannon E., Spiers H., Viana J., Pidsley R., Burrage J., Murphy T.M., Troakes C., et al. 2015. "Methylation QTLs in the Developing Brain and Their Enrichment in Schizophrenia Risk Loci." *Nature Neuroscience* 19 (1): 48–54.
Hanson M.A., & Gluckman P.D. 2008. "Developmental Origins of Health and Disease: New Insights." *Basic & Clinical Pharmacology & Toxicology* 102 (2): 90–93.
Hanson M.A., Godfrey K.M., Lillycrop K.A., Burdge G.C., & Gluckman P.D. 2011. "Developmental Plasticity and Developmental Origins of Non-Communicable Disease: Theoretical Considerations and Epigenetic Mechanisms." *Progress in Biophysics and Molecular Biology* 106 (1): 272–80.
Hanson M.A., Low F.M., & Gluckman P.D. 2011. "Epigenetic Epidemiology: The Rebirth of Soft Inheritance." *Annals of Nutrition and Metabolism* 58 (SUPPL. 2): 8–15.
Harbuz M.S., Chover-Gonzalez A.J., & Jessop D.S. 2003. "Hypothalamo-Pituitary-Adrenal Axis and Chronic Immune Activation." *Annals of the New York Academy of Sciences* 992: 99–106.
Harbuz M.S., Rees R.G., & Lightman S.L. 1993. "HPA Axis Responses to Acute Stress and Adrenalectomy during Adjuvant-Induced Arthritis in the Rat." *The American Journal of Physiology* 264 (1 Pt 2): R179–85.
Hard M.L., Abdolell M., Robinson B.H., & Koren G. 2005. "Gene-Expression Analysis after Alcohol Exposure in the Developing Mouse." *Journal of Laboratory and Clinical Medicine* 145 (1): 47–54.
Harper K.M., Tunc-Ozcan E., Graf E.N., & Redei E.E. 2014. "Intergenerational Effects of Prenatal Ethanol on Glucose Tolerance and Insulin Response." *Physiological Genomics* 46 (5). Bethesda, MD: American Physiological Society: 159–68.
Harris A., & Seckl J. 2011. "Glucocorticoids, Prenatal Stress and the Programming of Disease." *Hormones and Behavior* 59 (3): 279–89.
Hawrylycz M.J., Lein E.S., Guillozet-Bongaarts A.L., Shen E.H., Ng L., Miller J. a., Lagemaat L.N. van de, et al. 2012. "An Anatomically Comprehensive Atlas of the Adult Human Brain Transcriptome." *Nature* 489 (7416): 391–99.
Haycock P.C. 2009. "Fetal Alcohol Spectrum Disorders: The Epigenetic Perspective." *Biology of Reproduction* 81 (4): 607–17.
Haycock P.C., & Ramsay M. 2009. "Exposure of Mouse Embryos to Ethanol during Preimplantation Development: Effect on DNA Methylation in the h19 Imprinting Control Region." *Biology of Reproduction* 81 (4): 618–27.
He J., & Crews F.T. 2008. "Increased MCP-1 and Microglia in Various Regions of the Human Alcoholic Brain." *Experimental Neurology* 210 (2): 349–58.
Heijmans B.T., Tobi E.W., Stein A.D., Putter H., Blauw G.J., Susser E.S., Slagboom P.E., & Lumey L.H. 2008. "Persistent Epigenetic Differences Associated with Prenatal Exposure to Famine in Humans." *Proceedings of the National Academy of Sciences of the United States of America* 105 (44): 17046–49.

Hellemans K.G.C., Sliwowska J.H., Verma P., & Weinberg J. 2010. “Prenatal Alcohol Exposure: Fetal Programming and Later Life Vulnerability to Stress, Depression and Anxiety Disorders.” *Neuroscience and Biobehavioral Reviews* 34 (6): 791–807.
Hellemans K.G.C., Verma P., Yoon E., Yu W., & Weinberg J. 2008. “Prenatal Alcohol Exposure Increases Vulnerability to Stress and Anxiety-like Disorders in Adulthood.” *Annals of the New York Academy of Sciences* 1144: 154–75.
Hellemans K.G.C., Verma P., Yoon E., Yu W.K., Young A.H., & Weinberg J. 2010. “Prenatal Alcohol Exposure and Chronic Mild Stress Differentially Alter Depressive- and Anxiety-Like Behaviors in Male and Female Offspring.” *Alcoholism: Clinical and Experimental Research* 34 (4): 633–45.
Henikoff S., & Greally J.M. 2016. “Epigenetics, Cellular Memory and Gene Regulation.” *Current Biology* 26 (14): R644–48.
Herman J.P., & Cullinan W.E. 1997. “Neurocircuitry of Stress: Central Control of the Hypothalamo-Pituitary-Adrenocortical Axis.” *Trends in Neurosciences* 20 (2): 78–84.
Heyn H., Moran S., Hernando-Herraez I., Sayols S., Gomez A., Sandoval J., Monk D., et al. 2013. “DNA Methylation Contributes to Natural Human Variation.” *Genome Research* 23 (9): 1363–72.
Hicks S.D., Middleton F.A., & Miller M.W. 2010. “Ethanol-Induced Methylation of Cell Cycle Genes in Neural Stem Cells.” *Journal of Neurochemistry* 114 (6): 1767–80.
Hilakivi L. 1986. “Effects of Prenatal Alcohol Exposure on Neonatal Sleep-Wake Behaviour and Adult Alcohol Consumption in Rats.” *Acta Pharmacologica et Toxicologica* 59 (1): 36–42.
Hillemacher T., Frieling H., Hartl T., Wilhelm J., Kornhuber J., & Bleich S. 2009. “Promoter Specific Methylation of the Dopamine Transporter Gene Is Altered in Alcohol Dependence and Associated with Craving.” *Journal of Psychiatric Research* 43 (4): 388–92.
Hirayama T., & Yagi T. 2017. “Regulation of Clustered Protocadherin Genes in Individual Neurons.” *Seminars in Cell & Developmental Biology* 69 (September): 122–30.
Hofmann C., Glavas M., Yu W., & Weinberg J. 1999. “Glucocorticoid Fast Feedback Is Not Altered in Rats Prenatally Exposed to Ethanol.” *Alcoholism: Clinical and Experimental Research* 23 (5): 891–900.
Horvath S., Zhang Y., Langfelder P., Kahn R.S., Boks M.P., Eijk K. van, Berg L.H. van den, & Ophoff R.A. 2012. “Aging Effects on DNA Methylation Modules in Human Brain and Blood Tissue.” *Genome Biology* 13 (10): R97.
Howard J. 2013. “The Cytokine Hypothesis: A Neurodevelopmental Explanation for the Emergence of Schizophrenia Later in Life.” *Advances in Bioscience and Biotechnology* 4 (8): 81–88.
Hoyme H.E., Kalberg W.O., Elliott A.J., Blankenship J., Buckley D., Marais A.-S., Manning M.A., et al. 2016. “Updated Clinical Guidelines for Diagnosing Fetal Alcohol Spectrum Disorders.” *Pediatrics* 138 (2).
Hu Z.-L., Bao J., & Reecy J. 2008. “CateGOrizer: A Web-Based Program to Batch Analyze Gene Ontology Classification Categories.” *Online Journal of Bioinformatics* 9: 108–12.
Hwang J., Rajendrasozhan S., Yao H., Chung S., Sundar I.K., Huyck H.L., Pryhuber G.S., Kinnula V.L., & Rahman I. 2011. “FOXO3 Deficiency Leads to Increased Susceptibility to Cigarette Smoke-Induced Inflammation, Airspace Enlargement, and Chronic Obstructive Pulmonary Disease.” *Journal of Immunology (Baltimore, Md. : 1950)* 187 (2): 987–98.
Ikonomidou C., Bittigau P., Ishimaru M.J., Wozniak D.F., Koch C., Genz K., Price M.T., et al.

2000. “Ethanol-Induced Apoptotic Neurodegeneration and Fetal Alcohol Syndrome.” *Science* 287 (5455): 1056–60.
Illingworth R.S., & Bird A.P. 2009. “CpG Islands--’a Rough Guide’.” *Federation of European Biochemical Societies Letters* 583 (11): 1713–20.
International HapMap 3 Consortium, Altshuler D.M., Gibbs R.A., Peltonen L., Altshuler D.M., Gibbs R.A., Peltonen L., et al. 2010. “Integrating Common and Rare Genetic Variation in Diverse Human Populations.” *Nature* 467 (7311): 52–58.
Ipsiroglu O.S., McKellin W.H., Carey N., & Loock C. 2013. “‘They Silently Live in Terror…’ Why Sleep Problems and Night-Time Related Quality-of-Life Are Missed in Children with a Fetal Alcohol Spectrum Disorder.” *Social Science & Medicine* 79: 76–83.
Irizarry R.A., Ladd-Acosta C., Carvalho B., Wu H., Brandenburg S.A., Jeddeloh J.A., Wen B., & Feinberg A.P. 2008. “Comprehensive High-Throughput Arrays for Relative Methylation (CHARM).” *Genome Research* 18 (5): 780–90.
Irizarry R.A., Ladd-Acosta C., Wen B., Wu Z., Montano C., Onyango P., Cui H., et al. 2009a. “The Human Colon Cancer Methylome Shows Similar Hypo- and Hypermethylation at Conserved Tissue-Specific CpG Island Shores.” *Nature Genetics* 41 (2): 178–86.
Irizarry R.A., Ladd-Acosta C., Wen B., Wu Z., Montano C., Onyango P., Cui H., et al. 2009b. “Genome-Wide Methylation Analysis of Human Colon Cancer Reveals Similar Hypo- and Hypermethylation at Conserved Tissue-Specific CpG Island Shores.” *Nature Genetics* 41 (2): 178–86.
Ito S., D’Alessio A.C., Taranova O. V, Hong K., Sowers L.C., & Zhang Y. 2010. “Role of Tet Proteins in 5mC to 5hmC Conversion, ES-Cell Self-Renewal and Inner Cell Mass Specification.” *Nature* 466 (7310). Howard Hughes Medical Institute.: 1129–33.
Iwamoto K., Kakiuchi C., Bundo M., Ikeda K., & Kato T. 2004. “Molecular Characterization of Bipolar Disorder by Comparing Gene Expression Profiles of Postmortem Brains of Major Mental Disorders.” *Molecular Psychiatry* 9 (4): 406–16.
Jacobson L., & Sapolsky R. 1991. “The Role of the Hippocampus in Feedback Regulation of the Hypothalamic-Pituitary-Adrenocortical Axis.” *Endocrine Reviews* 12 (2): 118–34.
Jacobson S.W., Bihun J.T., & Chiodo L.M. 1999. “Effects of Prenatal Alcohol and Cocaine Exposure on Infant Cortisol Levels.” *Development and Psychopathology* 11 (2): 195–208.
Jacobson S.W., Jacobson J.L., Stanton M.E., Meintjes E.M., & Molteno C.D. 2011. “Biobehavioral Markers of Adverse Effect in Fetal Alcohol Spectrum Disorders.” *Neuropsychology Review* 21 (2): 148–66.
Jaffe A.E., Gao Y., Deep-Soboslay A., Tao R., Hyde T.M., Weinberger D.R., & Kleinman J.E. 2015. “Mapping DNA Methylation across Development, Genotype and Schizophrenia in the Human Frontal Cortex.” *Nature Neuroscience* 19 (1): 40–47.
Jankord R., & Herman J.P. 2008. “Limbic Regulation of Hypothalamo-Pituitary-Adrenocortical Function during Acute and Chronic Stress.” *Annals of the New York Academy of Sciences* 1148: 64–73.
Ji H., Wang Y., Jiang D., Liu G., Xu X., Dai D., Zhou X., et al. 2016. “Elevated DRD4 Promoter Methylation Increases the Risk of Alzheimer’s Disease in Males.” *Molecular Medicine Reports* 14 (3): 2732–38.
Jin L., Yoshida T., Ho R., Owens G.K., & Somlyo A. V. 2009. “The Actin-Associated Protein Palladin Is Required for Development of Normal Contractile Properties of Smooth Muscle Cells Derived from Embryoid Bodies.” *The Journal of Biological Chemistry* 284 (4): 2121–

30.
Johnson S., Knight R., Marmer D.J., & Steele R.W. 1981. “Immune Deficiency in Fetal Alcohol Syndrome.” *Pediatric Research* 15 (6): 908–11.
Jones K.L., & Smith D.W. 1973. “Recognition of the Fetal Alcohol Syndrome in Early Infancy.” *Lancet* 302 (7836): 999–1001.
Jones K.L., Smith D.W., Ulleland C.N., & Streissguth P. 1973. “Pattern of Malformation in Offspring of Chronic Alcoholic Mothers.” *Lancet* 1 (7815): 1267–71.
Jones M.J., Farré P., McEwen L.M., Macisaac J.L., Watt K., Neumann S.M., Emberly E., Cynader M.S., Virji-Babul N., & Kobor M.S. 2013. “Distinct DNA Methylation Patterns of Cognitive Impairment and Trisomy 21 in Down Syndrome.” *BMC Medical Genomics* 6: 58.
Jones M.J., Fejes A.P., & Kobor M.S. 2013. “DNA Methylation, Genotype and Gene Expression: Who Is Driving and Who Is along for the Ride?” *Genome Biology* 14 (7): 126.
Jones M.J., Goodman S.J., & Kobor M.S. 2015. “DNA Methylation and Healthy Human Aging.” *Aging Cell* 14 (6): 924–32.
Jones P.A. 2012. “Functions of DNA Methylation: Islands, Start Sites, Gene Bodies and beyond.” *Nature Reviews Genetics* 13 (7): 484–92.
Jones P.A., & Baylin S.B. 2007. “The Epigenomics of Cancer.” *Cell* 128 (4): 683–92.
Jones P.A., & Takai D. 2001. “The Role of DNA Methylation in Mammalian Epigenetics.” *Science* 293 (5532): 1068–70.
Jones T.B., Bailey B. a, & Sokol R.J. 2013. “Alcohol Use in Pregnancy: Insights in Screening and Intervention for the Clinician.” *Clinical Obstetrics and Gynecology* 56 (1): 114–23.
Joubert B.R., Håberg S.E., Nilsen R.M., Wang X., Vollset S.E., Murphy S.K., Huang Z., et al. 2012. “450K Epigenome-Wide Scan Identifies Differential DNA Methylation in Newborns Related to Maternal Smoking during Pregnancy.” *Environmental Health Perspectives* 120 (10): 1425–31.
Kaminen-Ahola N., Ahola A., Maga M., Mallitt K.A., Fahey P., Cox T.C., Whitelaw E., & Chong S. 2010. “Maternal Ethanol Consumption Alters the Epigenotype and the Phenotype of Offspring in a Mouse Model.” *PLoS Genetics* 6 (1).
Kaminsky Z., Tochigi M., Jia P., Pal M., Mill J., Kwan A., Ioshikhes I., et al. 2012. “A Multi-Tissue Analysis Identifies HLA Complex Group 9 Gene Methylation Differences in Bipolar Disorder.” *Molecular Psychiatry* 17 (7): 728–40.
Kawasawa Y.I., Mohammad S., Son A.I., Morizono H., Basha A., Salzberg A.C., Torii M., & Hashimoto-Torii K. 2017. “Genome-Wide Profiling of Differentially Spliced mRNAs in Human Fetal Cortical Tissue Exposed to Alcohol.” *Alcohol* 62: 1–9.
Kelleher E., & Corvin A. 2015. “Overlapping Etiology of Neurodevelopmental Disorders.” In *The Genetics of Neurodevelopmental Disorders*, 29–48. John Wiley & Sons, Inc.
Khalid O., Kim J.J., Kim H.S., Hoang M., Tu T.G., Elie O., Lee C., et al. 2014. “Gene Expression Signatures Affected by Alcohol-Induced DNA Methylomic Deregulation in Human Embryonic Stem Cells.” *Stem Cell Research* 12 (3): 791–806.
Kim S.H., Shin S.Y., Lee K.Y., Joo E.J., Song J.Y., Ahn Y.M., Lee Y.H., & Kim Y.S. 2012. “The Genetic Association of DUSP6 with Bipolar Disorder and Its Effect on ERK Activity.” *Progress in Neuro-Psychopharmacology and Biological Psychiatry* 37 (1): 41–49.
Kinde B., Gabel H.W., Gilbert C.S., Griffith E.C., & Greenberg M.E. 2015. “Reading the Unique DNA Methylation Landscape of the Brain: Non-CpG Methylation, Hydroxymethylation,

and MeCP2." *Proceedings of the National Academy of Sciences* 112 (22): 6800–6806.
Kleiber M.L., Laufer B.I., Stringer R.L., & Singh S.M. 2014. "Third Trimester-Equivalent Ethanol Exposure Is Characterized by an Acute Cellular Stress Response and an Ontogenetic Disruption of Genes Critical for Synaptic Establishment and Function in Mice." *Developmental Neuroscience* 36 (6): 499–519.
Kleiber M.L., Laufer B.I., Wright E., Diehl E.J., & Singh S.M. 2012. "Long-Term Alterations to the Brain Transcriptome in a Maternal Voluntary Consumption Model of Fetal Alcohol Spectrum Disorders." *Brain Research* 1458 (June): 18–33.
Kleiber M.L., Mantha K., Stringer R.L., & Singh S.M. 2013. "Neurodevelopmental Alcohol Exposure Elicits Long-Term Changes to Gene Expression That Alter Distinct Molecular Pathways Dependent on Timing of Exposure." *Journal of Neurodevelopmental Disorders* 5 (1): 6.
Kobor M.S., & Weinberg J. 2011. "Focus on: Epigenetics and Fetal Alcohol Spectrum Disorders." *Alcohol Research & Health : The Journal of the National Institute on Alcohol Abuse and Alcoholism* 34 (1): 29–37.
Kordi-Tamandani D.M., Sahranavard R., & Torkamanzehi A. 2013. "Analysis of Association between Dopamine Receptor Genes' Methylation and Their Expression Profile with the Risk of Schizophrenia." *Psychiatric Genetics* 23 (5): 183–87.
Koziol M.J., Bradshaw C.R., Allen G.E., Costa A.S.H., Frezza C., & Gurdon J.B. 2015. "Identification of Methylated Deoxyadenosines in Vertebrates Reveals Diversity in DNA Modifications." *Nature Structural & Molecular Biology* 23 (1). Nature Publishing Group: 24–30.
Kriaucionis S., & Heintz N. 2009. "The Nuclear DNA Base 5-Hydroxymethylcytosine Is Present in Purkinje Neurons and the Brain." *Science* 324 (5929): 929–30.
Krishnamoorthy M., Gerwe B.A., Scharer C.D., Sahasranaman V., Eilertson C.D., Nash R.J., Usta S.N., et al. 2013. "Ethanol Alters Proliferation and Differentiation of Normal and Chromosomally Abnormal Human Embryonic Stem Cell-Derived Neurospheres." *Birth Defects Research Part B - Developmental and Reproductive Toxicology* 98 (3): 283–95.
Kwak H.-S., Han J.-Y., Choi J.-S., Ahn H.-K., Kwak D.-W., Lee Y.-K., Koh S.-Y., Jeong G.-U., Velázquez-Armenta E.Y., & Nava-Ocampo A.A. 2014. "Dose-Response and Time-Response Analysis of Total Fatty Acid Ethyl Esters in Meconium as a Biomarker of Prenatal Alcohol Exposure." *Prenatal Diagnosis* 34 (9): 831–38.
Kwak H.-S., Han J.-Y., Choi J.-S., Ahn H.-K., Ryu H.-M., Chung H.-J., Cho D.-H., Shin C.-Y., Velazquez-Armenta E.Y., & Nava-Ocampo A.A. 2014. "Characterization of Phosphatidylethanol Blood Concentrations for Screening Alcohol Consumption in Early Pregnancy." *Clinical Toxicology* 52 (1): 25–31.
Ladd-Acosta C., Hansen K.D., Briem E., Fallin M.D., Kaufmann W.E., & Feinberg A.P. 2014. "Common DNA Methylation Alterations in Multiple Brain Regions in Autism." *Molecular Psychiatry* 19: 862–71.
Lam L.L., Emberly E., Fraser H.B., Neumann S.M., Chen E., Miller G.E., & Kobor M.S. 2012. "Factors Underlying Variable DNA Methylation in a Human Community Cohort." *Proceedings of the National Academy of Sciences* 109 (Supplement_2): 17253–60.
Lan N., Chiu M.P.Y., Ellis L., & Weinberg J. 2017. "Prenatal Alcohol Exposure and Prenatal Stress Differentially Alter Glucocorticoid Signaling in the Placenta and Fetal Brain." *Neuroscience* 342 (February): 167–79.

Lan N., Yamashita F., Halpert A.G., Sliwowska J.H., Viau V., & Weinberg J. 2009. "Effects of Prenatal Ethanol Exposure on Hypothalamic-Pituitary-Adrenal Function across the Estrous Cycle." *Alcoholism: Clinical and Experimental Research* 33 (6): 1075–88.
Lan N., Yamashita F., Halpert a G., Ellis L., Yu W.K., Viau V., & Weinberg J. 2006. "Prenatal Ethanol Exposure Alters the Effects of Gonadectomy on Hypothalamic-Pituitary-Adrenal Activity in Male Rats." *Journal of Neuroendocrinology* 18 (9): 672–84.
Langevin S.M., Houseman E.A., Christensen B.C., Wiencke J.K., Nelson H.H., Karagas M.R., Marsit C.J., & Kelsey K.T. 2011. "The Influence of Aging, Environmental Exposures and Local Sequence Features on the Variation of DNA Methylation in Blood." *Epigenetics* 6 (7): 908–19.
Laufer B.I., Diehl E.J., & Singh S.M. 2013. "Neurodevelopmental Epigenetic Etiologies: Insights from Studies on Mouse Models of Fetal Alcohol Spectrum Disorders." *Epigenomics* 5 (5): 465–68.
Laufer B.I., Kapalanga J., Castellani C.A., Diehl E.J., Yan L., & Singh S.M. 2015. "Associative DNA Methylation Changes in Children with Prenatal Alcohol Exposure." *Epigenomics* 7 (August): 1–16.
Laufer B.I., Mantha K., Kleiber M.L., Diehl E.J., Addison S.M.F., & Singh S.M. 2013. "Long-Lasting Alterations to DNA Methylation and ncRNAs Could Underlie the Effects of Fetal Alcohol Exposure in Mice." *Disease Models & Mechanisms* 6 (4): 977–92.
Laurent L., Wong E., Li G., Huynh T., Tsirigos A., Ong C.T., Low H.M., et al. 2010. "Dynamic Changes in the Human Methylome during Differentiation." *Genome Research* 20 (3): 320–31.
Lee C., Mayfield R.D., & Harris R.A. 2014. "Altered Gamma-Aminobutyric Acid Type B Receptor Subunit 1 Splicing In Alcoholics." *Biological Psychiatry* 75 (10): 765–73.
Lee H.K., Braynen W., Keshav K., & Pavlidis P. 2005. "ErmineJ: Tool for Functional Analysis of Gene Expression Data Sets." *BMC Bioinformatics* 6 (1): 269.
Lee H.K., Hsu A.K., Sajdak J., Qin J., & Pavlidis P. 2004. "Coexpression Analysis of Human Genes across Many Microarray Data Sets." *Genome Research* 14 (6): 1085–94.
Lee K. 2012. "Gender-Specific Relationships between Alcohol Drinking Patterns and Metabolic Syndrome: The Korea National Health and Nutrition Examination Survey 2008." *Public Health Nutrition* 15 (10): 1917–24.
Lee S., Imaki T., Vale W., & Rivier C. 1990. "Effect of Prenatal Exposure to Ethanol on the Activity of the Hypothalamic-Pituitary-Adrenal Axis of the Offspring: Importance of the Time of Exposure to Ethanol and Possible Modulating Mechanisms." *Molecular and Cellular Neuroscience* 1 (2): 168–77.
Lee S., & Rivier C. 1996. "Gender Differences in the Effect of Prenatal Alcohol Exposure on the Hypothalamic-Pituitary-Adrenal Axis Response to Immune Signals." *Psychoneuroendocrinology* 21 (2): 145–55.
Lee S., Schmidt D., Tilders F., & Rivier C. 2000. "Increased Activity of the Hypothalamic-Pituitary-Adrenal Axis of Rats Exposed to Alcohol in Utero: Role of Altered Pituitary and Hypothalamic Function." *Molecular and Cellular Neuroscience* 16 (4): 515–28.
Leek J.T., Johnson W.E., Parker H.S., Jaffe A.E., & Storey J.D. 2012. "The Sva Package for Removing Batch Effects and Other Unwanted Variation in High-Throughput Experiments." *Bioinformatics* 28 (6): 882–83.
Lemoine P., Harousseau H., Borteyru J., & Menuet J. 1968. "Les Enfants Des Parents

Alcoholiques: Anomalies Observées a Propos de 127 Cas." *Ouest Médical* 8: 476–82.
Lemoine P., Harousseau H., Borteyru J.P., & Menuet J.C. 2003. "Children of Alcoholic Parents--Observed Anomalies: Discussion of 127 Cases." *Therapeutic Drug Monitoring* 25 (2): 132–36.
Li H., & Durbin R. 2009. "Fast and Accurate Short Read Alignment with Burrows-Wheeler Transform." *Bioinformatics* 25 (14): 1754–60.
Li H., Handsaker B., Wysoker A., Fennell T., Ruan J., Homer N., Marth G., Abecasis G., & Durbin R. 2009. "The Sequence Alignment/Map Format and SAMtools." *Bioinformatics* 25 (16): 2078–79.
Li Z., Xiang Y., Chen J., Li Q., Shen J., Liu Y., Li W., et al. 2015. "Loci with Genome-Wide Associations with Schizophrenia in the Han Chinese Population." *The British Journal of Psychiatry* 207 (6): 490–94.
Lindner M., Thümmler K., Arthur A., Brunner S., Elliott C., McElroy D., Mohan H., et al. 2015. "Fibroblast Growth Factor Signalling in Multiple Sclerosis: Inhibition of Myelination and Induction of pro-Inflammatory Environment by FGF9." *Brain* 138 (7): 1875–93.
Lister R., Mukamel E.A., Nery J.R., Urich M., Puddifoot C.A., Johnson N.D., Lucero J., et al. 2013. "Global Epigenomic Reconfiguration during Mammalian Brain Development." *Science* 341 (6146): 1237905.
Lister R., Pelizzola M., Dowen R.H., Hawkins R.D., Hon G., Tonti-Filippini J., Nery J.R., et al. 2009. "Human DNA Methylomes at Base Resolution Show Widespread Epigenomic Differences." *Nature* 462 (7271): 315–22.
Lister R., Pelizzola M., Kida Y.S., Hawkins R.D., Nery J.R., Hon G., Antosiewicz-Bourget J., et al. 2012. "Hotspots of Aberrant Epigenomic Reprogramming in Human Induced Pluripotent Stem Cells." *Nature* 470 (7336): 68–73.
Liu X., Wu Z., Hayashi Y., & Nakanishi H. 2012. "Age-Dependent Neuroinflammatory Responses and Deficits in Long-Term Potentiation in the Hippocampus during Systemic Inflammation." *Neuroscience* 216 (August): 133–42.
Liu Y., Aryee M.J., Padyukov L., Fallin M.D., Hesselberg E., Runarsson A., Reinius L., et al. 2013. "Epigenome-Wide Association Data Implicate DNA Methylation as an Intermediary of Genetic Risk in Rheumatoid Arthritis." *Nature Biotechnology* 31 (2): 142–47.
Liu Y., Balaraman Y., Wang G., Nephew K.P., & Zhou F.C. 2009. "Alcohol Exposure Alters DNA Methylation Profiles in Mouse Embryos at Early Neurulation." *Epigenetics* 4 (7): 500–511.
Liyanage V.R.B., Zachariah R.M., Davie J.R., & Rastegar M. 2015. "Ethanol Deregulates Mecp2/MeCP2 in Differentiating Neural Stem Cells via Interplay between 5-Methylcytosine and 5-Hydroxymethylcytosine at the Mecp2 Regulatory Elements." *Experimental Neurology* 265 (March): 102–17.
Lowe R., Gemma C., Beyan H., Hawa M.I., Bazeos A., Leslie R.D., Montpetit A., Rakyan V.K., & Ramagopalan S. V. 2013. "Buccals Are Likely to Be a More Informative Surrogate Tissue than Blood for Epigenome-Wide Association Studies." *Epigenetics* 8 (4): 445–54.
Luo X., Kranzler H.R., Zuo L., Lappalainen J., Yang B., & Gelernter J. 2005. "ADH4 Gene Variation Is Associated with Alcohol Dependence and Drug Dependence in European Americans: Results from HWD Tests and Case-Control Association Studies." *Neuropsychopharmacology* 31 (5): 1085–95.
Lussier A.A., Stepien K.A., Neumann S.M., Pavlidis P., Kobor M.S., & Weinberg J. 2015.

"Prenatal Alcohol Exposure Alters Steady-State and Activated Gene Expression in the Adult Rat Brain." *Alcoholism: Clinical and Experimental Research* 39 (2): 251–61.
Lussier A.A., Weinberg J., & Kobor M.S. 2017. "Epigenetics Studies of Fetal Alcohol Spectrum Disorder: Where Are We Now?" *Epigenomics* 9 (3). Future Medicine: 291–311.
Lynch M.E., Kable J.A., & Coles C.D. 2015. "Prenatal Alcohol Exposure, Adaptive Function, and Entry into Adult Roles in a Prospective Study of Young Adults." *Neurotoxicology and Teratology* 51 (August): 52–60.
MacKay R.K., Colson N.J., Dodd P.R., & Lewohl J.M. 2011. "Differential Expression of 14-3-3 Isoforms in Human Alcoholic Brain." *Alcoholism: Clinical and Experimental Research* 35 (6): 1041–49.
Maier S.E., Cramer J.A., West J.R., & Sohrabji F. 1999. "Alcohol Exposure during the First Two Trimesters Equivalent Alters Granule Cell Number and Neurotrophin Expression in the Developing Rat Olfactory Bulb." *Journal of Neurobiology* 41 (3): 414–23.
Marjonen H., Sierra A., Nyman A., Rogojin V., Gröhn O., Linden A.M., Hautaniemi S., & Kaminen-Ahola N. 2015. "Early Maternal Alcohol Consumption Alters Hippocampal DNA Methylation, Gene Expression and Volume in a Mouse Model." *PLoS ONE* 10 (5).
Mathew D.E., Larsen K., Janeczek P., & Lewohl J.M. 2016. "Expression of 14-3-3 Transcript Isoforms in Response to Ethanol Exposure and Their Regulation by miRNAs." *Molecular and Cellular Neuroscience* 75 (September): 44–49.
Matthews S.G. 2002. "Early Programming of the Hypothalamo-Pituitary-Adrenal Axis." *Trends in Endocrinology and Metabolism* 13 (9): 373–80.
Mattson S.N., Crocker N., & Nguyen T.T. 2011. "Fetal Alcohol Spectrum Disorders: Neuropsychological and Behavioral Features." *Neuropsychology Review* 21 (2): 81–101.
Mattson S.N., Roesch S.C., Glass L., Deweese B.N., Coles C.D., Kable J.A., May P.A., et al. 2013. "Further Development of a Neurobehavioral Profile of Fetal Alcohol Spectrum Disorders." *Alcoholism: Clinical and Experimental Research* 37 (3): 517–28.
Maunakea A.K., Chepelev I., Cui K., & Zhao K. 2013. "Intragenic DNA Methylation Modulates Alternative Splicing by Recruiting MeCP2 to Promote Exon Recognition." *Cell Research* 23 (11): 1256–69.
Maunakea A.K., Nagarajan R.P., Bilenky M., Ballinger T.J., D'Souza C., Fouse S.D., Johnson B.E., et al. 2010. "Conserved Role of Intragenic DNA Methylation in Regulating Alternative Promoters." *Nature* 466 (7303): 253–57.
May P.A., Baete A., Russo J., Elliott A.J., Blankenship J., Kalberg W.O., Buckley D., et al. 2014. "Prevalence and Characteristics of Fetal Alcohol Spectrum Disorders." *Pediatrics* 134 (5): 855–66.
May P.A., Fiorentino D., Coriale G., Kalberg W.O., Hoyme H.E., Aragón A.S., Buckley D., et al. 2011. "Prevalence of Children with Severe Fetal Alcohol Spectrum Disorders in Communities Near Rome, Italy: New Estimated Rates Are Higher than Previous Estimates." *International Journal of Environmental Research and Public Health* 8 (6): 2331–51.
May P.A., & Gossage J.P. 2001. "Estimating the Prevalence of Fetal Alcohol Syndrome. A Summary." *Alcohol Research & Health : The Journal of the National Institute on Alcohol Abuse and Alcoholism* 25 (3): 159–67.
May P.A., Gossage J.P., Kalberg W.O., Robinson L.K., Buckley D., Manning M., & Hoyme H.E. 2009. "Prevalence and Epidemiologic Characteristics of FASD from Various Research

Methods with an Emphasis on Recent in-School Studies." *Developmental Disabilities Research Reviews* 15 (3): 176–92.
May P.A., Gossage J.P., White-Country M., Goodhart K., Decoteau S., Trujillo P.M., Kalberg W.O., Viljoen D.L., & Hoyme H.E. 2004. "Alcohol Consumption and Other Maternal Risk Factors for Fetal Alcohol Syndrome among Three Distinct Samples of Women Before, During, and after Pregnancy: The Risk Is Relative." *American Journal of Medical Genetics Part C: Seminars in Medical Genetics* 127C (1): 10–20.
May P.A., Keaster C., Bozeman R., Goodover J., Blankenship J., Kalberg W.O., Buckley D., et al. 2015. "Prevalence and Characteristics of Fetal Alcohol Syndrome and Partial Fetal Alcohol Syndrome in a Rocky Mountain Region City." *Drug & Alcohol Dependence* 155: 118–27.
McCormick C.M., & Mathews I.Z. 2010. "Adolescent Development, Hypothalamic-Pituitary-Adrenal Function, and Programming of Adult Learning and Memory." *Progress in Neuro-Psychopharmacology and Biological Psychiatry* 34 (5): 756–65.
McEwen B., & Stellar E. 1993. "Stress and the Individual. Mechanisms Leading to Disease." *Archives of Internal Medicine* 153 (18): 2093–2101.
McGill J., Meyerholz D.K., Edsen-Moore M., Young B., Coleman R.A., Schlueter A.J., Waldschmidt T.J., Cook R.T., & Legge K.L. 2009. "Fetal Exposure to Ethanol Has Long-Term Effects on the Severity of Influenza Virus Infections." *Journal of Immunology* 182 (12): 7803–8.
McLachlan K., Rasmussen C., Oberlander T.F., Loock C., Pei J., Andrew G., Reynolds J., & Weinberg J. 2016. "Dysregulation of the Cortisol Diurnal Rhythm Following Prenatal Alcohol Exposure and Early Life Adversity." *Alcohol* 53 (June): 9–18.
McQuire C., Paranjothy S., Hurt L., Mann M., Farewell D., & Kemp A. 2016. "Objective Measures of Prenatal Alcohol Exposure: A Systematic Review." *Pediatrics* 138 (3).
Meaney M.J. 2010. "Epigenetics and the Biological Definition of Gene X Environment Interactions." *Child Development* 81 (1): 41–79.
Mesa D.A., Kable J.A., Coles C.D., Jones K.L., Yevtushok L., Kulikovsky Y., Wertelecki W., Coleman T.P., Chambers C.D., & CIFASD the. 2017. "The Use of Cardiac Orienting Responses as an Early and Scalable Biomarker of Alcohol-Related Neurodevelopmental Impairment." *Alcoholism: Clinical and Experimental Research* 41 (1): 128–38.
Meyer K.D., & Jaffrey S.R. 2016. "Expanding the Diversity of DNA Base Modifications with N6-Methyldeoxyadenosine." *Genome Biology* 17 (5).
Meyer K.D., Saletore Y., Zumbo P., Elemento O., Mason C.E., & Jaffrey S.R. 2012. "Comprehensive Analysis of mRNA Methylation Reveals Enrichment in 3' UTRs and near Stop Codons." *Cell* 149 (7): 1635–46.
Moen E.L., Zhang X., Mu W., Delaney S.M., Wing C., McQuade J., Myers J., Godley L.A., Dolan M.E., & Zhang W. 2013. "Genome-Wide Variation of Cytosine Modifications Between European and African Populations and the Implications for Complex Traits." *Genetics* 194 (4): 987–96.
Moncada-Pazos A., Obaya A.J., Llamazares M., Heljasvaara R., Suárez M.F., Colado E., Noël A., Cal S., & López-Otín C. 2012. "ADAMTS-12 Metalloprotease Is Necessary for Normal Inflammatory Response." *The Journal of Biological Chemistry* 287 (47): 39554–63.
Moore E.M., & Riley E.P. 2015. "What Happens When Children with Fetal Alcohol Spectrum Disorders Become Adults?" *Current Developmental Disorders Reports* 2 (3): 219–27.

Moscatello K.M., Biber K.L., Jennings S.R., Chervenak R., & Wolcott R.M. 1999. “Effects of in Utero Alcohol Exposure on B Cell Development in Neonatal Spleen and Bone Marrow.” *Cellular Immunology* 191 (2): 124–30.

Mukhopadhyay P., Rezzoug F., Kaikaus J., Greene R.M., & Pisano M.M. 2013. “Alcohol Modulates Expression of DNA Methyltranferases and Methyl CpG-/CpG Domain-Binding Proteins in Murine Embryonic Fibroblasts.” *Reproductive Toxicology* 37: 40–48.

Murawski N., Moore E., Thomas J., & Riley E. 2015. “Advances in Diagnosis and Treatment of Fetal Alcohol Spectrum Disorders From Animal Models to Human Studies.” *Alcohol Research: Current Reviews* 37 (1): 97–108.

Nagre N.N., Subbanna S., Shivakumar M., Psychoyos D., & Basavarajappa B.S. 2015. “CB1-Receptor Knockout Neonatal Mice Are Protected against Ethanol-Induced Impairments of DNMT1, DNMT3A, and DNA Methylation.” *Journal of Neurochemistry* 132 (4): 429–42.

Nakashima A., Kawamoto T., Honda K.K., Ueshima T., Noshiro M., Iwata T., Fujimoto K., et al. 2008. “DEC1 Modulates the Circadian Phase of Clock Gene Expression.” *Molecular and Cellular Biology* 28 (12): 4080–92.

National Research Council. 2011. *Guide for the Care and Use of Laboratory Animals*. Eighth. Washington, DC: The National Academies Press.

Ngai Y.F., Sulistyoningrum D.C., O’Neill R., Innis S.M., Weinberg J., & Devlin A.M. 2015. “Prenatal Alcohol Exposure Alters Methyl Metabolism and Programs Serotonin Transporter and Glucocorticoid Receptor Expression in Brain.” *American Journal of Physiology. Regulatory, Integrative and Comparative Physiology* 309 (5): R613-22.

Nikolayeva O., & Robinson M.D. 2014. “edgeR for Differential RNA-Seq and ChIP-Seq Analysis: An Application to Stem Cell Biology.” *Methods in Molecular Biology* 1150: 45–79.

Nolan T., Hands R.E., & Bustin S. a. 2006. “Quantification of mRNA Using Real-Time RT-PCR.” *Nature Protocols* 1 (3): 1559–82.

Norman A.L., Crocker N., Mattson S.N., & Riley E.P. 2009. *Neuroimaging and Fetal Alcohol Spectrum Disorders*. *Developmental Disabilities Research Reviews*. Vol. 15.

Norman D.C., Chang M.P., Wong C.M., Branch B.J., Castle S., & Taylor A.N. 1991. “Changes with Age in the Proliferative Response of Splenic T Cells from Rats Exposed to Ethanol in Utero.” *Alcoholism: Clinical and Experimental Research* 15 (3): 428–32.

Okulicz-Kozaryn K., Borkowska M., & Brzózka K. 2017. “FASD Prevalence among Schoolchildren in Poland.” *Journal of Applied Research in Intellectual Disabilities* 30 (1): 61–70.

Oldehinkel A.J., & Bouma E.M.C. 2011. “Sensitivity to the Depressogenic Effect of Stress and HPA-Axis Reactivity in Adolescence: A Review of Gender Differences.” *Neuroscience & Biobehavioral Reviews* 35 (8): 1757–70.

Ooi S.K.T., & Bestor T.H. 2008. “The Colorful History of Active DNA Demethylation.” *Cell* 133 (7): 1145–48.

Osborn J.A., Kim C.K., Yu W., Herbert L., & Weinberg J. 1996. “Fetal Ethanol Exposure Alters Pituitary-Adrenal Sensitivity to Dexamethasone Suppression.” *Psychoneuroendocrinology* 21 (2): 127–43.

Osborne T.F. 2001. “CREating a SCAP-Less Liver Keeps SREBPs Pinned in the ER Membrane and Prevents Increased Lipid Synthesis in Response to Low Cholesterol and High Insulin.” *Genes & Development* 15 (15): 1873–78.

Ostrea E.M., Hernandez J.D., Bielawski D.M., Kan J.M., Leonardo G.M., Abela M.B., Church M.W., et al. 2006. “Fatty Acid Ethyl Esters in Meconium: Are They Biomarkers of Fetal Alcohol Exposure and Effect?” *Alcoholism: Clinical and Experimental Research* 30 (7): 1152–59.

Otero N.K.H., Thomas J.D., Saski C.A., Xia X., & Kelly S.J. 2012. “Choline Supplementation and DNA Methylation in the Hippocampus and Prefrontal Cortex of Rats Exposed to Alcohol During Development.” *Alcoholism: Clinical and Experimental Research* 36 (10): 1701–9.

Ouko L.A., Shantikumar K., Knezovich J., Haycock P., Schnugh D.J., & Ramsay M. 2009. “Effect of Alcohol Consumption on CpG Methylation in the Differentially Methylated Regions of H19 and IG-DMR in Male Gametes: Implications for Fetal Alcohol Spectrum Disorders.” *Alcoholism: Clinical and Experimental Research* 33 (9): 1615–27.

Ousman S.S., & Kubes P. 2012. “Immune Surveillance in the Central Nervous System.” *Nature Neuroscience* 15 (8): 1096–1101.

Ozer E., Sarioglu S., & Gure A. 2000. “Effects of Prenatal Ethanol Exposure on Neuronal Migration, Neuronogenesis and Brain Myelination in the Mice Brain.” *Clinical Neuropathology* 19 (1): 21–25.

Öztürk N.C., Resendiz M., Öztürk H., & Zhou F.C. 2017. “DNA Methylation Program in Normal and Alcohol-Induced Thinning Cortex.” *Alcohol* 60 (May): 135–47.

Pagnamenta A.T., Bacchelli E., Jonge M. V de, Mirza G., Scerri T.S., Minopoli F., Chiocchetti A., et al. 2010. “Characterization of a Family with Rare Deletions in CNTNAP5 and DOCK4 Suggests Novel Risk Loci for Autism and Dyslexia.” *Biological Psychiatry* 68 (4): 320–28.

Paley B., & O’Connor M.J. 2011. “Behavioral Interventions for Children and Adolescents With Fetal Alcohol Spectrum Disorders.” *Alcohol Research & Health* 34 (1): 64–75.

Panczakiewicz A.L., Glass L., Coles C.D., Kable J.A., Sowell E.R., Wozniak J.R., Jones K.L., Riley E.P., & Mattson S.N. 2016. “Neurobehavioral Deficits Consistent Across Age and Sex in Youth with Prenatal Alcohol Exposure.” *Alcoholism: Clinical and Experimental Research* 40 (9): 1971–81.

Pei J., Denys K., Hughes J., & Rasmussen C. 2011. “Mental Health Issues in Fetal Alcohol Spectrum Disorder.” *Journal of Mental Health* 20 (5): 473–83.

Pennington J.S., Shuvaeva T.I., & Pennington S.N. 2002. “Maternal Dietary Ethanol Consumption Is Associated With Hypertriglyceridemia in Adult Rat Offspring.” *Alcoholism: Clinical and Experimental Research* 26 (6): 848–55.

Perkins A., Lehmann C., Lawrence R.C., & Kelly S.J. 2013. “Alcohol Exposure during Development: Impact on the Epigenome.” *International Journal of Developmental Neuroscience* 31 (6): 391–97.

Peters T.J., & Buckley M. n.d. “DMRcate: Illumina 450 K Methylation Array Apatial Analysis Methods. R Package Version 1.2.0.”

Peters T.J., Buckley M.J., Statham A.L., Pidsley R., Samaras K., Lord R. V, Clark S.J., & Molloy P.L. 2015. “De Novo Identification of Differentially Methylated Regions in the Human Genome.” *Epigenetics & Chromatin* 8 (1): 1–31.

Petković G., & Barišić I. 2013. “Prevalence of Fetal Alcohol Syndrome and Maternal Characteristics in a Sample of Schoolchildren from a Rural Province of Croatia.” *International Journal of Environmental Research and Public Health* 10 (4): 1547–61.

Pfeifer G.P., Kadam S., & Jin S.-G. 2013. "5-Hydroxymethylcytosine and Its Potential Roles in Development and Cancer." *Epigenetics & Chromatin* 6 (1): 10.
Philibert R.A., Plume J.M., Gibbons F.X., Brody G.H., & Beach S.R.H. 2012. "The Impact of Recent Alcohol Use on Genome Wide DNA Methylation Signatures." *Frontiers in Genetics* 3: 54.
Pollard I. 2007. "Neuropharmacology of Drugs and Alcohol in Mother and Fetus." *Seminars in Fetal and Neonatal Medicine* 12 (2): 106–13.
Popova S., Lange S., Probst C., Gmel G., & Rehm J. 2017. "Estimation of National, Regional, and Global Prevalence of Alcohol Use during Pregnancy and Fetal Alcohol Syndrome: A Systematic Review and Meta-Analysis." *Lancet Global Health* 5 (3): e290–99.
Popova S., Lange S., Shield K., Mihic A., Chudley A.E., Mukherjee R.A.S., Bekmuradov D., & Rehm J. 2016. "Comorbidity of Fetal Alcohol Spectrum Disorder: A Systematic Review and Meta-Analysis." *Lancet* 6736 (15): 1–10.
Portales-Casamar E., Ch Ng C., Lui F., St-Georges N., Zoubarev A., Lai A.Y., Lee M., et al. 2013. "Neurocarta: Aggregating and Sharing Disease-Gene Relations for the Neurosciences." *BMC Genomics* 14 (1): 129.
Portales-Casamar E., Lussier A.A., Jones M.J., MacIsaac J.L., Edgar R.D., Mah S.M., Barhdadi A., et al. 2016. "DNA Methylation Signature of Human Fetal Alcohol Spectrum Disorder." *Epigenetics & Chromatin* 9 (25): 81–101.
Price M.E., Cotton A.M., Lam L.L., Farré P., Emberly E., Brown C.J., Robinson W.P., & Kobor M.S. 2013. "Additional Annotation Enhances Potential for Biologically-Relevant Analysis of the Illumina Infinium HumanMethylation450 BeadChip Array." *Epigenetics & Chromatin* 6 (1): 4.
Ptáček R., Kuželová H., & Stefano G.B. 2011. "Dopamine D4 Receptor Gene DRD4 and Its Association with Psychiatric Disorders." *Medical Science Monitor : International Medical Journal of Experimental and Clinical Research* 17 (9): RA215-RA220.
Quinlan A.R., & Hall I.M. 2010. "BEDTools: A Flexible Suite of Utilities for Comparing Genomic Features." *Bioinformatics* 26 (6): 841–42.
Quraishi B.M., Zhang H., Everson T.M., Ray M., Lockett G.A., Holloway J.W., Tetali S.R., et al. 2015. "Identifying CpG Sites Associated with Eczema via Random Forest Screening of Epigenome-Scale DNA Methylation." *Clinical Epigenetics* 7 (1): 68.
Raab R.M., Bullen J., Kelleher J., Mantzoros C., & Stephanopoulos G. 2005. "Regulation of Mouse Hepatic Genes in Response to Diet Induced Obesity, Insulin Resistance and Fasting Induced Weight Reduction." *Nutrition & Metabolism* 2 (1): 15.
Rakyan V.K., Down T.A., Balding D.J., & Beck S. 2011. "Epigenome-Wide Association Studies for Common Human Diseases." *Nature Reviews Genetics* 12 (8): 529–41.
Ramsahoye B.H., Biniszkiewicz D., Lyko F., Clark V., Bird A.P., & Jaenisch R. 2000. "Non-CpG Methylation Is Prevalent in Embryonic Stem Cells and May Be Mediated by DNA Methyltransferase 3a." *Proceedings of the National Academy of Sciences* 97 (10): 5237–42.
Ramsay D.S., Bendersky M.I., & Lewis M. 1996. "Effect of Prenatal Alcohol and Cigarette Exposure on Two- and Six-Month-Old Infants' Adrenocortical Reactivity to Stress." *Journal of Pediatric Psychology* 21 (6): 833–40.
Ramsay M. 2010. "Genetic and Epigenetic Insights into Fetal Alcohol Spectrum Disorders." *Genome Medicine* 2 (4). BioMed Central Ltd: 27.
Raychaudhuri S., Sandor C., Stahl E.A., Freudenberg J., Lee H.-S., Jia X., Alfredsson L., et al.

2012. “Five Amino Acids in Three HLA Proteins Explain Most of the Association between MHC and Seropositive Rheumatoid Arthritis.” *Nature Genetics* 44 (3): 291–96.
Redei E., Clark W.R., & McGivem R.F. 1989. “Alcohol Exposure in Utero Results in Diminished T-Cell Function and Alterations in Brain Corticotropin-Releasing Factor and ACTH Content.” *Alcoholism: Clinical and Experimental Research* 13 (3): 439–43.
Redei E., Halasz I., Li L.F., Prystowsky M.B., & Aird F. 1993. “Maternal Adrenalectomy Alters the Immune and Endocrine Functions of Fetal Alcohol-Exposed Male Offspring.” *Endocrinology* 133 (2): 452–60.
Reese S.E., Zhao S., Wu M.C., Joubert B.R., Parr C.L., Håberg S.E., Ueland P.M., et al. 2017. “DNA Methylation Score as a Biomarker in Newborns for Sustained Maternal Smoking during Pregnancy.” *Environmental Health Perspectives* 125 (4): 760–66.
Resendiz M., Chen Y., Ozturk N.C., & Zhou F.C. 2013. “Epigenetic Medicine and Fetal Alcohol Spectrum Disorders.” *Epigenomics* 5 (1): 73–86.
Reul J.M.H.M., & Kloet E.R. De. 1985. “Two Receptor Systems for Corticosterone in Rat Brain: Microdistribution and Differential Occupation.” *Endocrinology* 117 (6): 2505–11.
Reynolds J.N., Weinberg J., Clarren S., Beaulieu C., Rasmussen C., Kobor M., Dube M.-P., & Goldowitz D. 2011. “Fetal Alcohol Spectrum Disorders: Gene-Environment Interactions, Predictive Biomarkers, and the Relationship Between Structural Alterations in the Brain and Functional Outcomes.” *Seminars in Pediatric Neurology* 18 (1): 49–55.
Rice G.I., Toro Duany Y. del, Jenkinson E.M., Forte G.M.A., Anderson B.H., Ariaudo G., Bader-Meunier B., et al. 2014. “Gain-of-Function Mutations in IFIH1 Cause a Spectrum of Human Disease Phenotypes Associated with Upregulated Type I Interferon Signaling.” *Nature Genetics* 46 (5): 503–9.
Riley E.P., Infante M.A., & Warren K.R. 2011. “Fetal Alcohol Spectrum Disorders: An Overview.” *Neuropsychology Review* 21 (2): 73–80.
Robinson M.D., McCarthy D.J., & Smyth G.K. 2010. “edgeR: A Bioconductor Package for Differential Expression Analysis of Digital Gene Expression Data.” *Bioinformatics* 26 (1): 139–40.
Rogic S., Wong A., & Pavlidis P. 2016. “Meta-Analysis of Gene Expression Patterns in Animal Models of Prenatal Alcohol Exposure Suggests Role for Protein Synthesis Inhibition and Chromatin Remodeling.” *Alcoholism: Clinical and Experimental Research* 40 (4): 717–27.
Roozen S., Peters G.-J.Y., Kok G., Townend D., Nijhuis J., & Curfs L. 2016. “Worldwide Prevalence of Fetal Alcohol Spectrum Disorders: A Systematic Literature Review Including Meta-Analysis.” *Alcoholism: Clinical and Experimental Research* 40 (1): 18–32.
Ross-Innes C.S., Stark R., Teschendorff A.E., Holmes K.A., Ali H.R., Dunning M.J., Brown G.D., et al. 2012. “Differential Oestrogen Receptor Binding Is Associated with Clinical Outcome in Breast Cancer.” *Nature* 481 (7381): 389–93.
Russell M., Martier S.S., Sokol R.J., Mudar P., Jacobson S., & Jacobson J. 1996. “Detecting Risk Drinking during Pregnancy: A Comparison of Four Screening Questionnaires.” *American Journal of Public Health* 86 (10): 1435–39.
Sadakierska-Chudy A., Kostrzewa R.M., & Filip M. 2014. “A Comprehensive View of the Epigenetic Landscape Part I: DNA Methylation, Passive and Active DNA Demethylation Pathways and Histone Variants.” *Neurotoxicity Research* 27 (1): 84–97.
Sampson P.D., Streissguth A.P., Bookstein F.L., Little R.E., Clarren S.K., Dehaene P., Hanson J.W., & Graham J.M. 1997. “Incidence of Fetal Alcohol Syndrome and Prevalence of

Alcohol-Related Neurodevelopmental Disorder." *Teratology* 56 (5): 317–26.
Sánchez-Mora C., Ribasés M., Casas M., Bayés M., Bosch R., Fernàndez-Castillo N., Brunso L., et al. 2011. "Exploring DRD4 and Its Interaction with SLC6A3 as Possible Risk Factors for Adult ADHD: A Meta-Analysis in Four European Populations." *American Journal of Medical Genetics. Part B, Neuropsychiatric Genetics* 156B (5): 600–612.
Santiago M., Antunes C., Guedes M., Sousa N., & Marques C.J. 2014. "TET Enzymes and DNA Hydroxymethylation in Neural Development and Function — How Critical Are They?" *Genomics* 104 (5): 334–40.
Sarkola T., Eriksson P.C.J., Niemelä O., Sillanaukee P., & Halmesmäki E. 2000. "Mean Cell Volume and Gamma-Glutamyl Transferase Are Superior to Carbohydrate-Deficient Transferrin and Hemoglobin-Acetaldehyde Adducts in the Follow-up of Pregnant Women with Alcohol Abuse." *Acta Obstetricia et Gynecologica Scandinavica* 79 (5): 359–66.
Saxonov S., Berg P., & Brutlag D.L. 2006. "A Genome-Wide Analysis of CpG Dinucleotides in the Human Genome Distinguishes Two Distinct Classes of Promoters." *Proceedings of the National Academy of Sciences of the United States of America* 103 (5): 1412–17.
Schmittgen T.D., & Livak K.J. 2008. "Analyzing Real-Time PCR Data by the Comparative CT Method." *Nature Protocols* 3 (6): 1101–8.
Schott J.M., Crutch S.J., Carrasquillo M.M., Uphill J., Shakespeare T.J., Ryan N.S., Yong K.X., et al. 2016. "Genetic Risk Factors for the Posterior Cortical Atrophy Variant of Alzheimer's Disease." *Alzheimer's & Dementia* 12 (8): 862–71.
Schuebeler D. 2015. "Function and Information Content of DNA Methylation." *Nature* 517 (7534): 321–26.
Sei H., Sakata-Haga H., Ohta K., Sawada K., Morita Y., & Fukui Y. 2003. "Prenatal Exposure to Alcohol Alters the Light Response in Postnatal Circadian Rhythm." *Brain Research* 987 (1): 131–34.
Senturias Y., & Baldonado M. 2014. "Fetal Spectrum Disorders: An Overview of Ethical and Legal Issues for Healthcare Providers." *Current Problems in Pediatric and Adolescent Health Care* 44 (4): 102–4.
Shue E.H., Carson-Walter E.B., Liu Y., Winans B.N., Ali Z.S., Chen J., & Walter K.A. 2008. "Plasmalemmal Vesicle Associated Protein-1 (PV-1) Is a Marker of Blood-Brain Barrier Disruption in Rodent Models." *BMC Neuroscience* 9 (1): 29.
Shukla S., Kavak E., Gregory M., Imashimizu M., Shutinoski B., Kashlev M., Oberdoerffer P., Sandberg R., & Oberdoerffer S. 2011. "CTCF-Promoted RNA Polymerase II Pausing Links DNA Methylation to Splicing." *Nature* 479 (7371): 74–79.
Shulha H.P., Cheung I., Guo Y., Akbarian S., & Weng Z. 2013. "Coordinated Cell Type-Specific Epigenetic Remodeling in Prefrontal Cortex Begins before Birth and Continues into Early Adulthood." *PLoS Genetics* 9 (4): e1003433.
Sliwowska J.H., Lan N., Yamashita F., Halpert A.G., Viau V., & Weinberg J. 2008. "Effects of Prenatal Ethanol Exposure on Regulation of Basal Hypothalamic-Pituitary-Adrenal Activity and Hippocampal 5-HT1A Receptor mRNA Levels in Female Rats across the Estrous Cycle." *Psychoneuroendocrinology* 33 (8): 1111–23.
Smith A.C.M., Gropman A.L., Bailey-Wilson J.E., Goker-Alpan O., Elsea S.H., Blancato J., Lupski J.R., & Potocki L. 2002. "Hypercholesterolemia in Children with Smith-Magenis Syndrome: Del (17)(p11.2p11.2)." *Genetics in Medicine* 4 (3): 118–25.
Smith A.K., Kilaru V., Klengel T., Mercer K.B., Bradley B., Conneely K.N., Ressler K.J., &

Binder E.B. 2015. “DNA Extracted from Saliva for Methylation Studies of Psychiatric Traits: Evidence Tissue Specificity and Relatedness to Brain.” *American Journal of Medical Genetics, Part B: Neuropsychiatric Genetics* 168 (1): 36–44.
Smith Z.D., & Meissner A. 2013. “DNA Methylation: Roles in Mammalian Development.” *Nature Reviews Genetics* 14 (3): 204–20.
Smoot M.E., Ono K., Ruscheinski J., Wang P.-L., & Ideker T. 2011. “Cytoscape 2.8: New Features for Data Integration and Network Visualization.” *Bioinformatics* 27 (3): 431–32.
Smyth G.K. 2004. “Linear Models and Empirical Bayes Methods for Assessing Differential Expression in Microarray Experiments.” *Statistical Applications in Genetics and Molecular Biology* 3: Article3.
Smyth G.K. 2005. “Limma: Linear Models for Microarray Data.” In *Bioinformatics and Computational Biology Solutions Using R and Bioconductor*, edited by Robert Gentleman, Vincent J. Carey, Wolfgang Huber, Rafael A. Irizarry, and Sandrine Dudoit, 397–420. Springer New York.
Spanagel R., Rosenwasser A.M., Schumann G., & Sarkar D.K. 2005. “Alcohol Consumption and the Body’s Biological Clock.” *Alcoholism: Clinical and Experimental Research* 29 (8): 1550–57.
Spohr H.-L., & Steinhausen H.-C. 2008. “Fetal Alcohol Spectrum Disorders and Their Persisting Sequelae in Adult Life.” *Deutsches Ärzteblatt International* 105 (41): 693–98.
Squire L., Bloom F.E., Spitzer N.C., Squire L.R., Berg D., Lac S. du, & Ghosh A. 2008. *Fundamental Neuroscience*. Fundamental Neuroscience Series. Elsevier Science.
Stark R., & Brown G. 2011. “DiffBind: Differential Binding Analysis of ChIP-Seq Peak Data.”
Stojnic R., & Diez D. 2013. “PWMEnrich: PWM Enrichment Analysis.” *R Package Version* 4.
Stouder C., Somm E., & Paoloni-Giacobino A. 2011. “Prenatal Exposure to Ethanol: A Specific Effect on the H19 Gene in Sperm.” *Reproductive Toxicology* 31 (4): 507–12.
Stratton K., Howe C., & Battaglia F. 1996. *Fetal Alcohol Syndrome: Diagnosis, Epidemiology, Prevention and Treatment*. Washington, DC: National Academy Press.
Streissguth A.P., Bookstein F., Barr H., Sampson P., O’Malley K., & Young J. 2004. “Risk Factors for Adverse Life Outcomes in Fetal Alcohol Syndrome and Fetal Alcohol Effects.” *Journal of Developmental and Behavioral Pediatrics* 25 (4): 228–38.
Streissguth A.P., & O’Malley K. 2000. “Neuropsychiatric Implications and Long-Term Consequences of Fetal Alcohol Spectrum Disorders.” *Seminars in Clinical Neuropsychiatry* 5 (3): 177–90.
Streissguth A P, Clarren S.K., & Jones K.L. 1985. “Natural History of the Fetal Alcohol Syndrome: A 10-Year Follow-up of Eleven Patients.” *Lancet* 2 (8446): 85–91.
Subbanna S., Nagre N.N., Shivakumar M., Umapathy N.S., Psychoyos D., & Basavarajappa B.S. 2014. “Ethanol Induced Acetylation of Histone at G9a exon1 and G9a-Mediated Histone H3 Dimethylation Leads to Neurodegeneration in Neonatal Mice.” *Neuroscience* 258: 422–32.
Subbanna S., Shivakumar M., Umapathy N.S., Saito M., Mohan P.S., Kumar A., Nixon R. a., Verin A.D., Psychoyos D., & Basavarajappa B.S. 2013. “G9a-Mediated Histone Methylation Regulates Ethanol-Induced Neurodegeneration in the Neonatal Mouse Brain.” *Neurobiology of Disease* 54: 475–85.
Swanson J.M., Entringer S., Buss C., & Wadhwa P.D. 2009. “Developmental Origins of Health and Disease: Environmental Exposures.” *Seminars in Reproductive Medicine* 27 (5): 391–

402.
Tahiliani M., Koh K.P., Shen Y., Pastor W.A., Bandukwala H., Brudno Y., Agarwal S., et al. 2009. “Conversion of 5-Methylcytosine to 5-Hydroxymethylcytosine in Mammalian DNA by MLL Partner TET1.” *Science* 324 (5929): 930–35.
Taiwo O., Wilson G., Morris T., Seisenberger S., Reik W., Pearce D., Beck S., & Butcher L. 2012. “Methylome Analysis Using MeDIP-Seq with Low DNA Concentrations.” *Nature Protocols* 7 (4): 617–36.
Tate P.H., & Bird A.P. 1993. “Effects of DNA Methylation on DNA-Binding Proteins and Gene Expression.” *Current Opinion in Genetics & Development* 3 (2): 226–31.
Teschendorff A.E., Marabita F., Lechner M., Bartlett T., Tegner J., Gomez-Cabrero D., & Beck S. 2012. “A Beta-Mixture Quantile Normalisation Method for Correcting Probe Design Bias in Illumina Infinium 450k DNA Methylation Data.” *Bioinformatics* 29 (2): 189–96.
Thisse B., & Thisse C. 2005. “Functions and Regulations of Fibroblast Growth Factor Signaling during Embryonic Development.” *Developmental Biology* 287 (2): 390–402.
Thomas J.D., Biane J.S., O’Bryan K.A., O’Neill T.M., & Dominguez H.D. 2007. “Choline Supplementation Following Third-Trimester-Equivalent Alcohol Exposure Attenuates Behavioral Alterations in Rats.” *Behavioral Neuroscience* 121 (1): 120–30.
Thorisson G. a., Smith A. V., Krishnan L., & Stein L.D. 2005. “The International HapMap Project Web Site.” *Genome Research* 15 (11): 1592–93.
Tognini P., Napoli D., & Pizzorusso T. 2015. “Dynamic DNA Methylation in the Brain: A New Epigenetic Mark for Experience-Dependent Plasticity.” *Frontiers in Cellular Neuroscience* 9 (August): 611–71.
Topper L.A., Baculis B.C., & Valenzuela C.F. 2015. “Exposure of Neonatal Rats to Alcohol Has Differential Effects on Neuroinflammation and Neuronal Survival in the Cerebellum and Hippocampus.” *Journal of Neuroinflammation* 12 (1): 160.
Tseng P.-H., Cameron I.G.M., Pari G., Reynolds J.N., Munoz D.P., & Itti L. 2013. “High-Throughput Classification of Clinical Populations from Natural Viewing Eye Movements.” *Journal of Neurology* 260 (1): 275–84.
Uban K.A., Sliwowska J.H., Lieblich S., Ellis L.A., Yu W.K., Weinberg J., & Galea L.A.M. 2010. “Prenatal Alcohol Exposure Reduces the Proportion of Newly Produced Neurons and Glia in the Dentate Gyrus of the Hippocampus in Female Rats.” *Hormones and Behavior* 58 (5): 835–43.
Ulahannan N., & Greally J.M. 2015. “Genome-Wide Assays That Identify and Quantify Modified Cytosines in Human Disease Studies.” *Epigenetics & Chromatin* 8 (January): 5.
Ungerer M., Knezovich J., & Ramsay M. 2013. “In Utero Alcohol Exposure, Epigenetic Changes, and Their Consequences.” *Alcohol Research: Current Reviews* 35 (1): 37–46.
Vallés S., Pitarch J., Renau-Piqueras J., & Guerri C. 1997. “Ethanol Exposure Affects Glial Fibrillary Acidic Protein Gene Expression and Transcription during Rat Brain Development.” *Journal of Neurochemistry* 69: 2484–93.
Vandesompele J., Preter K. De, Pattyn F., Poppe B., Roy N. Van, Paepe A. De, & Speleman F. 2002. “Accurate Normalization of Real-Time Quantitative RT-PCR Data by Geometric Averaging of Multiple Internal Control Genes.” *Genome Biology* 3 (7): RESEARCH0034.
van Otterdijk S.D., & Michels K.B. 2016. “Transgenerational Epigenetic Inheritance in Mammals: How Good Is the Evidence?” *Federation of American Societies for Experimental Biology Journal* 30: 1–9.

Veazey K.J., Carnahan M.N., Muller D., Miranda R.C., & Golding M.C. 2013. "Alcohol-Induced Epigenetic Alterations to Developmentally Crucial Genes Regulating Neural Stemness and Differentiation." *Alcoholism: Clinical and Experimental Research* 37 (7): 1111–22.
Veazey K.J., Parnell S.E., Miranda R.C., & Golding M.C. 2015. "Dose-Dependent Alcohol-Induced Alterations in Chromatin Structure Persist beyond the Window of Exposure and Correlate with Fetal Alcohol Syndrome Birth Defects." *Epigenetics & Chromatin* 8 (1): 39.
Waddington C.H. 1968. "Towards a Theoretical Biology." *Nature* 218 (5141): 525–27.
Wagner J.R., Busche S., Ge B., Kwan T., Pastinen T., & Blanchette M. 2014. "The Relationship between DNA Methylation, Genetic and Expression Inter-Individual Variation in Untransformed Human Fibroblasts." *Genome Biology* 15 (2): R37.
Walton E., Hass J., Liu J., Roffman J.L., Bernardoni F., Roessner V., Kirsch M., Schackert G., Calhoun V., & Ehrlich S. 2016. "Correspondence of DNA Methylation Between Blood and Brain Tissue and Its Application to Schizophrenia Research." *Schizophrenia Bulletin* 42 (2). US: 406–14.
Wang T., Pan Q., Lin L., Szulwach K.E., Song C.X., He C., Wu H., et al. 2012. "Genome-Wide DNA Hydroxymethylation Changes Are Associated with Neurodevelopmental Genes in the Developing Human Cerebellum." *Human Molecular Genetics* 21 (26): 5500–5510.
Waschek J.A. 2013. "VIP and PACAP: Neuropeptide Modulators of CNS Inflammation, Injury, and Repair." *British Journal of Pharmacology* 169 (3): 512–23.
Weber M., Hellmann I., Stadler M.B., Ramos L., Pääbo S., Rebhan M., & Schübeler D. 2007. "Distribution, Silencing Potential and Evolutionary Impact of Promoter DNA Methylation in the Human Genome." *Nature Genetics* 39 (4): 457–66.
Weinberg J. 1993. "Neuroendocrine Effects of Prenatal Alcohol Exposure." *Annals of the New York Academy of Sciences* 697: 86–96.
Weinberg J., & Jerrells T.R. 1991. "Suppression of Immune Responsiveness: Sex Differences in Prenatal Ethanol Effects." *Alcoholism: Clinical and Experimental Research* 15 (3): 525–31.
Weinberg J., Sliwowska J.H., Lan N., & Hellemans K.G.C. 2008. "Prenatal Alcohol Exposure: Foetal Programming, the Hypothalamic-Pituitary-Adrenal Axis and Sex Differences in Outcome." *Journal of Neuroendocrinology* 20 (4): 470–88.
Welberg L.A.M., & Seckl J.R. 2001. "Prenatal Stress, Glucocorticoids and the Programming of the Brain." *Journal of Neuroendocrinology* 13 (2): 113–28.
Werts R.L., Calcar S.C. Van, Wargowski D.S., & Smith S.M. 2014. "Inappropriate Feeding Behaviors and Dietary Intakes in Children with Fetal Alcohol Spectrum Disorder or Probable Prenatal Alcohol Exposure." *Alcoholism: Clinical and Experimental Research* 38 (3): 871–78.
Weyrauch D., Schwartz M., Hart B., Klug M.G., & Burd L. 2017. "Comorbid Mental Disorders in Fetal Alcohol Spectrum Disorders: A Systematic Review." *Journal of Developmental & Behavioral Pediatrics* 38 (4): 283–91.
Wheeler D.L., Church D.M., Edgar R., Federhen S., Helmberg W., Madden T.L., Pontius J.U., et al. 2004. "Database Resources of the National Center for Biotechnology Information: Update." *Nucleic Acids Research* 32 (Database issue): D35–40.
Whitacre C.C. 2001. "Sex Differences in Autoimmune Disease." *Nature Immunology* 2 (9): 777–80.
Wolff G.L., Kodell R.L., Moore S.R., & Cooney C.A. 1998. "Maternal Epigenetics and Methyl

Supplements Affect Agouti Gene Expression in Avy/a Mice." *Federation of American Societies for Experimental Biology Journal* 12 (11): 949–57.
Wong M., & Munro S. 2014. "The Specificity of Vesicle Traffic to the Golgi Is Encoded in the Golgin Coiled-Coil Proteins." *Science* 346 (6209): 1256898.
Wu H., & Zhang Y. 2014. "Reversing DNA Methylation: Mechanisms, Genomics, and Biological Functions." *Cell* 156 (1–2): 45–68.
Xu W., Cohen-Woods S., Chen Q., Noor A., Knight J., Hosang G., Parikh S. V, et al. 2014. "Genome-Wide Association Study of Bipolar Disorder in Canadian and UK Populations Corroborates Disease Loci Including SYNE1 and CSMD1." *BMC Medical Genetics* 15 (January): 2.
Yuen R.K.C., Neumann S.M.A., Fok A.K., Peñaherrera M.S., McFadden D.E., Robinson W.P., & Kobor M.S. 2011. "Extensive Epigenetic Reprogramming in Human Somatic Tissues between Fetus and Adult." *Epigenetics & Chromatin* 4 (January): 7.
Zeng H., Kaul S., & Simons S.S. 2000. "Genomic Organization of Human GMEB-1 and Rat GMEB-2: Structural Conservation of Two Multifunctional Proteins." *Nucleic Acids Research* 28 (8): 1819–29.
Zhang B., & Horvath S. 2005. "A General Framework for Weighted Gene Co-Expression Network Analysis." *Statistical Applications in Genetics and Molecular Biology* 4: Article17.
Zhang C.R., Ho M.-F., Vega M.C.S., Burne T.H.J., & Chong S. 2015. "Prenatal Ethanol Exposure Alters Adult Hippocampal VGLUT2 Expression with Concomitant Changes in Promoter DNA Methylation, H3K4 Trimethylation and miR-467b-5p Levels." *Epigenetics & Chromatin* 8 (1): 40.
Zhang D., Cheng L., Badner J.A., Chen C., Chen Q., Luo W., Craig D.W., Redman M., Gershon E.S., & Liu C. 2010. "Genetic Control of Individual Differences in Gene-Specific Methylation in Human Brain." *The American Journal of Human Genetics* 86 (3): 411–19.
Zhang F.F., Cardarelli R., Carroll J., Fulda K.G., Kaur M., Gonzalez K., Vishwanatha J.K., Santella R.M., & Morabia A. 2011. "Significant Differences in Global Genomic DNA Methylation by Gender and Race/ethnicity in Peripheral Blood." *Epigenetics* 6 (5): 623–29.
Zhang H., Herman A.I., Kranzler H.R., Anton R.F., Zhao H., Zheng W., & Gelernter J. 2013. "Array-Based Profiling of DNA Methylation Changes Associated with Alcohol Dependence." *Alcoholism: Clinical and Experimental Research* 37 Suppl 1 (January): E108-115.
Zhang R., Miao Q., Wang C., Zhao R., Li W., Haile C.N., Hao W., & Zhang X.Y. 2013. "Genome-Wide DNA Methylation Analysis in Alcohol Dependence." *Addiction Biology* 18 (2): 392–403.
Zhang X., Lan N., Bach P., Nordstokke D., Yu W., Ellis L., Meadows G.G., & Weinberg J. 2012. "Prenatal Alcohol Exposure Alters the Course and Severity of Adjuvant-Induced Arthritis in Female Rats." *Brain, Behavior, and Immunity* 26 (3): 439–50.
Zhang X., Sliwowska J.H., & Weinberg J. 2005. "Prenatal Alcohol Exposure and Fetal Programming: Effects on Neuroendocrine and Immune Function." *Experimental Biology and Medicine* 230 (6): 376–88.
Zhang Y., Liu T., Meyer C. a, Eeckhoute J., Johnson D.S., Bernstein B.E., Nusbaum C., et al. 2008. "Model-Based Analysis of ChIP-Seq (MACS)." *Genome Biology* 9 (9): R137.
Zhou F.C., Balaraman Y., Teng M., Liu Y., Singh R.P., & Nephew K.P. 2011. "Alcohol Alters

DNA Methylation Patterns and Inhibits Neural Stem Cell Differentiation." *Alcoholism: Clinical and Experimental Research* 35 (4): 735–46.
Zhou F.C., Chen Y., & Love A. 2011. "Cellular DNA Methylation Program during Neurulation and Its Alteration by Alcohol Exposure." *Birth Defects Research Part A - Clinical and Molecular Teratology* 91 (8): 703–15.
Zhou F.C., Zhao Q., Liu Y., Goodlett C.R., Liang T., McClintick J.N., Edenberg H.J., & Li L. 2011. "Alteration of Gene Expression by Alcohol Exposure at Early Neurulation." *BMC Genomics* 12: 124.
Zhou W., Cao Q., Peng Y., Zhang Q.J., Castrillon D.H., DePinho R.A., & Liu Z.P. 2009. "FoxO4 Inhibits NF-κB and Protects Mice Against Colonic Injury and Inflammation." *Gastroenterology* 137 (4): 1403–14.
Ziller M.J., Gu H., Müller F., Donaghey J., Tsai L.T.-Y., Kohlbacher O., Jager P.L. De, et al. 2013. "Charting a Dynamic DNA Methylation Landscape of the Human Genome." *Nature* 500 (7463): 477–81.
Ziller M.J., Müller F., Liao J., Zhang Y., Gu H., Bock C., Boyle P., et al. 2011. "Genomic Distribution and Inter-Sample Variation of Non-CpG Methylation across Human Cell Types." *PLoS Genetics* 7 (12): e1002389-15.
Zimmerberg B., Ballard G.A., & Riley E.P. 1987. "The Development of Thermoregulation after Prenatal Exposure to Alcohol in Rats." *Psychopharmacology* 91 (4): 479–84.
Zoubarev A., Hamer K.M., Keshav K.D., McCarthy E.L., Santos J.R.C., Rossum T. Van, McDonald C., et al. 2012. "Gemma: A Resource for the Reuse, Sharing and Meta-Analysis of Expression Profiling Data." *Bioinformatics* 28 (17): 2272–73.

Appendices

Appendix A Supplementary materials for chapter 2

A.1 Supplementary figures

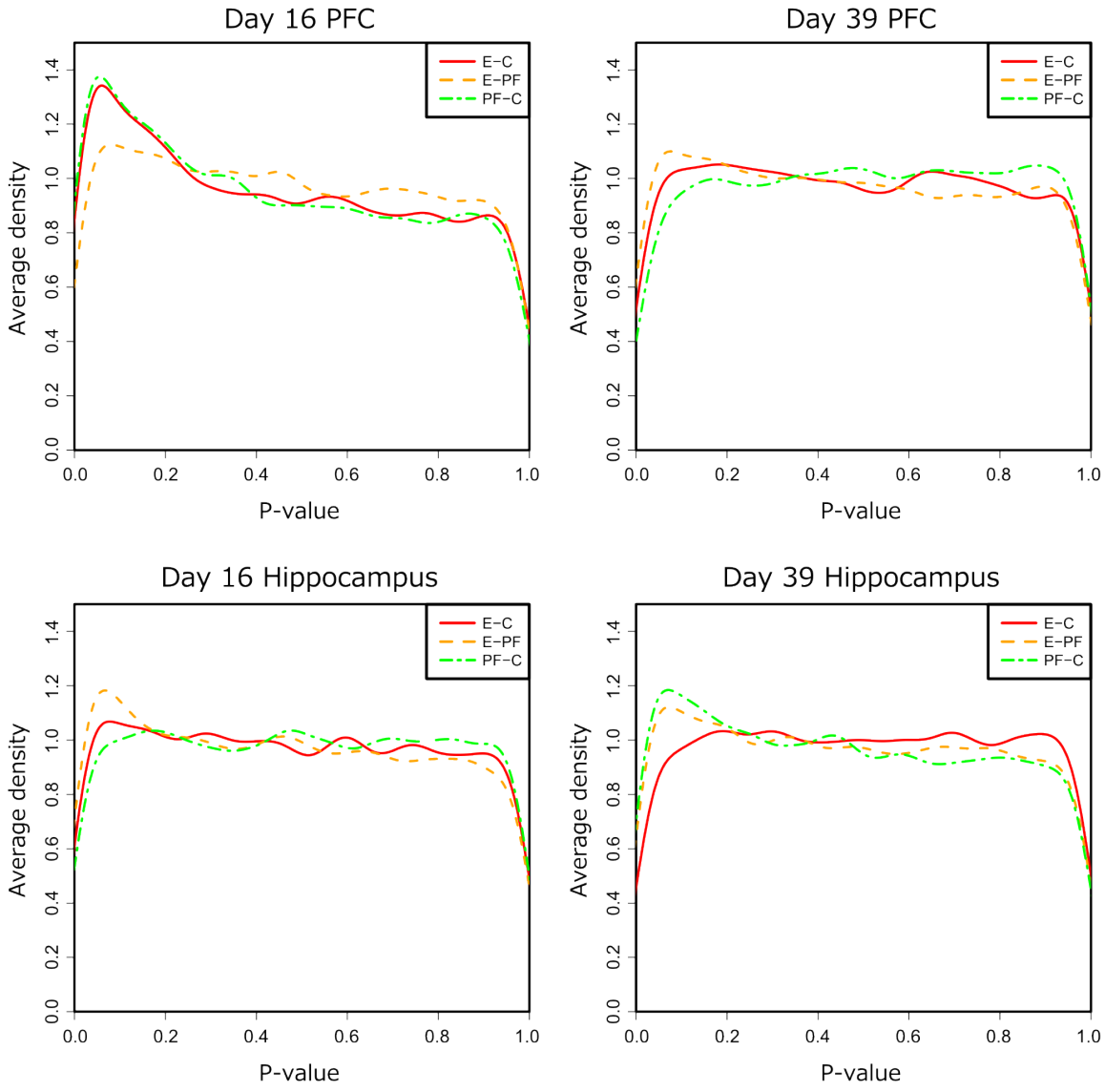

Supplementary figure 2.1: Plot of p-value distributions for gene expression differences among prenatal treatment groups, within the steady-state conditions, in **a)** PFC at Day 16 post-saline injection, **b)** PFC at Day 39 post-saline injection, **c)** HPC at Day 16 post-saline injection, and **d)** HPC at Day 39 post-saline injection. The greatest effects of prenatal ethanol exposure on gene

expression p-values were exhibited at D16 in PFC, followed by D16 HPC, as exhibited by enrichment of p-values towards zero for the ethanol contrasts (E-C, E-PF). No change in p-values was apparent in Day 39 PFC, and only a pair-fed effect was apparent in Day 39 HPC.

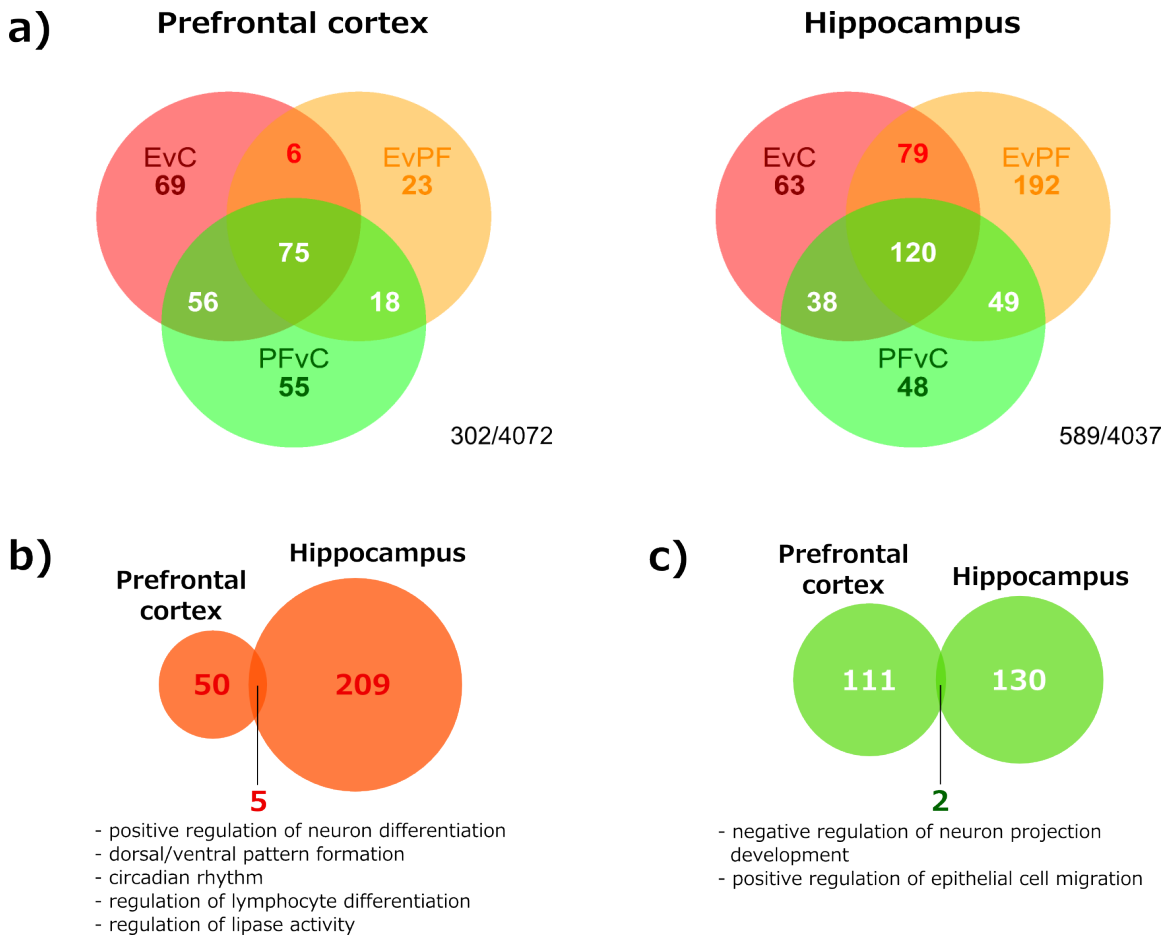

Supplementary figure 2.2: Venn diagrams demonstrating the number of Biological Processes significant for each contrast in Day 16 animals under steady-state conditions, and overlap of processes between different contrasts for PFC and HPC at FDR <1% **(a)**. FDR was increased to 10% to identify Biological Processes that showed overlapping changes in both tissues, specific to prenatal alcohol exposure **(b)** and pair-feeding **(c)**. FDR <10%.

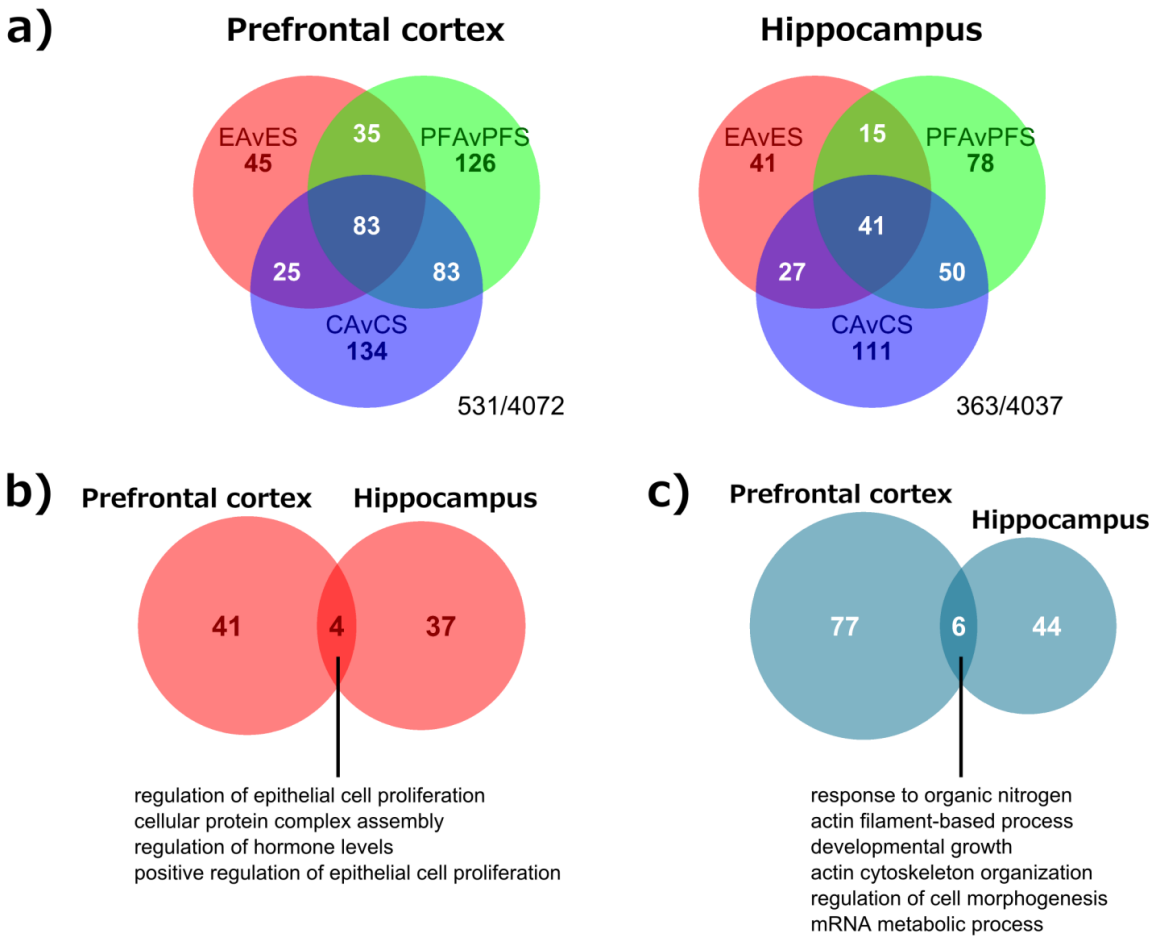

Supplementary figure 2.3: Venn diagrams demonstrating the number of Biological Processes significantly altered in the response to Adjuvant within each prenatal treatment group, and the overlap of processes enriched between groups **(a).** Many Biological Processes showed changes specific to prenatal alcohol exposure, and several overlapped between tissues **(b).** Other processes were common to the PF and C response to adjuvant, and several overlapped between tissues **(c)**. FDR <1%.

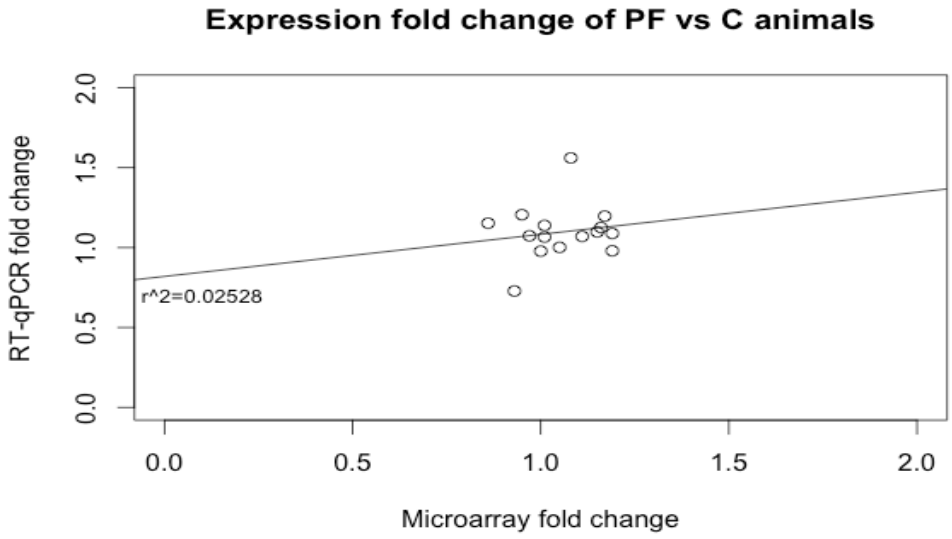

Supplementary figure 2.4: Fold changes in expression were not correlated between microarray and RT-qPCR results for PF vs C animals (r^2=0.02528, p=0.5714).

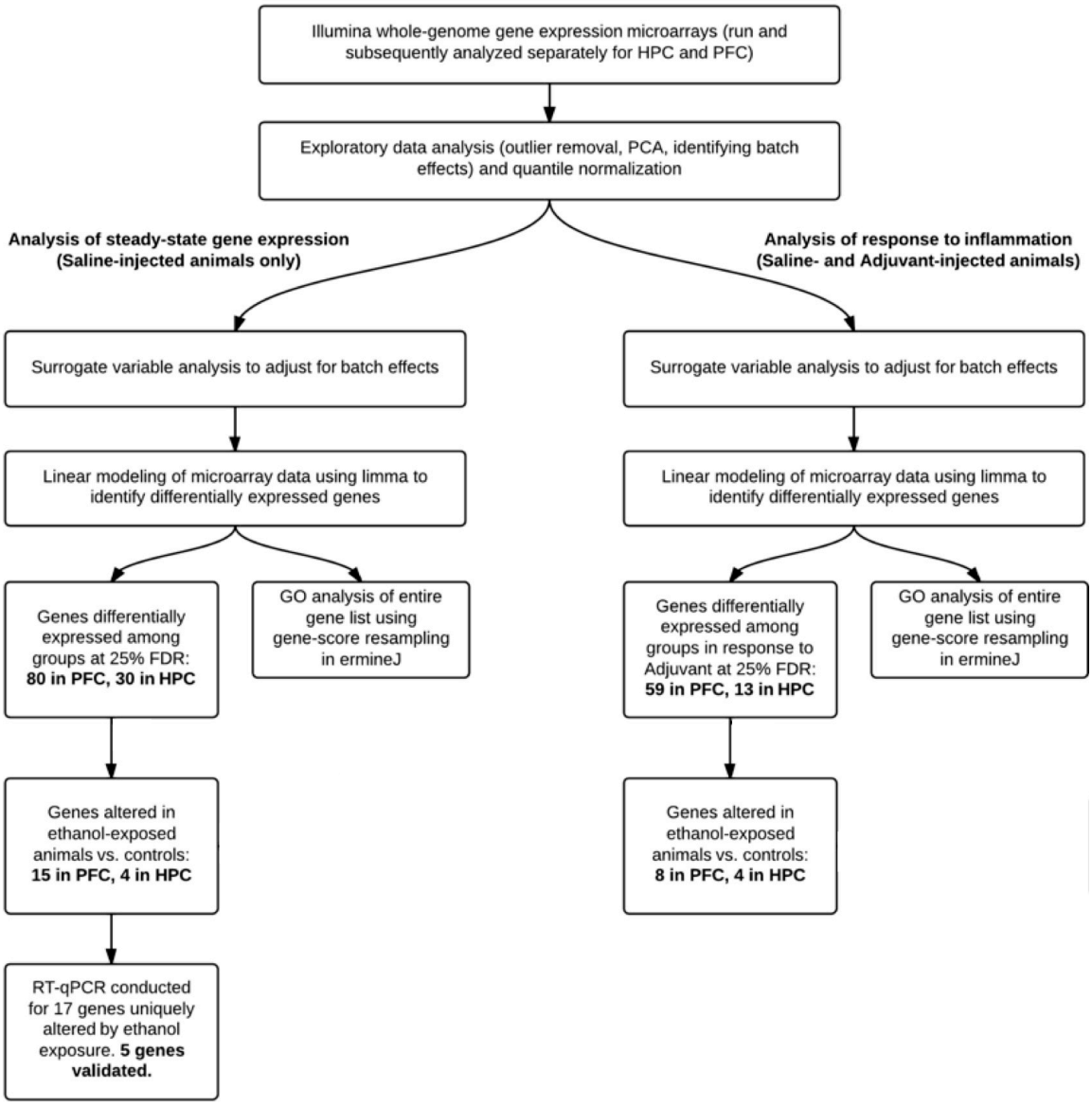

Supplementary figure 2.5: Overview of analyses and main findings for gene expression analysis.

A.2 Supplementary tables

Supplementary table 2.1 Candidate genes involved in the etiology of FASD, catalogued in NeuroCarta

Symbol	Gene name	Probe
Abca1	ATP-binding cassette, subfamily A (ABC1), member 1	ILMN_1650701
Abcg1	ATP-binding cassette, subfamily G (WHITE), member 1	ILMN_1354046
Actb	actin, beta	ILMN_1355039
Actb	actin, beta	ILMN_2038798
Actb	actin, beta	ILMN_2038799
Adcy8	adenylate cyclase 8 (brain)	ILMN_1350196
Akt1	v-akt murine thymoma viral oncogene homolog 1	ILMN_1353102
Alpl	alkaline phosphatase, liver/bone/kidney	ILMN_1372113
Apoe	apolipoprotein E	ILMN_1367529
Atoh1	atonal homolog 1 (Drosophila)	ILMN_1368168
Bad	BCL2-associated agonist of cell death	ILMN_1369751
Bcl2	B-cell CLL/lymphoma 2	ILMN_1366150
Bcl2l1	Bcl2-like 1	ILMN_1355163
Bcl2l1	Bcl2-like 1	ILMN_1365285
Bdnf	brain-derived neurotrophic factor	ILMN_1360447
Cacna1c	calcium channel, voltage-dependent, L type, alpha 1C subunit	ILMN_1370304
Casp3	caspase 3	ILMN_1349218
Cat	catalase	ILMN_1369530
Ccnd1	cyclin D1	ILMN_1350372
Ccnd2	cyclin D2	ILMN_1362471
Chat	choline O-acetyltransferase	ILMN_1363883
Creb1	cAMP responsive element binding protein 1	ILMN_1649829
Creb1	cAMP responsive element binding protein 1	ILMN_1376791
Cyba	cytochrome b-245, alpha polypeptide	ILMN_1366276
Dlg4	discs, large homolog 4 (Drosophila)	ILMN_1650748
Duox1	dual oxidase 1	ILMN_1367874
E2f1	E2F transcription factor 1	ILMN_1360877
Egfr	epidermal growth factor receptor	ILMN_1362571
Erbb2	v-erb-b2 erythroblastic leukemia viral oncogene homolog 2, neuro/glioblastoma derived oncogene homolog (avian)	ILMN_1350020
Fgfr2	fibroblast growth factor receptor 2	ILMN_1371701
Gad1	glutamate decarboxylase 1	ILMN_1351478
Gfap	glial fibrillary acidic protein	ILMN_1376423
Gpx1	glutathione peroxidase 1	ILMN_1372510
Gpx3	glutathione peroxidase 3	ILMN_1365802
Gria2	glutamate receptor, ionotropic, AMPA 2	ILMN_1356417
Gria3	glutamate receptor, ionotrophic, AMPA 3	ILMN_1368538
Gria4	glutamate receptor, ionotrophic, AMPA 4	ILMN_1371769
Grin1	glutamate receptor, ionotropic, N-methyl D-aspartate 1	ILMN_1365529
Grin2b	glutamate receptor, ionotropic, N-methyl D-aspartate 2B	ILMN_1366396
Grm5	glutamate receptor, metabotropic 5	ILMN_1361607
Gsk3b	glycogen synthase kinase 3 beta	ILMN_1349648
Gsr	glutathione reductase	ILMN_1352580
Gstm2	glutathione S-transferase mu 2	ILMN_1350896
Gstm3	glutathione S-transferase mu 3	ILMN_1374835
Hoxa1	homeo box A1	ILMN_1353666
Hoxb4	homeo box B4	ILMN_1363620

Symbol	Gene name	Probe
Hoxd4	homeo box D4	ILMN_1367426
Hoxd4	homeo box D4	ILMN_1353520
Igf1r	insulin-like growth factor 1 receptor	ILMN_1374575
Igf2	insulin-like growth factor 2	ILMN_1359301
Igf2r	insulin-like growth factor 2 receptor	ILMN_1349413
Insr	insulin receptor	ILMN_1360127
Irs1	insulin receptor substrate 1	ILMN_1360680
L1cam	L1 cell adhesion molecule	ILMN_1376861
Mapk1	mitogen activated protein kinase 1	ILMN_1349290
Mapt	microtubule-associated protein tau	ILMN_1354816
Ncf2	neutrophil cytosolic factor 2	ILMN_1365484
Ndufv1	NADH dehydrogenase (ubiquinone) flavoprotein 1	ILMN_1365082
Neurod1	neurogenic differentiation 1	ILMN_1363838
Ngfr	nerve growth factor receptor (TNFR superfamily, member 16)	ILMN_1365512
Notch1	notch 1	ILMN_1359640
Nox3	NADPH oxidase 3	ILMN_1376975
Noxa1	NADPH oxidase activator 1	ILMN_1365297
Noxo1	NADPH oxidase organizer 1	ILMN_1368197
Ntf3	neurotrophin 3	ILMN_1371735
Ntf4	neurotrophin 4	ILMN_1363013
Ntrk1	neurotrophic tyrosine kinase, receptor, type 1	ILMN_1370831
Ntrk2	neurotrophic tyrosine kinase, receptor, type 2	ILMN_1366426
Ntrk3	neurotrophic tyrosine kinase, receptor, type 3	ILMN_1362434
Plat	plasminogen activator, tissue	ILMN_1358127
Rac1	ras-related C3 botulinum toxin substrate 1	ILMN_1355225
Rara	retinoic acid receptor, alpha	ILMN_1368986
Rbp1	retinol binding protein 1, cellular	ILMN_1375320
S100b	S100 calcium binding protein B	ILMN_1373043
Sdha	succinate dehydrogenase complex, subunit A, flavoprotein (Fp)	ILMN_1357678
Serpine1	serpin peptidase inhibitor, clade E (nexin, plasminogen activator inhibitor type 1), member 1	ILMN_1376417
Serpine1	serpin peptidase inhibitor, clade E (nexin, plasminogen activator inhibitor type 1), member 1	ILMN_2040557
Sod1	superoxide dismutase 1, soluble	ILMN_1353544
Sod2	superoxide dismutase 2, mitochondrial	ILMN_1367263
Sod3	superoxide dismutase 3, extracellular	ILMN_1361581

Supplementary table 2.2A Correlation of expression profiles among all samples and among replicates in PFC microarray dataset

	Quantiles for Pearson correlations among samples					
	0%	**25%**	**50%**	**75%**	**100%**	**n**
All PFC samples	0.897	0.966	0.971	0.976	1.000	96
Hybridization replicate group 1	0.957	0.971	0.979	0.982	1.000	9
Amplification replicate	0.980	0.980	0.990	1.000	1.000	2

Supplementary table 2.2B Correlation of expression profiles among all samples and among replicates in HPC microarray dataset

	Quantiles for Pearson correlations among samples					
	0%	**25%**	**50%**	**75%**	**100%**	**n**
All HPC samples	0.925	0.958	0.965	0.971	1.000	96
Hybridization replicate group 1	0.964	0.970	0.974	0.984	1.000	4
Hybridization replicate group 2	0.971	0.972	0.986	0.990	1.000	4
Hybridization replicate group 3	0.957	0.963	0.980	0.989	1.000	4
Hybridization replicate group 4	0.961	0.968	0.971	0.982	1.000	4
Mean of replicates	0.963	0.968	0.978	0.986	1.000	

Supplementary table 2.3 Sequences of primers used for RT-qPCR.

Gene	Type	Accession	Forward primer (5'-3')	Reverse primer (5'-3')
Actb	Ref	NM_031144.2	CTGCCCTGGCTCCTAGCACCAT	CTCAGTAACAGTCCGCCTAGAAGCA
Hprt1	Ref	NM_012583.2	TGTGGCCAGTAAAGAACTAGCAGACGTT	GTGCAAATCAAAAGGGACGCAGCAACA
Pgk1	Ref	NM_053291.3	AGTCCTTCCTGGGGTGGATGCTCT	AGGGTTCCTGGTGCTGCGTCTT
Sdha	Ref	NM_130428.1	TGCCAGGGAAGATTACAAGGTGCGG	AGAGGGTGTGCTTCCTCCAGTGTTC
Ubc	Ref	NM_017314.1	CACCAAGAAGGTCAAACAGGA	GCAAGAACTTTATTCAAAGTGCAA
Acsl3	Target	NM_057107.1	ACTCCCGAAACTGGTCTGGTGACTGATG	ATCCGCTCAATGTCTGCCTGGTAGTGT
Ap1s2	Target	NM_001127531.2	TGTCACTGCCTAGTCGTCGGA	GCCAACCAATGCCACTTTGCTTCAG
Atp6ap1	Target	NM_031785.1	GGGTTAAGAATGAGCGGTACACTGGGG	ACTTCTGGCTTCTTGACAGGCAATCCTT
Dusp6	Target	NM_053883.2	GTGGGATGCGACAGGTTGTGAGGA	ACACCACGAACATCATGGAGCAAGTGAA
H2afv	Target	NM_001106019.1	CTGATCGGAAAGAAGGGGCAGCAGA	CACACACAGTGAGGACAGCAGGTCA
Med28	Target	NM_001107217.1	TGCAGCACAAGAAGCCAGCCGA	GGTCTGCTTCAGAGGTGCAGGTATGTT
Ndfip1	Target	NM_001013059.1	ACTGGCTCTGGTGGGTGTTCTTGGT	AGAACTCTGGTCCTGGGGAGATTTGAGA
Pex11g	Target	NM_001105902.1	AACGAGACTCAGATTCCCAGAGCGG	ATTTGAGCCCCTTTCCCACCCCA
Ppp1r14a	Target	NM_130403.1	GACGAGCTGCTGGAATTGGACAGTGA	GGACGAAGTCCTCTGTGGGATTCAGG
Rnasek	Target	NM_001137561.2	TTGGGACTGTTACCCTGGCGAGAC	TCCAGGGGTTGGGCAGCAGTTT
Tcf4	Target	NM_053369.1	AGAGAAGGTGTCCTCAGAGCCTCCC	GGTGGCAACTTGGACCCTTTCACATC
Cnih2	Target	NM_001025132.1	GGGCCAGGCAAAGCTCTAAACAGGG	GGCCCAAATTCCCCTGAAACGGACA
Loc688637	Target	XM_001067706.2	AGAGGCCATGCGGAGCTTTTTGAGT	AAATCACGCTTTCTGTCCAGCATCACCC
MCG125002	Target	NM_001034154.1	TCTAGCCCAAAGGAACCCAAAGCGG	GGCTGAACGTCTTCTGGTGGAGGA
Rgs3	Target	NM_019340.1	TGGCACATGAACGGTAATAGGAGAGCC	TGGGACCAGCAAATGCCCTGAAACT

Supplementary table 2.4A: Microarray expression results for common reference genes in PFC of Day 16 Saline animals.

Gene Symbol	Probe_ID (ILMN_)	Fold change			Average log2(exp)	F	p-value	q-value
		E:C	PF:C	E:PF				
Polr2a_mappe								
d	1372495	0.0043	-0.0666	0.0709	7.71	0.24	0.79	0.94
Tbp	1349379	0.0576	-0.0107	0.0683	8.04	0.29	0.75	0.93
Ubc	1350494	0.0879	-0.0244	0.1123	13.83	0.33	0.72	0.93
Pgk1	***1369074***	***0.0624***	***0.1493***	***-0.0869***	***12.30***	***0.52***	***0.60***	***0.89***
Sdha	1357678	0.1627	-0.0170	0.1797	10.53	0.83	0.45	0.84
Hmbs	1353365	0.0689	-0.0863	0.1552	8.13	0.96	0.40	0.82
Actb	***1355039***	***-0.1662***	***-0.1925***	***0.0263***	***12.13***	***1.12***	***0.35***	***0.79***
Hprt1	***1367708***	***0.1953***	***0.1306***	***0.0647***	***11.73***	***1.17***	***0.33***	***0.79***
Gusb	1350544	0.0857	0.1865	-0.1008	7.78	1.24	0.31	0.78
H2A.1	1372198	-0.1490	-0.0356	-0.1134	7.41	1.33	0.29	0.77
Gapdh	1649859	0.2458	-0.0535	0.2992	13.33	1.61	0.23	0.73
Tfrc	1360908	0.2191	0.1764	0.0427	7.13	2.02	0.16	0.70
Actb	***2038799***	***-0.2469***	***-0.1103***	***-0.1366***	***13.74***	***2.12***	***0.15***	***0.68***
Actb	***2038798***	***-0.3199***	***-0.4015***	***0.0816***	***11.87***	***2.89***	***0.083***	***0.63***
B2m	1368656	0.2073	-0.2072	0.4144	12.99	3.62	0.049	0.57
Ywhaz	1373913	-0.3891	0.1622	-0.5513	13.53	4.93	0.020	0.49

* Genes in bold were used as reference genes for RT-qPCR.

Supplementary table 2.4B: Microarray expression results for common reference genes in HPC of Day 16 Saline animals.

Gene Symbol	Probe ID (ILMN_)	Fold change			Average log2(exp)	F	p-value	q-value
		E:C	E:PF	PF:C				
Sdha	1357678	0.0006	0.0201	-0.0195	10.24	0.01	0.99	1.00
Gusb	1350544	-0.0643	-0.0581	-0.0062	7.83	0.18	0.84	0.98
Pgk1	***1369074***	***-0.1403***	***-0.0156***	***-0.1248***	***12.36***	***0.46***	***0.64***	***0.96***
Gapdh	1649859	0.1529	-0.0998	0.2527	12.95	0.64	0.54	0.95
Tfrc	1360908	0.0033	-0.1165	0.1198	7.01	0.65	0.54	0.95
Actb	***1355039***	***0.2317***	***-0.1115***	***0.3431***	***12.27***	***0.90***	***0.42***	***0.93***
Actb	***2038798***	***0.2406***	***-0.2054***	***0.4460***	***11.87***	***1.19***	***0.33***	***0.91***
Ubc	***1350494***	***0.3358***	***0.2165***	***0.1194***	***13.49***	***1.29***	***0.30***	***0.91***
Polr2a_mappe								
d	1372495	0.0352	-0.1551	0.1903	7.83	1.57	0.23	0.89
Hmbs	1353365	-0.1870	0.0817	-0.2686	8.22	1.68	0.21	0.88
Actb	***2038799***	***0.2694***	***-0.1511***	***0.4205***	***13.81***	***2.12***	***0.15***	***0.85***
Tbp	1349379	-0.1822	0.1249	-0.3070	8.32	2.49	0.11	0.83
H2A.1	1372198	0.0125	0.2517	-0.2391	7.83	3.00	0.07	0.78
Ywhaz	1373913	-0.3770	-0.2804	-0.0966	13.58	3.23	0.06	0.76
Hprt1	1367708	-0.3556	0.0844	-0.4400	11.66	3.49	0.05	0.75
B2m	1368656	-0.0322	0.2943	-0.3265	12.96	4.31	0.03	0.72

* Genes in bold were used as reference genes for RT-qPCR.

Supplementary table 2.5A: Genes showing common change in expression in PFC of E and PF compared to C animals under steady state conditions.

Gene Symbol	Gene Name	Average expression	F	p-value	q-value	Fold change		
						E:C	E:PF	PF:C
Rpusd1	RNA pseudouridylate synthase domain containing 1	9.4	11.9	5.7E-04	0.23	**0.68**	0.93	**0.73**
Nme2	NME/NM23 nucleoside diphosphate kinase 2	11.5	10.7	9.7E-04	0.25	**0.70**	0.89	**0.79**
Klhl24	kelch-like 24 (Drosophila)	9.6	10.7	9.4E-04	0.25	**0.69**	0.91	**0.75**
Ndrg2	N-myc downstream regulated gene 2	13.5	11.2	7.6E-04	0.23	**0.71**	0.95	**0.75**
ILMN_1370609	na	7.1	12.3	4.8E-04	0.23	**0.60**	1.10	**0.55**
Rasl10a	RAS-like, family 10, member A	8.5	13.3	3.2E-04	0.23	**0.74**	1.14	**0.64**
ILMN_1359879	na	9.2	10.9	8.6E-04	0.24	**0.76**	1.17	**0.65**
Grik5	glutamate receptor, ionotropic, kainate 5	9.4	12.6	4.3E-04	0.23	**1.33**	0.84	**1.58**
RGD1309651	similar to 1190005I06Rik protein	7.7	14.0	2.4E-04	0.22	**1.31**	0.88	**1.49**
ILMN_1368369	na	7.6	11.1	7.8E-04	0.23	**1.38**	0.92	**1.50**
Satb1	SATB homeobox 1	10.2	12.2	5.0E-04	0.23	**1.42**	0.91	**1.55**
Tmem178b	transmembrane protein 178B	9.5	15.5	1.4E-04	0.16	**1.37**	0.87	**1.56**
ILMN_1356747	na	14.1	10.7	9.7E-04	0.25	**1.41**	0.97	**1.45**
ILMN_1351805	na	12.1	12.0	5.4E-04	0.23	**1.45**	0.95	**1.53**
Mapkapk2	mitogen-activated protein kinase-activated protein kinase 2	8.4	11.9	5.7E-04	0.23	**1.33**	0.97	**1.38**
Igfbp7	insulin-like growth factor binding protein 7	11.9	11.2	7.6E-04	0.23	**1.43**	0.99	**1.45**
Nrxn3	neurexin 3	10.7	16.5	9.8E-05	0.13	**1.46**	0.86	**1.69**
Ywhaq	tyrosine 3-monooxygenase/tryptophan 5-monooxygenase activation protein, theta polypeptide	11.8	11.4	7.0E-04	0.23	**1.38**	1.01	**1.37**
ILMN_1352779	na	7.1	11.7	6.0E-04	0.23	**1.35**	1.00	**1.36**
Gpkow	G patch domain and KOW motifs	7.1	10.9	8.8E-04	0.24	**1.37**	1.04	**1.32**
LOC685828	hypothetical protein LOC685828	7.6	12.6	4.3E-04	0.23	**1.47**	0.99	**1.49**
Gabrr2	gamma-aminobutyric acid (GABA) A receptor, rho 2	7.1	12.5	4.3E-04	0.23	**1.37**	1.01	**1.36**
Chn1	chimerin (chimaerin) 1	13.3	11.6	6.5E-04	0.23	**1.51**	1.08	**1.40**
RGD1565784	RGD1565784	9.4	11.8	5.9E-04	0.23	**1.37**	1.05	**1.30**
ILMN_1366825	na	9.9	13.1	3.4E-04	0.23	**1.42**	1.01	**1.41**
Rpl27-l1	ribosomal protein L27-like 1	9.9	11.5	6.8E-04	0.23	**1.40**	1.16	**1.21**
ILMN_1366004	na	8.2	11.8	5.8E-04	0.23	**1.42**	1.11	**1.28**
ILMN_1359502	na	8.5	13.0	3.7E-04	0.23	**1.53**	1.06	**1.44**
ILMN_1366169	na	9.3	16.6	9.3E-05	0.13	**1.55**	0.98	**1.58**
ILMN_1367588	na	9.4	13.2	3.3E-04	0.23	**1.61**	1.18	**1.37**
ILMN_1359650	na	8.2	14.1	2.3E-04	0.22	**1.48**	1.10	**1.34**
RGD1309730	similar to RIKEN cDNA B230118H07	9.2	16.7	9.2E-05	0.13	**1.57**	1.02	**1.53**
Sep15	selenoprotein 15	11.3	18.0	5.9E-05	0.12	**1.55**	1.00	**1.55**

Gene Symbol	Gene Name	Average expression	F	p-value	q-value	Fold change		
						E:C	E:PF	PF:C
Hint3	histidine triad nucleotide binding protein 3	9.0	16.2	1.1E-04	0.14	**1.52**	1.07	**1.43**
ILMN_1352441	na	13.1	15.0	1.7E-04	0.18	**1.74**	1.19	**1.46**
ILMN_1366381	na	10.5	16.5	9.9E-05	0.13	**1.55**	1.07	**1.45**
Psma7	proteasome (prosome, macropain) subunit, alpha type 7	11.8	25.5	6.9E-06	0.06	**1.68**	0.86	**1.97**
ILMN_1368258	na	10.5	19.8	3.4E-05	0.10	**1.76**	1.05	**1.68**
LOC301193	similar to Discs large homolog 5 (Placenta and prostate DLG) (Discs large protein P-dlg)	10.5	21.4	2.1E-05	0.07	**1.74**	1.04	**1.67**

* Bold = p<0.05. na = probe had no specific alignment to current RefSeq RNA database

Supplementary table 2.5B: Genes showing common change in expression in HPC of E and PF compared to C animals under steady-state conditions.

Gene Symbol	Gene Name	Average Expression	F	p-value	q-value	Fold change		
						E:C	E:PF	PF:C
LOC100360417	RUN and SH3 domain containing 1-like	10.4	12.8	2.9E-04	0.21	**1.65**	1.10	**1.50**
Atp5a1	ATP synthase, H+ transporting, mitochondrial F1 complex, alpha subunit 1, cardiac muscle	13.1	13.5	2.2E-04	0.20	**1.35**	0.91	**1.48**
Acsl1	acyl-CoA synthetase long-chain family member 1	9.5	13.0	2.7E-04	0.21	**1.34**	0.91	**1.47**
Sqle	squalene epoxidase	10.0	14.1	1.7E-04	0.17	**1.44**	1.01	**1.42**

* Bold = p<0.05. na = probe had no specific alignment to current RefSeq RNA database

Supplementary table 2.6A: Genes differentially expressed in PFC among all 3 prenatal treatment groups under steady-state conditions.

Gene Symbol	Gene Name	Average expression	F	p-value	q-value	Fold change		
						E:C	E:PF	PF:C
Baiap2	BAI1-associated protein 2	10.8	10.6	9.8E-04	0.25	0.69	0.83	0.83
Lxn	latexin	8.3	15.8	1.2E-04	0.15	0.77	1.42	0.54
Tuba1a	tubulin, alpha 1A	14.1	25.2	7.5E-06	0.06	0.77	1.38	0.56
Tom1	target of myb1 homolog (chicken)	8.2	10.7	9.3E-04	0.25	0.83	1.17	0.71
Sumf1	sulfatase modifying factor 1	8.3	12.8	3.8E-04	0.23	1.17	1.45	0.81
Acat1	acetyl-CoA acetyltransferase 1	8.3	12.5	4.3E-04	0.23	1.20	0.80	1.49
Dynlrb1	dynein light chain roadblock-type 1	12.2	11.4	6.8E-04	0.23	1.21	0.79	1.54
Rnd2	Rho family GTPase 2	11.0	11.0	8.1E-04	0.23	1.22	0.85	1.43
Epn1	Epsin 1	8.7	22.7	1.4E-05	0.06	1.24	0.75	1.66
LOC100361558	histone H3.3B-like	11.4	11.8	5.9E-04	0.23	1.24	0.79	1.56
Acly	ATP citrate lyase	10.0	11.4	7.1E-04	0.23	1.25	0.78	1.60
Peo1	progressive external ophthalmoplegia 1	8.7	13.9	2.6E-04	0.22	1.26	0.80	1.58
Hbb-b1	hemoglobin, beta adult major chain	10.8	24.7	8.6E-06	0.06	1.28	1.73	0.74
Anxa4	annexin A4	9.8	13.7	2.7E-04	0.22	1.29	0.84	1.54
Ckb	creatine kinase, brain	12.8	16.5	9.8E-05	0.13	1.34	0.72	1.86
Scd	stearoyl-Coenzyme A desaturase 1	13.2	12.6	4.1E-04	0.23	1.36	0.78	1.75
LOC501223	similar to Discs large homolog 5 (Placenta and prostate DLG) (Discs large protein P-dlg)	11.2	13.9	2.5E-04	0.22	1.55	1.21	1.27
Rps27l3	ribosomal protein S27-like 3	7.4	18.5	5.0E-05	0.11	1.65	1.21	1.37
LOC363320	similar to Discs large homolog 5 (Placenta and prostate DLG) (Discs large protein P-dlg)	9.4	22.6	1.5E-05	0.06	1.90	1.26	1.50

*white fill (E<PF<C; C<PF<E), light grey fill (PF<E<C; C<E<PF), dark grey fill (E<C<PF; PF<C<E).

Supplementary table 2.6B: Genes differentially expressed in HPC among all 3 prenatal treatment groups under steady-state conditions.

Gene Symbol	Gene Name	Average expression	F	p-value	q-value	Fold change		
						E:C	E:PF	PF:C
Phlpp1	PH domain and leucine rich repeat protein phosphatase 1	10.2	12.7	3.1E-04	0.21	0.78	0.63	1.24
RGD1565117	similar to 40S ribosomal protein S26	9.6	22.4	9.5E-06	0.04	1.24	1.61	0.77
Trpv4	transient receptor potential cation channel, subfamily V, member 4	7.4	27.0	2.6E-06	0.02	1.26	1.84	0.69
Agap1	ArfGAP with GTPase domain, ankyrin repeat and PH domain 1	10.1	12.7	3.0E-04	0.21	1.30	0.81	1.59
Mgp	matrix Gla protein	9.0	12.9	2.8E-04	0.21	1.42	1.97	0.72
Col8a1	collagen, type VIII, alpha 1	7.9	17.2	5.2E-05	0.12	1.46	2.47	0.59
Igf2	insulin-like growth factor 2	11.8	13.4	2.3E-04	0.20	1.63	2.80	0.58

* light grey fill (PF<E<C; C<E<PF), dark grey fill (E<C<PF; PF<C<E).

Supplementary table 2.7A: Genes differentially expressed in PFC of Pair-fed vs both E and C animals under steady-state conditions.

Gene Symbol	Gene name	Average Expression	F	p-value	q-value	Fold change		
						PF:C	E:PF	E:C
ILMN_1358743	na	8.0	11.5	6.8E-04	0.23	**0.81**	**1.44**	1.17
Lrp1	low density lipoprotein receptor-related protein 1	8.8	12.4	4.6E-04	0.23	**1.38**	**0.69**	0.95
ILMN_1361625	na	9.8	11.4	6.9E-04	0.23	**1.58**	**0.72**	1.13
Ak2	adenylate kinase 2	9.9	13.4	3.1E-04	0.23	**1.69**	**0.67**	1.13
ILMN_1359487	na	10.6	11.0	8.3E-04	0.24	**1.53**	**0.76**	1.16
Ppp1r1b	protein phosphatase 1, regulatory (inhibitor) subunit 1B	10.8	11.7	6.2E-04	0.23	**1.47**	**0.72**	1.06
Park7	parkinson protein 7	12.2	12.5	4.4E-04	0.23	**0.70**	**1.38**	0.97

* Bold = p <0.05. na = probe had no specific alignment to current RefSeq RNA database.

Supplementary table 2.7B: Genes differentially expressed in HPC of Pair-fed vs both E and C animals under steady-state conditions.

Gene Symbol	Gene Name	Average Expression	F	p-value	q-value	Fold change		
						PF:C	E:PF	E:C
ILMN_1351851	na	8.9	12.4	3.5E-04	0.24	**0.77**	**1.49**	1.15
Sostdc1	sclerostin domain containing 1	8.7	26.4	3.1E-06	0.02	**0.28**	**4.40**	1.23
Nt5dc2	5'-nucleotidase domain containing 2	7.8	14.6	1.4E-04	0.15	**0.68**	**1.70**	1.16
Retsat	retinol saturase (all trans retinol 13,14 reductase)	8.4	15.8	8.7E-05	0.14	**1.68**	**0.49**	0.82
ILMN_1356875	na	10.0	22.2	1.0E-05	0.04	**0.46**	**2.68**	1.22
Aqp1	aquaporin 1	7.6	15.9	8.6E-05	0.14	**0.63**	**1.75**	1.10
Igfbp2	insulin-like growth factor binding protein 2	10.0	14.7	1.4E-04	0.15	**0.47**	**3.45**	1.62
Lxn	latexin	8.3	15.4	1.0E-04	0.14	**0.57**	**1.69**	0.96
Ttr	transthyretin	11.7	19.3	2.5E-05	0.08	**0.20**	**9.87**	1.96
Slco1a5	solute carrier organic anion transporter family, member 1a5	8.2	15.4	1.0E-04	0.14	**0.43**	**2.57**	1.11
Glb1l	galactosidase, beta 1-like	7.4	18.6	3.2E-05	0.09	**0.68**	**1.47**	1.00
Epn3	epsin 3	7.5	12.8	2.9E-04	0.21	**0.76**	**1.46**	1.11
F5	coagulation factor V (proaccelerin, labile factor)	8.6	17.8	4.3E-05	0.11	**0.33**	**4.27**	1.39
Cox8b	cytochrome c oxidase, subunit VIIIb	7.4	13.5	2.1E-04	0.20	**0.71**	**1.48**	1.06
Enpp2	ectonucleotide pyrophosphatase/phospho diesterase 2	12.7	27.2	2.5E-06	0.02	**0.47**	**2.45**	1.16

* Bold = p <0.05. na = probe had no specific alignment to current RefSeq RNA database.

Appendix B Supplementary materials for chapter 3

B.1 Supplementary figures

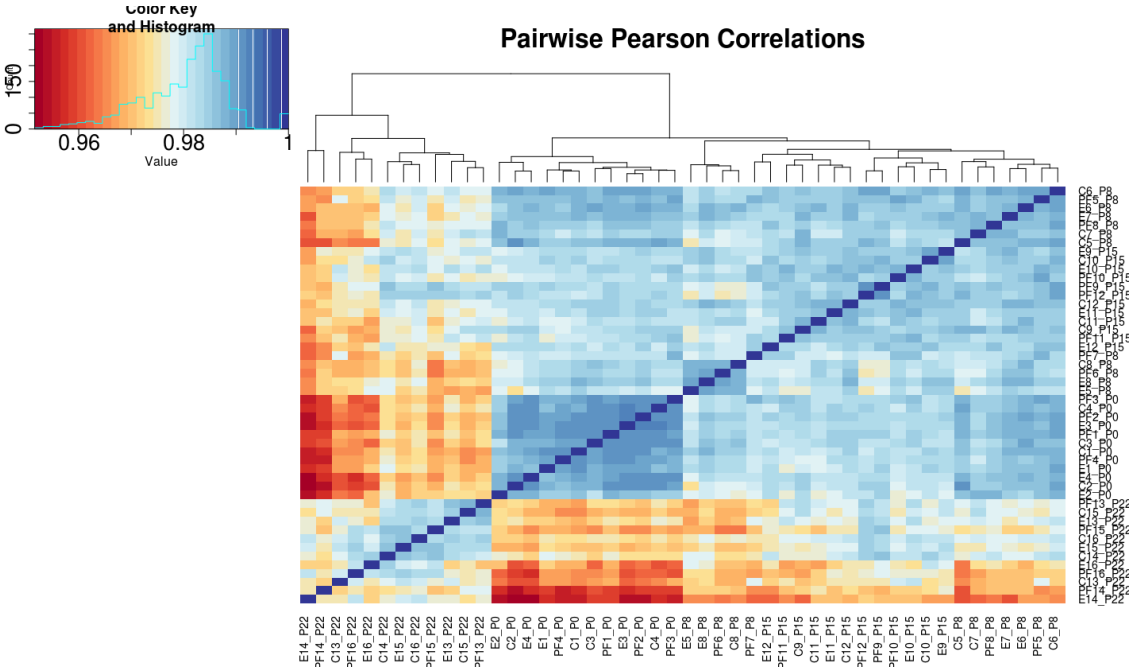

Supplementary figure 3.1. Pairwise Pearson correlations of meDIP-seq data for the developmental hypothalamus samples. Samples were generally highly correlated (r<0.95), with samples clustering most closely with animals of the same age.

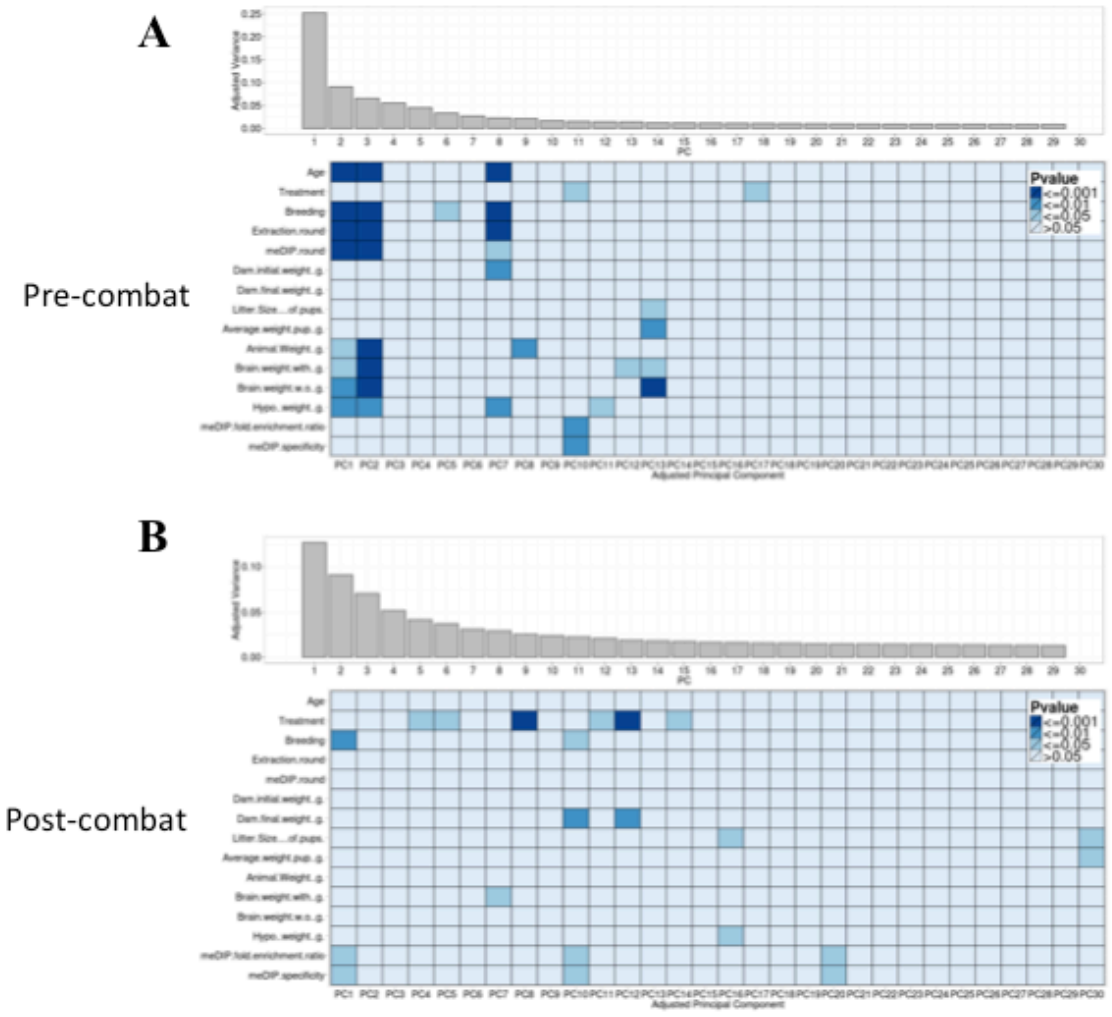

Supplementary figure 3.2. Principal component analysis of meDIP-seq data for the hypothalamus samples before and after ComBat correction. A) Principal component analysis of the normalized RPKM data revealed significant levels of variation associated with batch effects. MeDIP and DNA extraction rounds were significantly associated with a large proportion of variation within the dataset, and were also confounded with age. **B)** ComBat correction was performed on the RPKM data from the hypothalamic samples to correct the effects of MeDIP round and DNA extraction round. Partial effects of breeding remained in the dataset and prenatal

treatment was associated with a larger proportion of variance within the dataset after ComBat correction.

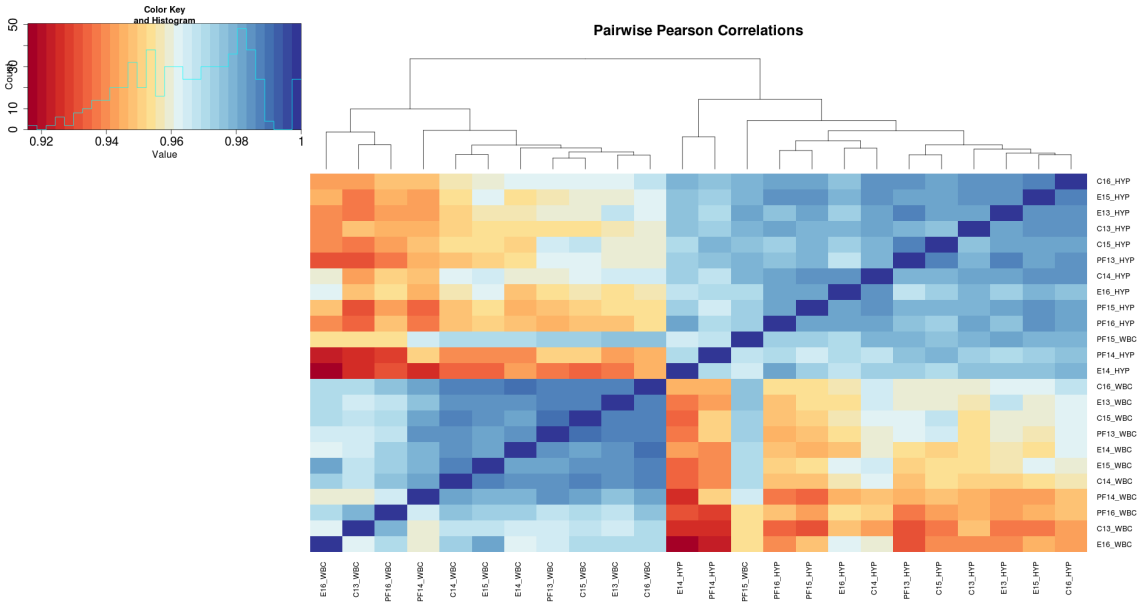

Supplementary figure 3.3. Pairwise Pearson correlations of meDIP-seq data for the hypothalamus and white blood cell samples on postnatal day 22. Samples in the BvB peakset were highly correlated within tissue (r>0.96), the main driver of DNA methylation patterns, and well correlated within the same animals (r>0.92). However, one PF WBC sample clustered with the hypothalamus samples, suggesting that it may have been mislabeled during processing.

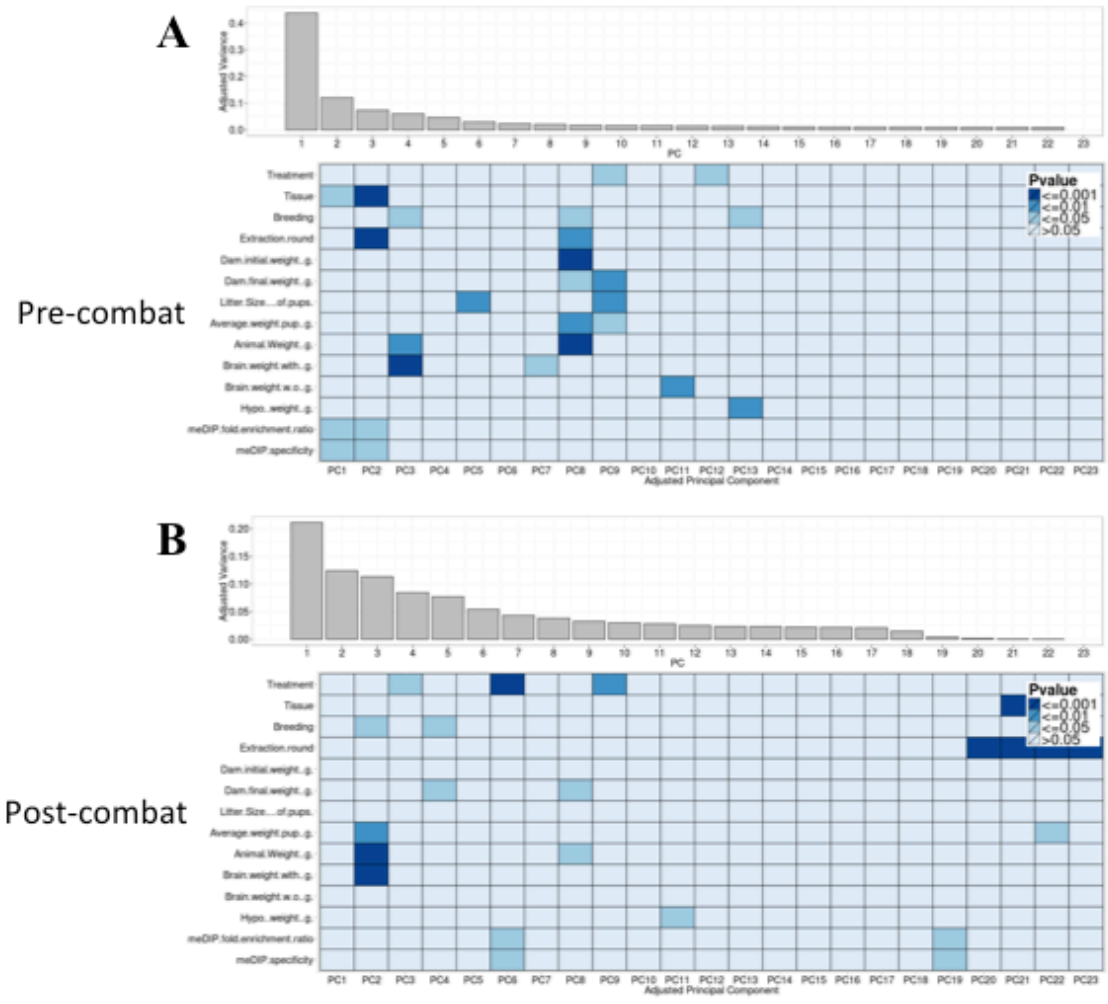

Supplementary figure 3.4. Principal component analysis of meDIP-seq data for the postnatal day 22 hypothalamus and white blood cell samples before and after ComBat correction. A) Principal component analysis of the normalized BvB RPKM data revealed significant levels of variation associated with DNA extraction round batch effects**.** Tissue type was the covariate most strongly associated with variance in the dataset, although it was slightly confounded with extraction round. B) ComBat correction was used to account for the effects of DNA extraction round in the BvB dataset, though this also removed cell-type associated

variation. Prenatal treatment was associated with a larger proportion of variance within the dataset following ComBat correction.

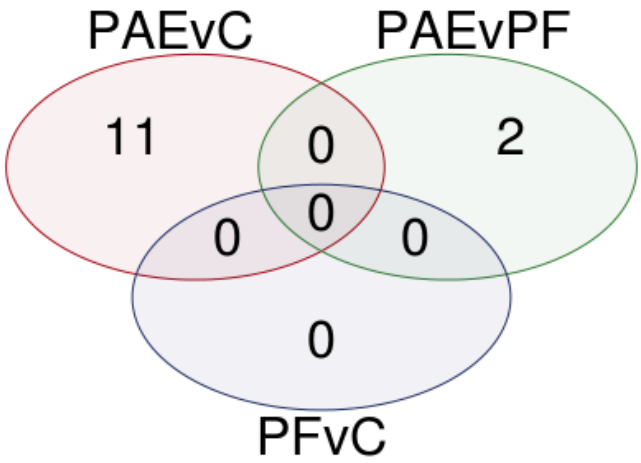

Supplementary figure 3.5. Cell-type associated DMRs. Linear modeling was performed on the 18,050 peaks located in cell-type associated meDIP-seq peaks, correcting for age and breeding. At an FDR<0.05, 11 DMRs were identified between PAE and controls (C; 6 neuron-, 3 oligodendrocyte-, 2 astrocyte-related), while 2 DMRs were found between PAE and PF (1 neuron-, 1 oligodendrocyte-related). No DMRs were identified between PF and controls, and no overlaps were identified.

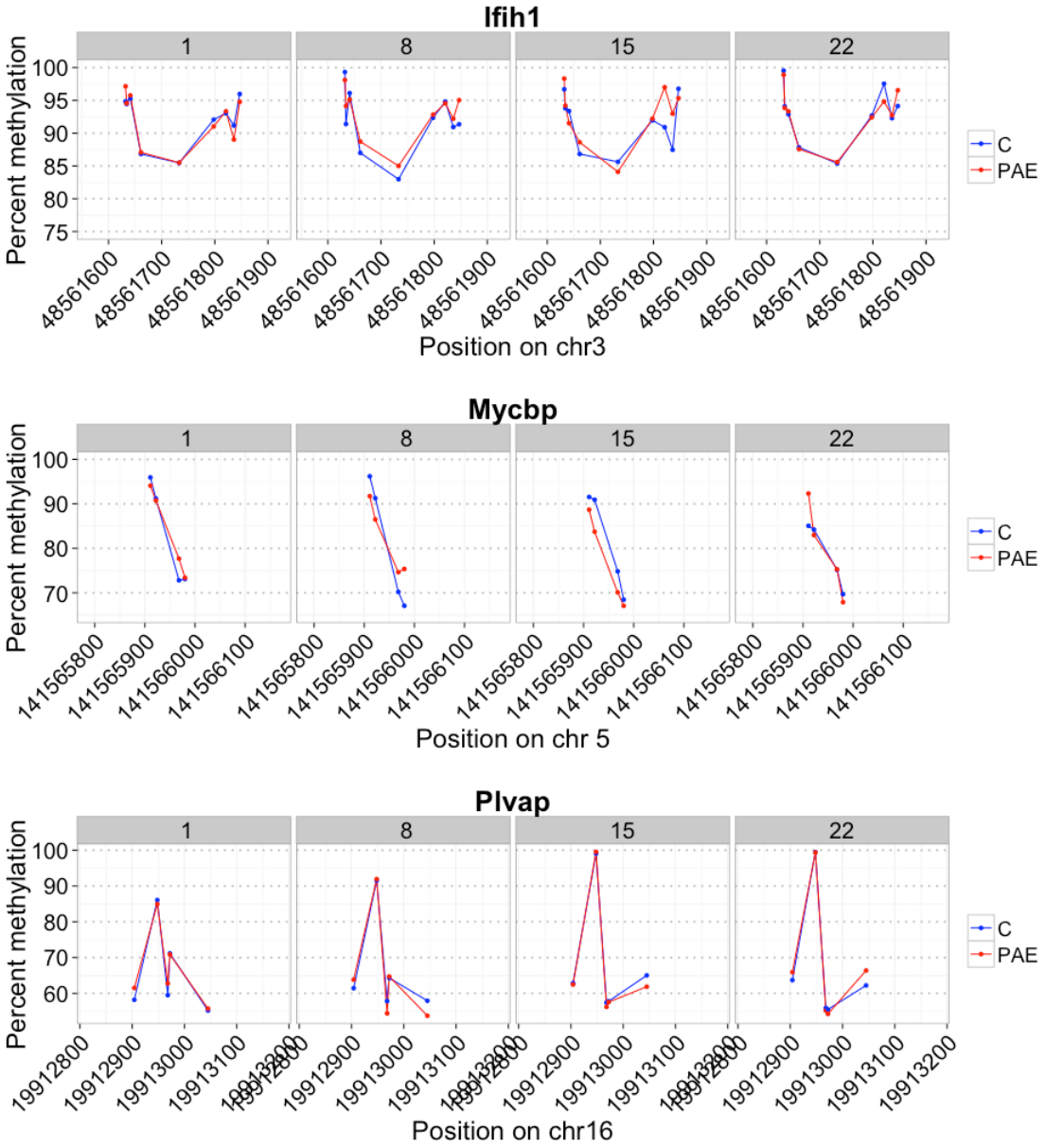

Supplementary figure 3.6. Additional bisulfite pyrosequencing data for the developmental hypothalamus samples. Three additional DMRs were verified by bisulfite pyrosequencing using the hypothamaus samples at P1, P8, P15, and P22. These were located within *Ifih1* (chr3:48,561,559-48,561,925), *Mycbp* (chr5:141,565,784-141,566,172), and *Plvap* (chr16:19,912,813-19,913,185). PAE = red; Control = blue.

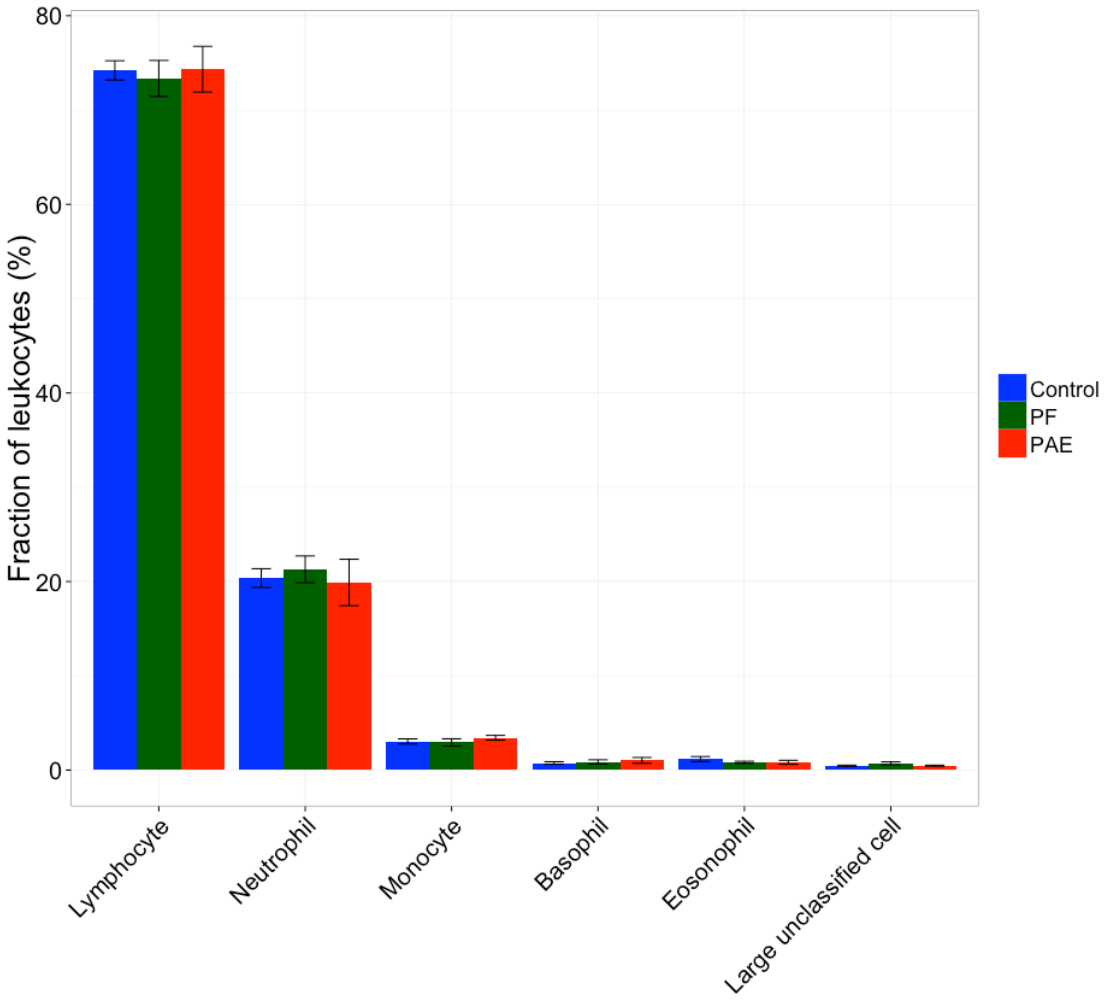

Supplementary figure 3.7. White blood cell composition on postnatal day 22. The composition of white blood cells from PAE, PF, and C animals on P22 was analyzed to obtain the proportions of lymphocytes, neutrophils, monocytes, basophils, eosoniphils, and large unclassified cells. No significant differences were observed between groups.

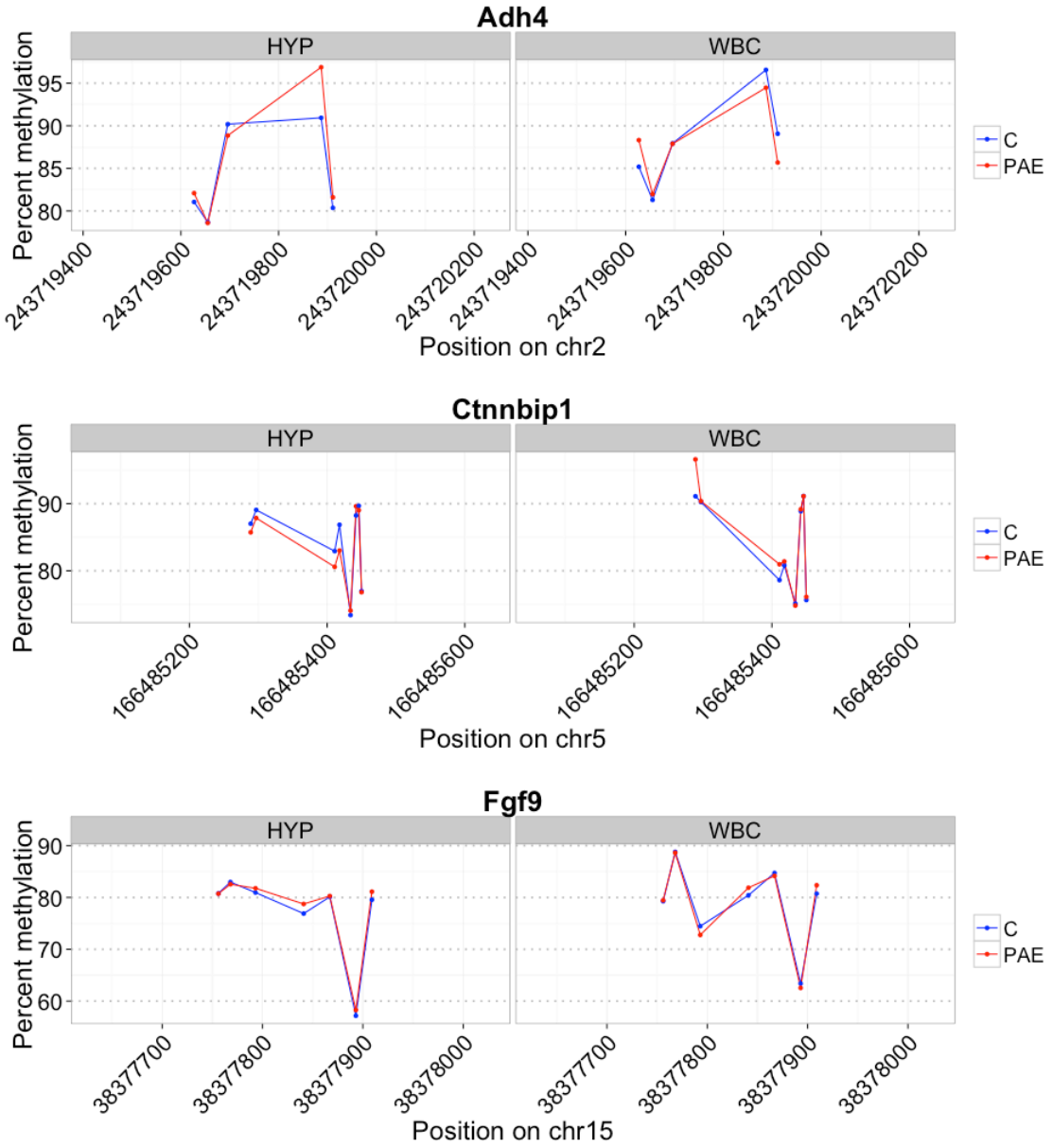

Supplementary figure 3.8. Bisulfite pyrosequencing data for the postnatal day 22 hypothalamus and white blood cell samples. DNA methylation patterns were analyzed in the final exon and 3' UTR of *Adh4* (chr2: 243,719,416-243,720,233), the first exon and 5' UTR of *Ctnnbip1* (chr5: 166,485,057-166,485,637), and the first intron of *Ffg9* (chr15: 38,377,629-38,378,027). PAE = red, Control = blue.

B.2 Supplementary tables

Supplementary table 3.1. White blood cell composition data in percentages

Group	Control	PF	PAE
N	7	5	5
Neutrophils	20.4 ± 1	21.3 ± 1.4	19.9 ± 2.5
Lymphocytes	74.2 ± 1	73.4 ± 1.9	74.3 ± 2.4
Monocytes	3 ± 0.3	2.9 ± 0.4	3.4 ± 0.3
Eosinophils	1.2 ± 0.3	0.8 ± 0.1	0.8 ± 0.2
Basophils	0.8 ± 0.1	0.9 ± 0.2	1 ± 0.3
Large unclassified cells	0.5 ± 0.1	0.7 ± 0.2	0.5 ± 0.1

Supplementary table 3.2. MeDIP-seq sample developmental data

Code	Age	Group	Tissue	Breeding	Animal Number	Dam initial weight (g)	Dam final weight (g)	Average weight/pup (g)	Extraction round	meDIP round
P0-hyp-C3	1	Con	hypo	NYB	42	313	491	7.41	5	2
P0-hyp-C1	1	Con	hypo	Dev-3	52	272	438	6.69	5	2
P0-hyp-C4	1	Con	hypo	NYB	51	299	474	5.8	6	2
P0-hyp-C2	1	Con	hypo	Dev-3	57	289	470	6.35	6	2
P0-hyp-E1	1	PAE	hypo	Dev-3	1	274	412	6.42	5	2
P0-hyp-E2	1	PAE	hypo	Dev-3	5	277	435	6.38	6	2
P0-hyp-E4	1	PAE	hypo	NYB	13	292	441	6.76	5	2
P0-hyp-E3	1	PAE	hypo	NYB	1	319	462	6.5	6	2
P0-hyp-PF4	1	PF	hypo	NYB	35	305	455	6.5	5	2
P0-hyp-PF1	1	PF	hypo	Dev-3	26	293	451	7.09	5	2
P0-hyp-PF3	1	PF	hypo	NYB	24	319	479	6.59	6	2
P0-hyp-PF2	1	PF	hypo	Dev-3	31	298	433	6.76	6	2
P8-hyp-C5	8	Con	hypo	Dev-4	41	312	496	6.63	3	2
P8-hyp-C7	8	Con	hypo	Dev-5	45	285	475	6.73	3	2
P8-hyp-C8	8	Con	hypo	Dev-5	46	274	530	7.29	4	2
P8-hyp-C6	8	Con	hypo	Dev-4	46	303	433	6.67	4	2
P8-hyp-E6	8	PAE	hypo	Dev-4	9	355	479	6.54	4	2
P8-hyp-E5	8	PAE	hypo	Dev-4	1	311	434	7	3	2
P8-hyp-E8	8	PAE	hypo	Dev-5	7	265	413	6.62	4	2
P8-hyp-E7	8	PAE	hypo	Dev-5	6	288	432	6.33	3	2
P8-hyp-PF6	8	PF	hypo	Dev-4	26	322.8	469	6.44	4	2
P8-hyp-PF8	8	PF	hypo	Dev-5	28	311	471	7.25	4	2
P8-hyp-PF5	8	PF	hypo	Dev-4	24	293	433	6.73	3	2
P8-hyp-PF7	8	PF	hypo	Dev-5	27	256	391	6.54	3	2

Code	Age	Group	Tissue	Breeding	Animal Number	Dam initial weight (g)	Dam final weight (g)	Average weight/pup (g)	Extraction round	meDIP round
P15-hyp-C12	15	Con	hypo	Dev-4	47	324	510	7.71	2	2
P15-hyp-C11	15	Con	hypo	Dev-4	44	304	446	6.64	1	2
P15-hyp-C9	15	Con	hypo	Dev-4	41	312	496	6.63	1	2
P15-hyp-C10	15	Con	hypo	Dev-4	43	303	529	6.69	2	2
P15-hyp-E11	15	PAE	hypo	Dev-4	3	300	455	6.61	1	2
P15-hyp-E10	15	PAE	hypo	Dev-4	2	306	411	6.78	2	2
P15-hyp-E12	15	PAE	hypo	Dev-4	6	330	431	6.7	2	2
P15-hyp-E9	15	PAE	hypo	Dev-4	1	311	434	7	1	2
P15-hyp-PF10	15	PF	hypo	Dev-4	24	293	433	6.73	2	2
P15-hyp-PF12	15	PF	hypo	Dev-4	28	319	461	9.22	1	2
P15-hyp-PF11	15	PF	hypo	Dev-4	27	304	479	6.8	2	2
P15-hyp-PF9	15	PF	hypo	Dev-4	22	298	470	5.76	1	2
P22-hyp-C14	22	Con	hypo	Dev-3	57	289	470	6.35	8	1
P22-hyp-C13	22	Con	hypo	Dev-3	54	290	466	6.75	7	1
P22-hyp-C15	22	Con	hypo	Dev-4	41	312	496	6.63	7	1
P22-hyp-C16	22	Con	hypo	Dev-4	44	304	446	6.66	11	1
P22-hyp-E15	22	PAE	hypo	Dev-4	1	311	434	7	7	1
P22-hyp-E13	22	PAE	hypo	Dev-3	13	283	413	6.49	8	1
P22-hyp-E14	22	PAE	hypo	Dev-3	14	292	424	6	8	1
P22-hyp-E16	22	PAE	hypo	Dev-4	3	300	455	6.61	8	1
P22-hyp-PF13	22	PF	hypo	Dev-3	35	282	425	6.414	11	1
P22-hyp-PF14	22	PF	hypo	Dev-3	36	270	418	5.24	8	1
P22-hyp-PF15	22	PF	hypo	Dev-4	22	298	470	5.76	8	1
P22-hyp-PF16	22	PF	hypo	Dev-4	25	291	404	7.29	7	1
P22-wbc-C16	22	Con	WBC	Dev-4	44	304	446	6.66	11	1
P22-wbc-C13	22	Con	WBC	Dev-3	54	290	466	6.75	9	1

Code	Age	Group	Tissue	Breeding	Animal Number	Dam initial weight (g)	Dam final weight (g)	Average weight/pup (g)	Extraction round	meDIP round
P22-wbc-C15	22	Con	WBC	Dev-4	41	312	496	6.63	9	1
P22-wbc-C14	22	Con	WBC	Dev-3	57	289	470	6.35	9	1
P22-wbc-E14	22	PAE	WBC	Dev-3	14	292	424	6	9	1
P22-wbc-E16	22	PAE	WBC	Dev-4	3	300	455	6.61	10	1
P22-wbc-E13	22	PAE	WBC	Dev-3	13	283	413	6.49	10	1
P22-wbc-E15	22	PAE	WBC	Dev-4	1	311	434	7	9	1
P22-wbc-PF14	22	PF	WBC	Dev-3	36	270	418	5.24	9	1
P22-wbc-PF13	22	PF	WBC	Dev-3	35	282	425	6.414	10	1
P22-wbc-PF16	22	PF	WBC	Dev-4	25	291	404	7.29	9	1
P22-wbc-PF15	22	PF	WBC	Dev-4	22	298	470	5.76	9	1

Supplementary table 3.3. Sequencing information

Tissue	Age	Group	Identifier	Index	Pool	Run	Raw reads	Filtered reads	Merged reads
Hypothalamus	P1	Control	C1	ATCACG	1	1	33,113,860	18,020,244	35,373,269
						2	31,784,264	17,353,025	
			C2	GATCAG	3	1	27,192,236	14,734,297	28,526,047
						2	25,679,030	13,791,750	
			C3	AACCCC	1	1	26,646,068	14,525,492	28,281,710
						2	25,133,374	13,756,218	
			C4	ACCCAG	2	1	25,186,902	13,665,101	26,376,060
						2	23,731,912	12,710,959	
		PAE	E1	AGCGCT	1	1	26,429,786	14,202,238	27,783,599
						2	25,157,078	13,581,361	
			E2	CAAAAG	2	1	27,380,852	14,706,678	28,436,281
						2	25,891,126	13,729,603	
			E3	CCAACA	2	1	31,992,216	17,277,335	33,361,893
						2	30,208,954	16,084,558	
			E4	CTAGCT	3	1	26,569,012	14,332,586	27,839,904
						2	25,246,104	13,507,318	
		PF	PF1	GATGCT	1	1	27,760,330	15,452,657	30,105,294
						2	26,223,882	14,652,637	
			PF2	TAATCG	3	1	30,779,018	16,827,587	32,670,305
						2	29,178,264	15,842,718	
			PF3	TGAATG	2	1	31,917,074	17,071,209	33,044,316
						2	30,248,814	15,973,107	
			PF4	AGTTCC	3	1	24,193,448	13,302,170	25,994,763
						2	23,266,440	12,692,593	

Tissue	Age	Group	Identifier	Index	Pool	Run	Raw reads	Filtered reads	Merged reads
Hypothalamus	P8	Control	C5	CGATGT	1	1	30,518,248	17,138,881	33,314,585
						2	28,796,732	16,175,704	
			C6	TAGCTT	2	1	31,254,738	17,351,755	33,473,392
						2	29,465,300	16,121,637	
			C7	AACTTG	3	1	28,431,432	15,611,842	30,284,774
						2	27,008,606	14,672,932	
			C8	ACCGGC	3	1	32,449,760	18,921,725	36,679,903
						2	30,725,390	17,758,178	
		PAE	E5	AGGCCG	1	1	33,548,916	19,547,947	38,470,718
						2	32,360,588	18,922,771	
			E6	CAACTA	2	1	35,583,836	19,250,990	37,249,626
						2	33,743,720	17,998,636	
			E7	CCACGC	3	1	34,376,176	18,454,863	35,902,562
						2	32,835,226	17,447,699	
			E8	CTATAC	1	1	34,721,986	18,826,227	36,717,315
						2	33,018,664	17,891,088	
		PF	PF5	GCAAGG	1	1	33,644,026	19,266,595	37,763,951
						2	32,201,456	18,497,356	
			PF6	TACAGC	2	1	32,825,210	18,529,959	35,897,122
						2	31,166,606	17,367,163	
			PF7	TGCCAT	3	1	35,456,476	19,656,204	38,177,496
						2	33,786,654	18,521,292	
			PF8	ATGTCA	2	1	29,446,168	16,802,092	32,429,973
						2	27,786,980	15,627,881	

Tissue	Age	Group	Identifier	Index	Pool	Run	Raw reads	Filtered reads	Merged reads
Hypothalamus	PN15	Control	C10	GGCTAC	2	1	35,268,414	20,979,814	40,584,612
						2	33,481,480	19,604,798	
			C11	AAGACT	1	1	38,296,066	22,439,953	43,542,043
						2	36,008,304	21,102,090	
			C12	ACGATA	3	1	36,590,934	21,441,076	41,501,439
						2	34,632,866	20,060,363	
			C9	TTAGGC	2	1	35,600,020	21,234,427	41,081,852
						2	33,762,840	19,847,425	
		PAE	E10	CACCGG	2	1	30,695,160	17,867,138	34,488,414
						2	28,993,480	16,621,276	
			E11	CCCATG	1	1	30,467,386	17,737,556	34,609,228
						2	28,955,916	16,871,672	
			E12	CTCAGA	3	1	38,501,180	23,567,190	45,620,926
						2	36,324,260	22,053,736	
			E9	ATAATT	3	1	37,520,694	22,115,457	42,698,321
						2	35,359,184	20,582,864	
		PF	PF10	TATAAT	1	1	37,575,902	22,133,777	42,876,537
						2	35,260,306	20,742,760	
			PF11	TGCTGG	2	1	34,648,014	20,322,751	39,225,192
						2	32,674,258	18,902,441	
			PF12	CCGTCC	1	1	25,605,012	15,284,658	29,763,216
						2	24,238,924	14,478,558	
			PF9	GCACTT	3	1	34,185,162	20,363,976	39,364,187
						2	32,217,998	19,000,211	

Tissue	Age	Group	Identifier	Index	Pool	Run	Raw reads	Filtered reads	Merged reads
Hypothalamus	P22	Control	C13	TGACCA	2	1	28,414,894	17,418,312	33,672,075
						2	26,924,380	16,253,763	
			C14	CTTGTA	1	1	29,515,800	17,903,092	34,695,180
						2	27,668,210	16,792,088	
			C15	AAGCGA	3	1	29,504,840	17,739,529	34,399,305
						2	28,037,190	16,659,776	
			C16	ACTCTC	1	1	30,471,106	18,210,924	35,346,488
						2	28,691,626	17,135,564	
		PAE	E13	ATACGG	1	1	30,684,776	17,630,787	34,240,873
						2	28,938,122	16,610,086	
			E14	CACGAT	2	1	30,423,746	18,388,642	35,419,868
						2	28,642,648	17,031,226	
			E15	GAGTGG	2	1	31,173,234	18,761,333	36,161,961
						2	29,292,372	17,400,628	
			E16	CTGCTG	3	1	32,570,020	19,094,631	36,832,208
						2	30,637,412	17,737,577	
		PF	PF13	GCCGCG	3	1	30,521,646	18,514,525	35,903,586
						2	28,936,906	17,389,061	
			PF14	TCATTC	2	1	29,311,830	17,565,565	33,861,425
						2	27,649,446	16,295,860	
			PF15	TGGCGC	1	1	30,520,304	17,902,814	34,882,050
						2	28,939,276	16,979,236	
			PF16	GTAGAG	3	1	29,568,090	18,172,937	35,013,277
						2	27,737,436	16,840,340	

Tissue	Age	Group	Identifier	Index	Pool	Run	Raw reads	Filtered reads	Merged reads
WBC	P22	Control	C13	ACAGTG	2	1	26,906,928	13,919,764	26,311,548
						2	25,535,086	12,391,784	
			C14	AAACAT	3	1	30,292,844	16,375,542	31,854,398
						2	28,983,878	15,478,856	
			C15	AAGGAC	3	1	27,956,550	14,821,280	28,956,709
						2	26,934,482	14,135,429	
			C16	ACTGAT	1	1	29,229,892	15,389,413	29,941,324
						2	27,646,582	14,551,911	
		PAE	E13	ATCCTA	3	1	28,367,834	15,486,836	30,100,768
						2	27,096,260	14,613,932	
			E14	CACTCA	2	1	28,585,764	15,081,785	29,259,531
						2	27,220,480	14,177,746	
			E15	CCGCAA	1	1	29,201,324	15,607,538	30,584,097
						2	28,006,024	14,976,559	
			E16	GAAACC	1	1	29,717,654	15,563,021	30,396,206
						2	28,278,420	14,833,185	
		PF	PF13	GCCTTA	3	1	28,467,842	15,798,190	30,752,305
						2	27,253,066	14,954,115	
			PF14	TCCCGA	1	1	29,075,498	15,667,697	30,472,297
						2	27,526,446	14,804,600	
			PF15	TTCGAA	2	1	29,904,506	16,430,391	31,722,602
						2	28,300,216	15,292,211	
			PF16	GTCCGC	2	1	24,674,412	12,894,418	24,427,455
						2	23,617,458	11,533,037	

* Pool 1 = PX0182, Pool 2 = PX0183, Pool 3 = PX0184, Run 1 = C5DN1ANXX, Run 2 = C5DWPANXX

Supplementary table 3.4. Primer sequences for bisulfite pyrosequencing

Analysis	DMR	Primer	Sequence
Developmental	*Plvap* chr16:19912813-19913185	F1	TTGGGTTAGGATTTGATTTAGTGT
		R1	Biotin-AATCTCATATTTTCCCCACTAATTTATT
		S1	GGATTTGATTTAGTGTTAGATA
		S2	GGTGATTTGAGTTTAGTTTTTAG
	Mycbp chr5:141565784-141566172	F1	TTGTAGTTGGTAGTTGTTTTGTAGAT
		R1	Biotin-TTCTATATTATCCTTCTTAAACCATTCACT
		S1	ATTTTTTGGTATTTTTAAAGTTAGA
	Drd4 chr1:214281174-214281640	F1	AGTTTGGAAGGGTGAAAGG
		R1	Biotin-AACAAAAAAACCTCCCTCTTTTC
		S1	GTTTTTTTTAGTGGTGTATAT
		S2	ATAGTGTTTTTAATTTTATTATTTATAT
		S3	GAGGTTAAGGGGTTTTA
	Ifih1 chr3:48561559-48561925	F1	AGTTGGTAATTTAGTGTAATTTTTGTTTG
		R1	biotin-AACACAACACTTCCTTTCTTTATT
		S1	TTGTTTGAAGAAGTAGTTATATAG
		S2	ATTTTATGTGTATATTTTTTTGGT
		S3	AATTTTAGAGTTATTGTTGGTAATTA
Tissue-concordant	*Adh4* chr2:243719416-243720233	F1	TGATGTTATAGATGGGGAAAGAT
		R1	Biotin-ATACTTAAACTCATAACTTTCCTTAACT
		S1	ATGGGGAAAGATGATAATA
		S2	AGATAAGTAGTATTTATTGTTGTATT
	Fgf9 chr15:38377629-38378027	F1	TGTATATATTTAGGGGGTATTGTGAA
		R1	Biotin-ACAAACAAATTTTCCTACTACCT
		S1	TTTGGGTTATTGTTGTTAAA
		S2	TTGAATATATTTATTTTTTTTGAAAATTATAG
	Ctnnbip1 chr5:166485057-166485637	F1	GGGAGGTTATTTGTTATAGTGAGT
		R1	Biotin-TATCCCAAATCCTTACCTACTTCT
		S1	TGTGTGGAGTAGTAGA
		S2	GTATTTTTAGATTATGATAGAGTTATG

Supplementary table 3.5. Annotated PAE-specific DMRs persisting across pre-weaning development of the hypothalamus

DMR	Direction	Gene symbol	Location	CpG Island
chr1:139741953:139742431	down		Intergenic	
chr1:15191610:15192035	down	Il20ra	Intron	
chr1:176085084:176085420	down		Intergenic	
chr1:214281174:214281640	up	Drd4	Exon; 3'UTR	
chr1:234096707:234097209	up		Intergenic	
chr1:24164308:24164875	up		Intergenic	
chr1:262677894:262678380	down	Hpse2	Intron	
chr10:86515501:86516299	up	Zpbp2	Intron/exon boundary	

DMR	Direction	Gene symbol	Location	CpG Island
chr11:10724344:10725282	down		Intergenic	
chr11:31024852:31025512	up		Intergenic	
chr11:71219854:71220604	up		Intergenic	
chr11:78732072:78732415	down		Intergenic	
chr12:43921015:43921537	up	RGD1562310	Exon; 3'UTR	
chr13:106810181:106810590	down	Ush2a	Intron/exon boundary	
chr13:62397424:62397837	down		Intergenic	
chr13:6442080:6442489	down	Cntnap5c	Intron	
chr14:15247402:15247937	down		Intergenic	
chr14:29220684:29221181	up		Intergenic	
chr14:35716091:35716595	up	Chic2	Intron	
chr14:89701233:89701608	down	Abca13	Intron	
chr15:10340174:10340716	down		Intergenic	
chr15:17047963:17048371	down		Intergenic	
chr15:66140998:66141718	down		Intergenic	
chr15:92709763:92710079	down		Intergenic	
chr16:17170588:17171040	up		Intergenic	
chr16:19912813:19913185	down	Plvap	Intron	
chr16:37619224:37619733	down		Intergenic	
chr16:41856506:41856951	down		Intergenic	
chr16:74651704:74652117	up	Tpte2	Intron	
chr16:8103352:8103846	up		Intergenic	
chr17:12596528:12597167	up		Intergenic	
chr17:40321029:40321439	down		Intergenic	
chr17:52612600:52612944	down		Intergenic	
chr17:70713643:70714128	down		Intergenic	
chr18:19915102:19915521	up		Intergenic	
chr18:41469757:41470143	down		Intergenic	
chr18:48789602:48790549	down		Intergenic	
chr19:11660067:11660621	down	Gnao1	Intron	
chr19:15777433:15777911	down		Intergenic	
chr19:42387827:42388317	down		Intergenic	
chr2:110616915:110617442	down		Intergenic	
chr2:127088880:127089374	down		Intergenic	
chr2:137850374:137850759	down		Intergenic	
chr2:140050486:140050870	down		Intergenic	
chr2:143692596:143693157	down		Intergenic	
chr2:161497496:161498141	down		Intergenic	
chr2:20558992:20559432	down		Intergenic	
chr2:215843043:215843572	down		Intergenic	

DMR	Direction	Gene symbol	Location	CpG Island
chr2:220525192:220525573	down	Palmd	Intron	
chr2:22513687:22514572	up		Intergenic	
chr2:229836382:229836753	down		Intergenic	
chr2:252425659:252425984	down		Intergenic	
chr2:25609554:25610159	up		Intergenic	
chr2:257310351:257310990	up	Gipc2	Intron	
chr2:38646120:38646704	down		Intergenic	
chr2:51638197:51638867	down		Intergenic	
chr2:75595569:75596105	up		Intergenic	
chr2:9358335:9358733	up		Intergenic	
chr20:2457035:2457456	down		Intergenic	
chr20:33453367:33454162	up		Intergenic	
chr20:47637214:47638161	up	Scml4	Intron	
chr3:104747852:104748440	down		Intergenic	
chr3:12053316:12053939	down		Intergenic	
chr3:138519119:138519451	down	Csrp2bp	Intron	
chr3:143201451:143202220	up		Intergenic	
chr3:156648220:156648604	down	Top1	Intron	
chr3:165424304:165424865	up		Intergenic	
chr3:167934957:167935603	up		Intergenic	
chr3:22603206:22603863	down		Intergenic	
chr3:24872200:24872928	down		Intergenic	
chr3:48561559:48561925	down	Ifih1	Intron/exon boundary	
chr3:65105079:65105674	up		Intergenic	
chr3:65324783:65325278	down		Intergenic	
chr3:70184226:70184782	down		Intergenic	
chr3:7434738:7435286	up	Ddx31	Intron	
chr4:150624486:150624887	up		Intergenic	
chr4:168837031:168837647	down	Gprc5a	Intron	
chr4:174485430:174486141	down		Intergenic	
chr4:182990407:182991016	down		Intergenic	
chr4:20511403:20511733	down		Intergenic	
chr4:43208183:43208612	down		Intergenic	
chr4:66719830:66720182	down	Tbxas1	Intron	
chr4:7482909:7483332	up		Intergenic	
chr5:118777373:118777836	up	Pgm1	Intron/exon boundary	
chr5:138504681:138505315	up	Zmynd12	Intron	
chr5:141565784:141566172	up	Mycbp	Intron	
chr5:156145583:156146099	down		Intergenic	
chr5:24846296:24847023	up		Intergenic	

DMR	Direction	Gene symbol	Location	CpG Island
chr5:37607753:37608583	down		Intergenic	
chr5:37986026:37986464	up		Intergenic	
chr5:60856339:60856751	down	Trmt10b	Intron/exon boundary	
chr5:68802664:68803213	down		Intergenic	
chr5:75657944:75658519	down	Lpar1	Intron	
chr6:119447228:119447764	up		Intergenic	
chr6:124978630:124979533	up		Intergenic	
chr6:141054659:141054986	up		Intergenic	
chr7:10808734:10809177	up		Intergenic	
chr7:110539701:110540189	down		Intergenic	
chr7:119688957:119689624	down	Tmprss6	Intron	
chr7:12861503:12862530	up	Hcn2	Intron/exon boundary	Yes
chr7:29983394:29984038	up	Ano4	Intron	
chr7:34231579:34231996	down		Intergenic	
chr7:39701627:39702039	down		Intergenic	
chr7:42660017:42660479	down		Intergenic	
chr7:58691577:58691930	up		Intergenic	
chr7:85674914:85675377	down		Intergenic	
chr8:119324904:119325855	up	Ccrl2	Intron/exon boundary	
chr8:127199227:127199648	up	Ctdspl	Intron	
chr8:127199227:127199648	up	Golga4	Intron	
chr8:127241188:127241611	down	Ctdspl	Intron	
chr8:127241188:127241611	down	Golga4	Intron	
chr8:21395317:21395763	down		Intergenic	
chr8:63476543:63476951	up	Rec114	Intron	
chr9:15545565:15546379	up		Intergenic	
chr9:20969820:20970520	up		Intergenic	
chr9:57883751:57884249	down		Intergenic	
chrUn_KL568409v1:220261:220784	up		Intergenic	
chrX:112031256:112031901	down	Mid2	Intron	
chrX:123442588:123443064	up		Intergenic	
chrX:9184168:9184644	down		Intergenic	

Supplementary table 3.6. Annotated PAE-specific tissue-concordant DMRs

DMR	Gene symbol	Location	CpG Island
chr1:101817110:101817545	Grwd1	Intron	
chr1:107194560:107195008		Intergenic	
chr1:15837095:15837641	LOC100911069	Intron	
chr1:15864955:15865332		Intergenic	
chr1:15923790:15924741	Pde7b	Intron	
chr1:196969305:196969803		Intergenic	
chr1:200209635:200210301	Sec23ip	Exon; 3' UTR	
chr1:204458884:204459389		Intergenic	
chr1:213019370:213019881		Intergenic	
chr1:213182167:213182721		Intergenic	
chr1:213270269:213271271		Intergenic	
chr1:242498350:242499595		Intergenic	
chr1:255332476:255332935		Intergenic	
chr1:28781411:28781929		Intergenic	
chr1:41175032:41175758		Intergenic	
chr1:47870742:47871490		Intergenic	
chr1:52860166:52860642		Intergenic	
chr1:74540044:74540657		Intergenic	
chr1:75812889:75813428		Intergenic	
chr1:99958512:99959133	Klk1c6	Intron	
chr10:10073982:10074605		Intergenic	
chr10:10909785:10910457		Intergenic	
chr10:22047700:22048388		Intergenic	
chr10:2521025:2521416		Intergenic	
chr10:26162626:26163113		Intergenic	
chr10:33049713:33050300		Intergenic	
chr10:33173764:33174779		Intergenic	
chr10:48610216:48610577	Ttc19	Intron	
chr10:52319608:52320654		Intergenic	
chr10:54524382:54524791	Stx8	Intron	
chr10:55465564:55466302		Intergenic	
chr10:56142404:56143430		Intergenic	
chr10:57734995:57735716	Nlrp1a	Intron	
chr10:68822951:68823429	Asic2	Intron	
chr10:98420150:98420680		Intergenic	
chr11:15449907:15450412	Usp25	Intron	
chr11:25607394:25608249		Intergenic	
chr11:37563059:37563612	Dscam	Intron	

DMR	Gene symbol	Location	CpG Island
chr11:53503523:53503944		Intergenic	
chr11:61199083:61199628		Intergenic	
chr11:61430001:61430590		Intergenic	
chr11:67451724:67452162		Intergenic	
chr11:73414606:73415256		Intergenic	
chr11:76843682:76844303	Uts2b	Intron	
chr11:82797763:82799768	Map3k13	Intron	
chr11:83023533:83024287		Intergenic	
chr12:15761494:15761955		Intergenic	
chr12:16828715:16829354		Intergenic	
chr12:29637821:29639566	Caln1	Intron	
chr12:29643946:29645192	Caln1	Intron	
chr12:29736869:29737477	Caln1	Intron	
chr12:29850352:29850897	Tyw1	Intron	
chr12:31065961:31066795		Intergenic	
chr12:34020071:34020891		Intergenic	
chr12:36232881:36233380	Tmem132b	Intron	
chr12:41558900:41559424	Tpcn1	Intron/exon boundary	
chr12:42210123:42210669		Intergenic	
chr12:43079102:43079674		Intergenic	
chr12:50909305:50909846		Intergenic	
chr13:100868490:100869695		Intergenic	Yes
chr13:102617677:102619172		Intergenic	
chr13:104818539:104818957		Intergenic	
chr13:10527965:10528451		Intergenic	
chr13:106979664:106980368	Ush2a	Intron	
chr13:107502115:107502538		Intergenic	
chr13:108465373:108465786		Intergenic	
chr13:108788476:108789657	Ptpn14	Intron	
chr13:12180618:12181092		Intergenic	
chr13:1790670:1791570		Intergenic	
chr13:19095660:19097231		Intergenic	
chr13:19116741:19118626		Intergenic	
chr13:2214879:2215562		Intergenic	
chr13:2440179:2440838		Intergenic	
chr13:2538677:2539280		Intergenic	
chr13:2550524:2551087		Intergenic	
chr13:2629949:2630705		Intergenic	
chr13:2632729:2633630		Intergenic	
chr13:3080853:3081925		Intergenic	

DMR	Gene symbol	Location	CpG Island
chr13:3518363:3519243		Intergenic	
chr13:35925680:35926363		Intergenic	
chr13:3714645:3715057		Intergenic	
chr13:43079999:43080407		Intergenic	
chr13:47698582:47699050		Intergenic	
chr13:48019856:48020481	Rassf5	Intron	
chr13:5171220:5172835		Intergenic	
chr13:6426133:6427027	Cntnap5c	Intron	
chr13:68800527:68801151	Trmt1l	Intron/exon boundary	
chr13:7043768:7044321	Cntnap5c	Intron	
chr13:70592814:70594019	Lamc2	Intron/exon boundary	
chr13:7065420:7065812	Cntnap5c	Intron	
chr13:8060704:8061382		Intergenic	
chr13:8090191:8090877		Intergenic	
chr13:8145292:8146028		Intergenic	
chr13:8386986:8387812		Intergenic	
chr13:8840844:8841233		Intergenic	
chr13:8865962:8866561		Intergenic	
chr13:9352429:9352926		Intergenic	
chr13:94516637:94517272		Intergenic	
chr13:95415525:95416328		Intergenic	
chr14:110799613:110800210	Vrk2	Intron	
chr14:15472278:15472836		Intergenic	
chr14:23719630:23720791		Intergenic	
chr14:88803125:88803626	Tns3	Intron	
chr14:88947856:88948313		Intergenic	
chr15:1541743:1542263	LOC681383	Intron	
chr15:24397254:24398708		Intergenic	
chr15:33965082:33965730		Intergenic	
chr15:38377629:38378027	Fgf9	Intron	
chr15:43112675:43113090		Intergenic	
chr15:47717609:47718058	Msra	Intron	
chr15:4941954:4942353	Nid2	Intron	
chr15:53469145:53469631		Intergenic	
chr15:54480009:54480746	Fndc3a	Intron	
chr15:55395690:55396182		Intergenic	
chr15:58360852:58361276		Intergenic	
chr15:73473804:73474268		Intergenic	
chr15:79218098:79218498		Intergenic	
chr16:22774739:22775525		Intergenic	

DMR	Gene symbol	Location	CpG Island
chr16:48479863:48480487		Intergenic	
chr16:59627092:59627549		Intergenic	
chr16:74994208:74994642		Intergenic	
chr16:88869199:88869771		Intergenic	
chr16:9998609:9999896		Intergenic	
chr17:1930700:1931243		Intergenic	
chr17:28755608:28756898		Intergenic	
chr17:29654228:29654663		Intergenic	
chr17:47853966:47854804		Intergenic	
chr17:51741559:51742069		Intergenic	
chr17:5174301:5174841		Intergenic	
chr17:67611431:67612810		Intergenic	
chr17:7443952:7444476		Intergenic	
chr17:74543902:74544458		Intergenic	
chr18:19561122:19561713		Intergenic	
chr18:26479481:26480151		Intergenic	
chr18:3755389:3755936		Intergenic	
chr18:40928839:40929459		Intergenic	
chr18:46337881:46338456		Intergenic	
chr18:46385964:46386475		Intergenic	
chr18:68973064:68973512	LOC361346	Intron	
chr18:86851313:86851845	Dok6	Intron	
chr19:24418007:24418408	Tbc1d9	Intron/exon boundary	
chr19:29358573:29359218		Intergenic	
chr19:30582479:30583315		Intergenic	
chr19:50583058:50583838		Intergenic	
chr19:54909295:54910046		Intergenic	
chr19:57264897:57265288		Intergenic	
chr19:58684491:58684952		Intergenic	
chr19:8001271:8001672		Intergenic	
chr19:9101115:9101871		Intergenic	
chr2:100576453:100577172		Intergenic	
chr2:120989562:120990862		Intergenic	
chr2:166074267:166074911	Ppm1l	Intron	
chr2:190076979:190077385		Intergenic	
chr2:20022744:20023453	Atg10	Intron	
chr2:203648149:203648573		Intergenic	
chr2:208075637:208076365	Kcnd3	Intron	
chr2:208075637:208076365	Kcnd3	Intron	
chr2:208075637:208076365	Kcnd3	Intron	

DMR	Gene symbol	Location	CpG Island
chr2:221348157:221348954		Intergenic	
chr2:228184208:228184842		Intergenic	
chr2:232135456:232136325	Tifa	Intron/exon boundary; 3' UTR	
chr2:24085832:24086430	Ap3b1	Intron	
chr2:243719416:243720233	Adh4	Intron/exon boundary; 3' UTR	
chr2:24721584:24722093	Pde8b	1st exon; Intron/exon boundary	
chr2:262708655:262709229		Intergenic	
chr2:266273656:266274228		Intergenic	
chr2:29291143:29291653		Intergenic	
chr2:32368744:32370108		Intergenic	
chr2:51832185:51832666		Intergenic	
chr2:52082131:52082682		Intergenic	
chr2:52863844:52864889		Intergenic	Yes
chr2:58622700:58623608		Intergenic	
chr2:6066999:6067900		Intergenic	
chr2:63210285:63210771	Cdh6	Intron	
chr2:72457804:72458303		Intergenic	
chr2:93469803:93470472		Intergenic	
chr20:31704044:31704497		Intergenic	
chr20:34367734:34368494	Slc35f1	Intron	
chr20:34470735:34471347		Intergenic	
chr20:49211454:49211905		Intergenic	
chr20:49627593:49628407		Intergenic	
chr3:121061430:121062178	LOC102550367	Intron	
chr3:122457208:122457945		Intergenic	
chr3:147572419:147573029		Intergenic	
chr3:157471957:157472440		Intergenic	
chr3:158114409:158114938	Ptprt	Intron	
chr3:163488431:163489121		Intergenic	
chr3:164180896:164181993	Slc9a8	Intron	
chr3:165828704:165829059		Intergenic	
chr3:171962462:171962893		Intergenic	
chr3:175607906:175608395		Intergenic	
chr3:21597908:21598331		Intergenic	
chr3:39088951:39089428		Intergenic	
chr3:45454549:45454984		Intergenic	
chr3:48004879:48005517	Slc4a10	Intron	
chr3:79256750:79257619	Ptprj	Intron/exon boundary	
chr3:84947374:84947867		Intergenic	
chr3:95269262:95269821	LOC691083	Intron	

DMR	Gene symbol	Location	CpG Island
chr3:95670322:95670727		Intergenic	
chr3:96090057:96090668		Intergenic	
chr4:10998474:10999573	Magi2	Intron	
chr4:111477535:111477970	Lrrtm4	Intron	
chr4:122270876:122271391		Intergenic	
chr4:124668174:124668889	Adamts9	Intron	
chr4:124873518:124873897		Intergenic	
chr4:141760520:141760948		Intergenic	
chr4:161260559:161261093		Intergenic	
chr4:167803157:167804132	Etv6	Intron	
chr4:17516038:17516612	Sema3e	Intron	
chr4:17791405:17791861		Intergenic	
chr4:17792850:17794297		Intergenic	
chr4:17798464:17800049		Intergenic	
chr4:17825133:17825775		Intergenic	
chr4:18650248:18650703		Intergenic	
chr4:26911942:26912456		Intergenic	
chr4:41088494:41089248		Intergenic	
chr4:51418020:51419045		Intergenic	
chr4:51892608:51893466	Pot1	Intron/exon boundary	
chr4:58840091:58840538	Podxl	Intron	
chr4:61955808:61956663		Intergenic	
chr4:65683298:65683739	Trim24	Intron/exon boundary	
chr4:81152751:81153537		Intergenic	
chr4:8719110:8719492		Intergenic	
chr4:89204967:89205584	Fam13a	Intron/exon boundary	
chr5:106393982:106394394		Intergenic	
chr5:147440928:147441720		Intergenic	
chr5:166485057:166485637	Ctnnbip1	5'UTR; 1st exon	
chr5:168677499:168679243	Camta1	Intron	
chr5:169919769:169920236		Intergenic	
chr5:26047051:26047604		Intergenic	
chr5:35366183:35366617		Intergenic	
chr5:35464085:35464515		Intergenic	
chr5:61882239:61882863		Intergenic	
chr5:67629981:67630562		Intergenic	
chr5:83060298:83060916		Intergenic	
chr5:83602076:83602690		Intergenic	
chr5:83649671:83650115		Intergenic	
chr5:84618382:84619503		Intergenic	

DMR	Gene symbol	Location	CpG Island
chr6:103914403:103916441		Intergenic	
chr6:109082698:109083739	Mlh3	Intron/exon boundary	
chr6:15773315:15773852		Intergenic	
chr6:28511897:28512337		Intergenic	
chr6:43218158:43218792		Intergenic	
chr6:44613686:44614353		Intergenic	
chr6:51046971:51047809		Intergenic	
chr6:53108700:53109636		Intergenic	
chr6:53112915:53113435		Intergenic	
chr6:54255811:54256413		Intergenic	
chr6:60514118:60515029		Intergenic	
chr6:60635422:60635989		Intergenic	
chr6:63841942:63842362		Intergenic	
chr7:104239546:104240006		Intergenic	
chr7:109815764:109816325		Intergenic	
chr7:110539631:110540182		Intergenic	
chr7:127168356:127168885		Intergenic	
chr7:145339032:145339991	Spt1	Promoter	
chr7:145556126:145556659		Intergenic	
chr7:18280334:18281065		Intergenic	
chr7:20723095:20723689		Intergenic	
chr7:25016890:25017352		Intergenic	
chr7:31345082:31345585	Anks1b	Intron	
chr7:42435928:42436444		Intergenic	
chr7:59493923:59494405	Kcnmb4	Intron	
chr7:66837966:66838405		Intergenic	
chr7:76318035:76318554		Intergenic	
chr7:79416202:79416811		Intergenic	
chr7:81043458:81044076		Intergenic	
chr7:92294378:92295000		Intergenic	
chr7:96399886:96400449		Intergenic	
chr8:101557978:101558429		Intergenic	
chr8:104109151:104109770	Tfdp2	Intron	
chr8:110166628:110167472		Intergenic	
chr8:110252343:110252979		Intergenic	
chr8:119867043:119867715		Intergenic	
chr8:128478205:128478631	Scn11a	Intron/exon boundary	
chr8:34038720:34039295		Intergenic	
chr8:39860982:39861801		Intergenic	
chr8:60106908:60107447		Intergenic	

DMR	Gene symbol	Location	CpG Island
chr8:7686400:7686908		Intergenic	
chr8:79706784:79707311	Pigb	Intron	
chr8:79839132:79840191		Intergenic	
chr8:96809632:96810068		Intergenic	
chr9:102613562:102614340		Intergenic	
chr9:113942634:113943096		Intergenic	
chr9:118717195:118717715	Dlgap1	Intron	
chr9:22522883:22523779		Intergenic	
chr9:37463415:37463844	Lgsn	Intron	
chr9:40835:41323		Intergenic	
chr9:47189340:47190123	Il18r1	Intron	
chr9:54282336:54282842	Gls	Exon; 3' UTR	
chr9:68420676:68421163	Pard3b	Intron	
chr9:83955944:83956465		Intergenic	
chr9:86655782:86656259		Intergenic	
chr9:95301397:95301957	Ugt1a1	Intron/exon boundary	
chr9:95301397:95301957	Ugt1a2	Intron/exon boundary	
chr9:95301397:95301957	Ugt1a3	Intron/exon boundary	
chr9:95301397:95301957	Ugt1a5	Intron/exon boundary	
chr9:95301397:95301957	Ugt1a6	Intron/exon boundary	
chr9:95301397:95301957	Ugt1a6	Intron/exon boundary	
chr9:95301397:95301957	Ugt1a7c	Intron/exon boundary	
chr9:95301397:95301957	Ugt1a8	Intron/exon boundary	
chr9:95301397:95301957	Ugt1a9	Intron/exon boundary	
chrUn_KL568295v1:15331:15829		Intergenic	Yes
chrUn_KL568307v1:11609:12122		Intergenic	
chrX:123235748:123236195		Intergenic	
chrX:27175013:27175448		Intergenic	
chrX:3922367:3922843		Intergenic	
chrX:83281162:83281867		Intergenic	
chrX:85550227:85551402		Intergenic	
chrX:87313178:87313849		Intergenic	

Appendix C Supplementary materials for chapter 4

C.1 Supplementary methods

Surrogate variable analysis (SVA)

The SVA with the full sample resulted in the identification of 15 surrogate variables (SVs), with the first 2 SVs representing 27 and 20% of the variance respectively and the others less than 6% each (Supplementary figure 4.2A). We applied linear regression to each SV using each known covariate as potential predictor. We tested 8 known covariates: Run (2 levels = dates when 450k arrays were processed), Chip (18 levels = Chip carrying the sample), location (96 levels = sample location on the array in each run), Plate_column (8 levels = column in 96-well plates), Plate_row (12 levels = row in 96-well plates), Sex (2 levels), Race (24 levels = self-declared ethnicity), and Age (continuous). For the discrete variables with more than two levels, the multiple regression model was built with dummy variables. This results in models that include different amounts of variables. To compare the different models against each other, we obtained the R squared values, adjusted for the number of variables in each model (Supplementary figure 4.2B). Most surrogate variables are best explained by technical covariates and less by biological covariates. However, it is clear that a lot of the variance remains unexplained by known covariates and justifies our use of the SVs in our model to better account for unknown undesirable variation.

Sensitivity analysis for family effect

The data includes 44 sets of siblings/cousins. To investigate whether this impacts our results, we ran an additional differential methylation analysis on the full sample, using the same model that includes the clinical factor (FASD vs. Control) + all 15 SVs identified, with the

addition of 'Family' as a random effect, using the lme4 R package. We compared the results from this analysis to the original analysis. The Spearman rank correlation is 0.9996. There are 1658 significant probes, 1601 overlap with the 1661 probes from the original analysis, 639 overlap with the 658 final probes after ethnicity adjustment (Supplementary table 1). The difference is minor and we conclude that the presence of families in our cohort do not impact significantly our results.

PAE vs FASD analysis

We performed an additional differential methylation analysis after excluding 27 FASD samples with no official diagnosis (denoted PAE for Prenatal Alcohol Exposure). This analysis, including 96 controls and 83 FASDd (FASD with diagnosis), resulted in 502 significant DM probes at a FDR of 0.05, 461 of which overlap with the 1661 probes from the original analysis. The Spearman rank correlation between the results from the original analysis and the analysis without PAE is 0.7927. In addition, we ran ANOVA analyses for the 658 significant probes after ethnicity adjustment, on Control vs. FASDd, Control vs. PAE, and FASDd vs. PAE. We observed that, for most of the probes, methylation in controls is significantly different from either FASDd or PAE, while FASDd vs. PAE doesn't lead to any significant results (Supplementary figure 4.9). We concluded from these results that the PAE samples are not significantly different from the FASDd samples and should be kept in the analysis as part of the broad FASD group.

Investigating ethnically-biased probes

To investigate ethnically-biased probes (denoted "ethnic" probes below), we ran a differential methylation analysis on the FASD samples, looking for differences between samples from the 2 ethnic clusters identified in the MDS analysis (49 samples in cluster 1 vs. 53 samples in cluster 2). It is important to note that the ethnicity bias is directional – the FASD Group is confounded with the ethnic cluster 2 and this is only problematic when the direction of change is the same (e.g. higher in FASD and higher in cluster 2). We thus calculated the one-sided p values and rank for all probes in the above analysis and investigated separately the up-methylated and down-methylated "ethnic" probes. We obtained 1105 probes significantly differentially up-methylated (FDR<0.05) and 594 probes differentially down-methylated (FDR<0.05) in the ethnic cluster 2. These overlap with 5 up-methylated and 4 down-methylated probes in FASD respectively, out of the 658 significant probes after ethnicity adjustment (Supplementary table 1). To investigate whether the ethnicity adjustment we performed was efficient at removing "ethnic" probes, we looked at the "ethnic" ranking of our significant FASD DM probes (Supplementary figure 4.4A). We performed a Receiver Operating Characteristic (ROC) analysis with the ethnic probes (Supplementary figure 4.4B). Our approach was to question how good the ethnic ranking was at predicting the 658 FASD DM probes, a high AUC indicating that the DM probes are in the top of the "ethnic" rank and thus very highly biased. Our results show that while the "ethnic" ranking can somewhat predict our 1661 FASD DM probes (AUC = 0.819 and 0.773 for up- and down-methylated probes respectively), it is much less effective at predicting our 658 FASD DM probes after ethnicity adjustment (AUC = 0.656 and 0.594 for up- and down-methylated probes respectively). These results confirm that our ethnicity adjustment is reducing the ethnic bias as expected.

Incorporating ethnicity as a set of covariates in the regression model

We investigated the option of incorporating the ethnicity as a covariate in the model, using the genotyping data available. There are 195 samples with both genotyping and methylation data, 103 FASD and 92 controls. We tested different models and decided to perform a linear regression analysis using Limma with a model that includes the clinical factor (FASD vs. Control) + Gender + C1 + C2 + C3 (First 3 components from the MDS analysis) + family as a random factor. The multiple-testing adjusted significance threshold was established at p = 1.2 x 10-7 (0.05/404030). No significant probes could be identified. This is expected because the FASD status is confounded with ethnicity and correcting for one will erase the small changes the can be observed in the other.

C.2 Supplementary figures

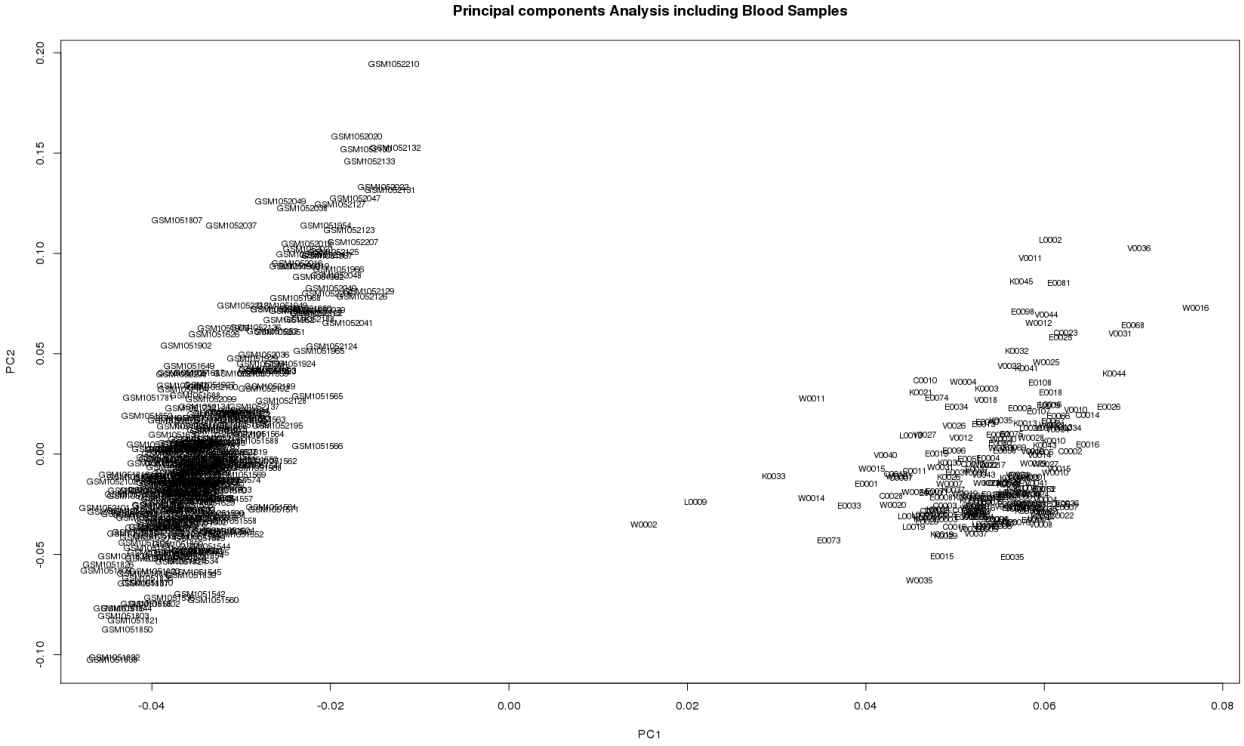

Supplementary figure 4.1. Principal component analysis of buccal epithelial cell and blood samples. The first two principal components, which typically associate with cell type, are depicted for the buccal epithelial cell (BEC) samples from the present study and blood samples obtained from the Gene Expression Omnibus (those beginning with GSM). As shown here, both tissue types cluster separately and little to no blood contamination of BECs is apparent in the dataset, though may be slightly contaminated (samples near center of graph).

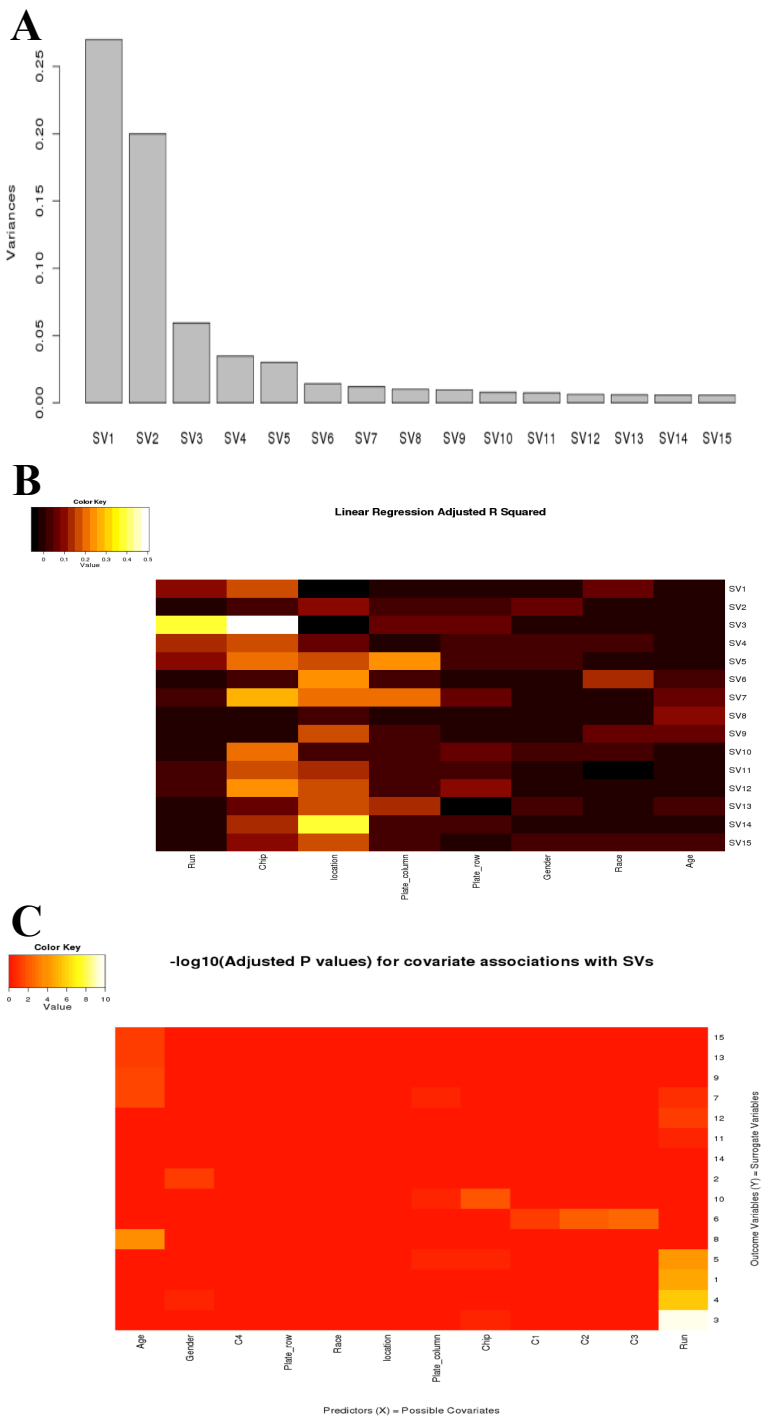

Supplementary figure 4.2. Exploration of surrogate variables. A. Scree plot of the percentage of variance represented by each surrogate variable generated from the entire dataset. B. Heatmap of R squared values from linear regression modeling of each SV with each known covariate. C.

Heatmap of adjusted p-values from linear regression modeling of each SV with known covariates and genetic clusters (C1 to C4).

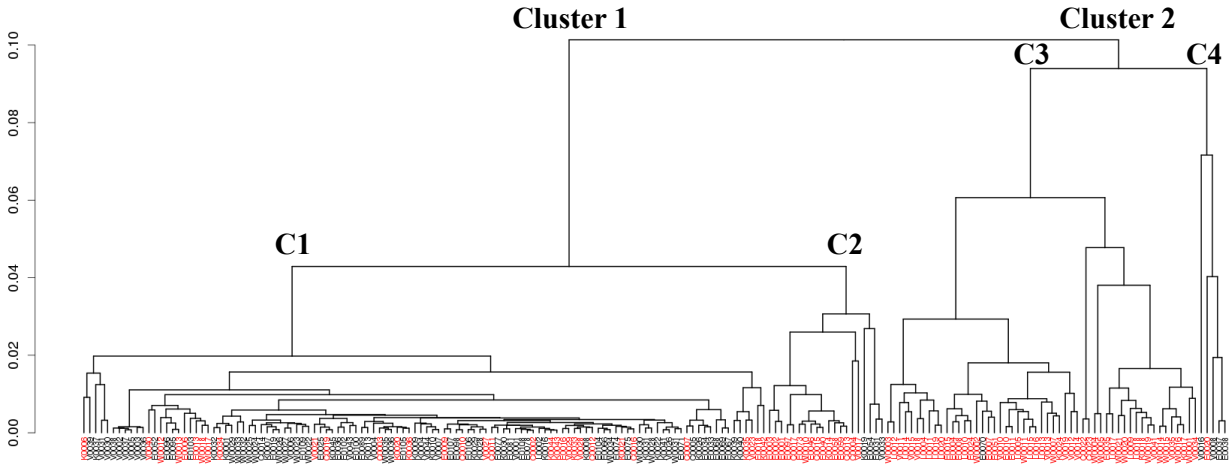

Supplementary figure 4.3. Hierarchical clustering of individuals based on MDS analysis of genotyping data. Children with FASD (red) and controls (black) were clustered based on genetic scores from SNP genotyping. Two major clusters were identified from the unsupervised hierarchical clustering, which were further subdivided into the genetic clusters C1 to C4.

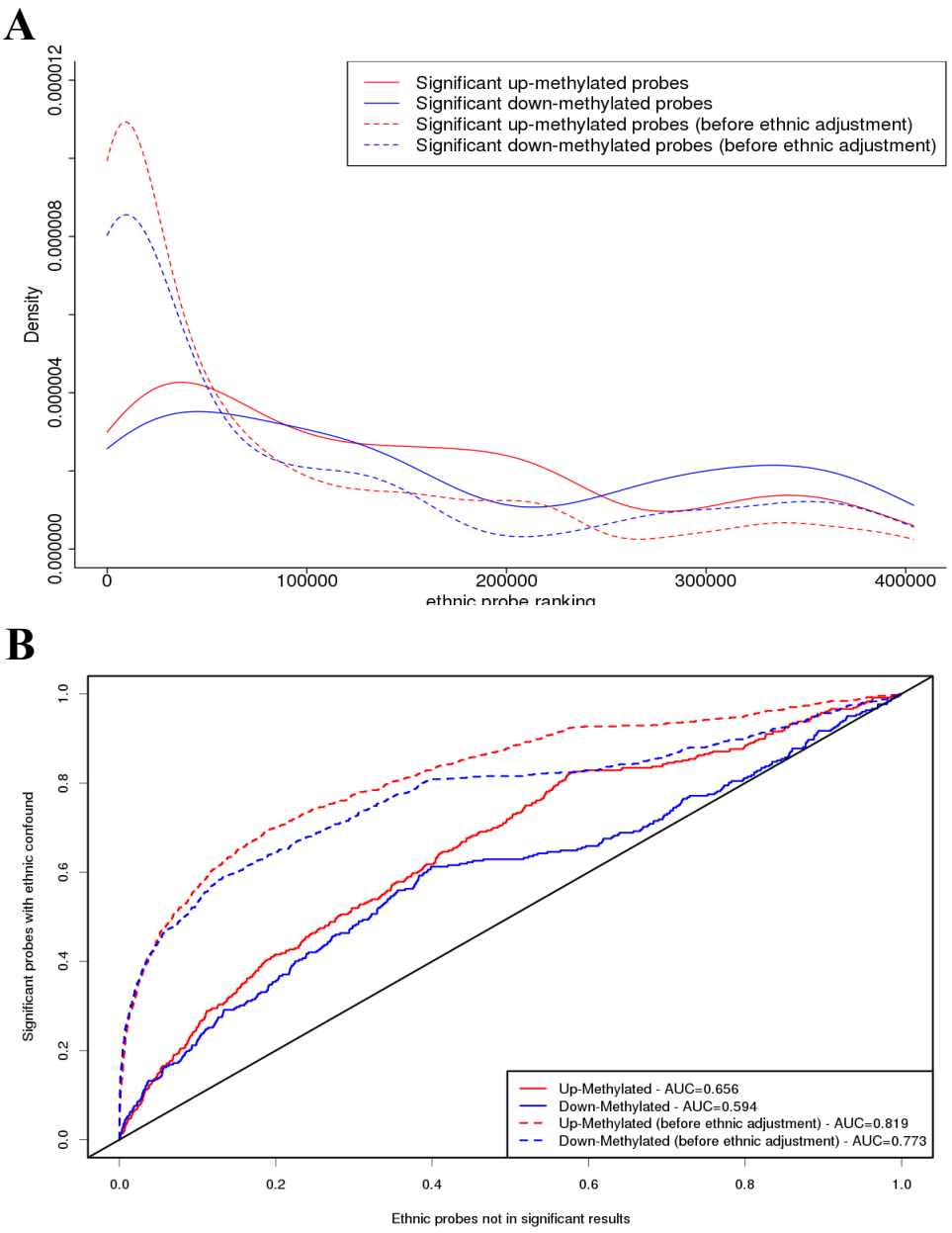

Supplementary figure 4.4. Analysis of ethnically-biased probes in the 658 DM probes. A. Distribution of "ethnic" rank in the significantly up- and down-methylated probes before and after ethnicity adjustment. B. ROC curve demonstrating that the "ethnic" probes are less able to predict the FASD DM probes after ethnicity adjustment.

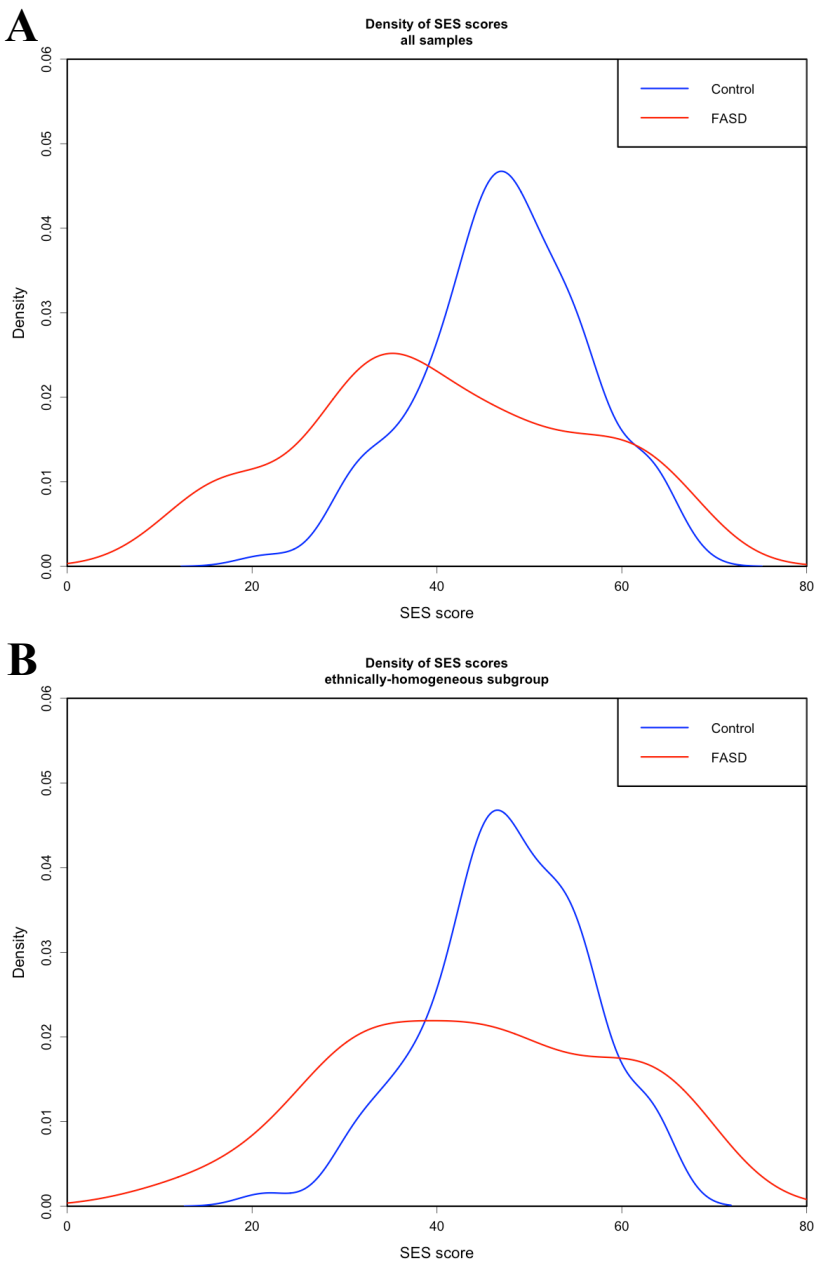

Supplementary figure 4.5. Distribution of socio-economic status scores for children in the FASD and control groups. A. In the full dataset, the distribution of socio-economic status (SES) scores is significantly different between groups (p=0.00017). B. By contrast, in the more ethnically homogeneous subgroup, the difference is no longer significant (p=0.16), suggesting

that these effects may have been partially corrected through the method used for genetic background correction.

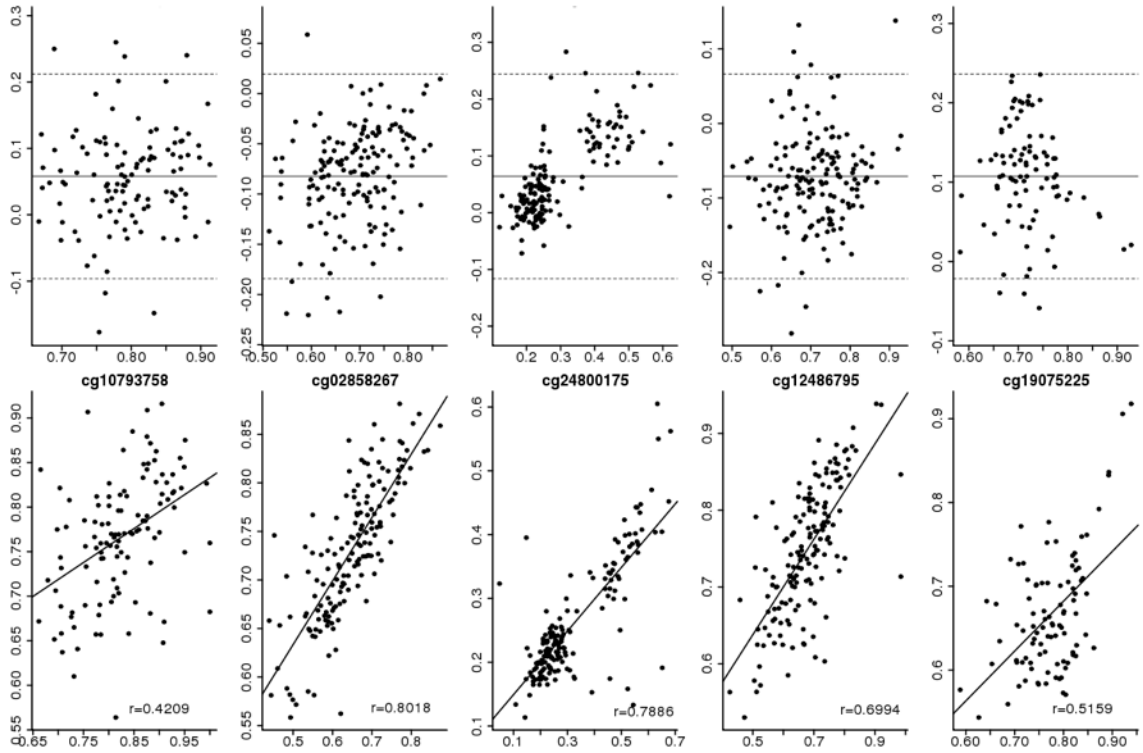

Supplementary figure 4.6. Pyrosequencing verification. Top row are Bland-Altman plots with the difference between the methylation values from the array and the pyrosequencing on the Y axis, and the average Beta values on the X axis. Bottom row are plots with the methylation level from the array on the Y axis and from the pyrosequencing on the X axis, with linear regression lines drawn as well as the Pearson correlation coefficient r.

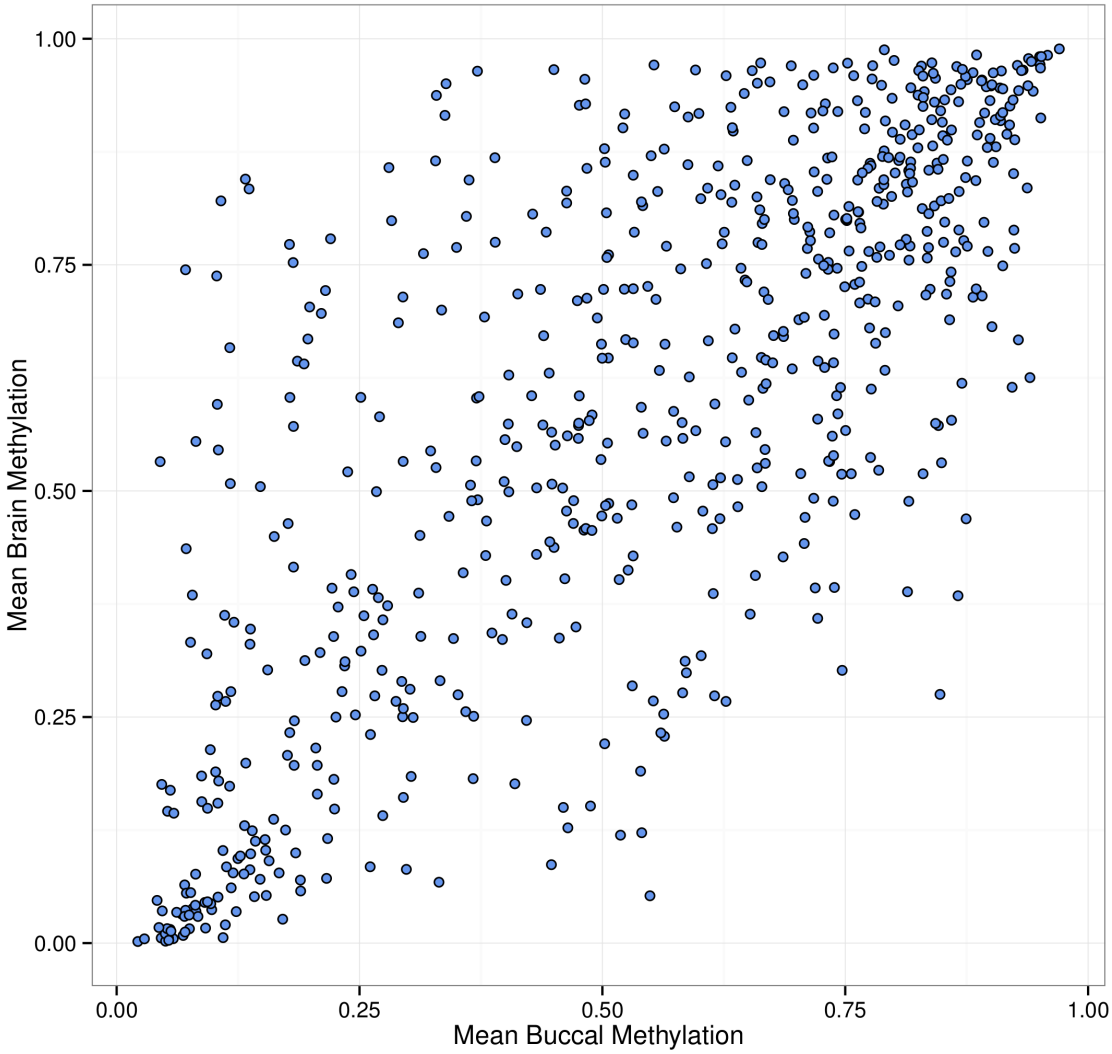

Supplementary figure 4.7. Correlation of buccal and brain methylation at 658 DM CpGs. Points represent an individual CpG methylation in brain and buccal. The overall correlation of mean methylation between buccal and brain samples was 0.76.

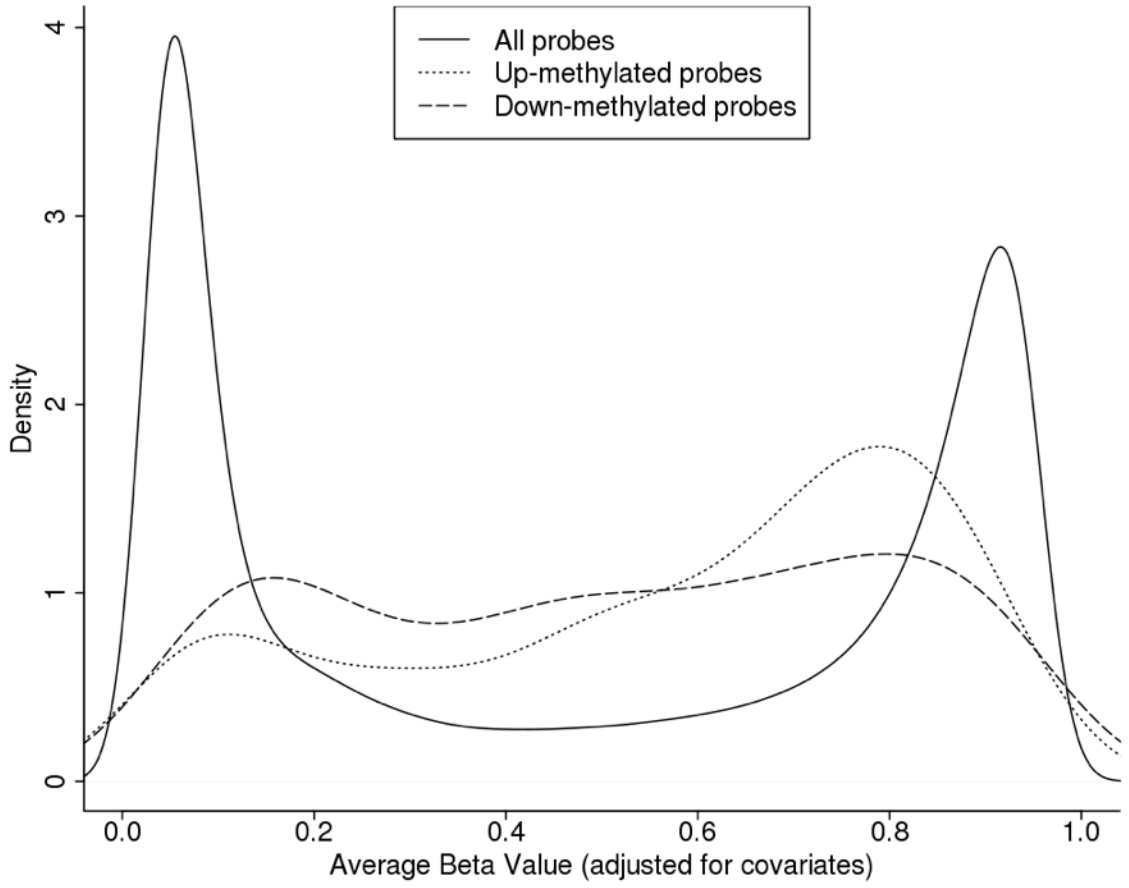

Supplementary figure 4.8. Average distribution of DNA Methylation. The distribution of average DNA methylation for all probes on the 450K array displayed a bimodal distribution, with probes clustering in the lowly (0-20%) and highly (80-100%) methylated ranges. By contrast, probes that were significantly differentially methylated in children with FASD versus controls were more prevalent in intermediately methylated regions (Student's t test; p = 2.5e-09).

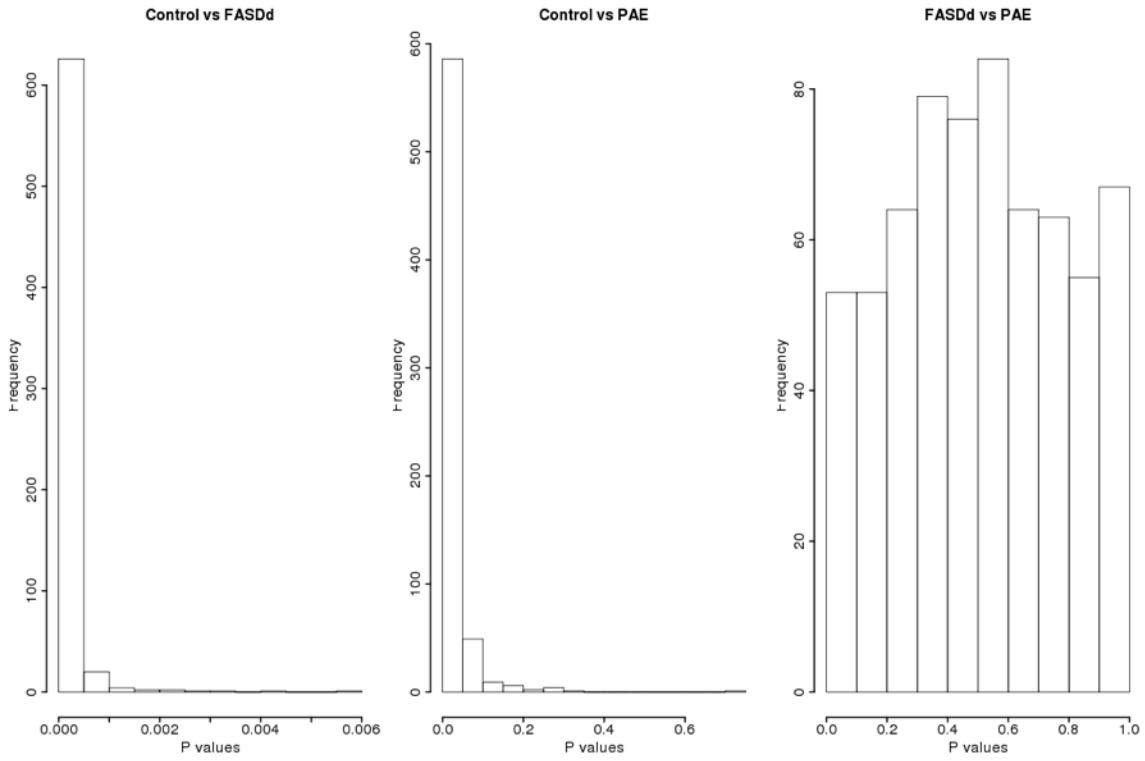

Supplementary figure 4.9. P-value distributions from ANOVA analyses on 658 significant probes. P-value distributions obtained from linear regression analyses were skewed to the left in controls versus both diagnosed FASD cases (FASDd) and children with PAE, but undiagnosed for FASD. By contrast, the p-value distribution comparing both groups of children with PAE revealed a relatively flat distribution, suggesting that there little differences in DNA methylation patterns between diagnosed and undiagnosed children with PAE.Supplementary tables

C.3 Supplementary tables

Supplementary table 4.1. Differentially methylated probes

Probe	p-value	FDR	Mean beta FASD	Mean beta Control	Δbeta
cg10482532	3.96E-07	2.44E-03	0.795	0.733	0.061
cg09895009	3.07E-05	2.13E-02	0.542	0.518	0.024
cg01655958	5.56E-07	2.84E-03	0.509	0.378	0.131
cg26693693	2.60E-08	6.92E-04	0.820	0.784	0.037
cg22691119	6.14E-06	9.73E-03	0.836	0.799	0.037
cg16414821	8.08E-05	3.25E-02	0.900	0.885	0.015
cg10793758	2.45E-06	6.40E-03	0.796	0.753	0.043
cg04707706	1.12E-05	1.25E-02	0.516	0.477	0.039
cg26736200	3.54E-05	2.30E-02	0.729	0.691	0.038
cg19075225	7.20E-06	1.01E-02	0.691	0.651	0.040
cg20293942	3.38E-05	2.24E-02	0.681	0.653	0.029
cg08064292	5.76E-06	9.66E-03	0.166	0.133	0.033
cg04833646	2.46E-05	1.88E-02	0.048	0.039	0.010
cg10946573	5.74E-05	2.76E-02	0.527	0.472	0.055
cg18715709	6.78E-05	2.97E-02	0.813	0.800	0.013
cg12893780	8.32E-08	1.41E-03	0.316	0.260	0.056
cg11959399	7.04E-05	3.01E-02	0.316	0.281	0.035
cg08329753	2.08E-08	6.45E-04	0.476	0.449	0.027
cg24511341	6.64E-09	3.36E-04	0.167	0.152	0.015
cg23418467	4.30E-05	2.47E-02	0.838	0.789	0.049
cg19360675	1.24E-04	3.92E-02	0.092	0.071	0.021
cg00043790	1.90E-05	1.66E-02	0.858	0.841	0.017
cg27120934	3.28E-05	2.21E-02	0.230	0.206	0.023
cg04456916	1.26E-04	3.94E-02	0.800	0.785	0.015
cg22239534	3.26E-07	2.44E-03	0.782	0.749	0.033
cg18057887	2.39E-05	1.86E-02	0.933	0.916	0.017
cg02728342	3.96E-05	2.39E-02	0.839	0.827	0.013
cg22129122	1.56E-07	1.63E-03	0.718	0.693	0.025
cg15339164	2.26E-05	1.82E-02	0.564	0.536	0.028
cg23660182	8.63E-05	3.36E-02	0.852	0.838	0.014
cg11030744	5.97E-07	2.84E-03	0.580	0.510	0.070
cg22910295	3.01E-06	6.79E-03	0.249	0.217	0.032
cg22010140	8.02E-06	1.07E-02	0.538	0.514	0.024
cg08212266	5.47E-06	9.48E-03	0.678	0.654	0.025
cg15073666	3.32E-06	7.18E-03	0.607	0.570	0.038
cg00012960	4.78E-05	2.57E-02	0.754	0.728	0.026
cg19092735	3.28E-06	7.17E-03	0.719	0.685	0.034

Probe	p-value	FDR	Mean beta FASD	Mean beta Control	Δbeta
cg12536502	9.81E-06	1.15E-02	0.085	0.074	0.011
cg24834889	6.84E-05	2.99E-02	0.107	0.091	0.017
cg02642958	1.79E-09	1.45E-04	0.478	0.405	0.073
cg02052956	3.74E-05	2.33E-02	0.455	0.440	0.016
cg22123885	1.07E-04	3.65E-02	0.823	0.783	0.039
cg01345586	3.86E-07	2.44E-03	0.592	0.560	0.032
cg20906524	3.99E-05	2.39E-02	0.734	0.714	0.020
cg21879102	2.33E-05	1.84E-02	0.556	0.523	0.033
cg08701816	6.65E-09	3.36E-04	0.734	0.695	0.039
cg03611029	1.08E-06	3.96E-03	0.685	0.650	0.035
cg19901523	2.14E-06	5.88E-03	0.729	0.689	0.039
cg01015062	1.46E-05	1.43E-02	0.828	0.809	0.019
cg25491704	7.29E-06	1.02E-02	0.889	0.859	0.031
cg18479249	2.45E-07	2.19E-03	0.385	0.351	0.034
cg20506745	9.72E-06	1.15E-02	0.760	0.734	0.027
cg12515485	5.36E-06	9.46E-03	0.553	0.507	0.046
cg27247225	4.88E-05	2.58E-02	0.509	0.484	0.025
cg09767675	1.82E-04	4.70E-02	0.768	0.753	0.016
cg13809095	1.11E-05	1.23E-02	0.487	0.460	0.027
cg09837169	2.54E-07	2.19E-03	0.806	0.777	0.029
cg14765933	1.40E-04	4.13E-02	0.841	0.827	0.015
cg25609517	1.39E-05	1.39E-02	0.716	0.613	0.103
cg08271366	1.40E-04	4.13E-02	0.524	0.482	0.043
cg24269657	5.89E-06	9.66E-03	0.290	0.262	0.028
cg03967266	9.99E-05	3.56E-02	0.783	0.761	0.022
cg15150463	1.13E-04	3.74E-02	0.734	0.715	0.019
cg02197634	8.11E-07	3.48E-03	0.792	0.705	0.087
cg21047695	6.45E-06	9.79E-03	0.408	0.367	0.042
cg24317217	3.36E-05	2.24E-02	0.755	0.739	0.017
cg00892368	1.88E-04	4.81E-02	0.487	0.464	0.023
cg22659953	2.75E-06	6.49E-03	0.771	0.737	0.034
cg24800175	4.18E-06	8.36E-03	0.294	0.234	0.059
cg12880095	6.89E-05	3.00E-02	0.232	0.180	0.052
cg01290710	7.35E-05	3.09E-02	0.770	0.753	0.017
cg17848054	1.93E-05	1.68E-02	0.270	0.234	0.036
cg13741289	1.89E-04	4.81E-02	0.029	0.027	0.002
cg08489410	1.25E-05	1.33E-02	0.921	0.904	0.017
cg01663696	1.04E-04	3.61E-02	0.629	0.603	0.026
cg05532178	2.80E-05	2.00E-02	0.730	0.707	0.023
cg07654559	7.14E-06	1.01E-02	0.118	0.106	0.011

Probe	p-value	FDR	Mean beta FASD	Mean beta Control	Δbeta
cg24506604	1.29E-04	3.99E-02	0.864	0.844	0.020
cg23161492	9.04E-05	3.41E-02	0.722	0.696	0.026
cg07470694	1.97E-04	4.89E-02	0.849	0.833	0.016
cg10804974	1.00E-05	1.15E-02	0.680	0.648	0.032
cg09459548	1.94E-05	1.68E-02	0.811	0.785	0.026
cg07007080	7.52E-06	1.04E-02	0.122	0.113	0.010
cg02814482	1.05E-04	3.62E-02	0.769	0.740	0.029
cg14549524	5.58E-06	9.53E-03	0.855	0.841	0.014
cg07500347	4.50E-06	8.48E-03	0.730	0.665	0.065
cg09066361	9.90E-05	3.55E-02	0.468	0.432	0.035
cg06812861	9.69E-07	3.93E-03	0.841	0.820	0.020
cg26231094	1.02E-06	3.96E-03	0.556	0.505	0.052
cg18174404	2.65E-05	1.95E-02	0.281	0.252	0.028
cg04151826	3.11E-05	2.14E-02	0.803	0.779	0.024
cg13881341	2.91E-06	6.72E-03	0.339	0.310	0.029
cg17352045	1.43E-05	1.41E-02	0.518	0.491	0.027
cg25236277	3.99E-07	2.44E-03	0.808	0.788	0.020
cg08535756	5.03E-06	8.99E-03	0.743	0.723	0.020
cg27409974	1.88E-06	5.50E-03	0.563	0.517	0.045
cg14556787	9.22E-05	3.44E-02	0.900	0.892	0.008
cg08102508	6.80E-06	9.99E-03	0.159	0.145	0.014
cg06915053	2.56E-05	1.91E-02	0.056	0.052	0.004
cg00464520	1.39E-04	4.13E-02	0.555	0.528	0.027
cg16096766	4.54E-06	8.48E-03	0.727	0.704	0.023
cg11253737	1.09E-04	3.68E-02	0.617	0.597	0.020
cg05665581	9.67E-05	3.52E-02	0.745	0.716	0.029
cg01206944	3.28E-05	2.21E-02	0.598	0.565	0.033
cg03411938	7.55E-05	3.12E-02	0.657	0.636	0.021
cg24499411	1.28E-04	3.97E-02	0.903	0.893	0.010
cg05252487	2.35E-06	6.19E-03	0.303	0.274	0.029
cg12192797	5.31E-05	2.70E-02	0.839	0.816	0.023
cg00610991	1.07E-04	3.64E-02	0.567	0.529	0.038
cg16614020	6.89E-06	1.00E-02	0.686	0.650	0.036
cg02487233	1.25E-04	3.94E-02	0.554	0.527	0.027
cg02361459	4.25E-06	8.45E-03	0.889	0.875	0.014
cg16409039	4.47E-05	2.50E-02	0.808	0.792	0.015
cg13557373	2.93E-05	2.05E-02	0.749	0.730	0.020
cg06121352	9.83E-07	3.93E-03	0.775	0.737	0.038
cg27135984	3.76E-05	2.33E-02	0.847	0.831	0.015
cg00971737	9.04E-05	3.41E-02	0.366	0.351	0.015

Probe	p-value	FDR	Mean beta FASD	Mean beta Control	Δbeta
cg19555986	4.60E-05	2.52E-02	0.054	0.047	0.008
cg17921548	1.05E-04	3.63E-02	0.746	0.723	0.023
cg11770664	1.28E-05	1.35E-02	0.622	0.596	0.026
cg19308397	5.76E-05	2.76E-02	0.823	0.807	0.016
cg17248961	1.06E-04	3.64E-02	0.842	0.828	0.013
cg19275200	3.83E-05	2.35E-02	0.909	0.899	0.011
cg10822352	1.13E-04	3.73E-02	0.517	0.491	0.026
cg06154313	8.25E-05	3.29E-02	0.267	0.253	0.014
cg02309230	9.28E-05	3.44E-02	0.882	0.868	0.015
cg03928546	9.21E-05	3.43E-02	0.103	0.093	0.010
cg19402173	8.13E-05	3.27E-02	0.079	0.073	0.006
cg01862688	9.27E-06	1.12E-02	0.578	0.552	0.027
cg26127778	4.31E-05	2.47E-02	0.046	0.040	0.005
cg08772837	2.92E-05	2.05E-02	0.798	0.782	0.016
cg23356309	9.01E-05	3.41E-02	0.876	0.859	0.017
cg04217218	6.23E-06	9.73E-03	0.672	0.649	0.023
cg02096656	2.35E-05	1.84E-02	0.179	0.163	0.015
cg08072202	6.24E-05	2.84E-02	0.583	0.563	0.020
cg14219900	2.81E-05	2.01E-02	0.407	0.382	0.026
cg12680326	1.28E-04	3.98E-02	0.071	0.066	0.005
cg00227156	2.26E-06	6.04E-03	0.080	0.070	0.010
cg25353064	1.36E-05	1.36E-02	0.857	0.847	0.010
cg16418105	9.31E-06	1.12E-02	0.764	0.736	0.028
cg21257581	8.05E-06	1.07E-02	0.730	0.714	0.016
cg24033103	2.53E-05	1.91E-02	0.829	0.804	0.026
cg04785587	7.12E-06	1.01E-02	0.778	0.752	0.027
cg27295595	5.98E-06	9.66E-03	0.535	0.501	0.035
cg08039322	2.03E-05	1.71E-02	0.082	0.075	0.007
cg25799797	1.15E-05	1.26E-02	0.746	0.719	0.027
cg10078335	8.90E-06	1.10E-02	0.796	0.737	0.059
cg05358814	8.79E-06	1.09E-02	0.053	0.042	0.010
cg08589214	5.62E-06	9.53E-03	0.834	0.797	0.037
cg27438218	3.99E-05	2.39E-02	0.588	0.560	0.028
cg09084256	4.15E-05	2.43E-02	0.484	0.465	0.019
cg00736201	1.31E-04	4.02E-02	0.909	0.901	0.008
cg17163363	1.03E-04	3.59E-02	0.303	0.280	0.022
cg01216369	2.27E-05	1.82E-02	0.878	0.864	0.014
cg10209089	9.99E-06	1.15E-02	0.525	0.505	0.019
cg14228272	1.76E-05	1.61E-02	0.644	0.617	0.027
cg02411950	1.09E-04	3.68E-02	0.088	0.080	0.008

Probe	p-value	FDR	Mean beta FASD	Mean beta Control	Δbeta
cg22940961	5.06E-05	2.64E-02	0.913	0.906	0.007
cg08796706	8.49E-05	3.33E-02	0.829	0.808	0.021
cg24127414	3.83E-05	2.35E-02	0.694	0.655	0.040
cg27129048	4.58E-06	8.48E-03	0.699	0.675	0.024
cg22070991	6.48E-05	2.90E-02	0.117	0.105	0.013
cg05178654	5.79E-05	2.76E-02	0.073	0.065	0.008
cg15032166	2.00E-05	1.71E-02	0.359	0.341	0.018
cg12856447	1.58E-05	1.50E-02	0.135	0.116	0.019
cg12734820	2.14E-05	1.75E-02	0.874	0.814	0.060
cg07626033	3.62E-06	7.65E-03	0.874	0.860	0.014
cg00648582	7.98E-05	3.23E-02	0.947	0.943	0.004
cg15928534	4.85E-05	2.58E-02	0.055	0.051	0.004
cg14841350	5.75E-05	2.76E-02	0.868	0.855	0.013
cg18147104	5.76E-05	2.76E-02	0.927	0.913	0.014
cg14166009	4.50E-05	2.50E-02	0.196	0.174	0.022
cg07723921	1.62E-04	4.45E-02	0.481	0.464	0.017
cg04622001	1.17E-06	4.11E-03	0.462	0.437	0.026
cg12486795	1.77E-04	4.63E-02	0.774	0.735	0.039
cg19037350	5.09E-05	2.65E-02	0.321	0.302	0.019
cg21048669	9.15E-05	3.42E-02	0.440	0.422	0.018
cg16782174	3.48E-05	2.29E-02	0.927	0.922	0.005
cg05813818	7.90E-07	3.47E-03	0.558	0.486	0.071
cg09681675	4.74E-06	8.70E-03	0.757	0.718	0.038
cg08076108	2.78E-05	2.00E-02	0.171	0.156	0.015
cg22672067	6.18E-05	2.83E-02	0.451	0.419	0.032
cg10350263	2.93E-06	6.72E-03	0.375	0.345	0.030
cg25059434	4.29E-05	2.47E-02	0.898	0.885	0.012
cg21857190	3.29E-05	2.21E-02	0.616	0.577	0.039
cg18489195	3.96E-05	2.39E-02	0.134	0.119	0.015
cg18054674	8.66E-11	1.97E-05	0.479	0.436	0.043
cg18865832	1.34E-05	1.36E-02	0.826	0.805	0.022
cg27384070	7.33E-06	1.02E-02	0.777	0.760	0.017
cg13712818	5.49E-06	9.48E-03	0.649	0.619	0.030
cg25182501	1.30E-04	4.01E-02	0.907	0.899	0.007
cg22702960	1.06E-04	3.64E-02	0.899	0.887	0.012
cg02666302	1.20E-04	3.85E-02	0.481	0.459	0.022
cg14379630	1.35E-05	1.36E-02	0.095	0.083	0.012
cg02858267	2.79E-05	2.00E-02	0.749	0.719	0.030
cg06913501	7.64E-06	1.04E-02	0.074	0.069	0.005
cg21117330	2.46E-07	2.19E-03	0.422	0.376	0.046

Probe	p-value	FDR	Mean beta FASD	Mean beta Control	Δbeta
cg14905731	7.70E-05	3.16E-02	0.902	0.890	0.012
cg20138186	3.35E-05	2.24E-02	0.749	0.730	0.019
cg21040775	7.70E-06	1.04E-02	0.227	0.203	0.024
cg07324496	1.41E-04	4.13E-02	0.694	0.651	0.044
cg09229169	1.53E-04	4.30E-02	0.847	0.839	0.007
cg01181415	3.49E-05	2.29E-02	0.309	0.294	0.016
cg06114363	5.33E-05	2.70E-02	0.846	0.830	0.016
cg01595666	9.21E-05	3.43E-02	0.622	0.606	0.015
cg16006738	8.66E-05	3.36E-02	0.753	0.737	0.016
cg25075776	1.14E-04	3.75E-02	0.654	0.628	0.025
cg05477514	1.94E-04	4.86E-02	0.134	0.126	0.009
cg01578398	4.86E-05	2.58E-02	0.139	0.131	0.008
cg20254763	1.38E-04	4.12E-02	0.724	0.699	0.026
cg26416341	6.57E-05	2.91E-02	0.067	0.059	0.008
cg16904330	9.04E-05	3.41E-02	0.612	0.592	0.021
cg00202441	1.78E-04	4.65E-02	0.268	0.251	0.017
cg12014113	1.00E-05	1.15E-02	0.889	0.879	0.010
cg13416249	2.12E-06	5.88E-03	0.817	0.766	0.051
cg09879382	1.99E-04	4.92E-02	0.766	0.738	0.029
cg14898768	5.21E-05	2.68E-02	0.843	0.826	0.017
cg01346077	2.03E-05	1.71E-02	0.122	0.107	0.015
cg00690809	7.75E-05	3.17E-02	0.749	0.728	0.021
cg03465782	8.95E-05	3.40E-02	0.022	0.020	0.002
cg02580969	6.17E-05	2.83E-02	0.707	0.690	0.017
cg03318904	4.55E-05	2.52E-02	0.572	0.556	0.016
cg05938607	5.03E-05	2.64E-02	0.627	0.598	0.028
cg16567202	6.82E-05	2.98E-02	0.823	0.812	0.012
cg13521077	1.35E-05	1.36E-02	0.757	0.734	0.023
cg07377907	8.87E-05	3.39E-02	0.809	0.794	0.015
cg09176023	1.39E-04	4.13E-02	0.822	0.788	0.033
cg25600027	4.78E-05	2.57E-02	0.045	0.041	0.004
cg26656658	1.88E-04	4.81E-02	0.798	0.777	0.022
cg11262093	8.39E-06	1.08E-02	0.859	0.847	0.012
cg11210069	4.03E-05	2.40E-02	0.700	0.674	0.026
cg10824677	1.20E-04	3.85E-02	0.911	0.901	0.010
cg12768523	2.03E-05	1.71E-02	0.666	0.640	0.025
cg05627398	3.71E-07	2.44E-03	0.663	0.635	0.028
cg20699141	1.47E-04	4.23E-02	0.480	0.459	0.021
cg08019384	1.56E-04	4.36E-02	0.701	0.676	0.025
cg21222426	4.29E-05	2.47E-02	0.183	0.166	0.017

Probe	p-value	FDR	Mean beta FASD	Mean beta Control	Δbeta
cg25842763	1.01E-04	3.56E-02	0.903	0.890	0.012
cg07880854	8.08E-06	1.07E-02	0.201	0.178	0.023
cg13502252	1.38E-04	4.12E-02	0.772	0.756	0.016
cg00408773	6.89E-05	3.00E-02	0.408	0.387	0.021
cg00063773	6.14E-05	2.83E-02	0.424	0.398	0.026
cg08108641	5.80E-05	2.76E-02	0.788	0.767	0.021
cg26880735	6.13E-06	9.73E-03	0.517	0.467	0.050
cg26723162	4.00E-05	2.39E-02	0.389	0.370	0.019
cg12008047	7.44E-05	3.11E-02	0.891	0.879	0.012
cg04234014	8.87E-05	3.39E-02	0.748	0.729	0.019
cg12285605	7.00E-06	1.00E-02	0.776	0.750	0.026
cg18237551	3.54E-05	2.30E-02	0.095	0.087	0.008
cg19748485	9.97E-05	3.55E-02	0.389	0.369	0.020
cg00956573	1.96E-04	4.89E-02	0.080	0.075	0.005
cg07251128	5.22E-05	2.68E-02	0.844	0.832	0.012
cg27151362	1.83E-05	1.63E-02	0.456	0.438	0.017
cg02760112	1.16E-05	1.26E-02	0.100	0.090	0.010
cg07830534	8.32E-05	3.30E-02	0.929	0.921	0.008
cg11944462	1.91E-04	4.83E-02	0.723	0.695	0.027
cg17059564	5.81E-07	2.84E-03	0.843	0.821	0.023
cg05491767	6.04E-05	2.80E-02	0.777	0.751	0.026
cg15734436	7.63E-05	3.14E-02	0.392	0.360	0.032
cg21462934	7.01E-06	1.00E-02	0.871	0.850	0.021
cg21030607	1.41E-04	4.14E-02	0.747	0.714	0.033
cg03359468	6.28E-05	2.86E-02	0.098	0.091	0.007
cg04009441	1.37E-04	4.11E-02	0.670	0.647	0.023
cg02773588	8.08E-05	3.25E-02	0.709	0.685	0.024
cg17914838	1.10E-04	3.68E-02	0.875	0.855	0.020
cg15023038	1.50E-04	4.26E-02	0.855	0.839	0.016
cg26614816	1.27E-04	3.96E-02	0.114	0.102	0.012
cg23978358	4.19E-05	2.45E-02	0.832	0.819	0.014
cg20306534	1.04E-04	3.62E-02	0.945	0.940	0.004
cg21051972	7.68E-06	1.04E-02	0.113	0.101	0.012
cg21785245	9.32E-05	3.45E-02	0.862	0.841	0.021
cg21225504	1.82E-04	4.70E-02	0.855	0.842	0.012
cg15636421	1.16E-04	3.78E-02	0.530	0.503	0.027
cg04180046	2.21E-07	2.12E-03	0.230	0.203	0.027
cg09436545	2.48E-05	1.88E-02	0.550	0.509	0.041
cg08388455	7.04E-05	3.01E-02	0.592	0.573	0.018
cg04089332	1.47E-04	4.22E-02	0.604	0.590	0.014

Probe	p-value	FDR	Mean beta FASD	Mean beta Control	Δbeta
cg12333845	3.62E-06	7.65E-03	0.511	0.485	0.026
cg02163378	4.70E-05	2.55E-02	0.637	0.609	0.028
cg21324308	2.05E-05	1.72E-02	0.734	0.712	0.022
cg09761265	9.43E-05	3.46E-02	0.786	0.766	0.019
cg21591807	5.44E-06	9.48E-03	0.874	0.861	0.013
cg23492399	5.18E-05	2.68E-02	0.151	0.127	0.025
cg03670369	7.14E-05	3.04E-02	0.961	0.956	0.004
cg02527881	9.91E-05	3.55E-02	0.630	0.585	0.045
cg00246301	1.28E-04	3.97E-02	0.915	0.906	0.010
cg18082362	5.40E-05	2.71E-02	0.234	0.216	0.019
cg05115862	1.93E-04	4.85E-02	0.884	0.860	0.024
cg02376887	7.56E-05	3.13E-02	0.861	0.843	0.018
cg14724749	1.44E-04	4.17E-02	0.449	0.413	0.036
cg10598595	1.02E-04	3.57E-02	0.043	0.039	0.004
cg05435295	7.66E-05	3.15E-02	0.630	0.612	0.018
cg20821838	1.65E-04	4.48E-02	0.906	0.894	0.012
cg09511421	7.32E-05	3.09E-02	0.346	0.315	0.031
cg16962008	4.51E-05	2.50E-02	0.152	0.138	0.014
cg18920097	1.09E-05	1.22E-02	0.271	0.254	0.017
cg19470832	4.41E-05	2.48E-02	0.780	0.756	0.024
cg15225534	1.43E-04	4.15E-02	0.921	0.915	0.006
cg21496518	5.87E-05	2.77E-02	0.308	0.295	0.013
cg10755035	1.25E-04	3.93E-02	0.470	0.447	0.023
cg26487259	1.73E-05	1.60E-02	0.689	0.644	0.044
cg11552868	1.11E-04	3.71E-02	0.785	0.768	0.017
cg19734433	1.00E-04	3.56E-02	0.566	0.539	0.027
cg20130789	1.20E-04	3.85E-02	0.916	0.904	0.012
cg20360285	1.40E-04	4.13E-02	0.845	0.834	0.011
cg27100140	4.22E-05	2.45E-02	0.498	0.480	0.018
cg20524128	4.29E-05	2.47E-02	0.194	0.182	0.012
cg23228529	5.43E-05	2.71E-02	0.341	0.276	0.065
cg10930290	1.70E-04	4.54E-02	0.799	0.778	0.021
cg22132788	8.87E-05	3.39E-02	0.295	0.261	0.034
cg05834603	1.15E-04	3.76E-02	0.848	0.835	0.013
cg03584351	1.81E-04	4.69E-02	0.678	0.650	0.028
cg06711175	1.07E-05	1.20E-02	0.663	0.639	0.024
cg15497724	1.75E-04	4.61E-02	0.748	0.713	0.035
cg12559474	2.01E-04	4.94E-02	0.648	0.622	0.026
cg22455271	9.64E-05	3.51E-02	0.735	0.712	0.023
cg03062564	2.68E-07	2.21E-03	0.164	0.144	0.020

Probe	p-value	FDR	Mean beta FASD	Mean beta Control	Δbeta
cg00812096	1.22E-04	3.87E-02	0.751	0.729	0.022
cg22924796	2.09E-05	1.73E-02	0.894	0.876	0.018
cg27370131	4.15E-05	2.43E-02	0.070	0.063	0.007
cg02539153	1.92E-04	4.83E-02	0.523	0.488	0.035
cg14204430	4.33E-05	2.47E-02	0.577	0.549	0.028
cg03667083	2.12E-05	1.75E-02	0.672	0.649	0.024
cg08268892	1.26E-04	3.94E-02	0.852	0.840	0.012
cg04450459	3.63E-05	2.31E-02	0.311	0.279	0.032
cg21481662	9.74E-05	3.53E-02	0.073	0.068	0.005
cg03829194	1.80E-04	4.67E-02	0.244	0.231	0.013
cg19100988	1.86E-04	4.76E-02	0.598	0.579	0.019
cg14827832	8.62E-06	1.09E-02	0.583	0.563	0.020
cg10831285	2.64E-05	1.95E-02	0.617	0.590	0.027
cg01353941	2.04E-04	4.98E-02	0.829	0.802	0.027
cg25967612	1.69E-04	4.52E-02	0.835	0.817	0.018
cg11024687	6.78E-05	2.97E-02	0.728	0.708	0.020
cg15484354	1.61E-04	4.43E-02	0.865	0.852	0.013
cg01787574	3.73E-05	2.33E-02	0.281	0.261	0.021
cg13118072	1.96E-04	4.88E-02	0.063	0.058	0.005
cg10135520	2.04E-04	4.98E-02	0.054	0.048	0.006
cg11353300	1.21E-04	3.85E-02	0.860	0.850	0.011
cg23348582	9.13E-05	3.42E-02	0.337	0.326	0.011
cg02139853	2.03E-04	4.98E-02	0.854	0.843	0.011
cg11663289	5.35E-07	2.84E-03	0.130	0.121	0.009
cg08289525	5.09E-07	2.78E-03	0.658	0.631	0.027
cg23930711	2.74E-07	2.21E-03	0.192	0.169	0.023
cg04417556	6.24E-05	2.84E-02	0.081	0.075	0.005
cg03817911	1.16E-04	3.77E-02	0.068	0.062	0.006
cg03357547	4.42E-06	8.48E-03	0.440	0.413	0.026
cg13010014	4.88E-06	8.81E-03	0.498	0.468	0.029
cg09914773	1.21E-05	1.30E-02	0.661	0.636	0.024
cg05389922	5.43E-05	2.71E-02	0.351	0.338	0.013
cg22573118	7.89E-05	3.21E-02	0.926	0.920	0.006
cg03625515	6.25E-06	9.73E-03	0.784	0.769	0.015
cg27105390	1.14E-04	3.75E-02	0.301	0.284	0.017
cg21838625	9.78E-05	3.53E-02	0.340	0.321	0.019
cg03032816	4.88E-05	2.58E-02	0.919	0.910	0.010
cg13785189	8.51E-05	3.34E-02	0.051	0.046	0.005
cg01134643	1.51E-04	4.27E-02	0.838	0.822	0.016
cg13485320	1.71E-09	1.45E-04	0.252	0.291	-0.039

Probe	p-value	FDR	Mean beta FASD	Mean beta Control	Δbeta
cg01031400	4.23E-09	2.85E-04	0.104	0.117	-0.013
cg02822788	9.85E-09	4.35E-04	0.435	0.477	-0.042
cg11900509	1.18E-08	4.35E-04	0.778	0.821	-0.042
cg01628053	2.07E-08	6.45E-04	0.652	0.704	-0.052
cg19566764	2.74E-08	6.92E-04	0.115	0.130	-0.016
cg15527515	4.26E-08	9.55E-04	0.165	0.214	-0.049
cg20307184	4.07E-08	9.55E-04	0.574	0.629	-0.055
cg13423554	5.17E-08	1.10E-03	0.121	0.147	-0.027
cg09245003	6.33E-08	1.28E-03	0.852	0.877	-0.025
cg23190089	8.73E-08	1.41E-03	0.624	0.663	-0.040
cg03919488	9.20E-08	1.43E-03	0.155	0.199	-0.044
cg14219124	1.02E-07	1.47E-03	0.061	0.073	-0.013
cg09939948	1.36E-07	1.60E-03	0.069	0.081	-0.012
cg05767421	1.43E-07	1.60E-03	0.165	0.186	-0.022
cg10944833	1.43E-07	1.60E-03	0.442	0.486	-0.044
cg13323489	1.57E-07	1.63E-03	0.649	0.674	-0.025
cg03663556	1.55E-07	1.63E-03	0.305	0.348	-0.043
cg08580187	2.28E-07	2.14E-03	0.769	0.792	-0.023
cg04134048	3.11E-07	2.41E-03	0.067	0.075	-0.008
cg24218620	3.16E-07	2.41E-03	0.248	0.279	-0.031
cg11966524	4.28E-07	2.44E-03	0.776	0.795	-0.020
cg09345786	3.93E-07	2.44E-03	0.446	0.477	-0.031
cg13075295	4.09E-07	2.44E-03	0.144	0.177	-0.033
cg04195855	4.04E-07	2.44E-03	0.196	0.261	-0.064
cg24033661	4.50E-07	2.53E-03	0.539	0.585	-0.046
cg21853021	4.67E-07	2.59E-03	0.341	0.390	-0.049
cg09654116	5.62E-07	2.84E-03	0.569	0.612	-0.043
cg09292069	5.86E-07	2.84E-03	0.704	0.735	-0.031
cg06711306	5.95E-07	2.84E-03	0.541	0.583	-0.042
cg25702651	6.47E-07	2.97E-03	0.250	0.335	-0.085
cg06382028	6.41E-07	2.97E-03	0.329	0.451	-0.122
cg24292665	7.71E-07	3.42E-03	0.357	0.383	-0.026
cg11953516	8.02E-07	3.48E-03	0.681	0.706	-0.026
cg00939684	9.75E-07	3.93E-03	0.768	0.785	-0.017
cg10537821	9.75E-07	3.93E-03	0.845	0.866	-0.021
cg11130630	1.04E-06	3.96E-03	0.673	0.711	-0.038
cg17098979	1.16E-06	4.11E-03	0.809	0.831	-0.022
cg05512869	1.29E-06	4.33E-03	0.680	0.718	-0.037
cg25949338	1.33E-06	4.33E-03	0.398	0.457	-0.059
cg20684180	1.40E-06	4.50E-03	0.110	0.126	-0.015

Probe	p-value	FDR	Mean beta FASD	Mean beta Control	Δbeta
cg01715680	1.54E-06	4.76E-03	0.646	0.687	-0.040
cg16072777	1.53E-06	4.76E-03	0.136	0.216	-0.080
cg19995899	1.70E-06	5.05E-03	0.860	0.884	-0.024
cg00371301	1.89E-06	5.50E-03	0.949	0.954	-0.005
cg27298830	1.97E-06	5.57E-03	0.862	0.883	-0.021
cg20703671	2.14E-06	5.88E-03	0.431	0.449	-0.017
cg02207200	2.23E-06	6.04E-03	0.090	0.112	-0.022
cg10070864	2.33E-06	6.19E-03	0.438	0.490	-0.052
cg07386859	2.49E-06	6.43E-03	0.851	0.874	-0.022
cg06297194	2.59E-06	6.46E-03	0.862	0.886	-0.024
cg23976431	2.55E-06	6.46E-03	0.472	0.503	-0.031
cg14195115	2.69E-06	6.49E-03	0.510	0.557	-0.047
cg04398451	2.73E-06	6.49E-03	0.796	0.855	-0.059
cg07927540	2.71E-06	6.49E-03	0.221	0.280	-0.059
cg19872095	2.81E-06	6.57E-03	0.603	0.641	-0.038
cg04099543	2.86E-06	6.64E-03	0.659	0.685	-0.026
cg04760708	3.06E-06	6.87E-03	0.852	0.872	-0.021
cg18064714	3.10E-06	6.92E-03	0.098	0.112	-0.015
cg08857221	3.14E-06	6.96E-03	0.615	0.657	-0.042
cg13916255	3.84E-06	8.08E-03	0.529	0.590	-0.061
cg17970176	3.94E-06	8.20E-03	0.739	0.769	-0.029
cg09245872	4.02E-06	8.21E-03	0.680	0.697	-0.018
cg01895612	4.01E-06	8.21E-03	0.724	0.751	-0.027
cg26112661	3.99E-06	8.21E-03	0.205	0.247	-0.041
cg23588928	4.11E-06	8.30E-03	0.909	0.921	-0.012
cg00588297	4.27E-06	8.45E-03	0.509	0.538	-0.029
cg14054283	4.31E-06	8.46E-03	0.352	0.397	-0.045
cg08570472	4.41E-06	8.48E-03	0.476	0.526	-0.050
cg17995197	4.54E-06	8.48E-03	0.463	0.519	-0.057
cg23948825	4.80E-06	8.73E-03	0.898	0.909	-0.011
cg20065463	4.78E-06	8.73E-03	0.163	0.195	-0.032
cg27118929	4.87E-06	8.81E-03	0.800	0.824	-0.024
cg12692682	5.87E-06	9.66E-03	0.629	0.662	-0.033
cg10707081	6.21E-06	9.73E-03	0.704	0.739	-0.034
cg17496887	6.08E-06	9.73E-03	0.759	0.800	-0.040
cg00077566	6.30E-06	9.73E-03	0.909	0.955	-0.046
cg00092400	6.42E-06	9.78E-03	0.623	0.656	-0.032
cg03757387	6.42E-06	9.78E-03	0.479	0.537	-0.058
cg02704570	6.53E-06	9.83E-03	0.733	0.749	-0.016
cg22893791	6.73E-06	9.94E-03	0.378	0.429	-0.051

Probe	p-value	FDR	Mean beta FASD	Mean beta Control	Δbeta
cg22283925	6.90E-06	1.00E-02	0.412	0.434	-0.022
cg22338356	6.87E-06	1.00E-02	0.509	0.555	-0.046
cg10238145	7.06E-06	1.00E-02	0.487	0.527	-0.040
cg06864895	7.76E-06	1.05E-02	0.200	0.239	-0.039
cg03230711	8.13E-06	1.07E-02	0.079	0.095	-0.016
cg18681352	7.99E-06	1.07E-02	0.195	0.214	-0.019
cg20961387	8.18E-06	1.07E-02	0.650	0.673	-0.023
cg08621957	8.19E-06	1.07E-02	0.503	0.542	-0.039
cg15867428	8.49E-06	1.08E-02	0.128	0.144	-0.016
cg16848712	8.75E-06	1.09E-02	0.241	0.260	-0.019
cg17198772	9.33E-06	1.12E-02	0.776	0.799	-0.023
cg17343167	9.29E-06	1.12E-02	0.431	0.461	-0.030
cg13055001	1.03E-05	1.16E-02	0.228	0.253	-0.025
cg04108939	1.10E-05	1.23E-02	0.076	0.083	-0.007
cg03583111	1.16E-05	1.26E-02	0.394	0.426	-0.032
cg26821681	1.16E-05	1.26E-02	0.573	0.606	-0.032
cg23069297	1.15E-05	1.26E-02	0.762	0.837	-0.075
cg05249460	1.23E-05	1.31E-02	0.771	0.791	-0.020
cg23586138	1.23E-05	1.31E-02	0.426	0.461	-0.035
cg07519373	1.24E-05	1.32E-02	0.711	0.757	-0.045
cg18235690	1.28E-05	1.35E-02	0.387	0.414	-0.027
cg01099220	1.34E-05	1.36E-02	0.124	0.141	-0.017
cg11737831	1.35E-05	1.36E-02	0.302	0.320	-0.018
cg17491622	1.32E-05	1.36E-02	0.260	0.287	-0.027
cg11335335	1.33E-05	1.36E-02	0.437	0.492	-0.056
cg19273668	1.36E-05	1.36E-02	0.938	0.944	-0.006
cg14387743	1.44E-05	1.41E-02	0.320	0.364	-0.044
cg24640156	1.50E-05	1.44E-02	0.768	0.830	-0.062
cg07266431	1.58E-05	1.50E-02	0.518	0.550	-0.032
cg26523175	1.61E-05	1.51E-02	0.301	0.350	-0.049
cg17121120	1.77E-05	1.62E-02	0.065	0.073	-0.007
cg20164964	1.81E-05	1.63E-02	0.318	0.354	-0.036
cg00625443	1.94E-05	1.68E-02	0.921	0.930	-0.009
cg26371345	1.96E-05	1.68E-02	0.332	0.389	-0.057
cg22767461	2.06E-05	1.72E-02	0.721	0.750	-0.028
cg23987134	2.09E-05	1.73E-02	0.704	0.733	-0.030
cg07527324	2.13E-05	1.75E-02	0.844	0.857	-0.013
cg15835339	2.21E-05	1.79E-02	0.825	0.847	-0.022
cg02467382	2.29E-05	1.82E-02	0.871	0.884	-0.014
cg08072217	2.28E-05	1.82E-02	0.466	0.503	-0.038

Probe	p-value	FDR	Mean beta FASD	Mean beta Control	Δbeta
cg08244301	2.30E-05	1.83E-02	0.729	0.743	-0.014
cg12604031	2.31E-05	1.83E-02	0.459	0.493	-0.034
cg12386061	2.35E-05	1.84E-02	0.094	0.107	-0.012
cg06261066	2.43E-05	1.87E-02	0.621	0.658	-0.037
cg01479187	2.63E-05	1.94E-02	0.100	0.115	-0.015
cg06943912	2.68E-05	1.96E-02	0.647	0.696	-0.050
cg04609875	2.84E-05	2.01E-02	0.636	0.664	-0.028
cg17132030	2.83E-05	2.01E-02	0.387	0.421	-0.035
cg18458509	2.86E-05	2.02E-02	0.772	0.797	-0.025
cg26470501	2.91E-05	2.05E-02	0.337	0.363	-0.026
cg26369418	2.98E-05	2.09E-02	0.762	0.781	-0.019
cg16046375	3.05E-05	2.13E-02	0.782	0.798	-0.016
cg11710912	3.11E-05	2.14E-02	0.219	0.240	-0.021
cg04656451	3.14E-05	2.16E-02	0.563	0.604	-0.041
cg05645661	3.21E-05	2.19E-02	0.837	0.851	-0.014
cg07043604	3.28E-05	2.21E-02	0.393	0.430	-0.037
cg04787675	3.39E-05	2.24E-02	0.090	0.100	-0.010
cg13430464	3.50E-05	2.29E-02	0.171	0.198	-0.027
cg17386185	3.51E-05	2.29E-02	0.098	0.109	-0.011
cg03626746	3.55E-05	2.30E-02	0.950	0.954	-0.005
cg02855981	3.55E-05	2.30E-02	0.926	0.933	-0.007
cg17342588	3.60E-05	2.30E-02	0.107	0.120	-0.013
cg27592868	3.58E-05	2.30E-02	0.529	0.554	-0.025
cg23617193	3.64E-05	2.31E-02	0.252	0.283	-0.030
cg25963822	3.76E-05	2.33E-02	0.056	0.062	-0.006
cg23476401	3.73E-05	2.33E-02	0.773	0.803	-0.030
cg15044041	3.69E-05	2.33E-02	0.572	0.604	-0.032
cg19697239	3.80E-05	2.35E-02	0.096	0.109	-0.013
cg21931938	3.81E-05	2.35E-02	0.740	0.755	-0.015
cg16439948	3.84E-05	2.35E-02	0.069	0.078	-0.009
cg02860108	3.85E-05	2.36E-02	0.896	0.904	-0.008
cg06814616	3.88E-05	2.36E-02	0.451	0.478	-0.027
cg01855013	3.90E-05	2.37E-02	0.362	0.379	-0.018
cg01746878	4.11E-05	2.42E-02	0.938	0.945	-0.006
cg17787876	4.11E-05	2.42E-02	0.386	0.415	-0.029
cg08506585	4.20E-05	2.45E-02	0.896	0.914	-0.018
cg04037470	4.22E-05	2.45E-02	0.053	0.062	-0.009
cg04215256	4.33E-05	2.47E-02	0.046	0.053	-0.007
cg27300742	4.36E-05	2.47E-02	0.854	0.872	-0.018
cg25670376	4.49E-05	2.50E-02	0.469	0.498	-0.029

Probe	p-value	FDR	Mean beta FASD	Mean beta Control	Δbeta
cg13439596	4.60E-05	2.52E-02	0.271	0.286	-0.015
cg04420752	4.61E-05	2.52E-02	0.877	0.900	-0.022
cg26932623	4.63E-05	2.52E-02	0.622	0.657	-0.035
cg11274371	4.68E-05	2.55E-02	0.085	0.096	-0.011
cg20359202	4.82E-05	2.58E-02	0.461	0.494	-0.033
cg06747543	4.83E-05	2.58E-02	0.163	0.197	-0.035
cg01439568	4.99E-05	2.63E-02	0.777	0.796	-0.019
cg21202862	5.22E-05	2.68E-02	0.910	0.917	-0.007
cg15026243	5.31E-05	2.70E-02	0.797	0.817	-0.020
cg20366110	5.28E-05	2.70E-02	0.544	0.570	-0.027
cg05769975	5.33E-05	2.70E-02	0.823	0.835	-0.012
cg26373071	5.38E-05	2.71E-02	0.852	0.867	-0.015
cg24630957	5.40E-05	2.71E-02	0.721	0.742	-0.021
cg02342791	5.44E-05	2.71E-02	0.276	0.310	-0.034
cg25954235	5.42E-05	2.71E-02	0.337	0.398	-0.060
cg08062387	5.63E-05	2.76E-02	0.694	0.728	-0.034
cg02030270	5.76E-05	2.76E-02	0.936	0.944	-0.008
cg09847753	5.80E-05	2.76E-02	0.105	0.116	-0.012
cg23237801	5.83E-05	2.76E-02	0.492	0.515	-0.023
cg26340050	5.71E-05	2.76E-02	0.616	0.644	-0.029
cg20876010	5.83E-05	2.76E-02	0.349	0.381	-0.032
cg04380576	5.81E-05	2.76E-02	0.539	0.571	-0.032
cg24927800	5.70E-05	2.76E-02	0.182	0.217	-0.035
cg00689651	5.95E-05	2.78E-02	0.051	0.057	-0.007
cg02413040	5.94E-05	2.78E-02	0.091	0.109	-0.018
cg09386376	5.92E-05	2.78E-02	0.596	0.651	-0.055
cg08376368	5.97E-05	2.79E-02	0.045	0.050	-0.005
cg05210798	6.00E-05	2.79E-02	0.064	0.072	-0.007
cg12438037	6.03E-05	2.80E-02	0.470	0.492	-0.022
cg04831327	6.06E-05	2.81E-02	0.817	0.840	-0.023
cg15887927	6.26E-05	2.85E-02	0.120	0.143	-0.023
cg02770683	6.31E-05	2.86E-02	0.950	0.954	-0.004
cg02512395	6.39E-05	2.88E-02	0.918	0.924	-0.006
cg00153543	6.41E-05	2.89E-02	0.526	0.560	-0.034
cg07107130	6.45E-05	2.90E-02	0.555	0.579	-0.024
cg18419977	6.47E-05	2.90E-02	0.713	0.741	-0.029
cg27110491	6.56E-05	2.91E-02	0.612	0.646	-0.034
cg13294084	6.73E-05	2.96E-02	0.878	0.907	-0.029
cg18182475	7.00E-05	3.01E-02	0.874	0.889	-0.014
cg18362003	6.97E-05	3.01E-02	0.843	0.860	-0.017

Probe	p-value	FDR	Mean beta FASD	Mean beta Control	Δbeta
cg05539265	6.99E-05	3.01E-02	0.762	0.802	-0.040
cg11107212	7.22E-05	3.06E-02	0.116	0.132	-0.016
cg03888765	7.40E-05	3.10E-02	0.970	0.972	-0.002
cg21008530	7.43E-05	3.10E-02	0.613	0.651	-0.038
cg27413421	7.73E-05	3.17E-02	0.730	0.748	-0.018
cg01291665	8.02E-05	3.24E-02	0.551	0.586	-0.035
cg17654567	8.04E-05	3.25E-02	0.897	0.907	-0.010
cg21563683	8.05E-05	3.25E-02	0.166	0.195	-0.029
cg24351857	8.15E-05	3.27E-02	0.133	0.141	-0.008
cg17324128	8.14E-05	3.27E-02	0.437	0.459	-0.021
cg08598287	8.19E-05	3.28E-02	0.688	0.707	-0.019
cg05206657	8.36E-05	3.30E-02	0.925	0.931	-0.006
cg04730355	8.35E-05	3.30E-02	0.151	0.178	-0.027
cg00686823	8.35E-05	3.30E-02	0.545	0.584	-0.039
cg20335425	8.44E-05	3.32E-02	0.301	0.330	-0.029
cg13625026	8.46E-05	3.32E-02	0.494	0.514	-0.020
cg13675051	8.53E-05	3.34E-02	0.733	0.760	-0.027
cg00945507	8.58E-05	3.36E-02	0.193	0.224	-0.030
cg11500660	8.66E-05	3.36E-02	0.044	0.048	-0.004
cg23358740	8.65E-05	3.36E-02	0.095	0.109	-0.014
cg17559809	8.71E-05	3.37E-02	0.104	0.117	-0.013
cg01074767	8.80E-05	3.38E-02	0.485	0.520	-0.035
cg22495058	9.04E-05	3.41E-02	0.473	0.494	-0.020
cg20143982	9.60E-05	3.51E-02	0.089	0.097	-0.008
cg12593541	9.76E-05	3.53E-02	0.176	0.208	-0.032
cg01784614	9.90E-05	3.55E-02	0.424	0.453	-0.029
cg02988698	9.93E-05	3.55E-02	0.124	0.150	-0.026
cg04060128	9.95E-05	3.55E-02	0.163	0.186	-0.023
cg23203302	1.01E-04	3.56E-02	0.882	0.891	-0.009
cg15825321	1.01E-04	3.56E-02	0.603	0.637	-0.034
cg10001715	1.02E-04	3.57E-02	0.850	0.862	-0.012
cg25230117	1.03E-04	3.59E-02	0.513	0.538	-0.026
cg06749854	1.06E-04	3.63E-02	0.735	0.752	-0.016
cg09412782	1.06E-04	3.64E-02	0.951	0.955	-0.005
cg14321284	1.06E-04	3.64E-02	0.494	0.514	-0.020
cg23495441	1.07E-04	3.65E-02	0.927	0.933	-0.006
cg01091565	1.07E-04	3.65E-02	0.468	0.498	-0.030
cg22873986	1.10E-04	3.68E-02	0.936	0.941	-0.006
cg07440826	1.10E-04	3.68E-02	0.083	0.091	-0.009
cg18776287	1.10E-04	3.68E-02	0.252	0.276	-0.024

Probe	p-value	FDR	Mean beta FASD	Mean beta Control	Δbeta
cg18153869	1.11E-04	3.70E-02	0.271	0.304	-0.033
cg03221025	1.11E-04	3.70E-02	0.760	0.775	-0.015
cg00756748	1.13E-04	3.73E-02	0.873	0.887	-0.013
cg01359236	1.13E-04	3.73E-02	0.191	0.205	-0.014
cg24330379	1.13E-04	3.74E-02	0.479	0.498	-0.019
cg05881135	1.15E-04	3.77E-02	0.171	0.197	-0.026
cg09187107	1.19E-04	3.84E-02	0.840	0.850	-0.010
cg00360077	1.19E-04	3.84E-02	0.678	0.722	-0.043
cg00839333	1.20E-04	3.85E-02	0.788	0.833	-0.045
cg25306006	1.22E-04	3.87E-02	0.785	0.798	-0.012
cg08864105	1.24E-04	3.90E-02	0.342	0.377	-0.035
cg06327965	1.26E-04	3.95E-02	0.226	0.243	-0.017
cg18728780	1.30E-04	4.01E-02	0.668	0.690	-0.022
cg26621408	1.34E-04	4.06E-02	0.873	0.882	-0.009
cg24605090	1.34E-04	4.06E-02	0.664	0.683	-0.019
cg07343703	1.35E-04	4.08E-02	0.659	0.681	-0.022
cg27491190	1.36E-04	4.08E-02	0.263	0.296	-0.033
cg25850044	1.39E-04	4.13E-02	0.140	0.155	-0.015
cg16558770	1.40E-04	4.13E-02	0.651	0.675	-0.024
cg26955579	1.40E-04	4.13E-02	0.852	0.863	-0.011
cg07179981	1.40E-04	4.13E-02	0.317	0.345	-0.028
cg00787726	1.42E-04	4.15E-02	0.308	0.336	-0.028
cg04439622	1.44E-04	4.16E-02	0.787	0.805	-0.018
cg13946872	1.44E-04	4.18E-02	0.870	0.880	-0.010
cg24212392	1.46E-04	4.20E-02	0.931	0.936	-0.005
cg17827803	1.46E-04	4.20E-02	0.781	0.799	-0.019
cg23978357	1.48E-04	4.23E-02	0.143	0.162	-0.019
cg08089041	1.50E-04	4.26E-02	0.106	0.127	-0.022
cg03078972	1.50E-04	4.27E-02	0.175	0.187	-0.012
cg14616251	1.50E-04	4.27E-02	0.207	0.224	-0.017
cg21032583	1.52E-04	4.30E-02	0.639	0.676	-0.037
cg26986871	1.54E-04	4.32E-02	0.573	0.611	-0.038
cg07234199	1.57E-04	4.38E-02	0.743	0.764	-0.021
cg23078194	1.57E-04	4.38E-02	0.146	0.159	-0.013
cg01812045	1.58E-04	4.39E-02	0.414	0.431	-0.017
cg18778727	1.58E-04	4.39E-02	0.810	0.825	-0.015
cg09311683	1.59E-04	4.39E-02	0.131	0.154	-0.024
cg15876968	1.60E-04	4.42E-02	0.343	0.369	-0.026
cg09133032	1.62E-04	4.45E-02	0.373	0.443	-0.070
cg09133511	1.64E-04	4.47E-02	0.574	0.595	-0.021

Probe	p-value	FDR	Mean beta FASD	Mean beta Control	Δbeta
cg11895451	1.65E-04	4.47E-02	0.370	0.405	-0.035
cg13109911	1.70E-04	4.52E-02	0.606	0.625	-0.020
cg16985708	1.73E-04	4.60E-02	0.182	0.209	-0.027
cg02510729	1.75E-04	4.61E-02	0.949	0.953	-0.004
ch.1.186147687F	1.77E-04	4.63E-02	0.038	0.044	-0.006
cg20003976	1.77E-04	4.63E-02	0.703	0.723	-0.020
cg16099687	1.77E-04	4.63E-02	0.583	0.624	-0.042
cg08937612	1.79E-04	4.66E-02	0.892	0.902	-0.010
cg04690793	1.82E-04	4.70E-02	0.933	0.938	-0.005
cg14499058	1.83E-04	4.71E-02	0.198	0.214	-0.016
cg05097643	1.83E-04	4.71E-02	0.225	0.247	-0.022
cg18437839	1.90E-04	4.82E-02	0.354	0.379	-0.025
cg19497798	1.90E-04	4.83E-02	0.730	0.747	-0.017
cg22118082	1.91E-04	4.83E-02	0.822	0.844	-0.022
cg22510032	1.91E-04	4.83E-02	0.102	0.113	-0.011
cg23406407	1.94E-04	4.86E-02	0.622	0.648	-0.025
cg23555395	1.95E-04	4.87E-02	0.610	0.638	-0.028
cg09278098	1.96E-04	4.89E-02	0.462	0.490	-0.027
cg15678825	2.00E-04	4.94E-02	0.200	0.245	-0.045
cg20694545	2.05E-04	5.00E-02	0.815	0.849	-0.033
cg20511832	2.05E-04	5.00E-02	0.214	0.229	-0.015

Supplementary table 4.2. Differentially methylated genes

EntrezGene ID	HGNC symbol	Direction of change	Alias
154664	ABCA13	DOWN	
34	ACADM	DOWN	
311	ANXA11	DOWN	
312	ANXA13	DOWN	
163	AP2B1	DOWN	
334	APLP2	DOWN	
55082	ARGLU1	DOWN	
57636	ARHGAP23	DOWN	
128272	ARHGEF19	DOWN	
9915	ARNT2	DOWN	
192134	B3GNT6	DOWN	
440465	BAIAP2-AS1	DOWN	FLJ90757
54971	BANP	DOWN	
602	BCL3	DOWN	
266675	BEST4	DOWN	
55727	BTBD7	DOWN	
84419	C15orf48	DOWN	
716	C1S	DOWN	
57685	CACHD1	DOWN	
799	CALCR	DOWN	
84674	CARD6	DOWN	
863	CBFA2T3	DOWN	
79879	CCDC134	DOWN	
54462	CCSER2	DOWN	FAM190B
1021	CDK6	DOWN	
25884	CHRDL2	DOWN	
1143	CHRNB4	DOWN	
81037	CLPTM1L	DOWN	
84570	COL25A1	DOWN	
51200	CPA4	DOWN	
1397	CRIP2	DOWN	
1437	CSF2	DOWN	
10217	CTDSPL	DOWN	
221955	DAGLB	DOWN	
79961	DENND2D	DOWN	
1674	DES	DOWN	
147015	DHRS13	DOWN	
9940	DLEC1	DOWN	
1815	DRD4	DOWN	

EntrezGene ID	HGNC symbol	Direction of change	Alias
10085	EDIL3	DOWN	
30844	EHD4	DOWN	
8178	ELL	DOWN	
55140	ELP3	DOWN	
1969	EPHA2	DOWN	
7957	EPM2A	DOWN	
115704	EVI5L	DOWN	
11336	EXOC3	DOWN	
58489	FAM108C1	DOWN	
57579	FAM135A	DOWN	
115572	FAM46B	DOWN	
2175	FANCA	DOWN	
85302	FBF1	DOWN	
730971	FLJ36777	DOWN	
2335	FN1	DOWN	
2350	FOLR2	DOWN	
442117	GALNTL6	DOWN	
150946	GAREML	DOWN	FAM59B
2646	GCKR	DOWN	
51608	GET4	DOWN	C7orf20
132158	GLYCTK	DOWN	
2783	GNB2	DOWN	
60313	GPBP1L1	DOWN	
9687	GREB1	DOWN	
57822	GRHL3	DOWN	
283120	H19	DOWN	
3029	HAGH	DOWN	
3083	HGFAC	DOWN	
59269	HIVEP3	DOWN	
57594	HOMEZ	DOWN	
3373	HYAL1	DOWN	
3632	INPP5A	DOWN	
25896	INTS7	DOWN	
84223	IQCG	DOWN	
26145	IRF2BP1	DOWN	
93107	KCNG4	DOWN	
27345	KCNMB4	DOWN	
9132	KCNQ4	DOWN	
83892	KCTD10	DOWN	
23325	KIAA1033	DOWN	

EntrezGene ID	HGNC symbol	Direction of change	Alias
57576	KIF17	DOWN	
3797	KIF3C	DOWN	
3827	KNG1	DOWN	
3910	LAMA4	DOWN	
254251	LCORL	DOWN	
145200	LINC00239	DOWN	C14orf72
154822	LINC00689	DOWN	LOC154822
285696	LOC285696	DOWN	
401010	LOC401010	DOWN	
4035	LRP1	DOWN	
9684	LRRC14	DOWN	
79705	LRRK1	DOWN	
284348	LYPD5	DOWN	
8379	MAD1L1	DOWN	
4116	MAGOH	DOWN	
114569	MAL2	DOWN	
54799	MBTD1	DOWN	
4209	MEF2D	DOWN	
4221	MEN1	DOWN	
55897	MESP1	DOWN	
399959	MIR100HG	DOWN	LOC399959
64928	MRPL14	DOWN	
51116	MRPS2	DOWN	
51168	MYO15A	DOWN	
4641	MYO1C	DOWN	
23138	N4BP3	DOWN	
54550	NECAB2	DOWN	
4772	NFATC1	DOWN	
4784	NFIX	DOWN	
4815	NINJ2	DOWN	
23530	NNT	DOWN	
79400	NOX5	DOWN	
9315	NREP	DOWN	C5orf13
9972	NUP153	DOWN	
220064	ORAOV1	DOWN	
114884	OSBPL10	DOWN	
5031	P2RY6	DOWN	
80227	PAAF1	DOWN	
124222	PAQR4	DOWN	
5101	PCDH9	DOWN	

EntrezGene ID	HGNC symbol	Direction of change	Alias
10954	PDIA5	DOWN	
10158	PDZK1IP1	DOWN	
8682	PEA15	DOWN	
5830	PEX5	DOWN	
148479	PHF13	DOWN	
5330	PLCB2	DOWN	
5359	PLSCR1	DOWN	
25953	PNKD	DOWN	
57460	PPM1H	DOWN	
5499	PPP1CA	DOWN	
5591	PRKDC	DOWN	
254427	PROSER2	DOWN	C10orf47
5799	PTPRN2	DOWN	
22821	RASA3	DOWN	
29890	RBM15B	DOWN	
9904	RBM19	DOWN	
54502	RBM47	DOWN	
3516	RBPJ	DOWN	
55920	RCC2	DOWN	
25897	RNF19A	DOWN	
55178	RNMTL1	DOWN	
861	RUNX1	DOWN	
338324	S100A7A	DOWN	
6279	S100A8	DOWN	
60485	SAV1	DOWN	
51435	SCARA3	DOWN	
23480	SEC61G	DOWN	
207107	SFTA1P	DOWN	
6457	SH3GL3	DOWN	
6461	SHB	DOWN	
9120	SLC16A6	DOWN	
5002	SLC22A18	DOWN	
376497	SLC27A1	DOWN	
54407	SLC38A2	DOWN	
57153	SLC44A2	DOWN	
6542	SLC7A2	DOWN	
23428	SLC7A8	DOWN	
54471	SMCR7L	DOWN	
64094	SMOC2	DOWN	
6615	SNAI1	DOWN	

EntrezGene ID	HGNC symbol	Direction of change	Alias
100124539	SNORA11B	DOWN	
677839	SNORA71C	DOWN	
6631	SNRPC	DOWN	
440352	SNX29P2	DOWN	RUNDC2C
221833	SP8	DOWN	
80725	SRCIN1	DOWN	
6430	SRSF5	DOWN	
23336	SYNM	DOWN	
6869	TACR1	DOWN	
7041	TGFB1I1	DOWN	
343641	TGM6	DOWN	
8793	TNFRSF10D	DOWN	
131601	TPRA1	DOWN	
83696	TRAPPC9	DOWN	
10107	TRIM10	DOWN	
10867	TSPAN9	DOWN	
7296	TXNRD1	DOWN	
7326	UBE2G1	DOWN	
7378	UPP1	DOWN	
7384	UQCRC1	DOWN	
55350	VNN3	DOWN	
391123	VSIG8	DOWN	
64856	VWA1	DOWN	
55779	WDR52	DOWN	
51741	WWOX	DOWN	
64131	XYLT1	DOWN	
80149	ZC3H12A	DOWN	
132625	ZFP42	DOWN	
79088	ZNF426	DOWN	
284346	ZNF575	DOWN	
374655	ZNF710	DOWN	
51279	C1RL	INCONSISTENT	
1740	DLG2	INCONSISTENT	
8448	DOC2A	INCONSISTENT	
165545	DQX1	INCONSISTENT	
83937	RASSF4	INCONSISTENT	
105	ADARB2	UP	
221442	ADCY10P1	UP	LOC221442
141	ADPRH	UP	
116987	AGAP1	UP	

EntrezGene ID	HGNC symbol	Direction of change	Alias
26289	AK5	UP	
1109	AKR1C4	UP	
285	ANGPT2	UP	
286	ANK1	UP	
290	ANPEP	UP	
57514	ARHGAP31	UP	CDGAP
9639	ARHGEF10	UP	
57492	ARID1B	UP	
9311	ASIC3	UP	ACCN3
57194	ATP10A	UP	
491	ATP2B2	UP	
10331	B3GNT3	UP	
80114	BICC1	UP	
665	BNIP3L	UP	
6046	BRD2	UP	
153579	BTNL9	UP	
715	C1R	UP	
150297	C22orf42	UP	
255119	C4orf22	UP	
154791	C7orf55	UP	
136288	C7orf57	UP	
773	CACNA1A	UP	
800	CALD1	UP	
813	CALU	UP	
11132	CAPN10	UP	
79587	CARS2	UP	
54897	CASZ1	UP	
126402	CCDC105	UP	
84865	CCDC142	UP	
1232	CCR3	UP	
961	CD47	UP	
993	CDC25A	UP	
1008	CDH10	UP	
1012	CDH13	UP	
1032	CDKN2D	UP	
1951	CELSR3	UP	
11113	CIT	UP	
10143	CLEC3A	UP	
22818	COPZ1	UP	
1353	COX11	UP	

EntrezGene ID	HGNC symbol	Direction of change	Alias
1369	CPN1	UP	
1395	CRHR2	UP	
1523	CUX1	UP	
1576	CYP3A4	UP	
10858	CYP46A1	UP	
54165	DCUN1D1	UP	
1804	DPP6	UP	
493861	EID3	UP	
1995	ELAVL3	UP	
24139	EML2	UP	
957	ENTPD5	UP	
2103	ESRRB	UP	
2113	ETS1	UP	
5393	EXOSC9	UP	
2155	F7	UP	
118670	FAM24A	UP	
129804	FBLN7	UP	
26291	FGF21	UP	
92973	FP588	UP	LOC92973
55691	FRMD4A	UP	
2560	GABRB1	UP	
9518	GDF15	UP	
389400	GFRAL	UP	
100126793	GHRLOS	UP	
57369	GJD2	UP	
2788	GNG7	UP	
2794	GNL1	UP	
257202	GPX6	UP	
2911	GRM1	UP	
2918	GRM8	UP	
2968	GTF2H4	UP	
3038	HAS3	UP	
54919	HEATR2	UP	
220296	HEPACAM	UP	
341208	HEPHL1	UP	
147746	HIPK4	UP	
80201	HKDC1	UP	
284459	HKR1	UP	
3115	HLA-DPB1	UP	
51155	HN1	UP	

EntrezGene ID	HGNC symbol	Direction of change	Alias
7087	ICAM5	UP	
152404	IGSF11	UP	
22997	IGSF9B	UP	
9922	IQSEC1	UP	
8514	KCNAB2	UP	
3752	KCND3	UP	
10984	KCNQ1OT1	UP	
57528	KCTD16	UP	
84634	KISS1R	UP	
162605	KRT28	UP	
144501	KRT80	UP	
3908	LAMA2	UP	
389541	LAMTOR4	UP	C7orf59
51056	LAP3	UP	
9113	LATS1	UP	
353142	LCE3A	UP	
55679	LIMS2	UP	
100133205	LINC00240	UP	C6orf41
283521	LINC00282	UP	FLJ37307
151300	LINC00608	UP	LOC151300
200879	LIPH	UP	
55885	LMO3	UP	
9053	MAP7	UP	
4146	MATN1	UP	
79143	MBOAT7	UP	
693139	MIR554	UP	
693233	MIR648	UP	
54148	MRPL39	UP	
64005	MYO1G	UP	
79923	NANOG	UP	
79804	NBLA00301	UP	
57727	NCOA5	UP	
64579	NDST4	UP	
58158	NEUROD4	UP	
23114	NFASC	UP	
4798	NFRKB	UP	
286183	NKAIN3	UP	
137814	NKX2-6	UP	
129521	NMS	UP	
10874	NMU	UP	

EntrezGene ID	HGNC symbol	Direction of change	Alias
9722	NOS1AP	UP	
55666	NPLOC4	UP	
140767	NRSN1	UP	
9378	NRXN1	UP	
84628	NTNG2	UP	
4948	OCA2	UP	
390201	OR10V1	UP	
255725	OR52B2	UP	
100309464	OTX2-AS1	UP	OTX2OS1
5027	P2RX7	UP	
23022	PALLD	UP	
5066	PAM	UP	
89932	PAPLN	UP	
399968	PATE4	UP	
56134	PCDHAC2	UP	
56125	PCDHB11	UP	
56122	PCDHB14	UP	
57717	PCDHB16	UP	
54660	PCDHB18	UP	
56132	PCDHB3	UP	
56127	PCDHB9	UP	
56111	PCDHGA4	UP	
56110	PCDHGA5	UP	
56109	PCDHGA6	UP	
56108	PCDHGA7	UP	
9708	PCDHGA8	UP	
64773	PCED1A	UP	FAM113A
192111	PGAM5	UP	
168507	PKD1L1	UP	
5357	PLS1	UP	
151742	PPM1L	UP	
100507444	PPP1R2P1	UP	
84432	PROK1	UP	
51334	PRR16	UP	
5745	PTH1R	UP	
55698	RADIL	UP	
23551	RASD2	UP	
55147	RBM23	UP	
5950	RBP4	UP	
57139	RGL3	UP	

EntrezGene ID	HGNC symbol	Direction of change	Alias
56963	RGMA	UP	
64221	ROBO3	UP	
221935	SDK1	UP	
6400	SEL1L	UP	
137868	SGCZ	UP	
9467	SH3BP5	UP	
50944	SHANK1	UP	
85358	SHANK3	UP	
284369	SIGLECL1	UP	C19orf75
113278	SLC52A3	UP	C20orf54
6529	SLC6A1	UP	
6531	SLC6A3	UP	
6546	SLC8A1	UP	
25992	SNED1	UP	
100033450	SNORD115-13	UP	
100033414	SNORD116-2	UP	
26765	SNORD12C	UP	
692205	SNORD89	UP	
83893	SPATA16	UP	
8128	ST8SIA2	UP	
64220	STRA6	UP	
252983	STXBP4	UP	
10454	TAB1	UP	MAP3K7IP1
6886	TAL1	UP	
125058	TBC1D16	UP	
202500	TCTE1	UP	
339669	TEX33	UP	C22orf33
26230	TIAM2	UP	
64759	TNS3	UP	
7726	TRIM26	UP	
54795	TRPM4	UP	
80727	TTYH3	UP	
114131	UCN3	UP	
9706	ULK2	UP	
55245	UQCC	UP	
55339	WDR33	UP	
84128	WDR75	UP	
9671	WSCD2	UP	
11060	WWP2	UP	
340481	ZDHHC21	UP	

EntrezGene ID	HGNC symbol	Direction of change	Alias
7730	ZNF177	UP	
7571	ZNF23	UP	
91975	ZNF300	UP	
257101	ZNF683	UP	

Supplementary table 4.3. Pyrosequencing primer sequences

Primer	Sequence
SNED1_cg19075225 F*	/5BiodT/TG TTG GAG GTT TAT GTT ATT AAT GTG
SNED1_cg19075225 R	CAA ACC CCT ACA AAA CCA AAT CAA T
SNED1_cg19075225 S	ACT ACT ATC ACA AAA AAC TAA TAC
SHANK3_cg10793758 R*	/5BiodT/TA CCA ACC CCC TCC TAC CTA AT
SHANK3_cg10793758 F	TAA TTT GAA GGG GGA GGT ATA GTT
SHANK3_cg10793758 S	GTT GTA AGA GGA GAA AGA
CACNAIA_cg24800175 F*	/5BiodT/GG GAA AAG AAG GAT AAG AGT ATA TTT G
CACNAIA_cg24800175 R	AAA TTC CAA ATC ACT AAA CAC AAT AAC
CACNAIA_cg24800175 S	CCT CCT TCT CTT CTA AC
NOSIAP_cg02858267 R*	/5BiodT/CC CCT CTA CTA CCT CTT ATC TCC
NOSIAP_cg02858267 F	GTA GGG TGG GTA AAG TTA GTT AAG T
NOSIAP_cg02858267 S	GTA GGT TTT TTG GTT TAG G
NOSIAP_cg12486795 F*	/5BiodT/TT TTG GGA GGT TTG GAG TTT ATT AAG T
NOSIAP_cg12486795 R	ACT TTA CCC TCC AAA ACA AAA TCT CAA TA
NOSIAP_cg12486795 S	ATA CAC ATT CAC TAA ACA TC

Supplementary table 4.4. List of imprinted genes

Gene	Aliases	Location	Expressed allele
DIRAS3	ARHI, NOEY2	1p31 AS	Paternal
RNU5D-1	U5DL, U5DS, RNU5D	1p34.1 AS	Paternal
TP73	P73	1p36.3	Maternal
LRRTM1		2p12 AS	Paternal
GPR1		2q33.3 AS	Paternal
ZDBF2		2q33.3	Paternal
NAP1L5	DRLM	4q22.1 AS	Paternal
FAM50B	X5L, D6S2654E	6p25.2	Paternal
AIM1	ST4, CRYBG1	6q21	Paternal
LIN28B	CSDD2	6q21	Paternal
PLAGL1	ZAC, LOT1, ZAC1, MGC126275, MGC126276, DKFZp781P1017	6q24-q25 AS	Paternal
HYMAI	NCRNA00020	6q24.2 AS	Paternal
SLC22A2*	OCT2, MGC32628	6q26 AS	Maternal
IGF2R	MPR1, MPRI, CD222, CIMPR, M6P-R	6q26	Biallelic
SLC22A3*	EMT, EMTH, OCT3	6q26-q27	Maternal
GRB10	RSS, IRBP, MEG1, GRB-IR, Grb-10, KIAA0207	7p12-p11.2 AS	Isoform Dependent
DDC	AADC	7p12.2 AS	Isoform Dependent
MAGI2	AIP1, AIP-1, ARIP1, SSCAM, MAGI-2, ACVRIP1	7q21 AS	Maternal
PEG10	EDR, HB-1, Mar2, MEF3L, Mart2, RGAG3	7q21	Paternal
SGCE	ESG, DYT11	7q21-q22 AS	Paternal
PPP1R9A	NRB1, NRBI, FLJ20068, KIAA1222, Neurabin-I	7q21.3	Maternal
DLX5		7q22 AS	Maternal
TFPI2	PP5, REF1, TFPI-2, FLJ21164	7q22 AS	Maternal
COPG2IT1	CIT1, COPG2AS, FLJ41646, NCRNA00170, DKFZP761N09121	7q32	Paternal
CPA4	CPA3	7q32	Maternal
MEST	PEG1, MGC8703, MGC111102, DKFZp686L18234	7q32	Paternal
MESTIT1	MEST-IT, PEG1-AS, MEST-AS1, MEST-IT1, NCRNA00040	7q32.2 AS	Paternal
KLF14	BTEB5	7q32.3 AS	Maternal
DLGAP2	DAP2, SAPAP2	8p23	Paternal
KCNK9	KT3.2, TASK3, K2p9.1, TASK-3, MGC138268, MGC138270	8q24.3 AS	Maternal
ZFAT-AS1	ZFATAS, ZFAT-AS, SAS-ZFAT, NCRNA00070	8q24.22	Paternal
ZFAT	AITD3, ZFAT1, ZNF406	8q24.22 AS	Paternal
GLIS3	ZNF515	9p24.2 AS	Paternal
INPP5F V2	SAC2, hSAC2, MSTP007, MSTPO47, FLJ13081, KIAA0966, MGC59773, MGC131851	10q26.11	Paternal
WT1-Alt trans	WT1, GUD, WAGR, WT33, WIT-2	11p13 AS	Paternal

Gene	Aliases	Location	Expressed allele
KCNQ1OT1	LIT1, KvDMR1, KCNQ10T1, KvLQT1-AS, long QT intronic transcript 1	11p15	Paternal
KCNQ1DN	BWRT, HSA404617	11p15.4	Maternal
OSBPL5	ORP5, OBPH1, FLJ42929	11p15.4 AS	Maternal
IGF2	INSIGF, pp9974, C11orf43, FLJ22066, FLJ44734	11p15.5 AS	Paternal
IGF2AS	PEG8, MGC168198	11p15.5	Paternal
PHLDA2	IPL, BRW1C, BWR1C, HLDA2, TSSC3	11p15.5 AS	Maternal
CDKN1C	BWS, WBS, p57, BWCR, KIP2	11p15.5 AS	Maternal
KCNQ1	LQT, RWS, WRS, LQT1, SQT2, ATFB1, ATFB3, JLNS1, KCNA8, KCNA9, Kv1.9, Kv7.1, KVLQT1, FLJ26167	11p15.5	Maternal
H19	ASM, BWS, ASM1, MGC4485, PRO2605, D11S813E	11p15.5 AS	Maternal
SLC22A18	HET, ITM, BWR1A, IMPT1, TSSC5, ORCTL2, BWSCR1A, SLC22A1L, p45-BWR1A, DKFZp667A184	11p15.5	Maternal
INS	ILPR, IRDN	11p15.5 AS	Paternal
ANO1	DOG1, TAOS2, ORAOV2, TMEM16A	11q13.3	Maternal
ZC3H12C	MCPIP3	11q22.3	Paternal
NTM	HNT, NTRI, IGLON2	11q25	Maternal
RBP5	CRBP3, CRBPIII, CRBP-III	12p13.31 AS	Maternal
RB1	RB, pRb, OSRC, pp110, p105-Rb	13q14.2	Maternal
DLK1	DLK, FA1, ZOG, pG2, PREF1, Pref-1	14q32	Paternal
MEG3	GTL2, FP504, prebp1, PRO0518, PRO2160, FLJ31163, FLJ42589	14q32	Maternal
RTL1	MART1, PEG11, LOC388015	14q32.31 AS	Paternal
MEG8	Rian	14q32.31	Maternal
MAGEL2	nM15, NDNL1	15q11-q12 AS	Paternal
NPAP1	C15orf2	15q11-q13	Unknown
UBE3A	AS, ANCR, E6-AP, HPVE6A, EPVE6AP, FLJ26981	15q11-q13 AS	Maternal
MKRN3	D15S9, RNF63, ZFP127, ZNF127, MGC88288	15q11-q13	Paternal
PWCR1	PET1, non-coding RNA in the Prader-Willi critical region	15q11.2	Paternal
SNORD108	HBII-437, HBII-437 C/D box snoRNA	15q11.2	Paternal
SNORD107	HBII-436, HBII-436 C/D box snoRNA	15q11.2	Paternal
SNORD116@	PET1, PWCR1, HBII-85	15q11.2	Paternal
SNRPN	SMN, PWCR, SM-D, RT-LI, HCERN3, SNRNP-N, FLJ33569, FLJ36996, FLJ39265, MGC29886, SNURF-SNRPN, DKFZp762N022, DKFZp686C0927, DKFZp761I1912, DKFZp686M12165	15q11.2	Paternal
ATP10A	ATPVA, ATPVC, ATP10C, KIAA0566	15q11.2 AS	Maternal
SNORD115@	HBII-52	15q11.2	Paternal
SNORD115-48	HBII-52-48	15q11.2	Paternal

Gene	Aliases	Location	Expressed allele
SNORD109B	HBII-438B, HBII-438B C/D box snoRNA	15q11.2	Paternal
SNORD109A	HBII-438A	15q11.2	Paternal
NDN	HsT16328	15q11.2-q12 AS	Paternal
SNURF		15q12	Paternal
SNORD64	HBII-13, HBII-13 snoRNA	15q12	Paternal
ZNF597		16p13.3 AS	Maternal
NAA60	HAT4, NAT15	16p13.3	Maternal
TCEB3C	HsT829, TCEB3L2, Elongin A3	18q21.1 AS	Maternal
DNMT1	AIM, DNMT, MCMT, CXXC9, HSN1E, ADCADN	19p13.2 AS	Paternal
ZIM2	ZNF656	19q13.4 AS	Paternal
MIMT1	MIM1, LINC00067, NCRNA00067	19q13.4	Paternal
PEG3	PW1, ZNF904, ZSCAN24	19q13.4 AS	Paternal
MIR371A	C19MC, MIR371, MIRN371, hsa-mir-371, hsa-mir-371a	19q13.42	Paternal
NLRP2	NBS1, PAN1, NALP2, PYPAF2, CLR19.9	19q13.42	Maternal
PSIMCT-1		20q11.2	Paternal
BLCAP	BC10	20q11.2-q12 AS	Isoform Dependent
NNAT	Peg5	20q11.2-q12	Paternal
MCTS2		20q11.21	Paternal
GDAP1L1	dJ881L22.1, dJ995J12.1.1	20q12	Paternal
SGK2	H-SGK2, dJ138B7.2	20q13.2	Paternal
GNAS	AHO, GSA, GSP, POH, GPSA, NESP, GNAS1, PHP1A, PHP1B, C20orf45, MGC33735, dJ309F20.1.1, dJ806M20.3.3	20q13.3	Isoform Dependent
L3MBTL	L3MBTL1, FLJ41181, KIAA0681, H-L(3)MBT, dJ138B7.3, DKFZp586P1522	20q13.12	Paternal
MIR296	MIRN296, miRNA296	20q13.32 AS	Paternal
MIR298	MIRN298, hsa-mir-298	20q13.32 AS	Paternal
SANG	SANG, Nespas	20q13.32	Paternal
GNASAS	SANG, NESPAS, GNAS1AS, NCRNA00075	20q13.32 AS	Paternal
DGCR6		22q11.21	Random
DGCR6L		22q11.21 AS	Random

Supplementary table 4.5. Differentially methylated regions associated with FASD

Rank	Chr	Start	End	Length	# probes	Associated gene	Location	Min FDR	Mean FDR	Mean beta FC	Max beta FC
1	chr6	33047056	33049505	2450	17	HLA-DPB1	Body	2.59E-50	1.61E-06	0.0348	0.0868
2	chr11	2919689	2921176	1488	20	SLC22A18AS, SLC22A18	Body, TSS1500, TSS200, 5'UTR	1.21E-29	1.46E-05	-0.0122	-0.0485
3	chr6	32846924	32847845	922	18	PPP1R2P1	Body	1.81E-20	9.39E-10	0.0156	0.0264
4	chr12	46767132	46768016	885	8	SLC38A2	TSS1500	1.98E-16	9.78E-09	-0.0201	-0.0389
5	chr19	37825307	37825679	373	7	HKR1	TSS1500, TSS200, 1stExon, 5'UTR	7.51E-16	9.51E-16	0.0156	0.0219
6	chr3	113160071	113160821	751	10	WDR52	5'UTR, 1stExon, TSS200, TSS1500	1.34E-14	6.02E-13	-0.0206	-0.0366
7	chr6	19180718	19181082	365	4			4.44E-14	5.05E-14	0.0311	0.0397
8	chr5	159894868	159895160	293	4			9.40E-14	1.18E-13	-0.0363	-0.0524
9	chr3	193587264	193587939	676	5			1.53E-13	2.47E-12	-0.0174	-0.0416
10	chr3	10149466	10150487	1022	11	C3orf24	5'UTR, 1stExon, TSS200, TSS1500	4.41E-13	1.88E-11	0.0211	0.0341
11	chr1	162336877	162337375	499	5	NOS1AP	Body, 3'UTR	4.69E-13	8.79E-13	0.0318	0.0391
12	chr1	6093770	6094993	1224	6	KCNAB2	5'UTR	9.78E-13	2.86E-07	0.0177	0.0261
13	chr13	113759771	113760286	516	6	F7	TSS1500, TSS200, Body	1.55E-10	1.96E-10	0.0181	0.0286
14	chr16	1598866	1599150	285	4	IFT140, TMEM204	Body	1.81E-10	4.34E-10	-0.0267	-0.0364
15	chr19	11517079	11517436	358	4	RGL3	Body	3.06E-10	5.34E-10	0.0256	0.0362
16	chr2	2581285	2581557	273	5			4.07E-10	1.00E-09	0.0191	0.0272

Rank	Chr	Start	End	Length	# probes	Associated gene	Location	Min FDR	Mean FDR	Mean beta FC	Max beta FC
17	chr15	74494781	74496040	1260	12	STRA6	5'UTR, 1stExon, TSS200, TSS1500	4.80E-10	1.06E-04	0.0137	0.0347
18	chr12	104697193	104697983	791	11	TXNRD1, EID3	5'UTR, Body, TSS1500, TSS200, 1stExon	5.49E-10	3.98E-08	0.0089	0.0237
19	chr17	695156	695661	506	3	RNMTL1	Body, 3'UTR	5.77E-10	3.23E-09	-0.0187	-0.0263
20	chr22	32554848	32555310	463	5	C22orf42	Body, TSS200	7.95E-10	7.91E-09	0.0142	0.0224
21	chr16	29796373	29796798	426	5			1.08E-09	1.49E-09	0.0247	0.0346
22	chr10	96990543	96991505	963	6			2.23E-09	2.12E-04	0.0223	0.0394
23	chr7	4869981	4870162	182	3	RADIL	Body	2.40E-09	2.48E-09	0.0209	0.0259
24	chr16	30485383	30485966	584	6	ITGAL	Body	7.18E-09	5.13E-08	0.0154	0.0216
25	chr7	98099806	98100419	614	7			2.14E-08	7.07E-07	-0.0079	-0.0166
26	chr15	90547692	90548043	352	3	ZNF710	5'UTR	4.18E-08	5.44E-07	-0.0117	-0.0232
27	chr5	140344290	140344745	456	4	PCDHA7, PCDHAC2, PCDHA12, PCDHA6, PCDHA10, PCDHA4, PCDHA11, PCDHA8, PCDHA1, PCDHA2, PCDHA9, PCDHA13, PCDHA5, PCDHAC1, PCDHA3	Body, TSS1500	4.73E-08	1.20E-07	0.0125	0.0187
28	chr8	120220410	120221797	1388	8	MAL2	TSS200, 1stExon, Body	1.26E-07	2.35E-03	-0.0036	-0.0218

Rank	Chr	Start	End	Length	# probes	Associated gene	Location	Min FDR	Mean FDR	Mean beta FC	Max beta FC
29	chr10	5406543	5407020	478	8	UCN3	TSS1500, TSS200, 1stExon, 5'UTR	1.32E-07	3.03E-07	0.0128	0.0160
30	chr10	70979777	70980067	291	4	HKDC1	TSS1500, 5'UTR, 1stExon	1.37E-07	1.40E-07	0.0171	0.0231
31	chr1	16533422	16534579	1158	8	ARHGEF19	Body	1.88E-07	1.11E-04	-0.0150	-0.0351
32	chr7	158815555	158816392	838	3	LOC154822	Body	2.36E-07	1.90E-05	-0.0083	-0.0433
33	chr4	116034871	116035232	362	4	NDST4	1stExon, 5'UTR, TSS200, TSS1500	5.96E-07	6.45E-07	0.0221	0.0310
34	chr2	242009513	242009588	76	2	SNED1	Body	6.41E-07	6.48E-07	0.0379	0.0403
35	chr10	102642531	102642752	222	3			7.68E-07	8.96E-07	0.0199	0.0280
36	chr8	48739161	48739256	96	2	PRKDC	Body	7.94E-07	8.04E-07	-0.0401	-0.0453
37	chr6	30848807	30848846	40	4			1.81E-06	1.82E-06	0.0196	0.0245
38	chr1	10847541	10847594	54	2	CASZ1	5'UTR	2.92E-06	2.92E-06	0.0184	0.0254
39	chr7	807596	809109	1514	9	HEATR2	Body	3.11E-06	3.69E-04	0.0181	0.0358
40	chr17	37123638	37124558	921	10	FBXO47	1stExon, 5'UTR, TSS200, TSS1500	3.94E-06	1.49E-04	0.0235	0.0343
41	chr11	69065333	69065779	447	3			5.59E-06	1.06E-04	-0.0126	-0.0255
42	chr20	741723	741937	215	3	C20orf54	Body	6.56E-06	7.34E-06	0.0232	0.0337
43	chr2	2797483	2797612	130	2			1.04E-05	1.22E-05	0.0221	0.0278
44	chr17	38183170	38184257	1088	7	MED24, SNORD124	Body, TSS1500, TSS200	1.52E-05	2.61E-04	-0.0048	0.0581
45	chr19	17918795	17919173	379	3	B3GNT3	Body	2.03E-05	2.37E-05	0.0143	0.0267
46	chr1	47688728	47689193	466	2	TAL1	Body	2.44E-05	2.57E-05	0.0180	0.0204
47	chr5	149980526	149980674	149	3	SYNPO	TSS200, 1stExon, 5'UTR	3.34E-05	3.69E-05	-0.0222	-0.0296

Rank	Chr	Start	End	Length	# probes	Associated gene	Location	Min FDR	Mean FDR	Mean beta FC	Max beta FC
48	chr19	18589848	18589894	47	2	ELL	Body	4.28E-05	4.30E-05	-0.0304	-0.0338
49	chr2	47382287	47382739	453	7	C2orf61	Body, 1stExon, 5'UTR, TSS200, TSS1500	4.40E-05	7.18E-05	0.0096	0.0205
50	chr5	141339086	141339777	692	4	PCDH12	TSS1500	4.48E-05	6.14E-04	0.0078	0.0128
51	chr16	69951706	69951820	115	2	WWP2	Body	5.32E-05	5.50E-05	0.0340	0.0365
52	chr3	50350760	50350790	31	3	HYAL1	TSS1500	5.49E-05	5.51E-05	-0.0211	-0.0323
53	chr8	105342214	105342491	278	4			6.39E-05	6.47E-05	-0.0240	-0.0349
54	chr12	111855825	111856652	828	7	SH2B3	5'UTR, Body	7.48E-05	3.26E-04	0.0162	0.0305
55	chr5	78365255	78366076	822	6	BHMT2, DMGDH	TSS1500, Body, TSS200	1.91E-04	3.86E-04	0.0136	0.0169
56	chr2	47915862	47916139	278	2			5.04E-04	5.06E-04	-0.0258	-0.0300
57	chr18	21852118	21852436	319	4	OSBPL1A	Body, 1stExon, 5'UTR, TSS200, TSS1500	6.26E-04	7.39E-04	-0.0058	-0.0089
58	chr7	922051	922235	185	3	C7orf20	Body	7.47E-04	1.24E-03	-0.0124	-0.0206
59	chr8	3141844	3141907	64	2	CSMD1	Body	1.19E-03	1.20E-03	0.0219	0.0263
60	chr19	23253218	23254131	914	6			1.36E-03	7.04E-03	0.0062	0.0175
61	chr1	24648203	24648984	782	5	GRHL3	TSS1500, Body	1.84E-03	5.18E-03	-0.0100	-0.0219
62	chr19	1472936	1473179	244	3	APC2	3'UTR	2.17E-03	2.25E-03	0.0154	0.0190
63	chr1	243645911	243647204	1294	8	SDCCAG8	Body	2.40E-03	1.23E-02	0.0101	0.0185
64	chr6	17016226	17016484	259	3			2.58E-03	2.95E-03	-0.0267	-0.0300
65	chr7	48131586	48132109	524	2	UPP1	5'UTR	2.67E-03	2.58E-02	-0.0154	-0.0327
66	chr7	48075568	48076004	437	5	C7orf57	5'UTR, Body	2.67E-03	9.45E-03	0.0051	0.0129

Rank	Chr	Start	End	Length	# probes	Associated gene	Location	Min FDR	Mean FDR	Mean beta FC	Max beta FC
67	chr2	121223534	121224327	794	8	LOC84931	Body, TSS200, TSS1500	3.01E-03	4.19E-03	0.0067	0.0158
68	chr2	242648702	242648761	60	3	ING5	Body	3.10E-03	3.12E-03	0.0007	0.0044
69	chr2	202901045	202901470	426	5	FZD7	1stExon, 3'UTR	3.22E-03	4.13E-03	0.0183	0.0277
70	chr15	32933661	32934185	525	7	SCG5	TSS1500, TSS200, 1stExon, 5'UTR	3.29E-03	1.73E-02	0.0090	0.0168
71	chr17	77965915	77966262	348	3	TBC1D16	Body	3.43E-03	3.92E-03	0.0069	0.0120
72	chr13	25085301	25085776	476	4	PARP4	5'UTR	4.35E-03	5.97E-03	-0.0122	-0.0173
73	chr16	7855305	7855622	318	3			4.53E-03	5.45E-03	0.0235	0.0321
74	chr13	49879669	49879770	102	3			4.91E-03	4.91E-03	0.0199	0.0232
75	chr4	95679808	95680414	607	3	BMPR1B	5'UTR	5.20E-03	1.18E-02	0.0100	0.0175
76	chr12	122396633	122396687	55	3	WDR66	Body	6.37E-03	6.39E-03	0.0120	0.0168
77	chr6	31148332	31148666	335	14			6.74E-03	7.19E-03	0.0134	0.0198
78	chr9	137251825	137252129	305	3	RXRA	Body	6.89E-03	9.87E-03	-0.0091	-0.0191
79	chr20	32255491	32256071	581	3	NECAB3, C20orf134	Body, 1stExon, 3'UTR	7.97E-03	1.00E-02	-0.0454	-0.0592
80	chr11	102638432	102638778	347	6			8.78E-03	9.34E-03	0.0098	0.0213
81	chr12	129309117	129309376	260	5	SLC15A4	TSS1500	9.67E-03	1.44E-02	-0.0058	-0.0128
82	chr1	21586831	21587174	344	3	ECE1	Body	1.02E-02	1.21E-02	0.0038	0.0051
83	chr15	100274128	100274248	121	3	LYSMD4	TSS1500	1.10E-02	1.43E-02	-0.0092	-0.0105
84	chr8	70855046	70855146	101	3			1.16E-02	1.19E-02	-0.0236	-0.0289
85	chr11	2596300	2596606	307	4	KCNQ1	Body	1.16E-02	1.64E-02	0.0016	-0.0097
86	chr17	40558061	40558245	185	3	PTRF	Body	1.48E-02	1.51E-02	0.0097	0.0218
87	chr14	32671389	32671882	494	3			1.66E-02	2.37E-02	-0.0068	-0.0116
88	chr7	48129814	48130197	384	5	UPP1	5'UTR	1.69E-02	2.96E-02	-0.0099	-0.0218
89	chr7	5536937	5537036	100	3	MIR589, FBXL18	TSS1500, Body	1.70E-02	1.85E-02	-0.0134	-0.0187

Rank	Chr	Start	End	Length	# probes	Associated gene	Location	Min FDR	Mean FDR	Mean beta FC	Max beta FC
90	chr18	14178949	14179364	416	2			1.79E-02	1.87E-02	-0.0324	-0.0334
91	chr19	10655622	10655686	65	2	ATG4D	Body	1.87E-02	1.88E-02	-0.0160	-0.0164
92	chr21	38074393	38074478	86	2	SIM2	Body	1.96E-02	2.13E-02	0.0167	0.0177
93	chr15	42371635	42371967	333	6	PLA2G4D	Body	2.03E-02	2.06E-02	-0.0118	-0.0162
94	chr3	9996954	9997177	224	2			2.31E-02	2.45E-02	0.0147	0.0187
95	chr19	49520450	49520532	83	3	LHB	TSS200	2.41E-02	2.53E-02	-0.0056	-0.0084
96	chr5	314553	314642	90	4	AHRR, PDCD6	Body, 3'UTR	2.50E-02	2.51E-02	-0.0021	-0.0053
97	chr12	30354611	30354663	53	2			2.56E-02	2.60E-02	-0.0196	-0.0235
98	chr1	76082568	76082888	321	3			2.63E-02	3.37E-02	0.0082	0.0107
99	chr11	129183160	129183282	123	4			3.08E-02	3.19E-02	0.0122	0.0171
100	chr14	104743900	104744168	269	3			3.22E-02	3.36E-02	0.0048	0.0109
101	chr17	76719591	76719640	50	4	CYTH1	Body	4.61E-02	4.74E-02	0.0104	0.0118

Appendix D Supplementary materials for chapter 5

D.1 Supplementary figures

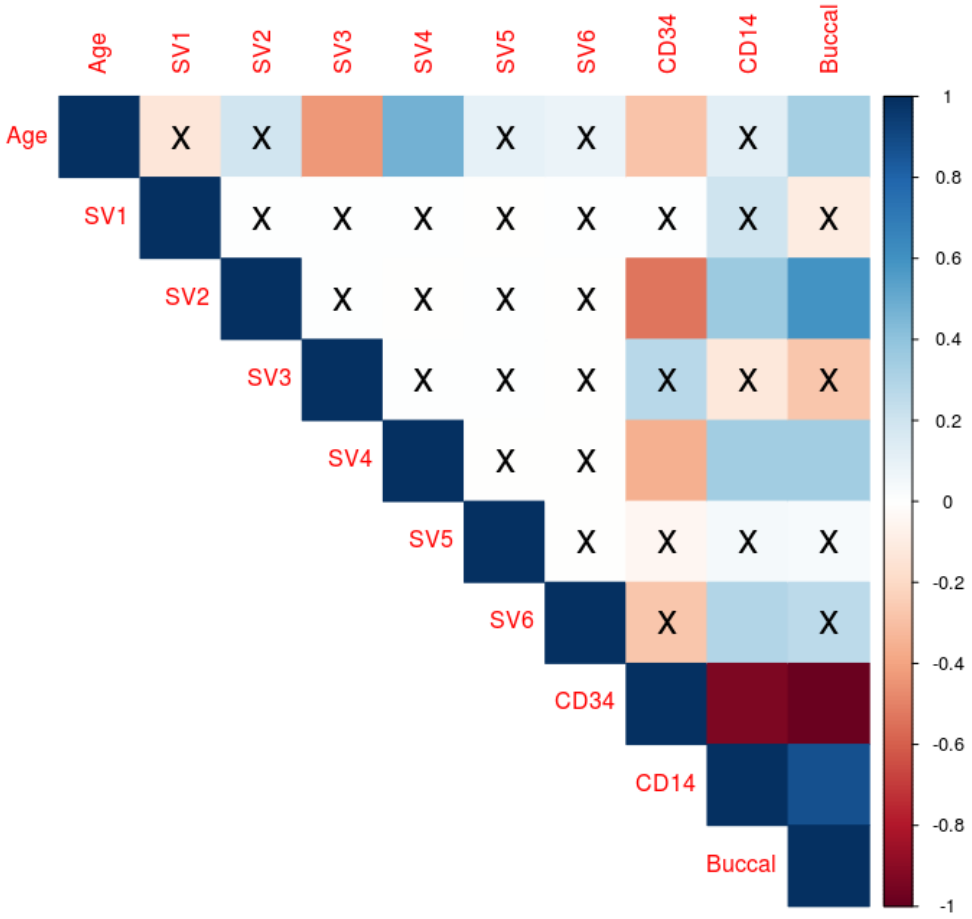

Supplementary figure 5.1. Surrogate variables were correlated with known sources of variation. Pearson correlations were performed between the 6 surrogate variables identified in the DNA methylation data and known covariates: age and predicted CD34+/CD14+/buccal proportions. SV2 and SV4 were highly correlated with cell type proportions, while SV3 and SV4 were correlated with age, suggesting that these SVs could be used to correct for these known sources of variance in the dataset. Squares with and X were not significant ($p>0.05$).

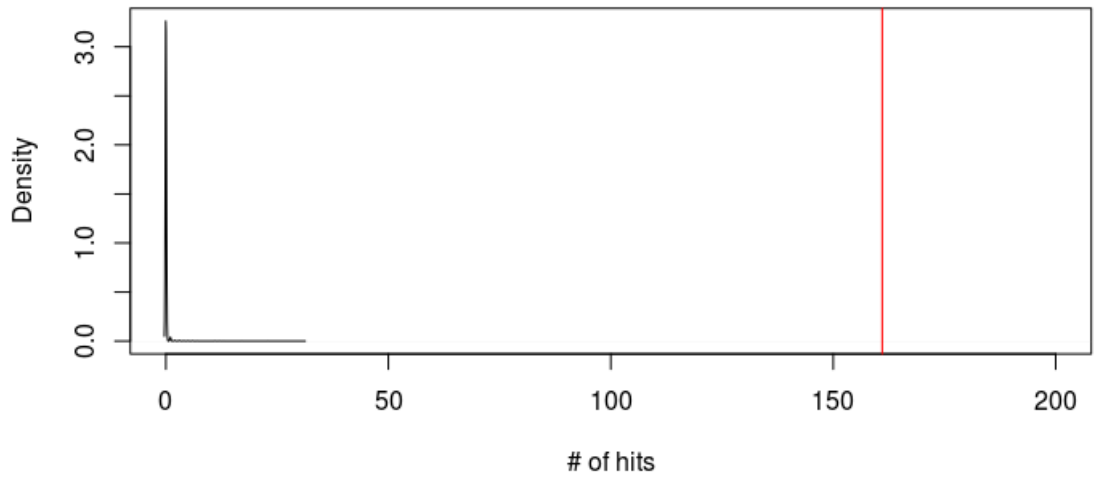

Supplementary figure 5.2. Number of hits in a random selection of sample group. Random group subsampling was performed 10,000 times to obtain the probability of validating differential methylation at 161/648 probes. As none showed more differentially methylated probes than the original replication cohort (maximum = 31 differentially methylated probes), the probability of validated 161/648 probes was < 1e-4.

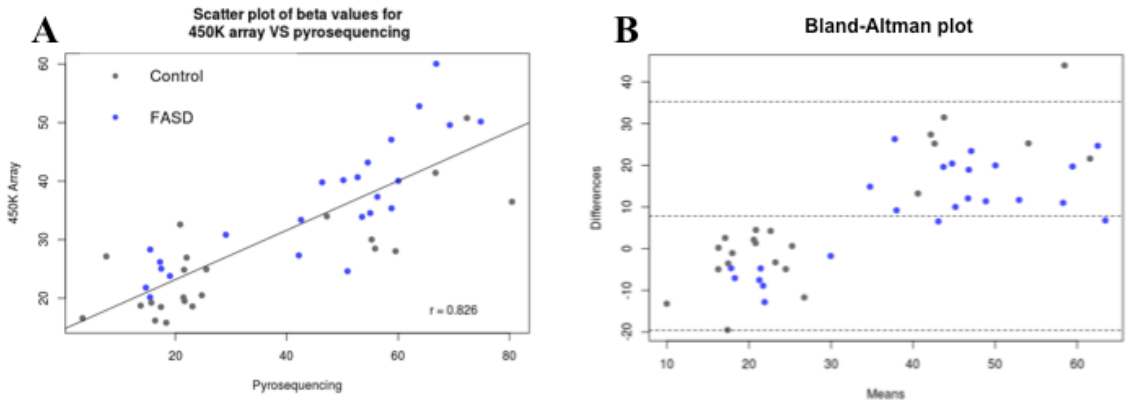

Supplementary figure 5.3. Scatter plot and Bland-Altman plots of bisulfite pyrosequencing and 450K array data. A) The values for the two methods were highly correlated (p = 0.826) for individuals with FASD (blue) and controls (grey). B) The Bland–Altman plot showed little difference when comparing the 450K array to pyrosequencing, suggesting good concordance between DNA methylation data from the two methods.

D.2 Supplementary tables

Supplementary table 5.1. Pyrosequencing primers

CpG	Primer	Sequence
cg24800175	CACNA1 F1-Biotin	GGGAAAAGAAGGATAAGAGTATATTTG
	CACNA1 R1	TCCCAACCTTCTTCCAAACCCTCATA
	CACNA1 S1	CCTCCTCTTCCAATAC

Supplementary table 5.2. Validated probes at a false-discovery rate (FDR) <0.05

CpG	p-value	FDR	Δbeta	Closest TSS	UCSC gene	UCSC location
cg21785245	5.54E-04	4.56E-03	0.033	AK5	AK5	Body
cg20130789	8.59E-03	3.48E-02	0.013	AKR1C4	AKR1C4	3'UTR
cg23161492	1.30E-05	3.11E-04	0.063	ANPEP	ANPEP	5'UTR
cg11900509	2.51E-03	1.35E-02	-0.048	ANXA11	ANXA11	5'UTR
cg09345786	1.98E-07	9.88E-06	-0.066	AP2B1	AP2B1	TSS1500
cg01206944	3.23E-03	1.63E-02	0.042	MIR4715	ATP10A	Body
cg05938607	1.43E-04	1.62E-03	0.055	BICC1	BICC1	Body
cg01715680	9.84E-05	1.36E-03	-0.089	BTBD7	BTBD7	Body
cg02666302	3.54E-03	1.72E-02	0.029	BTNL9	BTNL9	5'UTR
cg01291665	3.24E-04	3.00E-03	-0.064	LOC219731	C10orf47	Body
cg01074767	2.34E-03	1.29E-02	-0.048	C1RL	C1RL; LOC283314	TSS1500; Body
cg09084256	9.82E-05	1.36E-03	0.022	C22orf42	C22orf42	TSS200
cg02096656	1.08E-02	4.14E-02	0.014	LUC7L2	C7orf55	TSS1500
cg20876010	1.01E-02	3.95E-02	-0.030	CACHD1	CACHD1	Body
cg24800175	1.05E-04	1.36E-03	0.092	CACNA1A	CACNA1A	Body
cg19402173	4.68E-03	2.17E-02	0.009	CALU	CALU	1stExon; 5'UTR
cg13416249	3.59E-05	7.26E-04	0.061	CAPN10	CAPN10	Body
cg10078335	4.42E-05	8.43E-04	0.082	GPR35	CAPN10	Body
cg08589214	2.77E-03	1.47E-02	0.034	GPR35	CAPN10	Body
cg04622001	1.23E-02	4.62E-02	0.021	CASZ1	CASZ1	5'UTR
cg04833646	4.89E-03	2.25E-02	0.009	CDKN2D	CDKN2D	TSS200
cg02773588	1.20E-07	7.79E-06	0.044	CELSR3	CELSR3	1stExon
cg09847753	2.90E-03	1.50E-02	-0.014	PAAF1	CHCHD8; PAAF1	TSS1500; Body
cg19360675	4.83E-05	8.47E-04	0.040	COX11	COX11; STXBP4	TSS200
cg04439622	9.03E-03	3.59E-02	-0.027	CRIP2	CRIP2	Body
cg22873986	1.13E-03	7.47E-03	-0.008	DAGLB	DAGLB	Body
cg20699141	1.26E-03	8.18E-03	0.029	DCUN1D1	DCUN1D1	TSS1500
cg24927800	9.38E-05	1.35E-03	-0.052	DES	DES	1stExon

CpG	p-value	FDR	Δbeta	Closest TSS	UCSC gene	UCSC location
cg03583111	3.12E-04	2.93E-03	-0.045	DES	DES	1stExon
cg01812045	9.14E-03	3.61E-02	-0.028	DES	DES	1stExon
cg24218620	8.26E-07	2.68E-05	-0.060	DHRS13	DHRS13	Body
cg20694545	2.66E-05	5.75E-04	-0.051	DLG2	DLG2	Body
cg09386376	8.99E-03	3.59E-02	-0.068	DRD4	DRD4	Body
cg17559809	7.38E-03	3.08E-02	-0.011	EDIL3	EDIL3	TSS1500
cg06747543	1.35E-02	4.92E-02	-0.028	ELL	ELL	Body
cg02510729	3.04E-03	1.56E-02	-0.010	ELP3	ELP3	Body
cg00625443	1.88E-03	1.07E-02	-0.011	FAM108C1	FAM108C1	Body
cg23588928	7.96E-04	6.07E-03	-0.026	FAM135A	FAM135A	Body
cg05665581	1.94E-09	4.19E-07	0.056	FAM24A	FAM24A	TSS1500
cg05252487	9.72E-04	6.92E-03	0.026	FAM24A	FAM24A	5'UTR
cg08570472	8.92E-09	1.45E-06	-0.149	FAM59B	FAM59B	Body
cg25949338	1.89E-08	2.04E-06	-0.160	FAM59B	FAM59B	Body
cg17995197	1.13E-07	7.79E-06	-0.143	FAM59B	FAM59B	Body
cg22893791	2.62E-07	1.17E-05	-0.130	FAM59B	FAM59B	Body
cg19497798	2.67E-08	2.47E-06	-0.055	MRPL38	FBF1	Body
cg11030744	3.48E-03	1.72E-02	0.069	GHRLOS	GHRL; GHRLOS	Body
cg17386185	6.84E-05	1.11E-03	-0.015	GLYCTK	GLYCTK	TSS1500
cg08329753	4.73E-05	8.47E-04	0.022	GTF2H4	GTF2H4	Body
cg27300742	3.77E-03	1.81E-02	-0.016	H19	H19	TSS1500
cg23476401	4.10E-03	1.94E-02	-0.027	H19	H19	TSS1500
cg02814482	1.06E-02	4.10E-02	0.038	PANX1	HEPHL1	Body
cg01290710	3.84E-06	1.08E-04	0.031	HIPK4	HIPK4	Body
cg13423554	5.21E-03	2.35E-02	-0.020	HIVEP3	HIVEP3	5'UTR
cg25491704	1.63E-04	1.76E-03	0.041	HLA-DPA1	HLA-DPB1	Body
cg12893780	3.86E-04	3.34E-03	0.058	HLA-DPA1	HLA-DPB1	Body
cg02197634	4.38E-04	3.74E-03	0.086	HLA-DPA1	HLA-DPB1	Body
cg08796706	1.08E-03	7.27E-03	0.038	HLA-DPA1	HLA-DPB1	Body
cg15734436	2.34E-03	1.29E-02	0.030	HLA-DPB1	HLA-DPB1	Body
cg03611029	8.47E-04	6.38E-03	0.028	IQSEC1	IQSEC1	TSS1500
cg00043790	7.30E-05	1.15E-03	0.031	KCNAB2	KCNAB2	5'UTR
cg15867428	4.63E-05	8.47E-04	-0.021	KCNQ4	KCNQ4	Body
cg07830534	3.88E-03	1.85E-02	0.008	KRT28	KRT28	Body
cg24506604	1.69E-03	1.01E-02	0.026	KRT80	KRT80; KRT80	Body; Body
cg09895009	1.16E-04	1.44E-03	0.036	LCE3A	LCE3A	TSS1500
cg21032583	7.11E-03	3.01E-02	-0.045	IQCG	LMLN; IQCG	TSS1500; 5'UTR
cg23987134	1.05E-03	7.27E-03	-0.052	LOC285696	LOC285696	Body
cg24640156	5.26E-04	4.42E-03	-0.077	LOC401010	LOC401010	Body

cg04195855	2.89E-07	1.17E-05	-0.077	LRRK1	LRRK1	Body
CpG	**p-value**	**FDR**	**Δbeta**	**Closest TSS**	**UCSC gene**	**UCSC location**
cg26112661	1.71E-03	1.01E-02	-0.041	LOC100507564	MAGOH	TSS1500
cg26231094	2.89E-03	1.50E-02	0.050	TMC4	MBOAT7	Body; 3'UTR
cg01091565	5.45E-03	2.42E-02	-0.049	MESP1	MESP1	TSS1500
cg00227156	1.56E-03	9.80E-03	0.007	MIR648	MIR648; MICAL3	Body; 5'UTR
cg26371345	1.17E-02	4.44E-02	-0.068	MRPL14	MRPL14	5'UTR
cg12438037	9.04E-04	6.66E-03	-0.039	MRPS2	MRPS2	Body
cg18776287	3.27E-03	1.63E-02	-0.027	MRPS2	MRPS2	Body
cg14204430	1.07E-03	7.27E-03	0.046	NDST4	NDST4	TSS200
cg09511421	1.42E-07	8.37E-06	0.051	NDST4	NDST4	1stExon; 5'UTR
cg19470832	5.90E-04	4.67E-03	0.029	NEUROD4	NEUROD4	5'UTR
cg00689651	8.15E-03	3.32E-02	-0.006	LYL1	NFIX	3'UTR
cg19697239	1.20E-04	1.44E-03	-0.019	NINJ2	NINJ2	Body
cg21047695	1.38E-03	8.82E-03	0.037	UG0898H09	NKAIN3	Body
cg02858267	2.07E-03	1.17E-02	0.037	NOS1AP	NOS1AP	Body
cg27298830	3.75E-03	1.81E-02	-0.028	ZNF860	OSBPL10	Body
cg02163378	1.07E-04	1.36E-03	0.059	OTX2OS1	OTX2OS1	Body
cg23492399	1.83E-04	1.90E-03	0.030	PAM	PAM	5'UTR; 1stExon
cg05097643	1.75E-04	1.86E-03	-0.034	PAQR4	PAQR4	TSS1500
cg02539153	2.80E-07	1.17E-05	0.078	PCDHB18	PCDHB18	Body
cg22338356	1.06E-03	7.27E-03	-0.061	CEBPD	PRKDC	Body
cg17059564	1.72E-03	1.01E-02	0.032	RASD2	RASD2	5'UTR
cg11770664	4.11E-07	1.48E-05	0.036	C10orf10	RASSF4	Body
cg19566764	1.85E-04	1.90E-03	-0.012	RASSF4	RASSF4	5'UTR
cg09245003	8.59E-04	6.40E-03	-0.032	AX748314	RNMTL1	3'UTR
cg15835339	9.82E-04	6.92E-03	-0.037	SFTA1P	SFTA1P	Body
cg10793758	1.65E-03	1.01E-02	0.038	SHANK3	SHANK3	Body
cg14195115	2.48E-03	1.35E-02	-0.063	SHB	SHB	Body
cg06864895	1.03E-04	1.36E-03	-0.040	SLC38A2	SLC38A2	TSS1500
cg16848712	3.62E-04	3.21E-03	-0.032	SLC38A2	SLC38A2	TSS1500
cg27491190	6.51E-03	2.81E-02	-0.032	SLC38A2	SLC38A2	TSS1500
cg16614020	1.23E-08	1.59E-06	0.086	SLC6A3	SLC6A3	Body
cg22659953	1.10E-07	7.79E-06	0.060	SLC6A3	SLC6A3	Body
cg14765933	1.18E-04	1.44E-03	0.024	SLC6A3	SLC6A3	Body
cg07927540	5.19E-05	8.62E-04	-0.076	SMOC2	SMOC2	Body
cg19075225	3.53E-03	1.72E-02	0.031	SNED1	SNED1	Body
cg27592868	5.62E-03	2.48E-02	-0.047	SRCIN1	SRCIN1	Body
cg22672067	3.18E-03	1.62E-02	0.026	STRA6	STRA6	5'UTR; TSS1500; TSS200
cg05881135	1.82E-03	1.05E-02	-0.025	SYNM	SYNM	TSS1500

CpG	p-value	FDR	Δbeta	Closest TSS	UCSC gene	UCSC location
cg16006738	3.45E-04	3.11E-03	0.014	TAL1	TAL1	Body
cg15023038	1.10E-03	7.33E-03	0.017	TCTE1	TCTE1	Body
cg01855013	1.59E-03	9.88E-03	-0.033	TGFB1I1	TGFB1I1	3'UTR
cg04060128	1.70E-03	1.01E-02	-0.036	TGFB1I1	TGFB1I1	Body
cg09837169	7.55E-03	3.12E-02	0.029	TIAM2	TIAM2	TSS1500
cg16414821	9.34E-04	6.76E-03	0.025	MIR554	TUFT1; MIR554	Body; TSS1500
cg16567202	6.73E-04	5.19E-03	0.028	ULK2	ULK2	TSS1500
cg24330379	6.07E-04	4.74E-03	-0.037	UQCRC1	UQCRC1	TSS1500
cg15044041	8.54E-06	2.13E-04	-0.066	WDR52	WDR52	5'UTR; 1stExon
cg00736201	1.89E-04	1.92E-03	0.018	WSCD2	WSCD2	3'UTR
cg07519373	1.64E-03	1.01E-02	-0.056	OR7D2	ZNF426	TSS1500
cg17970176	1.41E-04	1.62E-03	-0.072	ZNF575	ZNF575	Body
cg19901523	4.63E-11	3.00E-08	0.063	LOC90925		
cg09311683	5.51E-10	1.78E-07	-0.056	TMEM239		
cg12880095	1.87E-07	9.88E-06	0.124	FAM57A		
cg25230117	3.99E-07	1.48E-05	-0.079	OTUD4		
cg13809095	7.28E-07	2.48E-05	0.069	REEP3		
cg00464520	1.78E-06	5.50E-05	0.057	VAX1		
cg03584351	2.77E-06	8.15E-05	0.070	C7orf50		
cg12192797	5.24E-06	1.36E-04	0.032	ZNF20		
cg08064292	5.26E-06	1.36E-04	0.037	BC024169		
cg14228272	2.26E-05	5.23E-04	0.056	KLC1		
cg21008530	2.61E-05	5.75E-04	-0.104	SNORA67		
cg03663556	3.32E-05	6.94E-04	-0.056	GRB10		
cg13323489	4.25E-05	8.34E-04	-0.045	AK091265		
cg04785587	4.99E-05	8.51E-04	0.039	TBRG4		
cg13712818	7.53E-05	1.16E-03	0.047	ANKFN1		
cg06382028	8.13E-05	1.22E-03	-0.130	LOC339166		
cg07343703	8.42E-05	1.24E-03	-0.054	AKT3		
cg01628053	1.22E-04	1.44E-03	-0.080	FGFR2		
cg18437839	1.52E-04	1.70E-03	-0.049	PHLDA3		
cg22239534	1.62E-04	1.76E-03	0.044	AK123632		
cg17198772	2.04E-04	2.03E-03	-0.036	PTDSS2		
cg22010140	2.18E-04	2.14E-03	0.046	AGT		
cg26932623	3.32E-04	3.03E-03	-0.053	ELF3		
cg15073666	3.85E-04	3.34E-03	0.046	BC036258		
cg15150463	5.56E-04	4.56E-03	0.026	GJA10		
cg06711306	9.38E-04	6.76E-03	-0.050	DQ658414		
cg23069297	1.19E-03	7.80E-03	-0.085	CXXC11		
cg02467382	1.41E-03	8.96E-03	-0.025	AK128400		

CpG	p-value	FDR	Δbeta	Closest TSS	UCSC gene	UCSC location
cg11737831	2.28E-03	1.27E-02	-0.017	WDR18		
cg18147104	2.79E-03	1.47E-02	0.008	BC011773		
cg10755035	4.35E-03	2.04E-02	0.034	MIR4472-1		
cg04009441	4.46E-03	2.08E-02	0.047	IPO11		
cg05539265	5.22E-03	2.35E-02	-0.063	IL1R1		
cg13625026	5.32E-03	2.38E-02	-0.025	MUC5B		
cg02376887	6.63E-03	2.85E-02	0.020	ERGIC2		
cg01353941	6.90E-03	2.94E-02	0.037	FGF12		
cg10209089	7.41E-03	3.08E-02	0.021	KCNA5		
cg14827832	7.42E-03	3.08E-02	0.019	DD413682		
cg13502252	8.86E-03	3.57E-02	0.036	SLC27A3		
cg26693693	1.09E-02	4.15E-02	0.025	COPS8		
cg26986871	1.21E-02	4.56E-02	-0.033	KLRK1		
cg25075776	1.27E-02	4.73E-02	0.027	DDR1		
cg10070864	1.28E-02	4.74E-02	-0.059	CGNL1		

Supplementary table 5.3. Weighting of probes for the DNA methylation predictors of FASD

Probe	648 probes	161 probes
cg00012960	0.00000	
cg00043790	0.00000	0.00068
cg00063773	1.17612	
cg00077566	0.00000	
cg00092400	0.00000	
cg00153543	0.00000	
cg00202441	0.00000	
cg00227156	0.49768	7.46591
cg00246301	0.00000	
cg00360077	4.04679	
cg00371301	0.00000	
cg00408773	0.00000	
cg00464520	1.08721	0.00007
cg00588297	0.00000	
cg00610991	0.50687	
cg00625443	0.28734	0.02802
cg00648582	0.08104	
cg00686823	0.00000	
cg00689651	0.00002	0.09672
cg00690809	0.00000	

Probe	648 probes	161 probes
cg00736201	0.00000	0.96332
cg00756748	5.82481	
cg00787726	1.07391	
cg00812096	0.81892	
cg00839333	3.28220	
cg00892368	0.00439	
cg00939684	0.00000	
cg00945507	23.05227	
cg00956573	0.04197	
cg00971737	0.00000	
cg01015062	0.05733	
cg01031400	17.49456	
cg01074767	0.00002	0.00614
cg01091565	0.00231	1.03663
cg01099220	0.10910	
cg01134643	0.00000	
cg01181415	0.00000	
cg01206944	0.95850	21.58166
cg01216369	0.00011	
cg01290710	0.00000	0.00000
cg01291665	0.65303	13.67013
cg01345586	0.83387	
cg01346077	0.00001	
cg01353941	22.20864	18.80239
cg01359236	0.00000	
cg01439568	0.00000	
cg01479187	4.66293	
cg01578398	0.00002	
cg01595666	0.00000	
cg01628053	1.06050	7.81963
cg01655958	13.92185	
cg01663696	0.01121	
cg01715680	18.84690	0.00000
cg01746878	0.04259	
cg01784614	0.00000	
cg01787574	0.00000	
cg01812045	0.00000	0.00054
cg01855013	0.00000	0.00987
cg01862688	5.08079	
cg01895612	1.35728	

Probe	648 probes	161 probes
cg02030270	10.74329	
cg02052956	0.00000	
cg02096656	0.00000	0.28157
cg02139853	1.36191	
cg02163378	0.00000	0.06075
cg02197634	12.84074	0.00004
cg02207200	0.00000	
cg02309230	0.00008	
cg02342791	5.11872	
cg02361459	0.00535	
cg02376887	0.00000	0.68816
cg02411950	0.00000	
cg02413040	0.00000	
cg02467382	0.00000	13.88709
cg02487233	0.00038	
cg02510729	1.48918	0.06494
cg02512395	0.00006	
cg02527881	0.00000	
cg02539153	36.24702	34.42112
cg02580969	0.00001	
cg02642958	100.00000	
cg02666302	0.68335	16.58075
cg02704570	0.00000	
cg02728342	0.00000	
cg02760112	0.00000	
cg02770683	0.00001	
cg02773588	0.00000	0.40718
cg02814482	0.00000	0.22423
cg02822788	0.00079	
cg02855981	9.03960	
cg02858267	0.61141	0.01587
cg02860108	0.02204	
cg02988698	0.00000	
cg03032816	0.00000	
cg03062564	0.00267	
cg03078972	0.81981	
cg03221025	0.02095	
cg03230711	2.52466	
cg03318904	0.00000	
cg03357547	0.00000	

Probe	648 probes	161 probes
cg03359468	22.79089	
cg03411938	0.00000	
cg03465782	0.00003	
cg03583111	0.00000	0.00000
cg03584351	0.42552	0.55664
cg03611029	0.29287	9.42709
cg03625515	0.00000	
cg03626746	0.78799	
cg03663556	69.54965	67.39943
cg03667083	0.00000	
cg03670369	0.00000	
cg03757387	0.00000	
cg03817911	0.00000	
cg03829194	0.00000	
cg03888765	0.00000	
cg03919488	1.71264	
cg03928546	0.00000	
cg03967266	2.75830	
cg04009441	0.00000	1.86221
cg04037470	0.00010	
cg04060128	0.00000	0.00000
cg04089332	0.00000	
cg04099543	0.00007	
cg04108939	0.00203	
cg04134048	0.00000	
cg04151826	0.00000	
cg04180046	0.00003	
cg04195855	34.78051	36.74883
cg04215256	0.00488	
cg04217218	4.12964	
cg04234014	1.01250	
cg04380576	0.00000	
cg04398451	13.97304	
cg04417556	0.00000	
cg04420752	0.00000	
cg04439622	0.00000	0.17927
cg04450459	0.00118	
cg04456916	0.00000	
cg04609875	0.00000	
cg04622001	0.00000	0.00000

Probe	648 probes	161 probes
cg04656451	0.00000	
cg04690793	0.00000	
cg04707706	0.00000	
cg04760708	6.03592	
cg04785587	0.00001	19.11033
cg04787675	0.00000	
cg04831327	0.00000	
cg04833646	0.38761	5.58295
cg05097643	0.00000	0.06231
cg05115862	0.00000	
cg05178654	0.00000	
cg05206657	0.00005	
cg05210798	0.00000	
cg05249460	16.79878	
cg05252487	68.85872	83.95361
cg05358814	0.00000	
cg05389922	0.00000	
cg05435295	0.00000	
cg05477514	0.00007	
cg05491767	31.42415	
cg05512869	0.00000	
cg05532178	0.00000	
cg05539265	0.00000	0.00007
cg05627398	23.01080	
cg05645661	0.00000	
cg05665581	0.00000	0.02406
cg05767421	13.62842	
cg05769975	0.00000	
cg05813818	8.40983	
cg05834603	0.00000	
cg05881135	0.65302	28.56234
cg05938607	0.10129	6.82553
cg06114363	0.42088	
cg06121352	0.00007	
cg06154313	3.25425	
cg06261066	0.00000	
cg06297194	0.00465	
cg06327965	0.00000	
cg06382028	8.29293	25.76629
cg06711175	11.17201	

Probe	648 probes	161 probes
cg06711306	0.00000	31.30020
cg06747543	0.00002	12.88855
cg06749854	0.00000	
cg06812861	0.00000	
cg06814616	0.22572	
cg06864895	0.00062	0.07451
cg06913501	0.00000	
cg06915053	0.00000	
cg06943912	0.00000	
cg07007080	0.01942	
cg07043604	0.00000	
cg07107130	0.00000	
cg07179981	0.00000	
cg07234199	0.05023	
cg07251128	0.00000	
cg07266431	0.00000	
cg07324496	0.33269	
cg07343703	0.00587	0.00012
cg07377907	0.00001	
cg07386859	0.25275	
cg07440826	0.00000	
cg07470694	0.00000	
cg07500347	0.01216	
cg07519373	0.00000	0.00037
cg07527324	0.00000	
cg07626033	98.80679	
cg07654559	0.00000	
cg07723921	0.00000	
cg07830534	7.77909	0.00000
cg07880854	11.28588	
cg07927540	6.18036	39.51676
cg08019384	0.00000	
cg08039322	0.54838	
cg08062387	0.00000	
cg08064292	0.00002	0.35367
cg08072202	0.00000	
cg08076108	0.00003	
cg08089041	0.00865	
cg08102508	0.00000	
cg08108641	0.00000	

Probe	648 probes	161 probes
cg08212266	0.00000	
cg08244301	0.00000	
cg08268892	0.00016	
cg08271366	0.00069	
cg08289525	0.96240	
cg08329753	0.00000	0.00000
cg08376368	0.00000	
cg08388455	0.00000	
cg08489410	0.17000	
cg08506585	0.00000	
cg08535756	0.02216	
cg08570472	0.00000	0.00000
cg08580187	0.00000	
cg08589214	0.00000	0.83765
cg08598287	0.00000	
cg08621957	0.00000	
cg08701816	33.59962	
cg08772837	0.00000	
cg08796706	0.00005	0.00145
cg08857221	0.00000	
cg08864105	2.85052	
cg08937612	0.00000	
cg09066361	0.00000	
cg09084256	0.15651	6.27706
cg09133032	27.31250	
cg09133511	0.00000	
cg09176023	0.00000	
cg09187107	0.00000	
cg09229169	1.42973	
cg09245003	0.00000	0.00000
cg09245872	3.13916	
cg09278098	0.00000	
cg09292069	0.00000	
cg09311683	0.02951	0.00001
cg09345786	0.00001	9.56301
cg09386376	0.00000	4.40759
cg09412782	0.18267	
cg09459548	0.00000	
cg09511421	31.51291	15.10552
cg09654116	46.78914	

Probe	648 probes	161 probes
cg09681675	19.30044	
cg09761265	0.00000	
cg09767675	0.00000	
cg09837169	0.00002	7.44888
cg09847753	0.00013	7.37818
cg09879382	1.78318	
cg09895009	0.00000	0.00000
cg09914773	0.00000	
cg09939948	0.00000	
cg10001715	0.00000	
cg10070864	0.92799	12.33404
cg10078335	0.49192	0.08805
cg10135520	0.20719	
cg10209089	0.00000	0.00000
cg10350263	0.00000	
cg10482532	0.00000	
cg10537821	0.73299	
cg10598595	9.16912	
cg10707081	2.51648	
cg10755035	0.00000	0.16147
cg10793758	0.33452	28.44001
cg10822352	0.00000	
cg10824677	0.20032	
cg10831285	0.00000	
cg10930290	0.03257	
cg10944833	0.00000	
cg11024687	0.85601	
cg11030744	0.00005	23.31113
cg11107212	0.00011	
cg11210069	2.06212	
cg11253737	0.00000	
cg11262093	8.08014	
cg11274371	0.00000	
cg11335335	0.00000	
cg11353300	0.00000	
cg11500660	0.00994	
cg11552868	1.33438	
cg11663289	0.00035	
cg11710912	0.00001	
cg11737831	0.00000	0.00000

Probe	648 probes	161 probes
cg11770664	0.00000	0.37258
cg11895451	5.76743	
cg11900509	51.93379	55.68059
cg11944462	0.00000	
cg11953516	0.00000	
cg11959399	1.20531	
cg11966524	0.11451	
cg12008047	0.00000	
cg12014113	4.71907	
cg12192797	18.72447	0.00736
cg12285605	0.00995	
cg12333845	0.00015	
cg12386061	0.01917	
cg12438037	0.00054	13.85449
cg12486795	0.00000	
cg12515485	6.34865	
cg12536502	0.00000	
cg12559474	0.16138	
cg12593541	0.00000	
cg12604031	0.00000	
cg12680326	0.70995	
cg12692682	0.00000	
cg12734820	0.00000	
cg12768523	0.00003	
cg12856447	0.00000	
cg12880095	0.00220	0.00000
cg12893780	0.31078	13.05657
cg13010014	1.52952	
cg13055001	0.00074	
cg13075295	33.53036	
cg13109911	0.00390	
cg13118072	0.00000	
cg13294084	0.00000	
cg13323489	0.00000	18.05434
cg13416249	0.03831	14.90409
cg13423554	0.00000	0.06305
cg13430464	0.00000	
cg13439596	0.00157	
cg13485320	39.64723	
cg13502252	0.00000	0.00007

Probe	648 probes	161 probes
cg13521077	8.45023	
cg13557373	0.00000	
cg13625026	0.00001	0.41028
cg13675051	0.00000	
cg13712818	0.00000	0.83343
cg13741289	0.00000	
cg13785189	0.00009	
cg13809095	0.61630	48.01921
cg13881341	0.00000	
cg13916255	0.44023	
cg13946872	0.00000	
cg14054283	35.08442	
cg14166009	0.00000	
cg14195115	0.26895	0.00000
cg14204430	0.00000	0.00000
cg14219124	0.52544	
cg14219900	0.00000	
cg14228272	0.09008	4.90270
cg14321284	0.00500	
cg14379630	4.13801	
cg14387743	0.00000	
cg14499058	0.00000	
cg14549524	0.00000	
cg14556787	0.00459	
cg14616251	1.21307	
cg14724749	74.22211	
cg14765933	0.00858	9.67642
cg14827832	0.12076	0.97822
cg14841350	0.00000	
cg14898768	0.00002	
cg14905731	0.00000	
cg15023038	0.00246	0.02988
cg15026243	0.00000	
cg15032166	0.00000	
cg15044041	0.01092	4.52516
cg15073666	19.39050	15.52385
cg15150463	0.00000	0.00141
cg15225534	2.93032	
cg15339164	0.00000	
cg15484354	12.21490	

Probe	648 probes	161 probes
cg15497724	0.00000	
cg15527515	0.00000	
cg15636421	0.00918	
cg15678825	0.06049	
cg15734436	0.03062	39.82044
cg15825321	0.00000	
cg15835339	0.00000	21.57562
cg15867428	0.00000	0.00129
cg15876968	0.00000	
cg15887927	0.00000	
cg15928534	0.00000	
cg16006738	0.00000	0.00000
cg16046375	0.00000	
cg16072777	23.36600	
cg16096766	0.14362	
cg16099687	0.00000	
cg16409039	0.00000	
cg16414821	0.01193	12.22966
cg16418105	1.42428	
cg16439948	0.00000	
cg16558770	0.00000	
cg16567202	0.00000	0.80691
cg16614020	99.61657	100.00000
cg16782174	0.20554	
cg16848712	0.01337	0.00872
cg16904330	0.00000	
cg16962008	4.86780	
cg16985708	2.86232	
cg17059564	0.00000	0.00699
cg17098979	0.00027	
cg17121120	0.06018	
cg17132030	22.13905	
cg17163363	0.00000	
cg17198772	0.00000	2.13934
cg17248961	5.82034	
cg17324128	0.00001	
cg17342588	0.00001	
cg17343167	0.00000	
cg17352045	12.14537	
cg17386185	0.00000	16.54185

Probe	648 probes	161 probes
cg17491622	0.00002	
cg17496887	0.00013	
cg17559809	0.00000	0.02259
cg17654567	0.00010	
cg17787876	0.00000	
cg17827803	0.00040	
cg17848054	0.53249	
cg17914838	2.82849	
cg17921548	61.39770	
cg17970176	10.28054	5.45559
cg17995197	0.27074	0.00000
cg18054674	10.46978	
cg18057887	0.00000	
cg18064714	0.00000	
cg18082362	0.00000	
cg18147104	0.00000	0.00181
cg18153869	9.61999	
cg18174404	0.00246	
cg18182475	0.00601	
cg18235690	14.38877	
cg18237551	0.00001	
cg18362003	0.27925	
cg18419977	0.65485	
cg18437839	0.00030	0.37884
cg18458509	0.00448	
cg18479249	0.00000	
cg18489195	0.17847	
cg18681352	0.00548	
cg18715709	0.00000	
cg18728780	0.00000	
cg18776287	0.00000	0.00000
cg18778727	2.32960	
cg18865832	0.00000	
cg18920097	0.00860	
cg19037350	0.01806	
cg19075225	0.00000	35.02488
cg19092735	0.03776	
cg19100988	0.00000	
cg19273668	4.66018	
cg19275200	0.06645	

Probe	648 probes	161 probes
cg19308397	0.00000	
cg19360675	0.56822	6.49140
cg19402173	39.01580	59.94469
cg19470832	1.33875	0.65186
cg19497798	0.00000	0.00059
cg19555986	0.00039	
cg19566764	52.61003	32.57136
cg19697239	0.98875	14.12348
cg19734433	0.00000	
cg19748485	0.33894	
cg19872095	13.06488	
cg19901523	0.00158	12.16287
cg19995899	0.00000	
cg20003976	0.00000	
cg20065463	0.00000	
cg20130789	0.00003	0.00316
cg20138186	0.00000	
cg20143982	0.00379	
cg20164964	3.73359	
cg20254763	0.00000	
cg20293942	0.01203	
cg20306534	0.00488	
cg20307184	0.00000	
cg20335425	0.00000	
cg20359202	1.47786	
cg20360285	0.00000	
cg20366110	0.11306	
cg20506745	0.00186	
cg20511832	0.00000	
cg20524128	0.06560	
cg20684180	0.00000	
cg20694545	0.00003	5.33391
cg20699141	0.00000	22.74435
cg20703671	0.01010	
cg20821838	0.00020	
cg20876010	0.00000	0.00000
cg20906524	0.00000	
cg20961387	0.00039	
cg21008530	0.00000	0.02070
cg21030607	0.00000	

Probe	648 probes	161 probes
cg21032583	0.00000	0.00000
cg21040775	0.00000	
cg21047695	9.30228	9.56906
cg21048669	0.00000	
cg21051972	0.00000	
cg21117330	2.25839	
cg21202862	0.00004	
cg21222426	0.00000	
cg21225504	0.00100	
cg21257581	0.00000	
cg21324308	0.00000	
cg21462934	0.00000	
cg21481662	0.00000	
cg21496518	0.00000	
cg21563683	0.00000	
cg21591807	0.00687	
cg21785245	0.00000	0.00000
cg21838625	0.00018	
cg21853021	0.00000	
cg21857190	4.54511	
cg21879102	0.00000	
cg21931938	0.00001	
cg22010140	0.09034	0.00099
cg22070991	0.03633	
cg22118082	0.00000	
cg22123885	0.01278	
cg22129122	0.02426	
cg22132788	0.00000	
cg22239534	3.69895	36.49658
cg22283925	4.55643	
cg22338356	0.04435	0.00000
cg22455271	0.00000	
cg22495058	0.00000	
cg22573118	0.00232	
cg22659953	74.01385	63.47089
cg22672067	3.66660	24.33809
cg22691119	28.08275	
cg22702960	0.00000	
cg22767461	0.47417	
cg22873986	0.52182	0.00188

Probe	648 probes	161 probes
cg22893791	0.00000	0.00000
cg22910295	0.00000	
cg22924796	1.78218	
cg22940961	0.00000	
cg23069297	0.04743	1.69723
cg23078194	0.00011	
cg23161492	6.88320	1.95704
cg23190089	0.43797	
cg23203302	0.00000	
cg23237801	0.00023	
cg23348582	0.00000	
cg23356309	0.00087	
cg23358740	0.00000	
cg23406407	0.00331	
cg23418467	0.00000	
cg23476401	0.01139	29.00413
cg23492399	0.06470	9.85625
cg23495441	0.00000	
cg23555395	0.00000	
cg23586138	0.00000	
cg23588928	0.00000	8.16590
cg23617193	0.00000	
cg23660182	0.00000	
cg23930711	17.57175	
cg23948825	0.18447	
cg23976431	2.51551	
cg23978357	0.00000	
cg23978358	0.00000	
cg23987134	0.00000	5.87866
cg24033103	0.02845	
cg24033661	0.00000	
cg24127414	0.18084	
cg24212392	0.00000	
cg24218620	11.13353	67.87875
cg24269657	0.00000	
cg24292665	0.00000	
cg24317217	0.00000	
cg24330379	0.00000	0.96532
cg24351857	0.00000	
cg24499411	0.00000	

Probe	648 probes	161 probes
cg24506604	0.00001	0.52984
cg24511341	11.73251	
cg24605090	0.00197	
cg24630957	0.19737	
cg24640156	69.97644	8.86757
cg24800175	76.84194	97.00374
cg24834889	0.00068	
cg24927800	0.00014	0.00000
cg25059434	14.40706	
cg25075776	0.00000	0.08255
cg25182501	0.00043	
cg25230117	0.00000	0.00004
cg25236277	54.52399	
cg25306006	0.00000	
cg25353064	0.37468	
cg25491704	0.00000	0.00000
cg25600027	0.00681	
cg25609517	0.10902	
cg25670376	0.16097	
cg25702651	10.55334	
cg25799797	14.15587	
cg25842763	0.00607	
cg25850044	0.00000	
cg25949338	0.00000	0.00000
cg25954235	30.68469	
cg25963822	9.90976	
cg25967612	0.19579	
cg26112661	0.00000	20.69830
cg26127778	9.48272	
cg26231094	23.31026	5.73678
cg26340050	0.01099	
cg26371345	0.00000	0.00000
cg26373071	0.08629	
cg26416341	0.00000	
cg26470501	0.00000	
cg26487259	0.08703	
cg26523175	0.03505	
cg26614816	3.26983	
cg26621408	1.16135	
cg26656658	0.00000	

Probe	648 probes	161 probes
cg26693693	0.00000	0.16349
cg26723162	0.00000	
cg26736200	6.22025	
cg26821681	0.25361	
cg26880735	4.85119	
cg26932623	0.00000	0.00000
cg26955579	0.00004	
cg26986871	0.00076	2.11947
cg27100140	0.00000	
cg27105390	0.11649	
cg27110491	20.53513	
cg27118929	0.00000	
cg27120934	0.00000	
cg27129048	0.67213	
cg27135984	0.00000	
cg27151362	0.00000	
cg27247225	0.00000	
cg27295595	0.00000	
cg27298830	0.00000	0.02450
cg27300742	0.00007	31.35286
cg27370131	0.00000	
cg27384070	0.00000	
cg27409974	0.00008	
cg27413421	0.00003	
cg27438218	0.61344	
cg27491190	0.00000	0.00209
cg27592868	1.72669	0.00001
ch.1.186147687F	0.00532	